

Guixia Kang
Nibelungenstr. 50
München, Deutschland

Time and frequency domain joint channel estimation in multi-carrier multi-branch systems

deutscher Titel:
**Gemeinsame Kanalschätzung im Zeit- und Frequenzbereich
für Mehrträgerübertragungsverfahren mit mehreren
Übertragungszweigen**

Vom Fachbereich Elektrotechnik und Informationstechnik
der Technischen Universität Kaiserslautern
zur Verleihung des akademischen Grades
Doktor der Ingenieurwissenschaften (Dr.-Ing.)
genehmigte Dissertation

von
Dr.-Eng. Guixia Kang
D 386

Tag der Einreichung: 27. Oktober 2004
Tag der mündlichen Prüfung: 18. Februar 2005

Dekan des Fachbereichs: Prof. Dr.-Ing. G. Huth

Vorsitzender der
Prüfungskommission: Prof. Dr.-Ing. R. Urbansky

1. Berichterstatter: Prof. Dr.-Ing. habil. Dr.-Ing. E. h. P. W. Baier
2. Berichterstatter: Prof. Dr.-Ing. habil. J. Götze

Preface

The available work is developed from Oct 2002 to Oct 2004 in line with my activity as a scientific researcher in the Future Radio department of ICM (Information Communication Mobile) of Siemens AG in Munich, Germany. I would like to thank all who have supported me on the accomplishment of this work.

My special appreciation is given to Mr. Prof. Dr.–Ing. habil. Dr.–Ing. E.h. P. W. Baier, the director of the Research Group for RF communications of the University of Kaiserslautern, for the many valuable suggestions and the support to my work. His constant readiness for discussion as well as the numerous proper references he gave me improved this work substantially.

My friends and colleagues in Siemens are appreciated for providing the pleasant atmosphere of academic exchange for the promotion of my work. Particularly, I would like to thank Dr.–Ing. E. Schulz for providing the necessary facilities and conditions for the research and Mr. Dr.–Ing. M. Weckerle for his concrete suggestions and discussions and review of my thesis work. With their help, my theoretical work was put into the context of some future wireless system concepts in the project of JRB3G (Joint Research Beyond 3G) for verification. Dr.–Ing. E. Costa, Mr. J. Eichinger, and Mr. A. Filippi are also thanked for the valuable discussions, and Mr. R. Halfmann is thanked for making the computer and software run effectively.

I thank also my friends in the the Research Group for RF communications of the University of Kaiserslautern for the fruitful discussions. Special thanks are given to Dr.–Ing. habil. T. Weber and Mr. I. Maniatis for the discussions on the joint channel estimation techniques, as well as to Mrs. Y. Liu for providing some simulation chains and for the discussion on the simulation tools and parameters.

My genuine appreciation is given also to Mr. Prof. Dr.–Ing. P. Zhang of Beijing University of Posts and Telecommunications, who has guided me into the fancy world of wireless communications.

I cordially thank to my family, in particular my parents, who made my education and training possible and always support me. Finally I thank my husband, Dr.–Ing. D. Liu, who gave me in this time a crucial support. I would like to dedicate this work to them.

Munich, October 2004

Guixia Kang

Contents

1	Introduction	1
1.1	JCE in the uplink of synchronous mobile wireless systems	1
1.1.1	General	1
1.1.2	Application scenarios of JCE	3
1.1.3	Time and frequency domain JCE	6
1.1.4	State of the art in JCE techniques	7
1.2	Multi-branch systems	8
1.3	Pilots for JCE	11
1.3.1	General	11
1.3.2	State of the art in pilot design for JCE	12
1.4	Goals of this thesis	13
1.5	Contents and important results	14
2	Mobile radio channel model	17
2.1	Introduction	17
2.2	WSSUS broadband channel model	19
2.2.1	Broadband channel characterization	19
2.2.2	Stochastic channel description	20
2.3	Beyond 3G channel	24
2.3.1	Channel parameters	24
2.3.2	Channel simulations	25
2.4	Multi-branch channel consideration	26
2.5	Interference model	29
3	JCE in multi-branch systems	31
3.1	Introduction	31
3.2	Description of the problems of JCE	32
3.3	Frequency domain representation of JCE	36
3.3.1	Discrete frequency model	36
3.3.2	FD-JCE algorithms	41
3.3.3	SNR degradation	43
3.3.4	MSE	45
3.3.5	Variation coefficient	47
3.4	Time domain representation of JCE	48
3.4.1	Introduction	48
3.4.2	The shift property of DFT	48
3.4.3	Discrete time model	50
3.4.4	TD-JCE	53
3.4.5	SNR degradation	54
3.4.6	MSE	55

3.5	List of estimators	55
4	Optimum and suboptimum pilots for JCE in noise limited systems	57
4.1	Introduction	57
4.2	Design criteria of optimum pilots	58
4.2.1	Frequency domain	58
4.2.2	Time domain	61
4.2.3	Equivalence between the time and frequency domain design criteria of optimum pilots	63
4.3	Optimum pilots	64
4.3.1	Introduction	64
4.3.2	Disjoint pilots	64
4.3.3	Walsh code based pilots	65
4.3.4	CAZAC code based pilots	67
4.3.5	Proof of the optimum pilots	71
4.4	Suboptimum pilots	72
4.5	Numerical results of SNR degradations	73
5	Pilot assignment in multiple SA environments	76
5.1	Introduction	76
5.2	Pilot assignment problem in interference environments	77
5.3	Variation coefficient simulation	79
5.4	Proposals of pilot assignment for multiple SAs	85
6	Application of JCE in OFDM and FMT based multi-branch systems	88
6.1	Introduction	88
6.2	Multi-carrier systems	88
6.2.1	Introduction	88
6.2.2	FB-MC modulation	89
6.2.3	OFDM modulation	90
6.2.4	FMT modulation	92
6.3	Time versus frequency domain JCE for OFDM and FMT systems	94
6.4	PAPR issue in OFDM systems	98
6.4.1	General	98
6.4.2	PAPR comparison of various pilots	99
6.5	Applications of various optimum pilots	101
7	Simulations of JCE in OFDM and FMT based multi-branch systems	102
7.1	General	102
7.2	Simulation scenarios	102
7.2.1	OFDM simulation parameters	102
7.2.2	FMT simulation parameters	104
7.2.3	Definition of SNR	106

7.3	Performance of JCE in the multi-branch OFDM system	107
7.3.1	Subchannel simulation	107
7.3.2	MSE simulation	109
7.3.3	BER simulation	114
7.4	Performance of JCE in multi-branch FMT systems	119
7.4.1	Subchannel simulation	119
7.4.2	MSE simulation	120
7.4.3	BER simulation	125
8	Summary	130
8.1	English	130
8.2	German	131
	Appendix	133
A.1	Abbreviations	133
A.2	Symbols	134
	References	140

1 Introduction

1.1 JCE in the uplink of synchronous mobile wireless systems

1.1.1 General

Recently, wireless communication systems are developing from the third generation (3G) into the beyond 3G or fourth generation (4G) due to the increasing demands of mobile user data services. In order to maximize the profit of the investment by the system operators on the scarce and, therefore, valuable spectrum resource, the beyond 3G systems will support high data rate services with higher spectral efficiency than previous systems over broadband channels [BBT02, BaM02, CS00, KJC⁺03]. Furthermore, the operators of the wireless communication systems expect to support more users transmitting simultaneously with acceptable quality of service (QoS) over the limited resource. Consequently, the system designers have to face the challenge of achieving higher system capacity. The important factor that limits the system capacity in multi-user simultaneous transmission is the multiple access interference (MAI) [Ver98]. In the broadband channels, the MAI problem becomes even worse because each user may produce multiple replicas of the transmitted signal at the receiver due to the frequency selectivity of the channel [Pro95, Rap96]. Various possibilities to mitigate or even cancel MAI are under investigation, such as the interference cancellation (IC) techniques [EGL93, KIH87] and joint detection (JD) [Ver98, SWB02] at the receiver and joint transmission (JT) [BMW⁺00] at the transmitter. In these approaches, the knowledge of the radio channels of these multiple active users, either their transfer functions (TF) or their channel impulse responses (CIR), is presupposed. One widely used method to estimate the radio channels is to periodically transmit training signals which are a-priori known to the receiver. The channel knowledge is achieved based on the received training signals caused by the transmitted training signals. The training signals, during the multi-user transmission process over the frequency selective channels, will also incur MAI like problems at the receiver. Therefore, it is necessary to introduce a MAI cancellation like technique into the channel estimation, and thereby the joint channel estimation (JCE) [SJ94, SMW⁺01] is derived. Different from traditional single user channel estimation techniques [Pro95], in JCE not only the channel knowledge of the considered user but also that of the interferers within a certain geographic area named cell or service area (SA) are estimated jointly. The well designed JCE can completely cancel the interference between different users in the channel estimation process.

In mobile wireless systems using frequency division multiple access (FDMA) and time division multiple access (TDMA) as for example in the second generation (2G) global

system for mobile communications (GSM) [GSM88], channel estimation is a relatively simple task because the signals of the active users are separated either in time or in frequency. In the asynchronous code division multiple access (CDMA) systems, such as the 2G IS-95 CDMA system [Gar99] and the 3G wideband CDMA (WCDMA) system [HT02], the signals associated with the active users which are not intended to be detected in the considered cell are treated as noise, and matched filtering or RAKE receivers [Pro95] are applied. The channel estimation in such asynchronous CDMA systems by using correlators is often suboptimal because the MAI cannot be cancelled. In synchronous CDMA systems, such as the 3G time division CDMA (TD-CDMA) system [BJW01] and the time division synchronous CDMA (TD-SCDMA) system [LL99], JCE is proposed in which the multi-user signals other than the input of the concerned user in the considered cell are treated as interference, which can be partly or even completely cancelled by introducing a MAI cancellation like technique into the channel estimation. The optimum maximum-likelihood (ML) channel estimator, in which the interference can be totally cancelled, and the suboptimum matched filtering (MF) channel estimator have been proposed [SJ94].

In contrast to the mobile wireless systems considering FDMA and/or TDMA, the signal processing for the downlink is different from that for the uplink in synchronous CDMA systems in the case that the base station (BS) is equipped with only one antenna. In this case of downlink, the signals associated with the multiple simultaneously active users are radiated from the same location, i.e. from the BS. Hence, all user signals are received at each mobile terminal (MT) over a single radio channel. Therefore, it is practical to radiate the same training sequence for all the active users and the channel estimation at each MT is similar to that used in mobile wireless systems in FDMA and/or TDMA scenarios. If the BS is equipped with more than one antenna, the signals received at each MT experience multiple radio channels. In the case that different data signals are transmitted by the antennas, the signals from one antenna will behave as interference to the others. Therefore, different training sequences should be sent by the different antennas so that the MAI cancellation like JCE can be carried out in the downlink. In this case, the downlink channel estimation issue will be the same as in the case of the synchronous uplink channel estimation. Moreover, in the time division duplex (TDD) CDMA systems, such as the TD-CDMA and the TD-SCDMA systems, the uplink and the downlink radio channels are equivalent if the duration for the uplink and downlink signal transmissions as well as a necessary guard time in between is less than the channel coherence time [Pro95]. In this case, the knowledge of the downlink channels can be obtained from the uplink channel estimation. In the following, only the channel estimation in the synchronous uplink systems is considered.

To summarize, JCE is typically applied in the uplink of synchronous CDMA systems. The reception of the multiple user signals which are radiated from the multiple separate MTs is associated with multiple separate wireless channels. Different training sequences are, therefore, transmitted by different users. A well designed JCE, such as the optimum

ML JCE [SJ94], can cancel the interference between different users in the considered cell or SA completely.

Due to the potential of the optimum solution provided by JCE, together with its support of JD techniques, JCE has been applied to the 3G mobile wireless communication systems such as the TD-CDMA and TD-SCDMA systems. JCE is also proposed in one of the beyond 3G air interface concepts: the **J**oint **T**ransmission and **D**etection **I**ntegrated **N**etwork (JOINT) concept [WMS⁺02].

1.1.2 Application scenarios of JCE

The JCE technique copes with the estimation of a multiple input single output (MISO) channel in a multi-point to point application scenario. The general MISO channel is illustrated in Fig. 1.1, in which the fading of each radio channel could be either flat (single path) or frequency selective (multi-path).

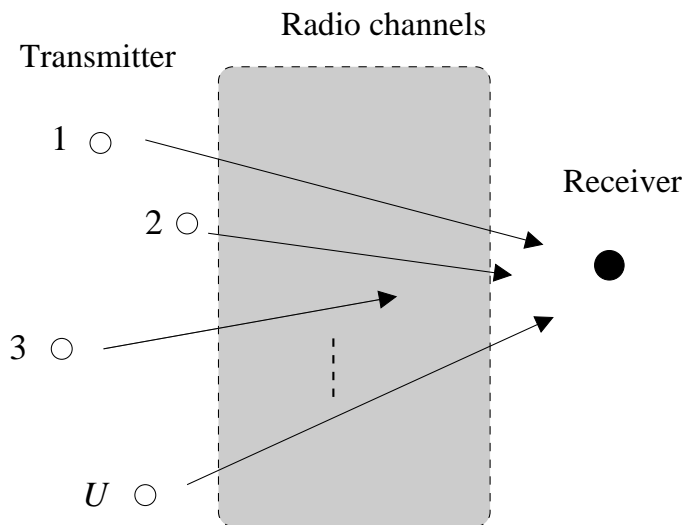


Fig. 1.1. A general MISO channel with U transmitters and one receiver.

In Fig. 1.1, there are U transmitters pouring signals into the radio channels. At the receiver, the signals from these U transmitters are received simultaneously. The JCE is carried out at the receiver to obtain the estimation of the U radio channels.

The JCE over the MISO channel can be applied in many system scenarios. In this subsection, two different system structures, i.e. the conventional cellular system [Rap96] and the JOINT architecture [WMS⁺02], will be recalled. The conventional cellular structure is shown in Fig. 1.2. In this structure, many MTs are distributed randomly in each cell

and communicate exclusively with the BS in that cell. In a certain time period, a few MTs are active simultaneously. As mentioned in Subsection 1.1.1, if the signals of these active MTs arrive in mutual synchronism at the BS, JCE can be carried out at the BS in order to simultaneously estimate the radio channels experienced by all the active MTs in the cell. TD-CDMA and TD-SCDMA systems are constructed as Fig. 1.2 in which JCE is performed at the BS.

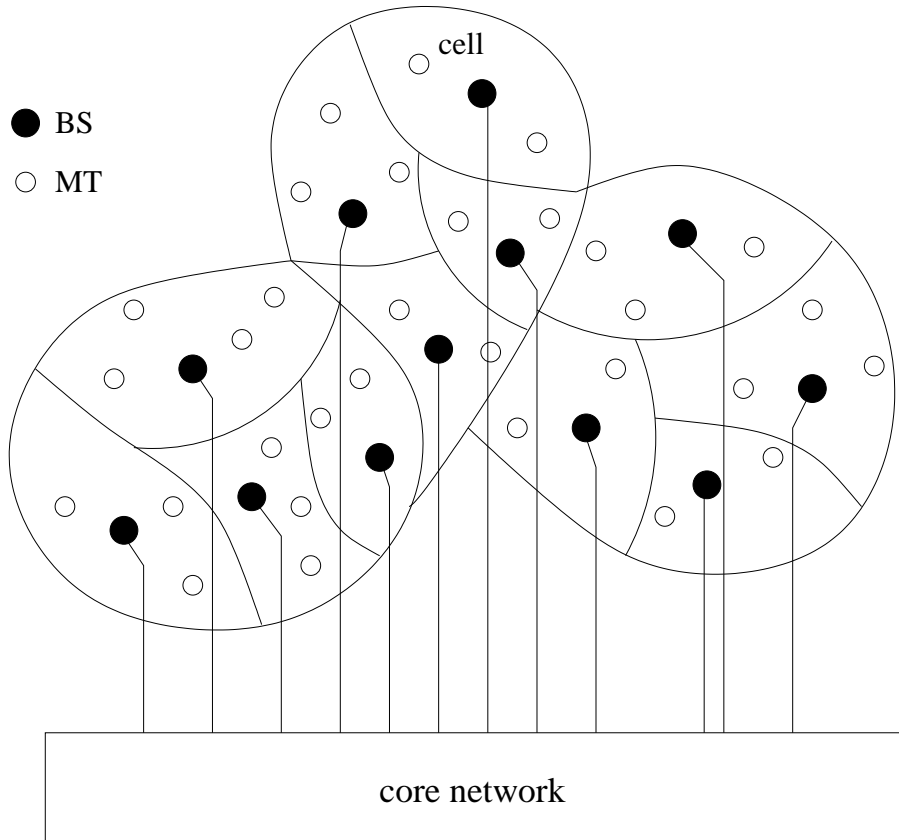


Fig. 1.2. Conventional cellular system, example with 12 cells.

Recently, compared with the cellular system structure of Fig. 1.2, another system architecture termed JOINT, see Subsection 1.1.1, is proposed for beyond 3G systems. The JOINT architecture [WMS⁺02] is shown in Fig. 1.3. Differently from the conventional cellular structure shown in Fig. 1.2, in the JOINT architecture a SA is introduced, in which many MTs and access points (APs) are distributed. Compared to that there is only one BS in each cell in the cellular structure, in the JOINT architecture there is one central unit (CU) in each SA. The MTs communicate with the CU via all APs. In a certain time period of the uplink transmission, the transmit signals of the simultaneously active MTs of a SA are received by all APs of the SA and fed to the CU, where they are jointly processed for the signal separation with the technique of JD [SWB02]. In the downlink, each MT of a SA is supported by the transmit signals radiated by all APs of

the SA. These signals are generated in the CU with the technique of JT [BMW⁺00].

JCE is proposed to be used in the JOINT concept [SMW⁺01]. It can be carried out in the synchronized uplink at each AP so that the channels experienced by all the active MTs in the considered SA to this AP can be estimated. The resulting knowledge of the channel from each MT to each SA is sent to the CU, based on which the data signals of the MTs are jointly detected by JD.

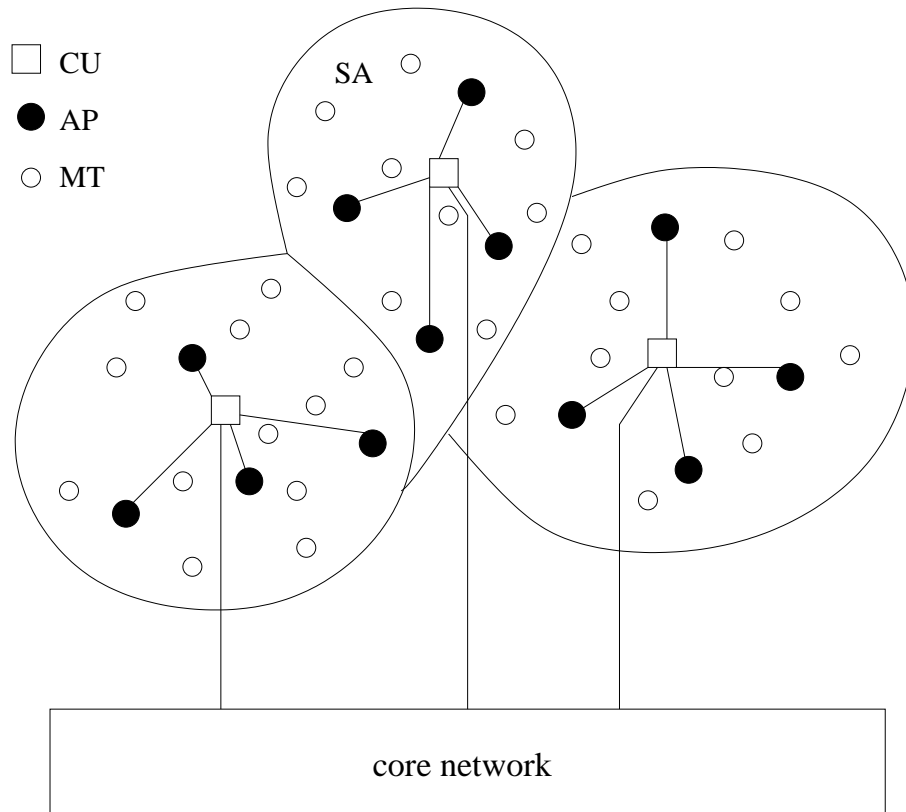


Fig. 1.3. Architecture of JOINT, example with 3 SAs [WMS⁺02].

The benefit of the JOINT architecture of Fig. 1.3 over the conventional cellular structure of Fig. 1.2 is discussed in [SWB02, WMS⁺02]. In the uplink of the cellular system structure, the signals radiated by the MTs not only impinge at their own BS, but also at the BSs of other cells, where they cannot be constructively utilized. In the downlink of the conventional cellular system structure, rather high transmit powers may be required at the BSs in order to compensate high losses of the propagation to MTs being far away from their BS or suffering from shadowing. These high transmit powers increase the interference observed at the MTs of other cells. In contrast to this situation, in the uplink of the JOINT concept, the transmit signals of the MTs are jointly processed at the CU in a manner that the signal energies received by the APs of the SA are exploited in an

optimum way characterized by simultaneously combating the impacts of inter symbol interference (ISI) and intra-SA MAI. In the downlink of the JOINT concept, the signals radiated by all APs are generated in the CU based on the data for each MT of the SA in such a way that the transmit signals for each MT have minimum powers and cause minimum interference at other MTs, and that the complexity of the MTs can be kept low.

Whereas the target scenarios of the conventional cellular systems are mainly outdoor environments, it is mentioned in [WMS⁺02] that the indoor mobile radio scenarios are viewed as the typical application area of JOINT.

1.1.3 Time and frequency domain JCE

The radio channels in the situation shown in Fig. 1.1 can be characterized in the time domain as channel impulse responses (CIRs). They can be equivalently characterized in the frequency domain as channel transfer functions (CTFs). In general, the estimation of the channel properties can be correspondingly classified into time domain channel estimation and frequency domain channel estimation [KWC04]. In time domain channel estimation, the training sequence is formed symbol by symbol in a certain time period, and the estimation of the time domain channel property, i.e. CIR, is based on the receive signal sampled in the time domain. In frequency domain channel estimation, the training sequence is formed symbol by symbol in a certain frequency band, and the estimation of the frequency domain channel property, i.e. CTF, is based on the receive signal sampled in the frequency domain.

In the TD-CDMA system, the CIRs of the synchronously active users are estimated by time domain JCE (TD-JCE), and the time domain JD is carried out afterwards. The realization of JCE in the JOINT concept is a mixture of time and frequency domain channel estimation. In the JOINT system concept, the orthogonal frequency division multiplexing (OFDM) [NP00] based multi-carrier transmission is adopted. Although the CTFs of the MTs are required by the frequency domain JD at the receiver and although the training sequences are allocated in the frequency domain, the CIRs are firstly estimated, and then, based on the CIRs, the CTFs are derived by discrete Fourier transformation (DFT). As shown in [SMW⁺01, MWS⁺02], in this way, the number of unknowns in the system equations can be reduced to a number which does not exceed the number of equations.

In the single user OFDM scenario, it is possible to apply a complete frequency domain channel estimation, by which the CTF of the single input single output (SISO) channel is directly estimated without resorting to the CIR at first [CD02]. In the following, for easier discrimination, the estimation aiming at the CTFs of channels, whether they are directly obtained or not, is termed frequency domain channel estimation.

1.1.4 State of the art in JCE techniques

The investigation on JCE accompanies the development of wireless communication systems. In the first generation (1G) and 2G systems, JCE is not used because the requirement on the system capacity in their eras was not as high as today. The capacity demand could be met by the multiple access technique of TDMA and/or FDMA within the allocated spectrum resource. With these techniques, the users are separated in time or in frequency so that only single user channel estimation technique is required.

JCE is originally a multi-user based technique. It is proposed for the TD-CDMA system and TD-SCDMA system for the 3G wireless communication systems to jointly estimate the wireless fading channels of the multiple users that are simultaneously active in the same frequency band and that are communicating with the same BS. In both systems, the CIRs of the active users are jointly estimated.

As stated in Subsection 1.1.1, the wireless communication systems are stepping into the beyond 3G or 4G which requires higher spectral efficiency for higher data rate transmission over broadband channels. Multi-carrier transmission techniques such as OFDM [NP00] are proposed to meet the ends and to reduce the complexity of channel equalization. Some novel channel estimation techniques are correspondingly emerging for the multi-carrier applications. The state of art of JCE in multi-user OFDM systems is that the training sequence for each users is allocated symbol by symbol in frequency and the received signal is sampled in the frequency domain with the inverse discrete Fourier transformation (IDFT) at the transmitter and the DFT at the receiver for fast implementation. As a result, a frequency domain JCE (FD-JCE) is generally proposed to estimate the broadband channels of multiple users. When the problem of unknowns surpassing the number of knowns in the equations of JCE is solved by changing the transformation domain from frequency into time for the channel properties [SMW⁺01], the traditional channel estimation methods, such as ML, least square (LS), weighted LS (WLS) and minimum mean square error (MMSE) estimations [Kay93] can be applied in multi-user OFDM systems. The JCE applied in the JOINT concept adopts this solution [WMS⁺02].

OFDM based systems take advantage of being robust to frequency selective fading and of doing with one tap per sub-channel equalizers with low complexity. However, they have also disadvantages such as the difficulty in subcarrier synchronization and sensitivity to the frequency offsets and nonlinear amplification [NP00]. Recently, another multi-carrier technique, filtered multi-tone (FMT), is drawing the attention of the researchers for the design of broadband beyond 3G wireless communication systems by referring the idea from very high speed digital subscriber lines [CEÖ⁺00, BTT02a]. Although FMT transmission requires more complicated equalization techniques at the receiver [BTT02], it is more robust to frequency offsets [CFW03]. Current research works on FMT based multi-carrier transmission include the modulation, the equalization techniques and the

design of prototype filters [CEÖ02, BTT02] in single user scenarios. Future development of FMT technique calls for its applications in multi-user and multi-antenna scenarios. Correspondingly, a lot of investigation in these scenarios should be carried out, such as the JCE technique.

As mentioned in Subsection 1.1.3, the JCE can be basically performed either in the time or the frequency domain. There is up to now little theoretical analysis on the relationship of the JCEs in these two domains. Also there are few researchers who have worked on the relationship of the training sequences for the TD-JCE and FD-JCE.

1.2 Multi-branch systems

JCE is typically proposed to address the issue of channel estimation in synchronous multi-user systems. In recent years, the multi-antenna transmit diversity based space-time coding techniques [TSC98, Ala98, Fos96] emerged thanks to their potential of high channel capacity [FG98, Tel95]. Among these techniques, the space-time block coding [Ala98] has been proposed for the 3G WCDMA system [WCDMA]. The space-time coding techniques are also promising for the beyond 3G systems. The channel estimation is one of the hot topics in the investigation of multi-antenna systems [LSA99, KCW⁺03], which involves the estimation of the multi-antenna fading channels at the receiver simultaneously.

Up to now, the channel estimation in multi-antenna systems and the JCE in multi-user systems are investigated separately. However, from the signal processing point of view, multi-antenna wireless channels and multi-user wireless channels have no intrinsic difference in the sense that both involve multiple transmit antennas that are communicating with a receiver within the same time-frequency resources, i.e. both are involved in the estimation of the MISO channel of Fig.1.1. So the channel estimation could be generally investigated for these two scenarios. The equivalence of channel estimation in a multi-user scenario and a multi-antenna scenario can be observed by comparing, e.g. the paper [SJ94] with [KCW⁺03, FAT03], for time domain channel estimation and the paper [SMW⁺01] with [LSA99] for frequency domain channel estimation. This equivalence is also mentioned in [VT01].

In the following, it is not distinguished between multiple antennas and multiple users for channel estimation. Instead, a new term of system structure, namely multiple branches or multi-branch scenarios, is introduced. Multi-branch systems refer to either multi-user or multi-antenna or the combination of multi-user and multi-antenna systems. More specifically, multiple branches refer to multiple transmit branches. We do not specify the number of receive branches or receivers. That is because, even if there are multiple receivers, each receiver can perform signal processing independently for channel estimation. Without

restricting generality, I consider only one receive branch in the thesis. That is the reason in Fig. 1.1 only one receiver is drawn.

It is assumed that the received signals transmitted by all the branches are synchronized at the receiver in the following.

Bandpass signal transmission in multi-branch systems can be efficiently described by the use of the equivalent low-pass domain representation of signals, in which the signals are expressed by their complex envelopes and vector representation of signals can be developed [Pro95]. Moreover, the model for the channel estimation in multi-branch systems can be decomposed into [Ver98, Kal95]:

- A physical transmission model. This represents in its interior the physical signal transmission and establishes, with respect to its input and output, the relation between the data symbols fed into the transmitter and the raw data estimates available in the receiver. Consequently, this model has to work time continuously in its interior and time discretely with respect to its input and output. In the concerned multi-branch systems, the physical transmission takes place over a time-continuous MISO channel of Fig. 1.1.
- A pre-processor at the transmitter before the physical transmission model and a post-processor in the Rx after the physical transmission model.

In this thesis, the equivalent low-pass representation of the signals for the investigation of JCE will be worked out. In Fig. 1.4, a general multi-branch system model for time domain channel estimation over the MISO channel of Fig.1.1 is illustrated. If we assume that there are K simultaneously active MTs in one cell or SA, with each MT $k, k = 1 \cdots K$, equipped with $K_{M,k}$ antennas, then the total number of branches is

$$U = \sum_{k=1}^K K_{M,k}, \quad (1.1)$$

with $u, u = 1 \cdots U$, representing the index of each branch. The physical transmission model for the aforementioned multi-branch transmission in the OFDM based and FMT based multi-carrier systems will be composed of the synthesis filter bank, the time-continuous $U \times 1$ MISO channel as well as the analysis filter bank, which will be further described in Chapter 6.

As shown in Fig. 1.4, the U time domain training sequences (TD training sequences), i.e. TD training sequence 1, TD training sequence 2, \cdots , TD training sequence U , are transmitted on the U branches. At each branch, a guard interval, which could be formed

by the cyclic prefix (CP) of the training sequence or any other formation, is appended to the training sequence to avoid the interference from the consecutively transmitted data symbols [DGE01]. The resulting U sequences for the U branches are then fed into the physical transmission model. At the receiver the guard is discarded prior to the further signal processing to retain the useful time domain receive signal (TD receive signal). The radio channels experienced by all branches are estimated jointly at the receiver, i.e. a TD-JCE is applied.

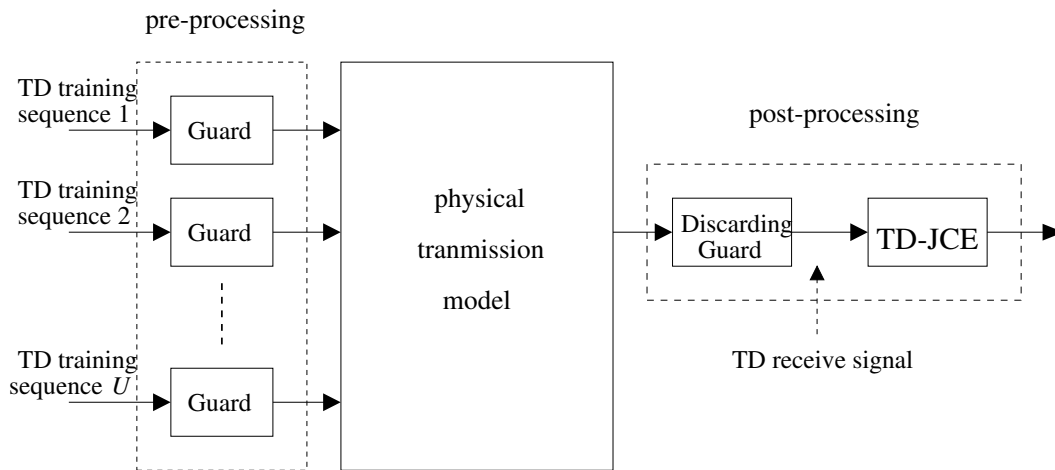


Fig. 1.4. Multi-branch system model in the time domain over the MISO channel.

The multi-branch system model can also be described in the frequency domain as shown in Fig. 1.5. In this structure, the U frequency domain training sequences (FD training sequences), i.e. FD training sequence 1, FD training sequence 2, \dots , FD training sequence U , are transmitted on the U branches. At each branch, the training sequence is first modulated by inverse fast Fourier transformation (IFFT) to transform signals from frequency domain into time domain, and then appended by a guard. In OFDM systems, which are conventionally based on the model of Fig. 1.5, the guard is achieved from the CP of the transmit signal, i.e. at the channel estimation stage, the CP of the training signal. The resulting signals including the guard interval are then fed into the physical transmission model in which a MISO channel of Fig. 1.1 is experienced. At the receiver, the guard interval is removed, and then the fast Fourier transformation (FFT) is passed. The frequency domain receive signal (FD domain receive signal) is therefore obtained for further signal processing. The radio channels experienced by all branches are estimated jointly at the receiver, i.e. a FD-JCE is applied.

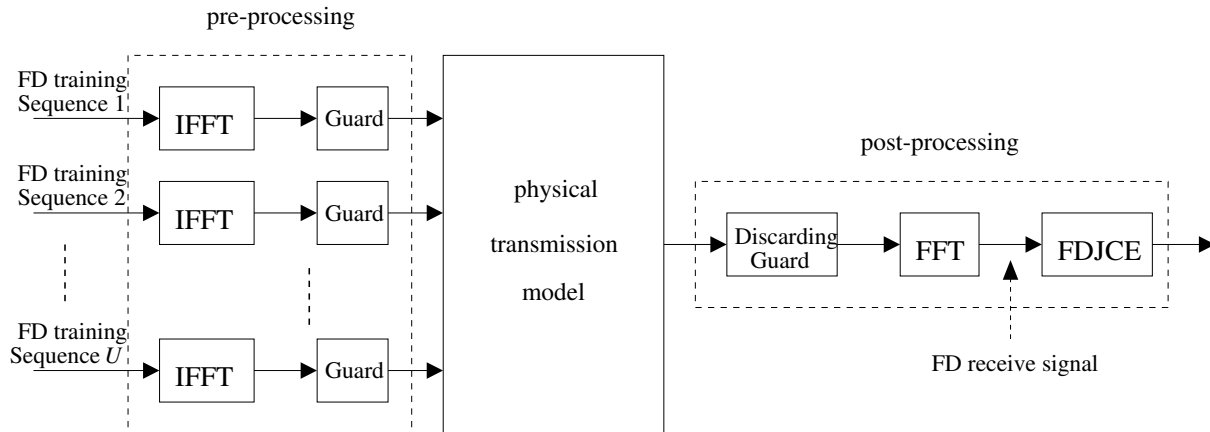


Fig. 1.5. Multi-branch system model in the frequency domain over the MISO channel.

1.3 Pilots for JCE

1.3.1 General

To get the knowledge of the broadband frequency selective channels, during some portion of the transmission interval, the transmitters of the multiple branches send training signals which have special patterns that allow to distinguish the different branches and which are a-priori known to the receiver [FAT03, BLM02, CM98]. These training signals are also called pilot signals or pilots in literature [MWS⁺02, YMC02, TM97].

As stated in Subsection 1.1.1, the optimum JCE, such as ML JCE, can be applied to multi-branch systems by which the interference from branches other than the considered one can be completely cancelled. However, compared with the matched filtering approach, the optimum JCE introduces a noise enhancement in the multi-branch case, which normally degrades the signal-to-noise ratio (SNR) at the receiver. SNR degradation [SJ94, MWS⁺02] is therefore introduced to evaluate the performance loss in a noisy environment. The noisy environment in the thesis refers to the case that either only one cell or SA exists in the system or many cells or SAs are present, but the superposition effect of the interferences from other cells or SAs than the considered cell or SA can be equivalently treated as noise. The other cases are referred to as interference environment.

This noise enhancement can be avoided by properly designing the pilot signals for the multiple branches. Pilots which are free of noise enhancement are called optimum pilots for the multiple branches. Optimum pilots cause no SNR degradation.

In contrast to the SNR degradation in a noisy environment, the performance of JCE in an interference environment can be evaluated by the variation coefficient [MWS⁺02]. It is observed that the pilot patterns of multiple branches will also influence the performance of JCE in interference environments [MWS⁺02].

Designing optimum pilots for the multiple branches is a hot topic in the research of JCE in recent years [CM98, BLM02, Li00]. Corresponding to the equivalence of JCE in multi-user and multi-antenna systems, which has been discussed in Section 1.2, the design of pilots in multi-user systems [SJ94, MWS⁺02, CM98] and in multi-antenna systems [FAT03, Li00] can be also equivalently coped with, although it has been developed actually in the context of two different applications. In this thesis, the design of pilots will be carried out in the more general multi-branch scenarios.

1.3.2 State of the art in pilot design for JCE

The development of JCE techniques is accompanied by the development of the pilot design. Since JCE has been addressed in the time and frequency domains, in multi-user and multi-antenna systems, and is involved in single carrier and multi-carrier transmissions, the design of pilots focuses also on such a variety of scenarios.

Up to now, the design of pilots has been addressed in the multi-user and multi-antenna scenarios separately. In [Li00], the design criteria of optimum pilots for the multiple transmit antennas in OFDM systems over multi-path fading channels is derived. The properties of optimum pilots are described. But the author did not give any example of the optimum pilots that would satisfy those properties. In [BLM02], the pilot tones, which multiplexes the available frequency resources with the data tone, is proposed as training sequences in OFDM systems. The property of optimum pilot tones for the multiple transmit antennas is given [BLM02]. However, the pilot tone is just a special case of pilot by which it is not obligatory to set some tones to be zeros. In addition, to derive the properties of optimum pilots, some researchers also take the method of exhaustive search [ChM00] or heuristic search [SJ94] for pilot design in multi-user systems. It is a big challenge to the computing process when the pilot is long and when the non-binary pilots is pursued with these search methods.

The state of the art of pilot design in the 3G wireless communication systems is that, although the design criterium of optimum pilots with 0 dB SNR degradation has been proposed [SJ94], there are no optimum pilots designed up to now and only suboptimum pilots derived by heuristic search [SJ94], or pseudo noise (PN) sequences [BC02] are proposed and applied [WCDMA, KCW⁺03].

Recently, with the development of beyond 3G systems, several kinds of pilots have been presented for the JCE in multi-user OFDM systems [MWS⁺02], namely disjoint pilots,

Walsh code based pilots and random pilots. However, up to now, there is no theoretical derivation on the design criteria of pilots in the systems, although simulation results show that some pilots, such as Walsh code based pilots and disjoint pilots, have 0 dB SNR degradation. Some pilots, such as Walsh code based pilots, challenge the implementation of OFDM transmission in the sense of peak-to-average power ratio (PAPR), which is not yet addressed in the investigation of pilots for JCE in OFDM systems. The design of pilots for the FMT based systems is also open.

1.4 Goals of this thesis

The previous research work concerning JCE and the design of pilots in multi-user or multi-antenna systems will be further improved and generalized in the thesis.

The design of optimum pilots for the 3G TD-CDMA and TD-SCDMA systems, in which time domain pilots are allocated for the multi-branch transmissions, as well as the design of optimum pilots for the beyond 3G multi-user OFDM systems such as the JOINT concept, in which frequency domain pilots are allocated for the multi-branch transmissions, will be investigated through theoretical analysis. The fruits after the investigation will be the optimum pilots for the above mentioned systems. The problem of non-linear amplifiers will be also taken into account in the process of pilot design. Since the channel estimation issue has never been addressed in FMT based multi-branch systems, the first focus for these systems will be to develop the suitable JCE scheme, and then propose the suitable pilots.

With the integration of multiple antennas and multiple users into a more general system structure of multiple branches, the JCE as well as the pilot design issues can be more generally dealt with. The theoretical analysis and the conclusions and results can be applied to many systems with the generalization.

Furthermore, the time and frequency domain signal processing will be incorporated into the research on JCE algorithm as well as the design of pilots. The relationship of the TD-JCE and FD-JCE as well as the time and frequency domain optimum pilots will be explained and clarified so that a special view on these issues is provided.

The goals of this thesis are:

- Propose and describe the multi-branch system model in the time and frequency domains.
- Elaborate the JCE algorithms in both the time and the frequency domain multi-branch systems.

- Derive theoretically the design criteria and properties of optimum pilots for TD-JCE and FD-JCE in noisy environments.
- Analyze the relationship between TD-JCE and FD-JCE and clarify the relationship of optimum pilots between TD-JCE and FD-JCE.
- Discuss and design optimum and suboptimum pilots for JCE in noisy environments and propose some new pilots.
- Discuss the design of pilots in interference environments.
- Analyze the suitability of TD-JCE and FD-JCE to various multi-branch multi-carrier systems.
- Investigate the performance of JCE in an OFDM based multi-branch multi-carrier system by simulation.
- Investigate the performance of JCE in a FMT based multi-branch multi-carrier system by simulation.

1.5 Contents and important results

This section briefly describes how the goals of this thesis presented in Section 1.4 are achieved. The structure and organizations of this thesis is already given by the table of contents.

Chapter 2 describes the mobile radio channel model, in particular the well known wide-sense stationary uncorrelated scattering (WSSUS) broadband radio channel model considered in the computer simulations in Chapter 7. The statistic channel description is adopted, by which the functions and the parameters characterizing the radio channel, such as the time-frequency correlation function, the coherence time, the coherence bandwidth, etc., are described. The beyond 3G channel parameters for both indoor and outdoor scenarios are then given, based on which the indoor and outdoor broadband channels are simulated. In addition, the interference model considered for the performance evaluation of JCE in terms of variation coefficient in Chapter 3, i.e. one strong interferer from the neighboring SA, is described. The aforementioned interference model is also used in Chapter 5 for investigating the issue of pilot assignment in multiple SA environments.

In Chapter 3, the problems met by JCE in multi-branch systems are firstly discussed. Three problems are paid particular attention to, i.e. the proper JCE algorithm for a certain transmission scheme, the pilot design in noisy environments, as well as the pilot assignment in interference environments. The following part of Chapter 3 as well as the following chapters, i.e. Chapter 4 to Chapter 6, aim to solve these problems. After

that, the frequency and the time domain representations of JCE are discussed separately. For each representation, the discrete system model, the JCE algorithms, as well as the performance evaluation of JCE, such as the SNR degradation, the mean square estimation error (MSE) and the variation coefficient, are presented. The frequency and the time domain representations of JCE, the frequency and the time domain JCE algorithms, as well as the frequency and the time domain performance evaluation criteria of JCE are proved to be equivalent in this chapter.

According to the SNR degradation evaluation of JCE in Chapter 3, the design criteria of optimum pilots in noisy environments for both the frequency and the time domain transmissions are derived in Chapter 4. It will be proved that the time and the frequency domain design criteria of optimum pilots are equivalent. Based on the equivalence, the optimum pilots designed in the frequency domain, after IDFT, will be shown to be the optimum pilots in the time domain for JCE in multi-branch systems. On the other hand, the optimum pilots designed in the time domain, after DFT, will be shown to be the optimum pilots in the frequency domain for JCE in multi-branch systems. The various optimum and suboptimum pilots for JCE in noisy environments are then constructed according to the design criteria. As optimum pilots, the disjoint pilots, the Walsh code based pilots and the constant amplitude zero autocorrelation (CAZAC) code based pilots are constructed. As suboptimum pilots, the random pilots are considered for performance comparison with the various optimum pilots in Chapter 4, 5 and 7. The numerical results of SNR degradations for the aforementioned pilots are then illustrated to verify the theoretical analysis.

In Chapter 5, the interference environments, i.e. the multiple SA scenarios, are considered for the pilot assignment. With the interference model of one strong interferer from the neighboring SA as described in Chapter 2, the pilot should be assigned in multiple SA environments in such a way that the variation coefficient for the considered SA is reduced. The correlation property of the pilots applied to the considered SA as well as the correlation property of the pilots applied to the considered SA and the neighboring SA influence the variation coefficient. It will be shown by simulations that the arrangement of different kinds of optimum pilots, e.g. disjoint pilots, Walsh code based pilots, and CAZAC code based pilots, to different SAs, or the arrangement of CAZAC code based pilots to the multiple SAs with a different mother CAZAC code in each SA, results in a good variation coefficient performance. The latter arrangement has the additional advantage of PAPR, which will be discussed in Chapter 6.

Chapter 6 addresses the application issues of JCE in multi-carrier systems based on OFDM or FMT transmissions. The OFDM and FMT transmission schemes are briefly introduced based on the description of a more general family of filter bank multi-carrier (FB-MC) modulation. The complexity evaluation of both time domain JCE and frequency domain JCE is then given, ending up with a curve illustrating the choice of time domain JCE

or frequency domain JCE according to their processing complexity. With the typical parameters chosen for the OFDM and FMT systems, it will be shown that in broadband channels the frequency domain JCE has less complexity for the OFDM systems, and the time domain JCE has less complexity for the FMT systems. Another important issue for the application of JCE is PAPR. The smaller the PAPR, the less the challenge of JCE to the implementation of the A/D, D/A converters as well as the RF power amplifier. It will be demonstrated that among disjoint pilots, Walsh code based pilots and CAZAC code based pilots, CAZAC code based pilots have the minimum PAPR of 0 dB.

Chapter 7 includes the simulation results of JCE in OFDM and FMT based multi-branch systems. The simulation results verify the theoretical analysis from Chapters 3 to 6.

A summary of this thesis in English and German is presented in Chapter 8.

2 Mobile radio channel model

2.1 Introduction

The mobile radio channel places fundamental limitations on the performance of wireless communication systems. The transmission path between the transmitter and the receiver can vary from simple line-of-sight (LOS) to one that is severely obstructed by buildings, mountains, and foliage. The speed of motion impacts how rapidly the signal level fades as a mobile terminal moves in space.

The received signal amplitude in mobile communications experiences fluctuations that can be divided into large-scale fading and small-scale fading. The large-scale fading is caused by shadowing effects in the propagation environment due to the morphology of the environment, and the small-scale fading, or simply fading, is mainly caused by changing interference of signals from scatterers around the receiver while the receiver moves a few wavelengths [Par92]. Since the small-scale fading describes the rapid fluctuation of the amplitude of a radio signal over very short travel distance of e.g. a few wavelengths or short time durations of the order of seconds, the large-scale path loss effects can be mitigated by power control and, hence, are generally ignored for the link level simulation, if perfect power control is assumed.

Through the numerous measurement campaigns performed in indoor [Zol93, Kat97] and outdoor environments [KMT96, FRB97], it is well known that in mobile radio communications a part of the electromagnetic energy radiated by the transmitter reaches the receiver by propagating through different paths [Par92, Pap00]. The performance of digital radio communication systems is strongly affected by multi-path propagation in the form of scattering, reflection, and refraction. The multipath in the radio channel creates small-scale fading effects. The three most important effects of the small-scale multi-path propagation are [Rap96]

- rapid changes in signal strength over a small travel distance or time interval,
- random frequency modulation due to varying Doppler shifts on different multi-path signals, and
- time dispersion caused by multi-path excess delays.

The time dispersive nature of the multi-path channels is normally quantified by their delay spread σ_τ , which can be determined from their power delay profile [Rap96]. The maximum multi-path excess delay τ_{\max} of the power delay profile is defined to be the time delay during which multi-path energy is smaller than a predefined threshold. The time

variance of the multi-path channels is described by the Doppler spread δ_{f_D} [Rap96]. It is defined as the range of frequencies over which the receive Doppler spectrum is essentially non-zero.

Due to the random characterization of the fading channels, it is necessary to investigate their statistical behavior, which leads to stochastic channel models. The simplest nondegenerate class of processes which exhibits uncorrelated dispersiveness in time delay and Doppler shifts is known as the wide-sense stationary uncorrelated scattering (WSSUS) model introduced by Bello [Bel63, Pro95, Hoe92]. The WSSUS channel model is widely used for the simulation of mobile communication systems with omnidirectional antennas [Pro95]. For the multi-antenna systems with beam-forming, directional models for mobile radio channels should be applied [ECS⁺98, COS01, Wec02], which are out of the discussion of this thesis.

Based on the WSSUS model, the statistical measures such as the coherence time T_C and the coherence bandwidth B_C can be obtained. Coherence time T_C is the time duration over which two receive signals have a strong potential for amplitude correlation. If the symbol duration T_s of the baseband signal is smaller than the channel coherence time T_C , then the channel variations are slower than the baseband signal variations, therefore the channel can be considered 'slow fading'. Otherwise the channel can be considered as fast fading [Rap96]. Coherence bandwidth B_C is the range of frequencies over which two frequency components have a strong potential for amplitude correlation. If the system bandwidth B is greater than the channel coherence bandwidth B_C , the channel can be considered to be 'frequency selective', and a broadband channel is characterized. Otherwise the channel is 'frequency non-selective' or 'flat', and a narrow-band channel is characterized. Frequency selective fading is due to time dispersion of the transmitted symbols within the channel. Thus the frequency selective channel induces ISI [Pro95].

In this chapter, the mathematical description of the WSSUS channel model and its statistical properties will be introduced in Section 2.2, which refers mainly to [Gal01, Hoe92]. Since in this thesis the channel estimation problems for the beyond 3G systems are targeted, in Section 2.3 the parameters of the beyond 3G channel, which is generated from the WSSUS channel model, will be given for the indoor and outdoor environments. The beyond 3G channel model in these two scenarios will be also simulated in this section. For the concerned multi-branch transmissions the generation of the multiple independent WSSUS channels will be proposed and simulated in Section 2.4. The interference model, which is particularly useful for the evaluation of channel estimation in multi-cell or multi-SA scenarios, will be introduced in Section 2.5.

Throughout the thesis, signals, CIRs and CTFs are represented by complex vectors and matrices. All complex quantities are underlined, and vectors and matrices are in bold face. Furthermore, $()^*$ and $()^T$ designate the complex conjugate and the transpose, respectively.

The complex conjugate transpose $()^{*T}$ is also called complex Hermitian and expressed as $()^H$. The operator $[\cdot]_{x,y}$ yields the element in the x -th row and the y -th column, and $[\cdot]_{x_1,y_1}^{x_2,y_2}$ yields the submatrix bounded by the rows x_1, x_2 and the columns y_1, y_2 of a matrix in bracket. The frequency domain quantities are marked by a tilde, whereas the time domain quantities are printed without distinguishing marks. The expressions $\text{diag}(\cdot)$, $E\cdot$ and $\text{tr}\cdot$ denote the diagonal matrix containing the diagonal elements of the matrix in the argument, the expectation operation and trace operation, respectively.

2.2 WSSUS broadband channel model

2.2.1 Broadband channel characterization

The notion of WSSUS was proposed by Bello [Bel63] to model the fading phenomenon. The WSSUS channel model is fully determined by a two-dimensional scattering function in terms of the echo delay τ due to multi-path, and the Doppler shift f_D due to the vehicle movement [Hoe92]. It is shown [Bel63] that such a channel is effectively wide-sense stationary (WSS) in both the time and frequency domains.

As introduced in Section 2.1, mobile radio communications suffer from multi-path propagation of the transmitted signal. The transmitted signal reaches the receiver either only as scattered signal (No line-of-sight (NLOS)) or as directed path as well as scattered signal LOS. Let us assume the number of paths of the radio channel to be W_τ . The received signals over the different paths experience time delays $\tau_{w_\tau}, w_\tau = 1 \cdots W_\tau$, according to the distance of the reflection points and phase rotations $\varphi_{w_\tau}, w_\tau = 1 \cdots W_\tau$. As long as the communication environment remains unchanged and neither the transmitter nor the receiver is moving the channel is static over time, or 'time-invariant'. With a Kronecker delta function $\delta(\cdot)$, the time-invariant CIR

$$\underline{h}(\tau) = \frac{1}{\sqrt{W_\tau}} \sum_{w_\tau=1}^{W_\tau} e^{j\varphi_{w_\tau}} \delta(\tau - \tau_{w_\tau}) \quad (2.1)$$

is obtained as the superposition of a large number W_τ of received paths [Sch89].

The Fourier transform of the time-invariant CIR $\underline{h}(\tau)$ of (2.1) determines the time-invariant CTF

$$\tilde{h}(f) = \frac{1}{\sqrt{W_\tau}} \sum_{w_\tau=1}^{W_\tau} e^{j\varphi_{w_\tau}} e^{-j2\pi f\tau_{w_\tau}}. \quad (2.2)$$

A movement of either the transmitter or the receiver introduces individual Doppler shifts $f_{D,w_\tau}, w_\tau = 1 \cdots W_\tau$, to all W_τ propagation paths. The Doppler shifts f_{D,w_τ} of the

propagation paths introduces a 'time-variance' to the time-invariant CIR $\underline{h}(\tau)$ of (2.1) which is caused by the phase rotation on each path over time. The Doppler shift f_{D,w_τ} of each path is determined by the carrier frequency f_c as well as the vehicle speed v and the direction ψ_{w_τ} of the movement of the terminal relative to the direction from which the signal of that path is received [Rap96]

$$f_{D,w_\tau} = \frac{f_c v}{c} \cos(\psi_{w_\tau}) = f_{D_{\max}} \cos(\psi_{w_\tau}), w_\tau = 1 \cdots W_\tau \quad (2.3)$$

in which $f_{D_{\max}}$ represents the maximum Doppler shift and c represents the speed of light.

With the influence of the Doppler shifts $f_{D,w_\tau}, w_\tau = 1 \cdots W_\tau$, the time-variant CIR

$$\underline{h}(\tau, t) = \frac{1}{\sqrt{W_\tau}} \sum_{w_\tau=1}^{W_\tau} e^{j\varphi_{w_\tau}} e^{j2\pi f_{D,w_\tau} t} \delta(\tau - \tau_{w_\tau}) \quad (2.4)$$

can be obtained. By taking the Fourier transformation of the time-variant CIR $\underline{h}(\tau, t)$ of (2.4) with respect to the delay τ , the time-variant CTF

$$\tilde{\underline{h}}(f, t) = \frac{1}{\sqrt{W_\tau}} \sum_{w_\tau=1}^{W_\tau} e^{j\varphi_{w_\tau}} e^{j2\pi f_{D,w_\tau} t} e^{-j2\pi f \tau_{w_\tau}} \quad (2.5)$$

can be obtained.

The time-variant CTF $\tilde{\underline{h}}(f, t)$ of (2.5) is a random variable and, therefore, can be statistically described. According to the central limit theorem [Pro95] in the NLOS scenario, a large number of randomly superimposed signal paths leads to a Gaussian distribution of the time-variant CTF $\tilde{\underline{h}}(f, t)$ of (2.5), whose probability density function (pdf) is given by [Pro95]

$$p(\tilde{\underline{h}}) = \frac{1}{2\pi\sigma_h^2} e^{-\frac{|\tilde{\underline{h}}|^2}{2\sigma_h^2}}, \quad (2.6)$$

in which σ_h^2 represents the variance of the time-variant CTF $\tilde{\underline{h}}(f, t)$ of (2.5).

The absolute value of the time-variant CTF $\tilde{\underline{h}}(f, t)$ of (2.5) follows a Rayleigh distribution, whose pdf is given by [Pro95]

$$p(|\tilde{\underline{h}}|) = \frac{|\tilde{\underline{h}}|}{\sigma_h^2} e^{-\frac{|\tilde{\underline{h}}|^2}{2\sigma_h^2}}. \quad (2.7)$$

2.2.2 Stochastic channel description

The time delay τ_{w_τ} , the phase rotation φ_{w_τ} and the Doppler shift f_{D,w_τ} in (2.4) characterize one specific channel realization related to a certain topography of the surrounding environment. For computer simulations, a stochastic channel model which adopts the

statistic properties of a transmission scenario but neglects the exact topography of the environment should be defined [Bel63, Gal01]. During the simulation process a pseudo-random realization of the channel is generated which follows the statistical properties of the selected transmission scenario. The actual channel can be interpreted as one possible realization of the stochastic channel model which contains the same statistical information as all other channel realizations [Gal01].

A number of correlation functions can be defined which are sufficient to characterize the stochastic channel [Bel63]. The autocorrelation function of the time-variant CIR $\underline{h}(\tau, t)$ of (2.4) is given by

$$\underline{\phi}_h(\tau_1, \tau_2, t_1, t_2) = \mathbb{E}\{\underline{h}(\tau_1, t_1)\underline{h}^*(\tau_2, t_2)\}. \quad (2.8)$$

(2.8) describes on one hand the distribution of the average receive power over varying delays for a given observation time, and on the other hand the changes in the distribution of the receive power over time.

Under the assumption of a WSS stochastic process the autocorrelation function $\underline{\phi}_h(\tau_1, \tau_2, t_1, t_2)$ of (2.8) of the time-variant CIR $\underline{h}(\tau, t)$ of (2.4) does not depend on the absolute time t but depend on the time difference

$$\Delta t = t_2 - t_1 \quad (2.9)$$

of the observation times. Therefore, (2.8) turns out to be

$$\underline{\phi}_h(\tau_1, \tau_2, \Delta t) = \mathbb{E}\{\underline{h}(\tau_1, t)\underline{h}^*(\tau_2, t + \Delta t)\}. \quad (2.10)$$

Moreover, in most radio transmission situations the signal attenuations and phase rotations of different propagation paths are uncorrelated. This fact is most often denoted as uncorrelated scattering of the signals since the received signal paths are assumed to be caused by independent scattering objects. With this assumption the autocorrelation function $\underline{\phi}_h(\tau_1, \tau_2, t_1, t_2)$ of (2.8) can be further simplified to [Hoe92]

$$\underline{\phi}_h(\tau_1, \tau_2, \Delta t) = \underline{\phi}_h(\tau, \Delta t)\delta(\tau_2 - \tau_1), \quad (2.11)$$

which can be completely described by the autocorrelation function $\underline{\phi}_h(\tau, \Delta t)$.

By letting

$$\Delta t = 0 \quad (2.12)$$

the autocorrelation function $\underline{\phi}_h(\tau, \Delta t)$ in (2.11) turns out to be

$$\underline{\phi}_h(\tau, 0) = \underline{\phi}_h(\tau), \quad (2.13)$$

which is the average power of the time-invariant CIR $\underline{h}(\tau)$ of (2.1) with respect to the multi-path excess delay τ . $\underline{\phi}_h(\tau)$ in (2.13) is therefore also known as the power delay profile of the channel [Pro95].

Typically, the power delay profile $\underline{\phi}_h(\tau)$ in (2.13) of a radio channel is an exponentially decreasing function with the delay τ . It is often characterized by its maximum multi-path excess delay τ_{\max} for which the average power of the time-invariant CIR $\underline{h}(\tau)$ of (2.1) is reduced by 30 dB. The model of an exponentially decreasing power delay profile has been adopted as part of the COST 207 [COS89] project during the development of the GSM system. It will also be adopted in the beyond 3G WSSUS channel model in this thesis used for the simulations in Chapter 8.

By taking the Fourier transformation of the autocorrelation function $\underline{\phi}_h(\tau, \Delta t)$ in (2.11) of the time-invariant CIR $\underline{h}(\tau)$ of (2.1), the scattering function

$$\underline{\phi}_h(\tau, f_D) = \int_{-\infty}^{\infty} \underline{\phi}_h(\tau, \Delta t) e^{j2\pi\Delta t f_D} d\Delta t \quad (2.14)$$

is obtained, which is also recognized as the time-frequency correlation function of the time-invariant CIR $\underline{h}(\tau)$ of (2.1).

It is proved [Hoe92] that the scattering function $\underline{\phi}_h(\tau, f_D)$ of (2.14) is proportional to the joint pdf $p(\tau, f_D)$ of the Doppler shifts f_D and time delays τ of the independent propagation paths, i.e.

$$\underline{\phi}_h(\tau, f_D) \propto p(\tau, f_D). \quad (2.15)$$

By calculating the integral of $p(\tau, f_D)$ in (2.15), the marginal distributions, i.e. the pdf of the Doppler shift f_D

$$p(f_D) \propto \underline{\phi}_h(f_D) = \int_0^{\infty} \underline{\phi}_h(\tau, f_D) d\tau \quad (2.16)$$

and the pdf of the delay τ

$$p(\tau) \propto \underline{\phi}_h(\tau) = \int_{-\infty}^{\infty} \underline{\phi}_h(\tau, f_D) df_D, \quad (2.17)$$

can be obtained. The pdfs of the Doppler shift $p(f_D)$ in (2.16) and of the delay $p(\tau)$ in (2.17) can be utilized to generate the random Doppler shifts f_{D,w_τ} , $w_\tau = 1 \cdots W_\tau$, and the delays τ_{w_τ} , $w_\tau = 1 \cdots W_\tau$, for characterizing a realization of the radio channel. It is furthermore assumed that the two random variables of the delay τ and the Doppler shift f_D are independent and, therefore, the joint pdf $p(\tau, f_D)$ in (2.15) can be written as

$$p(\tau, f_D) = p(f_D)p(\tau). \quad (2.18)$$

The moments of the pdf of the Doppler shift $p(f_D)$ in (2.16) and the pdf of the delay $p(\tau)$ in (2.17) can be used to characterize the properties of the stochastic channel model [Pro95]. The standard deviation of the pdf of the delay $p(\tau)$ of (2.17) is known as the delay spread σ_τ and the standard deviation of the pdf of the Doppler shift $p(f_D)$ of (2.16) is known as the Doppler spread δ_{f_D} of the channel, respectively.

Normally, the random variable of the initial phases φ is assumed to be uniformly distributed [Hoe92, Gal01], i.e. its pdf follows

$$p(\varphi) = \begin{cases} \frac{1}{2\pi} & \varphi \in [0, 2\pi) \\ 0 & \text{else} \end{cases} \quad (2.19)$$

The phase rotations $\varphi_{w_\tau}, w_\tau = 1 \cdots W_\tau$, in (2.4) are taken from the random samples of φ .

For an exponentially decreasing power delay profile the multi-path excess delays τ are taken from an exponential pdf [Hoe92, Gal01]

$$p(\tau) = \begin{cases} \frac{a}{1-e^{-a\tau_{\max}}} e^{-a\tau} & 0 \leq \tau < \tau_{\max} \\ 0 & \text{else} \end{cases}, a = \frac{3\ln(10)}{\tau_{\max}} \quad (2.20)$$

The time delays $\tau_{w_\tau}, w_\tau = 1 \cdots W_\tau$, in (2.4) are taken from the random samples of τ .

If the directions of arrival of the paths are equally probably distributed, then the pdf of the Doppler shift f_D follows a Jakes distribution [Hoe92] of

$$p(f_D) = \begin{cases} \frac{1}{\pi f_{D\max} \sqrt{1 - \left(\frac{f_D}{f_{D\max}}\right)^2}} & |f_D| < f_{D\max} \\ 0 & \text{else} \end{cases} \quad (2.21)$$

$f_{D,w_\tau}, w_\tau = 1 \cdots W_\tau$, in (2.4) are taken from the random samples of f_D .

Additionally, from the autocorrelation function $\underline{\phi}_h(\tau, \Delta t)$ in (2.11) the time-frequency correlation function

$$\tilde{\underline{\phi}}_h(\Delta f, \Delta t) = \int_{-\infty}^{\infty} \underline{\phi}_h(\tau, \Delta t) e^{j2\pi\Delta f\tau} d\tau. \quad (2.22)$$

can be calculated, which measures the correlation of the time-variant CTF $\tilde{\underline{h}}(t, f)$ of (2.5) in time and frequency directions.

Based on (2.22), the coherence time T_C and the coherence bandwidth B_C of the channel can be defined, respectively, as the time and the frequency with which the absolute value of the time correlation function $\tilde{\underline{\phi}}_h(0, \Delta t)$ and the frequency correlation function $\tilde{\underline{\phi}}_h(\Delta f, 0)$ obtained from the time-frequency correlation function $\tilde{\underline{\phi}}_h(\Delta f, \Delta t)$ of (2.22) are reduced to half of their maximum values, i.e. [Pro95]

$$|\tilde{\underline{\phi}}_h(0, T_C)| = \frac{1}{2} |\tilde{\underline{\phi}}_h(0, 0)| \quad (2.23)$$

and

$$|\tilde{\underline{\phi}}_h(B_C, 0)| = \frac{1}{2} |\tilde{\underline{\phi}}_h(0, 0)| \quad (2.24)$$

are satisfied.

The coherence bandwidth B_C in (2.24) is inversely proportional to the delay spread σ_τ and is a measure for the frequency selectivity of the channel [Rap96, Pro95]. With a broadband channel, the maximum multi-path excess delay τ_{\max} will be much larger than the symbol duration and, therefore, will disturb consecutive symbols, i.e. the ISI appears. For example, for a system bandwidth B of 20 MHz, the maximum multi-path excess delay τ_{\max} of 5 μs will be approximately 100 times larger than the symbol duration T_s of 50 ns, which is derived approximately by the inverse of the system bandwidth B . This implies that amount of resolvable paths and severe ISI effects can be observed for the transmission of this system over the broadband channel.

The coherence bandwidth B_C can be roughly calculated as the inverse of the maximum multi-path excess delay τ_{\max} [Rap96], i.e.

$$B_C \approx \frac{1}{\tau_{\max}} \quad (2.25)$$

satisfies.

The coherence time T_C in (2.23) describes the time-variance of the channel. It is inversely proportional to the Doppler spread σ_{f_D} [Rap96]. For a coherence time T_C much greater than the symbol duration T_s the channel will not change within the duration of amount of symbols. Therefore, the coherence time influences the frequency of carrying out channel estimation and of inserting pilots. The shorter the coherence time, the more often the channel estimation should be carried out.

The coherence time T_C can be roughly estimated as the inverse of the maximum Doppler shift $f_{D_{\max}}$, i.e.

$$T_C \approx \frac{1}{f_{D_{\max}}} \quad (2.26)$$

satisfies.

2.3 Beyond 3G channel

2.3.1 Channel parameters

The application scenarios of the channel estimation techniques, although are not limited to, are the beyond 3G systems in this thesis. The beyond 3G channel is constructed as the WSSUS channel described in Section 2.2 with specific parameters. To simulate the performance of JCE in various beyond 3G system concepts, which will be focused in Chapter 8, it is necessary to have a common channel parameter basis in the simulations in order to come to comparable results. Mainly two scenarios, an indoor scenario with lower

mobility and an outdoor scenario with higher mobility are defined, which are referred to also as the indoor channel and the outdoor channel. The parameters of the considered beyond 3G indoor and outdoor channels are summarized in Table 2.1 [Gal01].

As shown in Table 2.1, the system bandwidth B of 20MHz is defined over the carrier frequency f_c of 5.5GHz. The maximum multi-path excess delay τ_{\max} of $0.8 \mu\text{s}$ for the indoor channel and $5 \mu\text{s}$ for the outdoor channel are anticipated, which, according to (2.25), correspond approximately to the coherence bandwidth B_C of 1.25 MHz for the indoor channel and 200 kHz for the outdoor channel, respectively. The maximum supportable vehicle speed v_{\max} of 3 km/h in the indoor channel and v_{\max} of 200 km/h in the outdoor channel are considered. With the carrier frequency f_c and the maximum vehicle speed v_{\max} , according to (2.3), the maximum Doppler shift $f_{D_{\max}}$ of 15.28 Hz for the indoor channel and 1.028 kHz for the outdoor channel can be obtained. With the knowledge of the maximum Doppler shift $f_{D_{\max}}$, the coherence time T_C can be approximately estimated as 65 ms in the indoor channel and 0.98 ms in the outdoor channel according to (2.26). The exponential power delay profile is adopted in the channel realization.

Table 2.1. Beyond 3G Channel Parameters.

Channel Parameters	Indoor	Outdoor
System bandwidth B	20 MHz	20 MHz
Carrier frequency f_c	5.5 GHz	5.5 GHz
Maximum vehicle speed v_{\max}	3km/h	200km/h
Power delay profile	exponential	exponential
Maximum multi-path excess delay τ_{\max}	$0.8 \mu\text{s}$	$5 \mu\text{s}$
Coherence bandwidth B_C	1.25 MHz	200 kHz
Maximum Doppler frequency $f_{D_{\max}}$	15.28 Hz	1.028 kHz
Coherence time T_C	65 ms	0.98 ms

2.3.2 Channel simulations

The WSSUS channel described in Section 2.2 with the parameters given in Table 2.1 is simulated in Fig. 2.1 and Fig. 2.2 for the two scenarios of indoor and outdoor, respectively. The f -axis represents the frequency in MHz and the t -axis represents the propagation time in ms. The amplitude of the time-variant CTF $\tilde{h}(f, t)$ of (2.5), i.e. $|\tilde{h}(f, t)|$, in dB is shown to be varying with time t and frequency f . It is seen in Fig. 2.1 that the indoor channel exhibits a slow time variance and a moderate frequency selectivity, whereas we see in Fig. 2.2 that the outdoor channel fluctuates strongly in both time and frequency directions. According to Table 2.1, the coherence bandwidth B_C is about 1.25 MHz in an indoor environment and 200 kHz in an outdoor environment, which can be roughly read from

the f -axis in Fig. 2.1 and Fig. 2.2, respectively. The coherence time T_C is about 65 ms in an indoor environment and 0.98 ms in an outdoor environment, which can be roughly read from the t -axis in the corresponding Fig. 2.1 and 2.2, respectively.

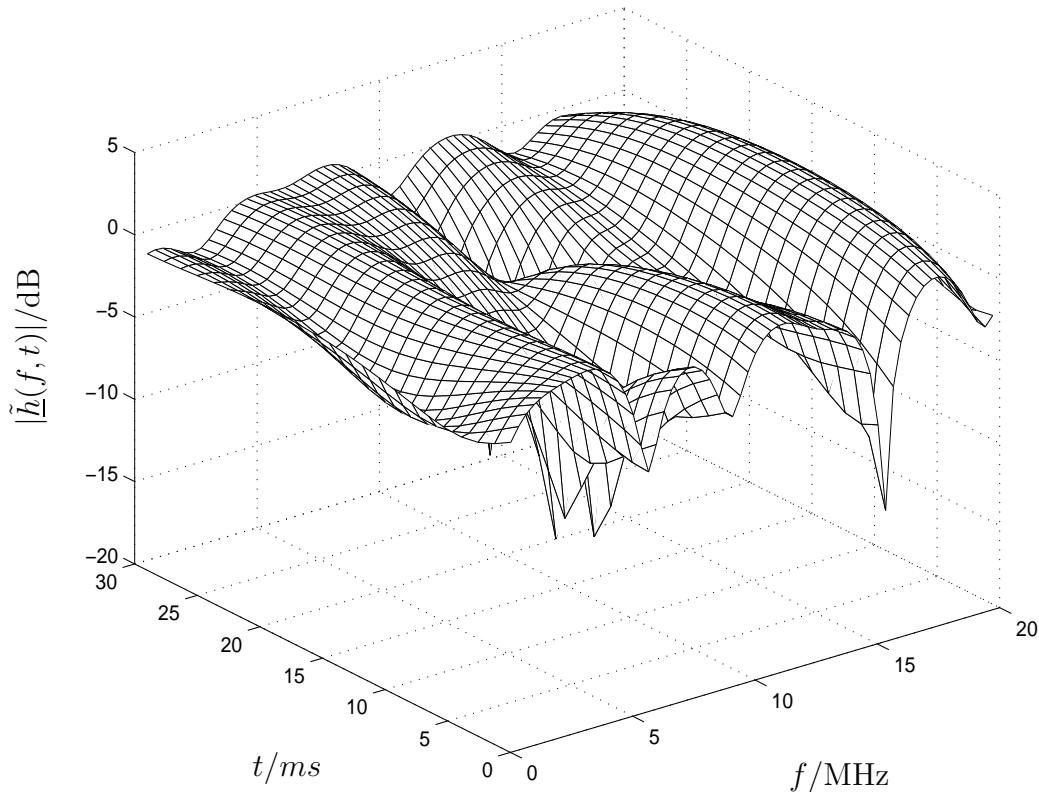


Fig. 2.1. The magnitude of the time-variant CTF $\tilde{h}(f, t)$ of (2.5), i.e. $|\tilde{h}(f, t)|$, for the WSSUS broadband indoor channel.

Comparing Fig. 2.2 with Fig. 2.1, we can understand that the channel estimation in the outdoor environment, due to its strong time variance and frequency selectivity, is much more challenging than the one in the indoor environment.

2.4 Multi-branch channel consideration

The frequency selective fading channel between each transmit branch u and the receiver can be characterized by a CIR vector

$$\underline{\mathbf{h}}^{(u)} = \left(\underline{h}_1^{(u)} \cdots \underline{h}_W^{(u)} \right)^T, \quad u = 1 \cdots U, \quad (2.27)$$

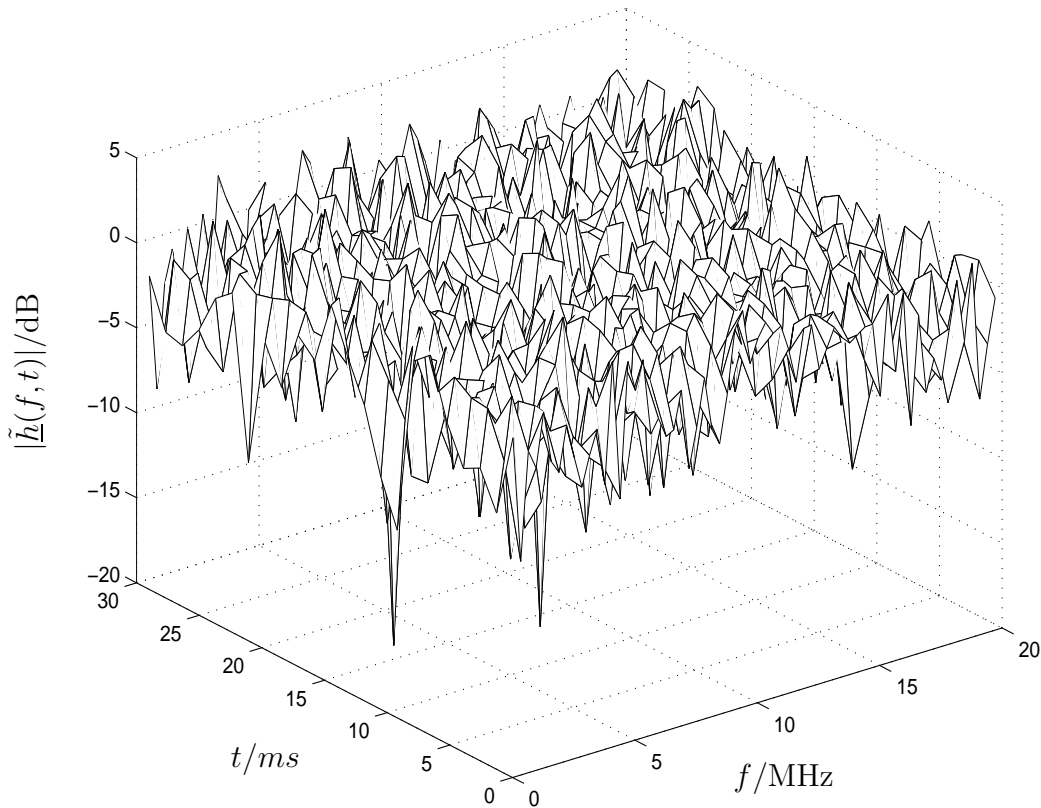


Fig. 2.2. The amplitude of the time-variant CTF $\tilde{\underline{h}}(f, t)$ of (2.5), i.e. $|\tilde{\underline{h}}(f, t)|$, for the WSSUS broadband outdoor channel.

of dimension W , with W representing the number of channel coefficients. Different from the CIR expression $\underline{h}(\tau)$ in (2.1) with a number W_τ of paths, in the vector expression (2.27) for the CIR $\underline{\mathbf{h}}^{(u)}$, only a limited number W of channel coefficients is considered. With (2.27) the total CIR vector for the U branches

$$\underline{\mathbf{h}} = \left(\underline{\mathbf{h}}^{(1)\text{T}} \ \dots \ \underline{\mathbf{h}}^{(U)\text{T}} \right)^{\text{T}} \quad (2.28)$$

of dimension UW is obtained.

The correlation matrix of the total CIR vector $\underline{\mathbf{h}}$ of (2.28) is expressed as [Wec02]

$$\underline{\mathbf{R}}_{\mathbf{h}} = \text{E}\{\underline{\mathbf{h}} \underline{\mathbf{h}}^{\text{H}}\}. \quad (2.29)$$

If the WSSUS channel realizations for any two branches are uncorrelated, the correlation matrix $\underline{\mathbf{R}}_{\mathbf{h}}$ of (2.29) should be diagonal matrix.

Let us consider the case of two branches, i.e. U equals to 2. The channels for the two branches are generated with two different random seeds. In Fig. 2.3, one random representation of the correlation matrix \mathbf{R}_h of (2.29) is simulated with the number of channel coefficients W assumed to be 10. Therefore, the correlation matrix \mathbf{R}_h consists of 20 rows and 20 columns. The elements in \mathbf{R}_h are expressed as $\underline{R}_h(i, j), i = 1 \cdots UW, j = 1 \cdots UW$. It is seen from Fig. 2.3 that \mathbf{R}_h has several peaks on the diagonal and two other peaks among the off-diagonal elements. All other elements of \mathbf{R}_h have low values. Although from the simulation result of Fig. 2.3 we could not say that the two channels are completely independent, it is still reasonable to think that the two channels are approximately independent. Therefore, for the simulation works in Chapter 7 the multi-branch WSSUS channels are generated with different random seeds on each branch.

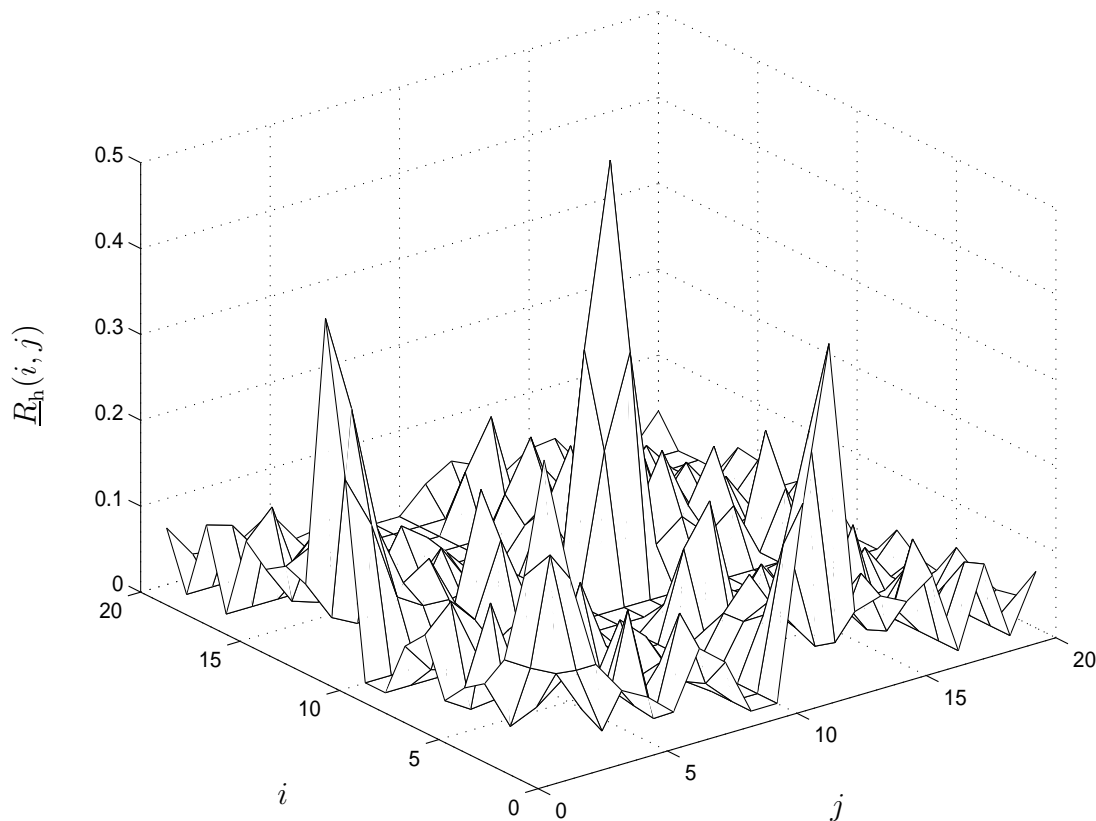


Fig. 2.3. Correlation matrix \mathbf{R}_h of (2.29) of the two branch WSSUS broadband channels.

2.5 Interference model

In order to investigate the channel estimation, i.e. the design of pilots in particular, in interference environments, an interference scenario that takes into account the neighboring cell or SA is required. This section describes a method for modelling intercell MAI in cellular mobile radio systems. Intercell MAI is the co-channel interference which affects reception of desired signals at the receiver in the reference SA and which is caused by the users in the other cells [BKN⁺94a]. The intercell MAI modelling presented below is used in the link level simulations of the uplink.

Fig. 2.4 illustrates the considered case in the presence of interference. Two neighboring SAs, the reference SA1 and the interfering SA2, are presented in the figure. Both SAs use the same frequency band. Interference occurs between adjacent SAs due to the MTs which are simultaneously active in each of the SAs. For the reference SA1 all MTs from the adjacent SA2 are interferers, and typically, a few of the interferers are stronger than the rest. In Fig. 2.4, the worse case of a single strong interferer is considered. This model is used for the calculation of the variation coefficient in Chapter 3 and the investigation of the performance of various pilots in interference environments in Chapter 5.

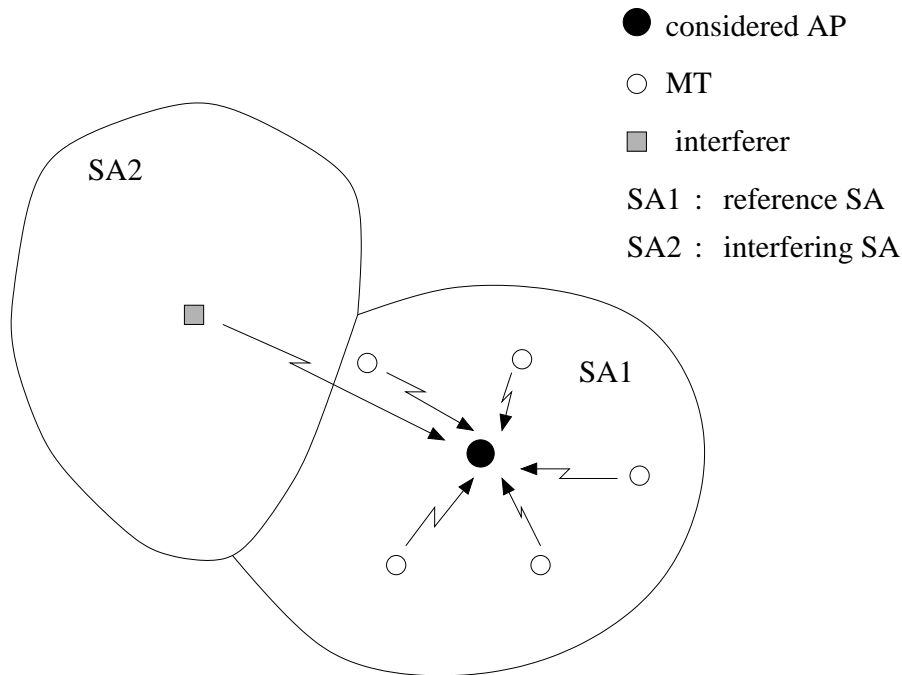


Fig. 2.4. Interference scenario.

As a side information, besides intercell MAI, two other kinds of interference will affect the transmission quality, i.e. the interference between the channel coefficients and intracell

MAI. ISI is caused by the superposition of signal components originating in temporally adjacent transmitted data symbols, as mentioned in Section 2.1, while intracell MAI is caused by the user signals other than the desired user signal those are simultaneously present in the same frequency band in the cell or SA under consideration [Pro95, Kle96]. Both the interference between the channel coefficients and intracell MAI can be eliminated by the well-designed JCE scheme [SJ94, SMW⁺01], which will be discussed in Chapter 3. However, the intercell MAI cannot be cancelled with the traditional single branch channel estimation scheme and even not with the JCE scheme, since the pilots used by the branches in the neighboring cell or SA are unknown to the receivers in the considered cell or SA.

3 JCE in multi-branch systems

3.1 Introduction

As mentioned in Subsection 1.1.3, the channel estimation can be carried out either in the time domain or in the frequency domain, corresponding to the signals and the channels represented either in the time domain or in the frequency domain. The JCE processed in different domains has different typical application scenarios, such as the TD-JCE in the uplink of synchronous multi-user CDMA systems and the FD-JCE in the uplink of synchronous multi-user OFDM systems. However, the application of JCE is not restricted to these typical scenarios. For example, the FD-JCE can be also applied to the multi-antenna OFDM systems [LSA99]. In this chapter, the discussion of JCE is not limited to any particular transmission scenario, but generally treated by considering multi-branch systems with signals represented in both the time and frequency domains. The derivations and conclusions may be applied to many applications of wireless communication systems, such as single carrier multi-user CDMA systems [SJ94], OFDM based multi-carrier multi-user systems [SMW⁺01, MWS⁺02, KMW⁺04] as well as FMT based multi-carrier multiple antenna systems [KWC04a].

The frequency domain representation and the time domain representation of a multi-branch linear transmission system are inherently equivalent. For example, the equivalence between the time and the frequency domain representations of JCE will be discussed in Section 3.4. Based on this observation, the multi-branch system is mainly represented in one domain, e.g. the frequency domain in this chapter. A discrete frequency model of the multi-branch systems will be obtained in Subsection 3.3.1. Various FD-JCE schemes, discussed in Subsection 3.3.2, will be derived based on the discrete frequency model. The equivalence between the discrete time representation and the discrete frequency representation for the multi-branch systems can be observed by the shift property of the DFT, which will be discussed in Subsection 3.4.2. Based on this equivalence, the discrete time model for the multi-branch systems and the various TD-JCE schemes will be obtained from their frequency domain counterparts in Subsections 3.4.3 and 3.4.4, respectively.

As stated in Subsection 1.3.1, the performance of JCE can be evaluated in noisy environments by the SNR degradation and in interference environments by the variation coefficient. The SNR degradation provides us with the numerical results of the relative performance loss for a certain JCE algorithm compared with a reference method. If the reference method is chosen as the matched filtering JCE (MF-JCE) with neglecting interference between the channel coefficients and MAI [SJ94, Kle96], then the SNR degradation describes the performance loss of a certain JCE algorithm for a multi-branch system with respect to the single-branch scenario. The variation coefficient provides us

with the statistical fluctuation of interference [MWS⁺02]. Moreover, if we aim to statistically evaluate the difference of the estimated channel with respect to the real channel, then the MSE [Kay93] can be introduced.

The performance evaluation of FD-JCE in terms of the SNR degradation, the MSE and the variation coefficient will be derived in Subsections 3.3.3, 3.3.4 and 3.3.5, respectively. The performance evaluation of TD-JCE in terms of the SNR degradation and the MSE will be derived in Subsections 3.4.5 and 3.4.6, respectively.

3.2 Description of the problems of JCE

Before investigating JCE for the linear multi-branch transmission systems, the problems met by JCE should be explained. Without loss of generality, the signals and variables in this section will be expressed in the time domain, i.e. Fig. 1.4 will be referred to.

As shown in Fig. 1.4, the multi-branch system comprises U branches. U is the sum of the number of all antenna elements of the K MTs together, where each MT $k, k = 1 \cdots K$, is equipped with $K_{M,k}$ antennas, see (1.1). In order to carry out JCE, U pilots are transmitted by the U branches so that the CIR vectors $\underline{\mathbf{h}}^{(u)}, u = 1 \cdots U$, of (2.27) of the U radio channels of Fig. 1.1 can be simultaneously distinguished and estimated at the receiver. At each branch u , a branch specific pilot vector, i.e. the TD training sequence $\underline{\mathbf{p}}^{(u)}, u = 1 \cdots U$, in Fig. 1.4,

$$\underline{\mathbf{p}}^{(u)} = \left(\underline{p}_1^{(u)} \cdots \underline{p}_{L_p}^{(u)} \right)^T, \quad u = 1 \cdots U, \quad (3.1)$$

of dimension L_p , which is a-priori known at the receiver, is considered in the channel estimation process. $\underline{\mathbf{p}}^{(u)}$ of (3.1) is composed of L_p discrete time complex symbols $\underline{p}_{l_p}^{(u)}, u = 1 \cdots U, l_p = 1 \cdots L_p$.

With a linear system model, according to Fig. 3.2, the problems of JCE can be described. As shown in Fig. 3.2, the task of JCE in a multi-branch system is that, from a receive signal vector

$$\underline{\mathbf{r}} = \left(r_1 \cdots r_{L_p} \right)^T \quad (3.2)$$

of dimension L_p , based on the a-priori knowledge of the number of channel coefficients W as well as the pilot vector $\underline{\mathbf{p}}^{(u)}, u = 1 \cdots U$, of (3.1) transmitted by all the U branches, the CIR vectors $\underline{\mathbf{h}}^{(u)}, u = 1 \cdots U$, of (2.27) experienced by all the U branches are jointly estimated as the estimated CIR vectors

$$\hat{\underline{\mathbf{h}}}^{(u)} = \left(\hat{h}_1^{(u)} \cdots \hat{h}_W^{(u)} \right)^T, \quad u = 1 \cdots U, \quad (3.3)$$

of dimension W for the U branches, based on which a total estimated CIR vector

$$\hat{\mathbf{h}} = \left(\hat{\mathbf{h}}^{(1)\text{T}} \cdots \hat{\mathbf{h}}^{(U)\text{T}} \right)^{\text{T}} \quad (3.4)$$

of dimension UW is obtained.

It is worth noting that the dimension of \mathbf{r} of (3.2) is only then equal to L_p , if we work with a prefix before the pilot vector $\mathbf{p}^{(u)}$ of (3.1) and do not consider the total of the receive signal. This statement can be illustrated in Fig. 3.1 for the receive signals for the u -th, $u = 1 \cdots U$, branch, i.e. $r_1^{(u)}$ to $r_{L_p+W-1}^{(u)}$, which are obtained from the convolution of the transmit pilot signal $\mathbf{p}^{(u)}$ of (3.1) of dimension L_p and the CIR $\mathbf{h}^{(u)}$ of (2.27) of dimension W . The relationship between $r_{l_p}^{(u)}$, $l_p = 1 \cdots L_p$, and the elements $r_{(l_p)}$ in the receive signal vector \mathbf{r} of (3.2) is

$$r_{(l_p)} = \sum_{u=1}^U r_{l_p}^{(u)}, \quad l_p = 1 \cdots L_p. \quad (3.5)$$

The shadowed parts in Figs. 3.1 (c) and (d) illustrate the data symbols transmitted after the pilot signal $\mathbf{p}^{(u)}$ of (3.1). It is seen in Fig. 3.1 that with a prefix in front of the pilot signal $\mathbf{p}^{(u)}$ of (3.1), $r_1^{(u)}$ to $r_{L_p}^{(u)}$ correspond to the receive signals which are free of the interference from the consecutively transmitted data symbols, while $r_{L_p+1}^{(u)}$ to $r_{L_p+W-1}^{(u)}$ correspond to the receive signals with the interference. For channel estimation, only the L_p receive signals which are free of the interference, i.e. $r_1^{(u)}$ to $r_{L_p}^{(u)}$, are taken into account.

If for the received noise vector

$$\mathbf{n} = \left(n_1 \cdots n_{L_p} \right)^{\text{T}} \quad (3.6)$$

of dimension L_p the covariance matrix

$$\mathbf{R}_n = \text{E}\{\mathbf{n} \mathbf{n}^{\text{H}}\} \quad (3.7)$$

is also a-priori known, this knowledge can be used to improve the estimation performance.

According to estimation theory [Kay93], based on various algorithms such as MF, LS, WLS and MMSE, various estimators can be correspondingly developed. All these estimators require the a-priori knowledge of the number W of channel coefficients as well as the transmitted pilot vectors $\mathbf{p}^{(u)}$, $u = 1 \cdots U$, of (3.1). The WLS estimators require additionally the a-priori knowledge of the noise covariance matrix \mathbf{R}_n of (3.7), while the MMSE estimator requires additionally the a-priori knowledge of the noise covariance matrix \mathbf{R}_n of (3.7) and the covariance matrix of the total CIR vector \mathbf{R}_h of (2.29). The MMSE estimator normally outperforms the other estimators. However, more a-priori knowledge is needed by the MMSE estimator which makes the MMSE estimator more

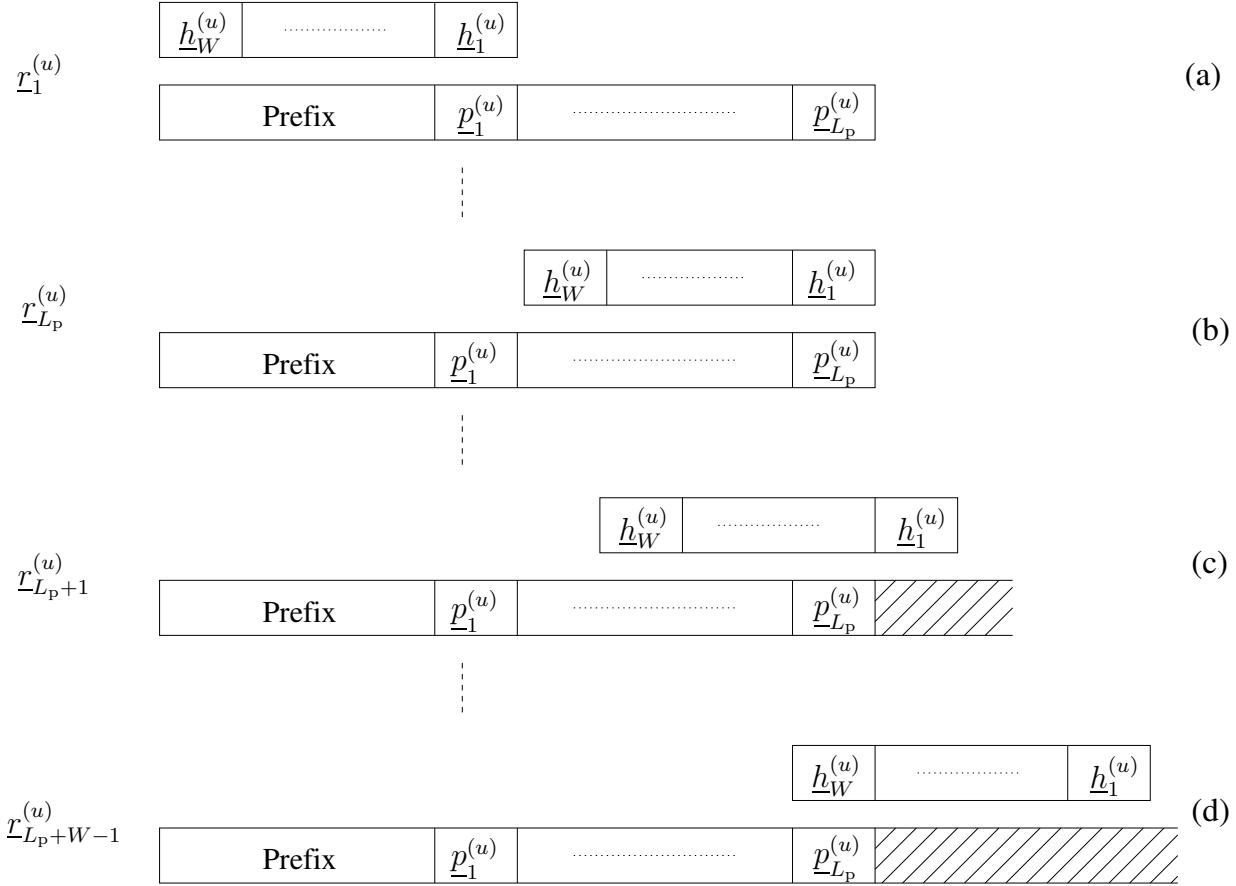


Fig. 3.1. Generation of the receive signals.

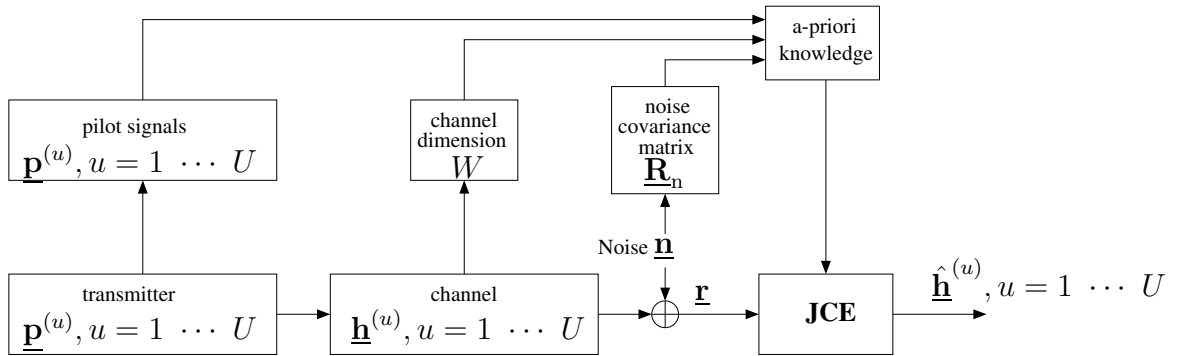


Fig. 3.2. Description of the problems of JCE.

complicated to implement than the other estimators and which restricts its applications in practical systems. Therefore, the MMSE estimation is not considered in this thesis.

If the noise vector \mathbf{n} of (3.6) is complex Gaussian with power σ^2 of the real and the imaginary parts, i.e. the noise covariance matrix satisfies

$$\mathbf{R}_{\mathbf{n}} = 2\sigma^2\mathbf{I}_{L_p}, \quad (3.8)$$

in which \mathbf{I}_{L_p} is a $L_p \times L_p$ identity matrix, then the WLS estimate will become the LS estimate and both are identical to the ML estimate [Kay93].

The unbiased estimation of the total CIR vector \mathbf{h} of (2.28) requires

$$E\{\hat{\mathbf{h}}\} = \mathbf{h}. \quad (3.9)$$

An estimation by which (3.9) cannot be fulfilled is biased. Both the LS and the WLS estimations are unbiased [Kay93]. If the noise \mathbf{n} is not Gaussian, then the WLS estimation is expected to outperform the LS estimation. MF estimation is biased since the interference between the channel coefficients is not considered.

From the above discussions, the performance of channel estimation varies with the availability of the a-priori knowledge, i.e. the number of channel coefficients W , the transmitted pilot vectors $\mathbf{p}^{(u)}$, $u = 1 \cdots U$, of (3.1) as well as the noise covariance matrix $\mathbf{R}_{\mathbf{n}}$ of (3.7). Besides, different channel estimation algorithms such as MF, LS and WLS estimations have different implementation complexity. Therefore, the first problem of JCE is to select a suitable algorithm for the multi-branch applications by jointly considering the available a-priori knowledge, the noise covariance matrix $\mathbf{R}_{\mathbf{n}}$ of (3.7), the estimation performance and the complexity.

It is observed that the performance of JCE in terms of MSE or SNR degradation depends on the transmitted pilots [SJ94, MWS⁺02]. For example, for the widely applied LS JCE algorithm, if the estimated CIR vector $\hat{\mathbf{h}}^{(u)}$ of (3.3) is required to statistically deviate as little as possible from the true CIR vector $\mathbf{h}^{(u)}$ of (2.27) in the sense of MSE [Kay93], then some pilots can result in the minimum achievable MSE [KMW⁺04]. With these pilots, the SNR degradation of a particular channel estimation scheme in comparison to the SNR-minimized scheme, i.e. the MF channel estimation, is also minimized, i.e. 0 dB SNR degradation can be achieved [SJ94, MWS⁺02]. The pilots by which the minimum MSE and the 0 dB SNR degradation can be achieved are called the optimum pilots. Therefore, the second problem met by JCE in the multi-branch systems is how to design the optimum pilots for the multiple branch transmissions by which both the MSE and the SNR degradation can be minimized.

The performance of JCE in noisy environments is generally evaluated by the SNR degradation [SJ94, SMW⁺01]. In interference environments, i.e. if more than one cell or SA is considered in the systems, it is normally the interference originating in the adjacent cells and SAs that limits the system performance. The smaller the fluctuation of the interference, the more similar the behavior of the interference to additive white Gaussian noise

(AWGN), and the better the overall system performance. The performance of JCE in interference environments is generally evaluated by the variation coefficient [Fis76]. The smaller the variation coefficient, the better the overall system performance. It is observed that the variation coefficient for JCE depends on the pilots being chosen for the reference SA and the neighboring SA [MWS⁺02]. Therefore, the third problem met by JCE is how to design the pilots for the branches in the reference SA and its neighboring SAs so that the variation coefficient can be reduced and simultaneously the SNR degradation in each SA can be minimized.

The above mentioned three problems should be solved by the investigation of JCE no matter the TD-JCE or the FD-JCE is carried out. Besides, the implementation of a JCE algorithm in the time domain or in the frequency domain has different complexity. For a certain transmission scheme of a wireless communication system, it is also the task of the system designer to choose a JCE scheme processed in a suitable domain with moderate complexity to meet the overall system requirements.

Envisaging the problems of JCE in multi-branch systems described above, in this chapter I focus on the first problem of deriving the JCE algorithms for multi-branch systems. Besides, the performance criteria of JCE such as the MSE, the SNR degradation and the variation coefficient will be also discussed in this chapter. In Chapter 4 the second problem of designing the optimum pilots for the multi-branch systems in noisy environments with one considered SA will be dealt with. The third problem of how to assign pilots for the multiple branches in the considered SA and its neighboring SAs will be discussed in Chapter 5. The choice of the suitable process domain for JCE based on the complexity evaluation of time and frequency domain processing will be addressed in Chapter 6.

3.3 Frequency domain representation of JCE

3.3.1 Discrete frequency model

In this section, the discrete frequency transmission model based on the frequency domain multi-branch transmission of Fig. 1.5 considering the MISO channel of Fig. 1.1 will be described. Since the transmitted signals shown in the physical transmission model of Fig. 1.5 are normally represented in the time domain, the considered signals before the IFFT at the transmitter and after the FFT at the receiver are represented in the frequency domain.

The signals on each branch $u, u = 1 \cdots U$, are supposed to be transmitted on N_F subcarriers. It is assumed that each branch u experiences a frequency selective channel whose CIR vector $\underline{\mathbf{h}}^{(u)}$ of (2.27) can be represented by W channel coefficients. At each branch

$u, u = 1 \cdots U$, a branch specific frequency domain pilot vector, i.e. the FD training sequence u in Fig. 1.5,

$$\tilde{\underline{\mathbf{p}}}^{(u)} = \left(\tilde{\underline{\mathbf{p}}}_1^{(u)} \cdots \tilde{\underline{\mathbf{p}}}_{N_F}^{(u)} \right)^T, u = 1 \cdots U, \quad (3.10)$$

of dimension N_F is transmitted. Without loss of generality, the pilot vector $\tilde{\underline{\mathbf{p}}}^{(u)}$ of (3.10) on each branch is assumed to occupy all the N_F subcarriers for channel estimation, composing an OFDM symbol. The U pilot vectors $\tilde{\underline{\mathbf{p}}}^{(u)}, u = 1 \cdots U$, are assumed to have the same energy

$$E_p = \frac{1}{2} \tilde{\underline{\mathbf{p}}}^{(u)H} \tilde{\underline{\mathbf{p}}}^{(u)}, u = 1 \cdots U. \quad (3.11)$$

The pilot and the data are assumed to be multiplexed in time, i.e. OFDM symbol by symbol. Fig. 3.3 illustrates the multiplexing block structure of pilot and data concerned for a frequency representation of the multi-branch systems of Fig. 1.5. Notice that transmissions on different branches can be introduced as different transmissions in the spatial domain.

After the IDFT of each pilot vector $\tilde{\underline{\mathbf{p}}}^{(u)}$ of (3.10), a time domain pilot vector $\underline{\mathbf{p}}^{(u)}$ of (3.1) of dimension L_p is obtained. L_p is equal to N_F . With the Fourier matrix [BC02]

$$\tilde{\underline{\mathcal{F}}} = \begin{pmatrix} 1 & 1 & 1 & \cdots & 1 \\ 1 & e^{-j\frac{2\pi}{N_F}} & e^{-j\frac{2\pi \times 2}{N_F}} & \vdots & e^{-j\frac{2\pi(N_F-1)}{N_F}} \\ 1 & e^{-j\frac{2\pi \times 2}{N_F}} & e^{-j\frac{2\pi \times 4}{N_F}} & \vdots & e^{-j\frac{2\pi \times 2(N_F-1)}{N_F}} \\ \vdots & \vdots & \vdots & \ddots & \vdots \\ 1 & e^{-j\frac{2\pi(N_F-1)}{N_F}} & e^{-j\frac{2\pi \times 2(N_F-1)}{N_F}} & \vdots & e^{-j\frac{2\pi(N_F-1)^2}{N_F}} \end{pmatrix} \quad (3.12)$$

of dimension $N_F \times N_F$, the relationship between the frequency domain pilot vector $\tilde{\underline{\mathbf{p}}}^{(u)}$ of (3.10) and the time domain pilot vector $\underline{\mathbf{p}}^{(u)}$ of (3.1) is given by

$$\tilde{\underline{\mathbf{p}}}^{(u)} = \tilde{\underline{\mathcal{F}}} \underline{\mathbf{p}}^{(u)}, u = 1 \cdots U. \quad (3.13)$$

As indicated in Fig. 1.5, a guard vector

$$\underline{\mathbf{g}}^{(u)} = \left(\underline{\mathbf{g}}_1^{(u)} \cdots \underline{\mathbf{g}}_{L_G}^{(u)} \right)^T, u = 1 \cdots U, \quad (3.14)$$

of dimension L_G is then placed in front of the time domain pilot vector $\underline{\mathbf{p}}^{(u)}$ of (3.1) for transmission to provide protection between two transmit blocks. With W denoting the number of channel coefficients, the condition $L_G \geq W - 1$ should be satisfied for the interference free transmission. The time multiplexing structure of the pilot vector $\underline{\mathbf{p}}^{(u)}$ of (3.1) and the guard vector $\underline{\mathbf{g}}^{(u)}$ of (3.14) is illustrated in Fig. 3.4.

In [SJ94], the extended pilot vector

$$\underline{\mathbf{p}}_E^{(u)} = \left(\underline{\mathbf{g}}^{(u)T} \underline{\mathbf{p}}^{(u)T} \right)^T \quad (3.15)$$

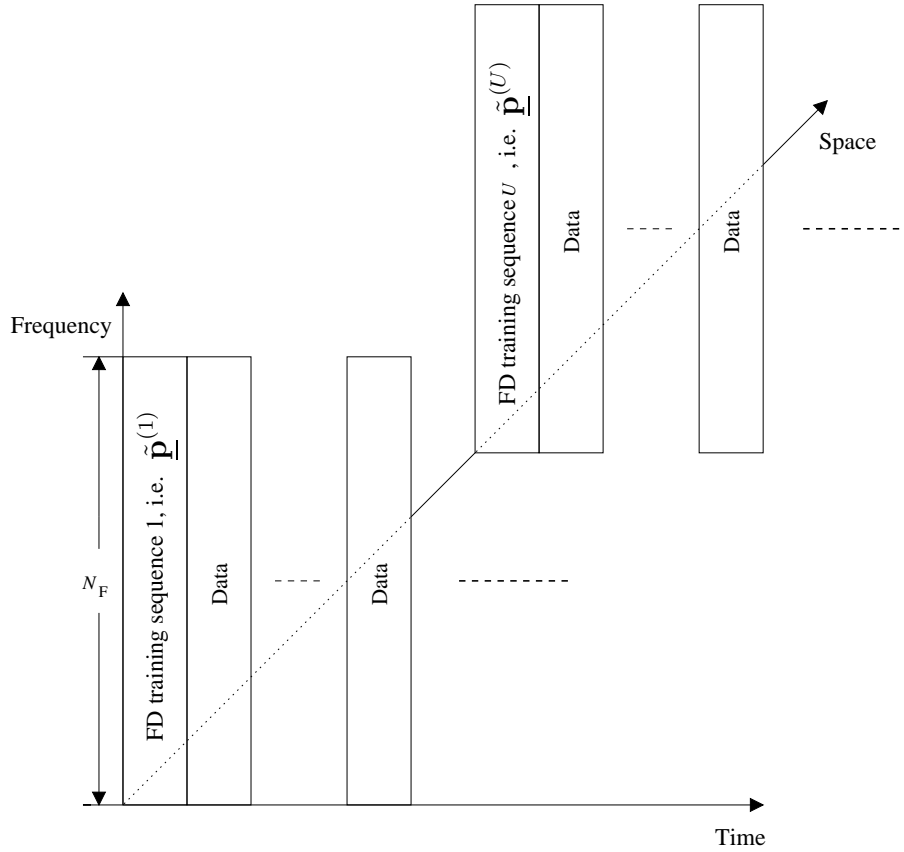


Fig. 3.3. Multiplexing structure of the pilot and the data concerned for a frequency domain representation of the multi-branch system of Fig. 1.5.

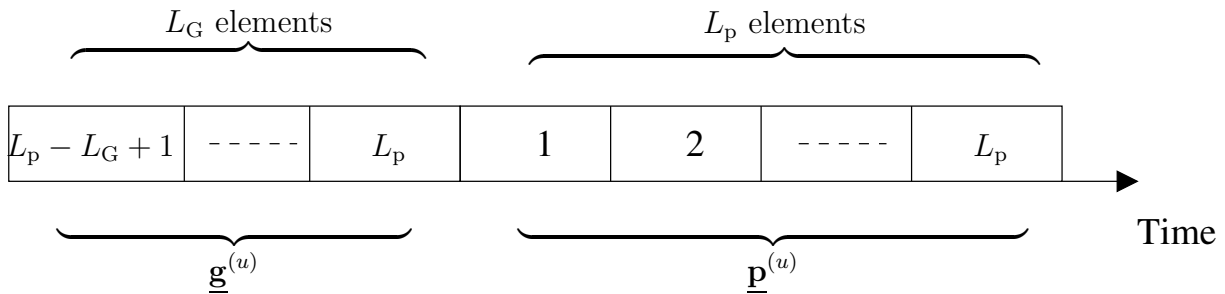


Fig. 3.4. Time multiplexing structure of the pilot vector $\mathbf{p}^{(u)}$ of dimension L_p and the guard vector $\mathbf{g}^{(u)}$ of dimension L_G .

of dimension L_p plus L_G is considered in the pilot design process for each branch $u, u = 1 \cdots U$. At the receiver the leading L_G received samples are discarded and only the L_p received samples are retained for channel estimation. For the U branches, with the

assumption that the extended pilot vectors $\underline{\mathbf{p}}_{\text{E}}^{(u)}$, $u = 1 \cdots U$, of (3.15) for the U branches are independently designed, the degree of freedom \mathfrak{f} for designing the U extended pilot vectors is [SJ94]

$$\mathfrak{f} = U(L_{\text{G}} + L_{\text{p}}), \quad (3.16)$$

provided that an exhaustive search method is used for the pilot design [SJ94]. The degree of freedom \mathfrak{f} is reduced if the extended pilot vector $\underline{\mathbf{p}}_{\text{E}}^{(u)}$ of (3.15) of each branch consists of $\underline{\mathbf{p}}^{(u)}$ of dimension L_{p} plus L_{G} elements taken from $\underline{\mathbf{p}}^{(u)}$ [SJ94]. The degree of freedom \mathfrak{f} for designing the U extended pilot vectors in this case will be

$$\mathfrak{f} = UL_{\text{p}}. \quad (3.17)$$

(3.17) can be fulfilled by introducing a cyclic prefix to the pilot vector $\underline{\mathbf{p}}^{(u)}$ of (3.1). This cyclic prefix on the other hand forms the guard vector $\underline{\mathbf{g}}^{(u)}$ of (3.14), which is composed of the cyclic shifts of the last L_{G} symbols of the pilot vector $\underline{\mathbf{p}}^{(u)}$ of (3.1), i.e.

$$\underline{\mathbf{g}}^{(u)} = \left(\underline{p}_{L_{\text{p}}-L_{\text{G}}+1}^{(u)} \cdots \underline{p}_{L_{\text{p}}-1}^{(u)} \underline{p}_{L_{\text{p}}}^{(u)} \right)^{\text{T}}, \quad u = 1 \cdots U. \quad (3.18)$$

As a side information, if, instead of the pilot, the data are transmitted, the cyclic prefix structure will be beneficial to the equalization and detection. With the cyclic prefix, the linear convolution of the transmitted signal with the CIR becomes the circular convolution so that the time domain convolution will be equivalent to the frequency domain multiplication [BT02]. With this equivalence, the frequency domain equalization can be realized by just multiplying the inverse of the CTF matrix by the frequency domain receive signal [BP95]. Hence the complexity of equalization can be significantly reduced, especially if broadband single carrier systems are considered [FAB02]. Comparing with the time domain equalization to broadband single carrier systems, where a huge number of channel coefficients must be estimated, the frequency domain equalization is much less complicated because the equalization is performed on a block of data at a time and the operations on this block involve an efficient FFT operation and a simple channel inversion operation [FAB02]. This makes the frequency domain equalization, and originally, the structure with a cyclic prefix, particularly attractive to the broadband applications. In OFDM-based multi-carrier systems the cyclic prefix is applied to the transmitted signal so that the receive signals contain mutually orthogonal sinusoidal sections with constant envelope, which are in the receiver processed by FFT [NP00].

The radio channel between each transmit branch u and the receiver can be characterized by the CIR vector $\underline{\mathbf{h}}^{(u)}$ of (2.27), or by a CTF vector

$$\tilde{\underline{\mathbf{h}}}^{(u)} = \left(\tilde{\underline{h}}_1^{(u)} \cdots \tilde{\underline{h}}_{N_{\text{F}}}^{(u)} \right)^{\text{T}}, \quad u = 1 \cdots U, \quad (3.19)$$

of dimension N_{F} . With (3.19), the total CTF vector

$$\tilde{\underline{\mathbf{h}}} = \left(\tilde{\underline{\mathbf{h}}}^{(1)\text{T}} \cdots \tilde{\underline{\mathbf{h}}}^{(U)\text{T}} \right)^{\text{T}} \quad (3.20)$$

of dimension UN_F of all U branches is obtained.

With the typical OFDM system applications of the frequency domain multi-branch system model of Fig. 1.5, it is verified that the number of channel coefficients W of the CIR vector $\underline{\mathbf{h}}^{(u)}$ of (2.27) is smaller than the dimension N_F of the CTF vector $\underline{\mathbf{h}}^{(u)}$ of (3.19) [NP00].

Let us consider a blockdiagonal matrix

$$\underline{\tilde{\mathcal{F}}}_{W,\text{tot}} = \begin{pmatrix} \left[\underline{\tilde{\mathcal{F}}} \right]_{N_F,W}^{1,1} & \cdots & \mathbf{0} \\ \vdots & \ddots & \vdots \\ \mathbf{0} & \cdots & \left[\underline{\tilde{\mathcal{F}}} \right]_{N_F,W}^{1,1} \end{pmatrix} \quad (3.21)$$

of dimension $(UN_F) \times (UW)$, whose blocks

$$\underline{\tilde{\mathcal{F}}}_W = \left[\underline{\tilde{\mathcal{F}}} \right]_{N_F,W}^{1,1} \quad (3.22)$$

are matrices containing the first W columns of the Fourier matrix $\underline{\tilde{\mathcal{F}}}$ of (3.12). With (3.21), the total CIR vector $\underline{\mathbf{h}}$ of (2.28) and the total CTF vector $\underline{\mathbf{h}}$ of (3.20) are related by [SMW⁺01, MWS⁺02]

$$\underline{\mathbf{h}} = \underline{\tilde{\mathcal{F}}}_{W,\text{tot}} \underline{\mathbf{h}}. \quad (3.23)$$

With a branch specific pilot matrix

$$\underline{\tilde{\mathbf{P}}}^{(u)} = \text{diag} \left(\tilde{p}_1^{(u)} \cdots \tilde{p}_{N_F}^{(u)} \right)^T, \quad u = 1 \cdots U, \quad (3.24)$$

of dimension $N_F \times N_F$, whose diagonal elements are composed of the components of $\underline{\tilde{\mathbf{p}}}^{(u)}$ of (3.10), a total pilot matrix

$$\underline{\tilde{\mathbf{P}}} = \left(\underline{\tilde{\mathbf{P}}}^{(1)} \cdots \underline{\tilde{\mathbf{P}}}^{(U)} \right) \quad (3.25)$$

of dimension $N_F \times (UN_F)$ is obtained.

With a noise vector

$$\underline{\tilde{\mathbf{n}}} = \left(\tilde{n}_1 \cdots \tilde{n}_{N_F} \right)^T \quad (3.26)$$

of dimension N_F at the receiver, together with the total CTF vector $\underline{\mathbf{h}}$ of (3.20) and the total pilot matrix $\underline{\tilde{\mathbf{P}}}$ of (3.25), the FD receive signal vector

$$\underline{\tilde{\mathbf{r}}} = \underline{\tilde{\mathbf{P}}} \underline{\mathbf{h}} + \underline{\tilde{\mathbf{n}}} \quad (3.27)$$

illustrated in Fig. 1.5 and having the dimension N_F is obtained.

There are UN_F unknown frequency samples in the total CTF vector $\tilde{\mathbf{h}}$ of (3.20) but only N_F samples in the frequency domain receive signal vector $\tilde{\mathbf{r}}$ of (3.27). Therefore, the linear set of equations described by (3.27) is underdetermined.

Substituting (3.23) into (3.27) gives

$$\tilde{\mathbf{r}} = \underbrace{\tilde{\mathbf{P}} \tilde{\mathcal{F}}_{W,\text{tot}}}_{\tilde{\mathbf{G}}} \mathbf{h} + \tilde{\mathbf{n}}, \quad (3.28)$$

in which $\tilde{\mathbf{G}}$ is a matrix of dimension $N_F \times (UW)$.

In the linear multi-branch system described by (3.28), there are UW unknown channel coefficients and N_F received samples. In the case

$$N_F \geq UW, \quad (3.29)$$

(3.28) is an overdetermined or a determined linear set of equations. (3.28) is assumed to be fulfilled in the following and will be used to derive the FD-JCE algorithms in the Subsection 3.3.2.

3.3.2 FD-JCE algorithms

In this subsection, three different FD-JCE algorithms will be derived based on the discrete frequency representation of the multi-branch transmission model described in Subsection 3.3.1. In order to reduce the number of unknowns, the total CIR vector \mathbf{h} of (2.28) is firstly estimated, based on which the total CTF vector $\tilde{\mathbf{h}}$ of (3.20) is obtained. In both cases, the pilot vectors contained in matrix $\tilde{\mathbf{G}}$ and the received signal vector $\tilde{\mathbf{r}}$ in (3.28) are expressed in the frequency domain. According to the classification in Subsection 1.1.3, the estimation in both cases is called FD-JCE.

Under the assumption of the linear system, the FD-JCE at the receiver in Fig. 1.5 is assumed to be linear by multiplying the receive signal vector $\tilde{\mathbf{r}}$ in (3.28) with an estimation matrix $\tilde{\mathbf{M}}$ of dimension $(UW) \times N_F$, i.e.

$$\hat{\mathbf{h}} = \tilde{\mathbf{M}} \tilde{\mathbf{r}} = \tilde{\mathbf{M}} \tilde{\mathbf{G}} \mathbf{h} + \tilde{\mathbf{M}} \tilde{\mathbf{n}}. \quad (3.30)$$

Various choices of the estimation matrix $\tilde{\mathbf{M}}$ result in various FD-JCE algorithms. The unbiased estimation requires (3.9) to be fulfilled.

Without any a-priori knowledge about the statistical properties of the noise $\tilde{\mathbf{n}}$ of (3.26), the conventional method of digital signal processing in the receiver for channel estimation is correlation by an estimation matrix $\tilde{\mathbf{M}}$ matched to the matrix $\tilde{\mathbf{G}}$ [Kay93], i.e.

$$\tilde{\mathbf{M}} = \tilde{\mathbf{G}}^H. \quad (3.31)$$

Substituting (3.31) into (3.30), a frequency domain MF JCE (FD-MF-JCE)

$$\hat{\mathbf{h}}_{\text{MF}} = \tilde{\mathbf{G}}^{\text{H}} \tilde{\mathbf{r}} = \tilde{\mathbf{G}}^{\text{H}} \tilde{\mathbf{G}} \mathbf{h} + \tilde{\mathbf{G}}^{\text{H}} \tilde{\mathbf{n}}. \quad (3.32)$$

of the total CIR vector \mathbf{h} of (2.28) is obtained. The a-priori knowledge required by the FD-MF-JCE in (3.32) is the number of channel coefficients W and the transmitted frequency domain pilot vectors $\tilde{\mathbf{p}}^{(u)}$, $u = 1 \cdots U$, of (3.10). The FD-MF-JCE $\hat{\mathbf{h}}_{\text{MF}}$ of (3.32) is biased since it does not take into account the interference between the channel coefficients.

With the estimation matrix

$$\tilde{\mathbf{M}} = (\tilde{\mathbf{G}}^{\text{H}} \tilde{\mathbf{G}})^{-1} \tilde{\mathbf{G}}^{\text{H}} \quad (3.33)$$

of dimension $(UW) \times N_{\text{F}}$, by substituting (3.33) into (3.30), an unbiased frequency domain LS JCE (FD-LS-JCE)

$$\hat{\mathbf{h}}_{\text{LS}} = (\tilde{\mathbf{G}}^{\text{H}} \tilde{\mathbf{G}})^{-1} \tilde{\mathbf{G}}^{\text{H}} \tilde{\mathbf{r}} = \mathbf{h} + (\tilde{\mathbf{G}}^{\text{H}} \tilde{\mathbf{G}})^{-1} \tilde{\mathbf{G}}^{\text{H}} \tilde{\mathbf{n}} \quad (3.34)$$

of the total CIR vector \mathbf{h} of (2.28) is obtained. In (3.34) the number of channel coefficients W and the transmitted frequency domain pilot vectors $\tilde{\mathbf{p}}^{(u)}$, $u = 1 \cdots U$, of (3.10) should be a-priori known.

If the frequency domain noise covariance matrix

$$\tilde{\mathbf{R}}_{\mathbf{n}} = \text{E}\{\tilde{\mathbf{n}} \tilde{\mathbf{n}}^{\text{H}}\} \quad (3.35)$$

is also a-priori known, the estimation matrix

$$\tilde{\mathbf{M}} = (\tilde{\mathbf{G}}^{\text{H}} \tilde{\mathbf{R}}_{\mathbf{n}}^{-1} \tilde{\mathbf{G}})^{-1} \tilde{\mathbf{G}}^{\text{H}} \tilde{\mathbf{R}}_{\mathbf{n}}^{-1} \quad (3.36)$$

of dimension $(UW) \times N_{\text{F}}$ can be used to obtain an unbiased frequency domain WLS JCE (FD-WLS-JCE)

$$\hat{\mathbf{h}}_{\text{WLS}} = (\tilde{\mathbf{G}}^{\text{H}} \tilde{\mathbf{R}}_{\mathbf{n}}^{-1} \tilde{\mathbf{G}})^{-1} \tilde{\mathbf{G}}^{\text{H}} \tilde{\mathbf{R}}_{\mathbf{n}}^{-1} \tilde{\mathbf{r}} = \mathbf{h} + (\tilde{\mathbf{G}}^{\text{H}} \tilde{\mathbf{R}}_{\mathbf{n}}^{-1} \tilde{\mathbf{G}})^{-1} \tilde{\mathbf{G}}^{\text{H}} \tilde{\mathbf{R}}_{\mathbf{n}}^{-1} \tilde{\mathbf{n}} \quad (3.37)$$

of the total CIR vector \mathbf{h} of (2.28).

In the case of AWGN with the covariance matrix, we have

$$\tilde{\mathbf{R}}_{\mathbf{n}} = \sigma^2 \mathbf{I}_{N_{\text{F}}}, \quad (3.38)$$

in which $\mathbf{I}_{N_{\text{F}}}$ is a $N_{\text{F}} \times N_{\text{F}}$ identity matrix. In this case, the FD-WLS-JCE $\hat{\mathbf{h}}_{\text{WLS}}$ of (3.37) will be reduced to the FD-LS-JCE $\hat{\mathbf{h}}_{\text{LS}}$ of (3.34).

The FD-JCE, i.e. in particular the FD-MF-JCE, the FD-LS-JCE and the FD-WLS-JCE for the multi-branch systems described in the frequency domain is only feasible when the

number of unknown channel coefficients UW in the total CIR vector $\underline{\mathbf{h}}$ of (2.28) does not exceed the number of components N_F in the frequency domain receive vector $\tilde{\mathbf{r}}$ of (3.28).

By substituting (3.32) into (3.23), the FD-MF-JCE

$$\hat{\underline{\mathbf{h}}}_{\text{MF}} = \underbrace{\tilde{\mathcal{F}}_{\text{W,tot}} \tilde{\mathbf{G}}^{\text{H}}}_{\underline{\mathbf{Z}}_{\text{MF}}} \tilde{\mathbf{r}} = \tilde{\mathcal{F}}_{\text{W,tot}} \tilde{\mathcal{F}}_{\text{W,tot}}^{\text{H}} \tilde{\mathbf{P}}^{\text{H}} \tilde{\mathbf{P}} \tilde{\underline{\mathbf{h}}} + \underline{\mathbf{Z}}_{\text{MF}} \tilde{\underline{\mathbf{n}}} \quad (3.39)$$

of the total CTF vector $\tilde{\underline{\mathbf{h}}}$ of (3.20) is derived, in which $\underline{\mathbf{Z}}_{\text{MF}}$ is a matrix of dimension $(UN_F) \times N_F$.

Furthermore, by substituting (3.34) into (3.23), the FD-LS-JCE

$$\hat{\underline{\mathbf{h}}}_{\text{LS}} = \underbrace{\tilde{\mathcal{F}}_{\text{W,tot}} \left(\tilde{\mathbf{G}}^{\text{H}} \tilde{\mathbf{G}} \right)^{-1} \tilde{\mathbf{G}}^{\text{H}}}_{\underline{\mathbf{Z}}_{\text{LS}}} \tilde{\mathbf{r}} = \tilde{\underline{\mathbf{h}}} + \underline{\mathbf{Z}}_{\text{LS}} \tilde{\underline{\mathbf{n}}} \quad (3.40)$$

of the total CTF vector $\tilde{\underline{\mathbf{h}}}$ of (3.20) is derived, in which $\underline{\mathbf{Z}}_{\text{LS}}$ is a matrix of dimension $(UN_F) \times N_F$.

Finally, the FD-WLS-JCE

$$\hat{\underline{\mathbf{h}}}_{\text{WLS}} = \underbrace{\tilde{\mathcal{F}}_{\text{W,tot}} \left(\tilde{\mathbf{G}}^{\text{H}} \tilde{\mathbf{R}}_{\text{n}}^{-1} \tilde{\mathbf{G}} \right)^{-1} \tilde{\mathbf{G}}^{\text{H}} \tilde{\mathbf{R}}_{\text{n}}^{-1}}_{\underline{\mathbf{Z}}_{\text{WLS}}} \tilde{\mathbf{r}} = \tilde{\underline{\mathbf{h}}} + \underline{\mathbf{Z}}_{\text{WLS}} \tilde{\underline{\mathbf{n}}} \quad (3.41)$$

of the total CTF vector $\tilde{\underline{\mathbf{h}}}$ of (3.20) is obtained by substituting (3.37) into (3.23), in which $\underline{\mathbf{Z}}_{\text{WLS}}$ is a matrix of dimension $(UN_F) \times N_F$.

3.3.3 SNR degradation

The SNR degradation is defined as the ratio of the SNR obtained at the output of a reference channel estimator of a single branch system, and the SNR obtained at the output of the JCE in the multi-branch system [Kle96]. As the reference method, the FD-MF-JCE case is considered. The performance of the FD-LS-JCE and FD-WLS-JCE will be compared with the FD-MF-JCE for the SNR degradation evaluation.

It is assumed that for the reference method all N_F available subcarriers are used for pilot transmission on the single branch as in [MWS⁺02]. This reference system actually corresponds to the FD-MF-JCE scheme. From (3.39), with the pilot energy E_p of (3.11), the number of considered channel coefficients W and the power of the complex noise $2\sigma^2$,

the SNR of the estimation $\hat{\underline{h}}_j$ of component j , $j = 1 \cdots UN_F$, of the estimated total CTF vector $\hat{\underline{\mathbf{h}}}_{\text{MF}}$ at the output of the FD-MF-JCE

$$\tilde{\gamma}_{\text{ref},j} = \frac{E_p}{2W\sigma^2} |\tilde{h}_j|^2 \quad (3.42)$$

is obtained [MWS⁺02].

From (3.40), the SNR of the estimation $\hat{\underline{h}}_j$ of component j , $j = 1 \cdots UN_F$, of the estimated total CTF vector $\hat{\underline{\mathbf{h}}}_{\text{LS}}$ at the output of the FD-LS-JCE

$$\tilde{\gamma}_{\text{LS},j} = \frac{E\{|\tilde{\underline{\mathbf{h}}}_j|^2\}}{E\{|\underline{\mathbf{Z}}_{\text{LS}}\tilde{\underline{\mathbf{h}}}_j|^2\}} = \frac{|\tilde{h}_j|^2}{2\sigma^2[\underline{\mathbf{Z}}_{\text{LS}}\underline{\mathbf{Z}}_{\text{LS}}^{\text{H}}]_{j,j}} \quad (3.43)$$

is derived [SMW⁺01].

Furthermore, considering the FD-WLS-JCE and taking into account (3.41), the corresponding SNR of the estimation $\hat{\underline{h}}_j$ of component j , $j = 1 \cdots UN_F$, of the estimated total CTF vector $\hat{\underline{\mathbf{h}}}_{\text{WLS}}$ at the output of the FD-WLS-JCE is given by

$$\tilde{\gamma}_{\text{WLS},j} = \frac{E\{|\tilde{\underline{\mathbf{h}}}_j|^2\}}{E\{|\underline{\mathbf{Z}}_{\text{WLS}}\tilde{\underline{\mathbf{h}}}_j|^2\}} = \frac{|\tilde{h}_j|^2}{2\sigma^2[\underline{\mathbf{Z}}_{\text{WLS}}\underline{\mathbf{Z}}_{\text{WLS}}^{\text{H}}]_{j,j}}. \quad (3.44)$$

Hence, considering (3.42) and (3.43), the SNR degradation of $\hat{\underline{h}}_j$ by considering FD-LS-JCE with respect to the reference system

$$\tilde{\delta}_{\text{MF-LS},j} = \frac{\tilde{\gamma}_{\text{ref},j}}{\tilde{\gamma}_{\text{LS},j}} = \frac{E_p}{W} [\underline{\mathbf{Z}}_{\text{LS}}\underline{\mathbf{Z}}_{\text{LS}}^{\text{H}}]_{j,j} \quad (3.45)$$

is obtained.

By taking into account (3.42) and (3.44), the SNR degradation of FD-WLS-JCE with respect to the reference system

$$\tilde{\delta}_{\text{MF-WLS},j} = \frac{\tilde{\gamma}_{\text{ref},j}}{\tilde{\gamma}_{\text{WLS},j}} = \frac{E_p}{W} [\underline{\mathbf{Z}}_{\text{WLS}}\underline{\mathbf{Z}}_{\text{WLS}}^{\text{H}}]_{j,j} \quad (3.46)$$

is obtained.

In order to perform FD-JCE in multi-branch environments without noise enhancement as compared with the single-branch FD-MF-JCE scenario, 0 dB SNR degradation is required.

3.3.4 MSE

It is shown by (3.45) and (3.46) that the SNR degradation provides us with the analytical numerical results of the performance loss for a considered JCE scheme compared with a reference channel estimation method of a single branch system. In order to statistically evaluate the difference of the estimated channel e.g. the estimated CIR $\hat{\mathbf{h}}$ with respect to the true channel, e.g. the true CIR \mathbf{h} of (2.28), i.e. the channel estimation error, the MSE

$$\epsilon = E\{|\hat{\mathbf{h}} - \mathbf{h}|^2\} \quad (3.47)$$

can be evaluated. Similarly, the MSE

$$\tilde{\epsilon} = E\{|\hat{\tilde{\mathbf{h}}} - \tilde{\mathbf{h}}|^2\} \quad (3.48)$$

for the estimated CTF $\hat{\tilde{\mathbf{h}}}$ with respect to the real CTF $\tilde{\mathbf{h}}$ of (3.20) can be evaluated. By considering the relationship of the CTF and the CIR, which is given by (3.23), the relationship between the MSE ϵ of (3.47) and the MSE $\tilde{\epsilon}$ of (3.48)

$$\tilde{\epsilon} = N_F \epsilon \quad (3.49)$$

can be obtained.

In this subsection, the MSE of the unbiased FD-LS-JCE of (3.34) is calculated by referring to (3.47). By replacing $\hat{\mathbf{h}}$ in (3.47) by $\hat{\mathbf{h}}_{\text{LS}}$ of (3.40), and by using the exchangeability of the trace and expectation operations, the MSE of the FD-LS-JCE is derived as

$$\epsilon_{\text{LS}} = 2\sigma^2 \text{tr}\{((\tilde{\mathbf{G}}^H \tilde{\mathbf{G}})^{-1})\} \quad (3.50)$$

with the assumption of AWGN represented by the noise vector $\tilde{\mathbf{n}}$ of (3.26) with the covariance matrix $\tilde{\mathbf{R}}_{\mathbf{n}}$ of (3.38).

By considering the construction of matrix $\tilde{\mathbf{G}}$ in (3.28), it is seen in (3.50) that the MSE ϵ_{LS} of the FD-LS-JCE is influenced by the transmitted pilot vectors $\tilde{\mathbf{p}}^{(u)}$, $u = 1 \cdots U$, of (3.10) on the U branches.

With the assumption in (3.11) that the pilot vectors $\tilde{\mathbf{p}}^{(u)}$, $u = 1 \cdots U$, transmitted on the U branches have the same energy E_p , and if we consider the matrix $\tilde{\mathbf{G}}$ as specified in (3.28), the trace operation $\text{tr}\{(\tilde{\mathbf{G}}^H \tilde{\mathbf{G}})$ in (3.50) can be expressed as

$$\text{tr}\{(\tilde{\mathbf{G}}^H \tilde{\mathbf{G}})\} = \text{tr}\{\tilde{\mathcal{F}}_{W,\text{tot}}^H \tilde{\mathbf{P}}^H \tilde{\mathbf{P}} \tilde{\mathcal{F}}_{W,\text{tot}}\} = UW E_p. \quad (3.51)$$

The matrix $\tilde{\mathbf{G}}^H \tilde{\mathbf{G}}$ is a nonsingular positive definite matrix, so that the decomposition

$$\tilde{\mathbf{G}}^H \tilde{\mathbf{G}} = \tilde{\mathbf{V}} \text{diag}(\tilde{\lambda}_1 \cdots \tilde{\lambda}_{UW}) \tilde{\mathbf{V}}^H \quad (3.52)$$

holds, in which $\tilde{\mathbf{V}}$ is a unitary matrix and $\tilde{\lambda}_j, j = 1 \cdots UW$, are the eigenvalues of the matrix $\tilde{\mathbf{G}}^H \tilde{\mathbf{G}}$, which gives

$$\text{tr}\{(\tilde{\mathbf{G}}^H \tilde{\mathbf{G}})\} = \sum_{j=1}^{UW} \tilde{\lambda}_j. \quad (3.53)$$

Taking (3.51) and (3.53) into account we obtain

$$\sum_{j=1}^{UW} \tilde{\lambda}_j = UWE_p. \quad (3.54)$$

Based on (3.50) and (3.52) the MSE ϵ_{LS} of the FD-LS-JCE

$$\epsilon_{\text{LS}} = 2\sigma^2 \sum_{j=1}^{UW} \frac{1}{\tilde{\lambda}_j} \quad (3.55)$$

is determined by the eigenvalues of the matrix $\tilde{\mathbf{G}}^H \tilde{\mathbf{G}}$.

The minimum of the MSE ϵ_{LS} of (3.55) can be derived from the Lagrange cost function [Arf85]

$$J = 2\sigma^2 \sum_{j=1}^{UW} \frac{1}{\tilde{\lambda}_j} + \beta \left(\sum_{j=1}^{UW} \tilde{\lambda}_j - UWE_p \right) \quad (3.56)$$

based on the condition (3.54) and with a Lagrange multiplier β . From (3.56), the minimum MSE can be achieved if and only if

$$\tilde{\lambda}_j = E_p, j = 1 \cdots UW. \quad (3.57)$$

Substituting (3.57) into (3.55) we derive the minimum MSE

$$\epsilon_{\text{LS},\min} = \frac{2UW\sigma^2}{E_p} \quad (3.58)$$

for the FD-LS-JCE. The normalized minimum MSE

$$\epsilon'_{\text{LS},\min} = \frac{2W\sigma^2}{E_p} \quad (3.59)$$

is derived by multiplying the minimum MSE $\epsilon_{\text{LS},\min}$ of (3.58) with factor $1/U$.

3.3.5 Variation coefficient

The SNR degradations $\tilde{\delta}_{\text{MF-LS},j}$ of (3.45) and $\tilde{\delta}_{\text{MF-WLS},j}$ of (3.46) allow to quantify the performance of JCE in the presence of noise in single cell or SA scenarios. However, in mobile radio systems, the interference originating from adjacent cells or SAs limits the system performance. The interference model of a single strong interferer as described in Section 2.5 is considered and the FD-LS-JCE of (3.40) is applied at the receiver of the considered SA in the analysis of the variation coefficient [MWS⁺02]. The disturbance of the noise vector $\tilde{\mathbf{n}}$ of (3.26) on the receive vector $\tilde{\mathbf{r}}$ of (3.28) is omitted in the analysis since the interferer is strong.

Introducing the pilot matrix of the interferer

$$\tilde{\mathbf{P}}_{\text{I}} = \text{diag} \left\{ \tilde{p}_{\text{I},1} \cdots \tilde{p}_{\text{I},N_{\text{F}}} \right\} \quad (3.60)$$

of dimension $N_{\text{F}} \times N_{\text{F}}$ of the considered strong interferer from the neighboring SA, and by considering the CTF vector of the interferer

$$\tilde{\mathbf{h}}_{\text{I}} = (\tilde{h}_{\text{I},1} \cdots \tilde{h}_{\text{I},N_{\text{F}}})^{\text{T}} \quad (3.61)$$

of dimension N_{F} that represents the CTF between the strong interferer and the receiver in the considered SA, the interfered receive vector

$$\tilde{\mathbf{r}}_{\text{A}} = \tilde{\mathbf{P}} \tilde{\mathbf{h}} + \tilde{\mathbf{P}}_{\text{I}} \tilde{\mathbf{h}}_{\text{I}} \quad (3.62)$$

is obtained [MWS⁺02].

Applying the FD-LS-JCE of (3.40) to the interfered receive vector $\tilde{\mathbf{r}}_{\text{A}}$ of (3.62), the estimate of the total CTF vector

$$\hat{\mathbf{h}}_{\text{LS,A}} = \tilde{\mathbf{Z}}_{\text{LS}} \tilde{\mathbf{r}}_{\text{A}} = \tilde{\mathbf{Z}}_{\text{LS}} \tilde{\mathbf{P}} \tilde{\mathbf{h}} + \tilde{\mathbf{Z}}_{\text{LS}} \tilde{\mathbf{P}}_{\text{I}} \tilde{\mathbf{h}}_{\text{I}} \quad (3.63)$$

results. The right part of the summation in (3.63) stands for the estimation error in the presence of one strong interferer, from which the channel estimation error

$$\hat{\mathbf{h}}_{\text{LS,A}} - \tilde{\mathbf{h}} = \tilde{\mathcal{F}}_{\text{W,tot}} \left(\tilde{\mathcal{F}}_{\text{W,tot}}^{\text{H}} \tilde{\mathbf{P}}^{\text{H}} \tilde{\mathbf{P}} \tilde{\mathcal{F}}_{\text{W,tot}} \right)^{-1} \tilde{\mathcal{F}}_{\text{W,tot}}^{\text{H}} \tilde{\mathbf{P}}^{\text{H}} \tilde{\mathbf{P}}_{\text{I}} \tilde{\mathbf{h}}_{\text{I}} \quad (3.64)$$

results. With the interference power

$$\tilde{I}^{(j)} = \left[\left(\hat{\mathbf{h}}_{\text{LS,A}} - \tilde{\mathbf{h}} \right) \left(\hat{\mathbf{h}}_{\text{LS,A}} - \tilde{\mathbf{h}} \right)^{\text{H}} \right]_{j,j}, \quad j = 1 \cdots UN_{\text{F}}, \quad (3.65)$$

on the j -th component $\hat{h}_{\text{LS,A}}^{(j)}$ of the total CTF vector $\hat{\mathbf{h}}_{\text{LS,A}}$ of (3.63), the mean value of the interference power $\tilde{I}^{(j)}$ of (3.65) can be expressed as

$$\bar{\tilde{I}} = \frac{1}{UN_{\text{F}}} \sum_{j=1}^{UN_{\text{F}}} \tilde{I}^{(j)}. \quad (3.66)$$

Then, the mean square deviation of the interference power $\tilde{I}^{(j)}$ of (3.65)

$$\tilde{\sigma}_I^2 = \frac{1}{UN_F - 1} \sum_{j=1}^{UN_F} \left(\tilde{I}^{(j)} - \tilde{I} \right)^2 \quad (3.67)$$

is obtained [MWS⁺02].

The variation coefficient v_c [Fis76] is defined as the square root of the mean square deviation $\tilde{\sigma}_I^2$ of (3.67) normalized by the mean value of the interference power \tilde{I} of (3.66), i.e.

$$v_c = \frac{\sqrt{\tilde{\sigma}_I^2}}{\tilde{I}}. \quad (3.68)$$

The variation coefficient v_c of (3.68) is a random variable, if random channels are considered. The smaller the variation coefficient v_c , the smaller the fluctuation of the interference power $\tilde{I}^{(j)}$ of (3.65) over all subcarriers and over all branches, i.e. the behavior of the interference will be more similar to that of white noise, which is equivalent to the scenario of no inter SA interference. The system with smaller variation coefficient v_c of (3.68) will result in better performance on the system level.

3.4 Time domain representation of JCE

3.4.1 Introduction

In the previous Section 3.3, the frequency domain representation of the multi-branch systems as shown in Fig. 1.5 has been described. The MF, LS and WLS based FD-JCE algorithms have been discussed and their performance in terms of SNR degradation, MSE as well as variation coefficient v_c has been analyzed. In this section, a shift property of DFT is used to explain the equivalence between the time and the frequency domain representations of the multi-branch systems of Fig. 1.4 and Fig. 1.5. Based on this equivalence, the discrete time model of the multi-branch system, the MF, LS and WLS based TD-JCE algorithms as well as their performance evaluation in terms of the SNR degradation and MSE will be derived from their frequency domain counterparts.

3.4.2 The shift property of DFT

The equivalent expression of $\tilde{\mathbf{G}}$ in (3.28) will be firstly introduced. With

$$\underline{\mathbf{P}}^{(u)} = \begin{pmatrix} \underline{p}_1^{(u)} & \underline{p}_{L_p}^{(u)} & \cdots & \underline{p}_{L_p - W + 2}^{(u)} \\ \underline{p}_2^{(u)} & \underline{p}_1^{(u)} & \cdots & \underline{p}_{L_p - W + 3}^{(u)} \\ \vdots & \vdots & \ddots & \vdots \\ \underline{p}_{L_p}^{(u)} & \underline{p}_{L_p - 1}^{(u)} & \cdots & \underline{p}_{L_p - W + 1}^{(u)} \end{pmatrix}, u = 1 \cdots U, \quad (3.69)$$

of dimension $L_p \times W$, a total time domain pilot matrix [SJ94, KCW⁺03, KWC04a]

$$\underline{\mathbf{P}} = \left(\underline{\mathbf{P}}^{(1)} \dots \underline{\mathbf{P}}^{(U)} \right) \quad (3.70)$$

of dimension $L_p \times (UW)$ is obtained. With the Fourier matrix $\tilde{\mathcal{F}}$ of dimension $N_F \times N_F$ of (3.12), by assuming that L_p is equal to N_F , the matrix $\tilde{\mathbf{G}}$ can be derived as

$$\tilde{\mathbf{G}} = \tilde{\mathcal{F}} \underline{\mathbf{P}}, \quad (3.71)$$

which can be proved in the following way: By expressing the frequency domain pilot vector $\tilde{\mathbf{p}}^{(u)}$ of (3.10) to be the Fourier transformation of the time domain pilot vector $\underline{\mathbf{p}}^{(u)}$ of (3.1) on each branch $u, u = 1 \dots U$, i.e. (3.13) is satisfied, the total frequency domain pilot matrix $\tilde{\mathbf{P}}$ of (3.25) can be expressed as

$$\tilde{\mathbf{P}} = \left(\text{diag} \left(\tilde{\mathcal{F}} \underline{\mathbf{p}}^{(1)} \right) \dots \text{diag} \left(\tilde{\mathcal{F}} \underline{\mathbf{p}}^{(U)} \right) \right). \quad (3.72)$$

From (3.72) and the definition of the matrix $\tilde{\mathbf{G}}$ as in (3.28), we derive

$$\tilde{\mathbf{G}} = \left(\text{diag} \left(\tilde{\mathcal{F}} \underline{\mathbf{p}}^{(1)} \right) \tilde{\mathcal{F}}_W \dots \text{diag} \left(\tilde{\mathcal{F}} \underline{\mathbf{p}}^{(U)} \right) \tilde{\mathcal{F}}_W \right), \quad (3.73)$$

in which the matrix $\tilde{\mathcal{F}}_W$ is defined in (3.22).

From (3.73) and (3.70), the prove of (3.71) turns out to be

$$\left(\text{diag} \left(\tilde{\mathcal{F}} \underline{\mathbf{p}}^{(1)} \right) \tilde{\mathcal{F}}_W \dots \text{diag} \left(\tilde{\mathcal{F}} \underline{\mathbf{p}}^{(U)} \right) \tilde{\mathcal{F}}_W \right) = \left(\tilde{\mathcal{F}} \underline{\mathbf{P}}^{(1)} \dots \tilde{\mathcal{F}} \underline{\mathbf{P}}^{(U)} \right). \quad (3.74)$$

Therefore, it is only necessary to equivalently prove the relation

$$\text{diag} \left(\tilde{\mathcal{F}} \underline{\mathbf{p}}^{(u)} \right) \tilde{\mathcal{F}}_W = \tilde{\mathcal{F}} \underline{\mathbf{P}}^{(u)}, u = 1 \dots U. \quad (3.75)$$

The right side of (3.75) is reformulated as

$$\begin{aligned} \tilde{\mathcal{F}} \underline{\mathbf{P}}^{(u)} &= \begin{pmatrix} 1 & 1 & \dots & 1 \\ 1 & e^{-j\frac{2\pi}{L_p}} & \dots & e^{-j\frac{2\pi(L_p-1)}{L_p}} \\ \vdots & \vdots & \ddots & \vdots \\ 1 & e^{-j\frac{2\pi(L_p-1)}{L_p}} & \dots & e^{-j\frac{2\pi(L_p-1)^2}{L_p}} \end{pmatrix} \begin{pmatrix} \underline{p}_1^{(u)} & \underline{p}_{L_p}^{(u)} & \dots & \underline{p}_{L_p-W+2}^{(u)} \\ \underline{p}_2^{(u)} & \underline{p}_1^{(u)} & \dots & \underline{p}_{L_p-W+3}^{(u)} \\ \vdots & \vdots & \ddots & \vdots \\ \underline{p}_{L_p}^{(u)} & \underline{p}_{L_p-1}^{(u)} & \dots & \underline{p}_{L_p-W+1}^{(u)} \end{pmatrix} \\ &= \begin{pmatrix} \sum_{l=1}^{L_p} \underline{p}_l^{(u)} & \dots & \sum_{l=1}^{L_p} \underline{p}_l^{(u)} \\ \sum_{l=1}^{L_p} \underline{p}_l^{(u)} e^{-j\frac{2\pi(l-1)}{L_p}} & \dots & \left(\sum_{l=1}^{L_p} \underline{p}_l^{(u)} e^{-j\frac{2\pi(l-1)}{L_p}} \right) e^{-j\frac{2\pi(W-1)}{L_p}} \\ \vdots & \ddots & \vdots \\ \sum_{l=1}^{L_p} \underline{p}_l^{(u)} e^{-j\frac{2\pi(l_p-1)(l-1)}{L_p}} & \dots & \left(\sum_{l=1}^{L_p} \underline{p}_l^{(u)} e^{-j\frac{2\pi(l_p-1)(l-1)}{L_p}} \right) e^{-j\frac{2\pi(l_p-1)(W-1)}{L_p}} \end{pmatrix}, \end{aligned} \quad (3.76)$$

which appears to be the same with the reformulation of the left side of (3.75), i.e.

$$\begin{aligned}
& \text{diag} \left(\tilde{\mathcal{F}} \underline{\mathbf{p}}^{(u)} \right) \tilde{\mathcal{F}}_{\mathbf{W}} \\
&= \text{diag} \left\{ \left(\begin{array}{ccc} 1 & \dots & 1 \\ 1 & \dots & e^{-j \frac{2\pi(L_{\mathbf{P}}-1)}{L_{\mathbf{P}}}} \\ \vdots & \ddots & \vdots \\ 1 & \dots & e^{-j \frac{2\pi(L_{\mathbf{P}}-1)^2}{L_{\mathbf{P}}}} \end{array} \right) \left(\begin{array}{c} p_1^{(u)} \\ p_2^{(u)} \\ \vdots \\ p_{L_{\mathbf{P}}}^{(u)} \end{array} \right) \right\} \left(\begin{array}{ccc} 1 & \dots & 1 \\ 1 & \dots & e^{-j \frac{2\pi(W-1)}{L_{\mathbf{P}}}} \\ \vdots & \ddots & \vdots \\ 1 & \dots & e^{-j \frac{2\pi(L_{\mathbf{P}}-1)(W-1)}{L_{\mathbf{P}}}} \end{array} \right) \\
&= \left(\begin{array}{ccc} \sum_{l=1}^{L_{\mathbf{P}}} p_l^{(u)} & \dots & 0 \\ 0 & \ddots & 0 \\ 0 & \dots & \sum_{l=1}^{L_{\mathbf{P}}} p_l^{(u)} e^{-j \frac{2\pi(L_{\mathbf{P}}-1)(l-1)}{L_{\mathbf{P}}}} \end{array} \right) \left(\begin{array}{ccc} 1 & \dots & 1 \\ 1 & \dots & e^{-j \frac{2\pi(W-1)}{L_{\mathbf{P}}}} \\ \vdots & \ddots & \vdots \\ 1 & \dots & e^{-j \frac{2\pi(L_{\mathbf{P}}-1)(W-1)}{L_{\mathbf{P}}}} \end{array} \right) \quad (3.77) \\
&= \left(\begin{array}{ccc} \sum_{l=1}^{L_{\mathbf{P}}} p_l^{(u)} & \dots & \sum_{l=1}^{L_{\mathbf{P}}} p_l^{(u)} \\ \sum_{l=1}^{L_{\mathbf{P}}} p_l^{(u)} e^{-j \frac{2\pi(l-1)}{L_{\mathbf{P}}}} & \dots & \left(\sum_{l=1}^{L_{\mathbf{P}}} p_l^{(u)} e^{-j \frac{2\pi(l-1)}{L_{\mathbf{P}}}} \right) e^{-j \frac{2\pi(W-1)}{L_{\mathbf{P}}}} \\ \vdots & \ddots & \vdots \\ \sum_{l=1}^{L_{\mathbf{P}}} p_l^{(u)} e^{-j \frac{2\pi(l_{\mathbf{P}}-1)(l-1)}{L_{\mathbf{P}}}} & \dots & \left(\sum_{l=1}^{L_{\mathbf{P}}} p_l^{(u)} e^{-j \frac{2\pi(l_{\mathbf{P}}-1)(l-1)}{L_{\mathbf{P}}}} \right) e^{-j \frac{2\pi(l_{\mathbf{P}}-1)(W-1)}{L_{\mathbf{P}}}} \end{array} \right)
\end{aligned}$$

From (3.76) and (3.77), (3.75) is proved. As a result, (3.71) is proved, too.

3.4.3 Discrete time model

The discrete time model of the time domain multi-branch system of Fig. 1.4 can be obtained from the discrete frequency model of the frequency domain multi-branch system of Fig. 1.5 which is described in Section 3.3.1. Let us suppose the time domain receive signal vector to be $\underline{\mathbf{r}}$ with dimension $L_{\mathbf{p}}$, which is the IDFT of the frequency domain receive signal vector $\tilde{\underline{\mathbf{r}}}$ of (3.28) with dimension $N_{\mathbf{F}}$. $L_{\mathbf{p}}$ is equal to $N_{\mathbf{F}}$ in the derivation. With the inverse of the Fourier matrix $\tilde{\mathcal{F}}$ of (3.12), i.e. $\tilde{\mathcal{F}}^{-1}$, of dimension $N_{\mathbf{F}} \times N_{\mathbf{F}}$, and with the frequency domain receive vector $\tilde{\underline{\mathbf{r}}}$ of (3.28), the time domain receive vector

$$\underline{\mathbf{r}} = \tilde{\mathcal{F}}^{-1} \tilde{\underline{\mathbf{r}}} = \tilde{\mathcal{F}}^{-1} \tilde{\underline{\mathbf{G}}} \underline{\mathbf{h}} + \tilde{\mathcal{F}}^{-1} \tilde{\underline{\mathbf{n}}} \quad (3.78)$$

of dimension $L_{\mathbf{p}}$ is obtained, in which $L_{\mathbf{p}}$ is assumed to be equal to $N_{\mathbf{F}}$.

With the time domain total pilot matrix $\underline{\mathbf{P}}$ of (3.70) and considering the equivalent expression of $\tilde{\underline{\mathbf{G}}}$ in (3.71), together with the time domain noise vector

$$\underline{\mathbf{n}} = \left(\underline{\mathbf{n}}_1 \cdots \underline{\mathbf{n}}_{L_{\mathbf{p}}} \right)^{\text{T}} \quad (3.79)$$

of dimension L_p , which is the IDFT of the frequency domain noise vector $\tilde{\mathbf{n}}$ of (3.26), i.e.

$$\mathbf{n} = \tilde{\mathcal{F}}^{-1} \tilde{\mathbf{n}}, \quad (3.80)$$

the time domain receive signal vector \mathbf{r} of (3.78) can be derived as

$$\mathbf{r} = \mathbf{P} \mathbf{h} + \mathbf{n}. \quad (3.81)$$

In (3.81), there are UW unknown channel coefficients and L_p known received signals. In the case

$$UW \leq L_p, \quad (3.82)$$

it is a determined linear set of equations by which the solutions of the unknown channel coefficients can be obtained.

(3.81) gives us the discrete time model of the linear multi-branch system shown in Fig. 1.4 using matrix vector notation. The time multiplexing structure of the pilot vector $\mathbf{p}^{(u)}$ of (3.1) and the guard vector $\mathbf{g}^{(u)}$ of (3.18) on each branch of Fig. 1.4 is illustrated in Fig. 3.4, in which the guard vector $\mathbf{g}^{(u)}$ is composed of the cyclic prefix of the pilot vector $\mathbf{p}^{(u)}$, see (3.18). This discrete time model of the time domain multi-branch systems of Fig. 1.4 has been applied to many systems, such as the single carrier multi-user CDMA system [SJ94] and the FMT-based multi-carrier multi-antenna system [KWC04a].

For a single carrier system, the multiplexing structure of the guard, the pilot and the data from the time domain multi-branch model of Fig. 1.4 with U branches is illustrated in Fig. 3.5. In this scheme, the U branches occupy the same frequency resource of bandwidth B for the transmission of the guard $\mathbf{g}^{(u)}$, the TD training sequence u or the pilot vector $\mathbf{p}^{(u)}$, and the data serially in time. However, the multiple branches are separated e.g. in the code domain in the sense that each branch transmits its own branch specific pilot signature. Such a transmit block structure as shown in Fig. 3.5 is e.g. typical for synchronous CDMA systems [SJ94].

For the multi-carrier transmission systems of the FMT-based transmission with N_F sub-carriers, the multiplexing structure of the guard, the pilot and the data is shown in Fig. 3.6, which is basically the extension of the multiplexing structure of Fig. 3.5 into the frequency domain by N_F copies. At each frequency resource of subband of bandwidth B_{n_F} , $n_F = 1 \cdots N_F$, the pilot vectors $\mathbf{p}^{(u)}$, $u = 1 \cdots U$, of U branches are transmitted within a certain time duration while separated in the code domain such that each branch transmits its own branch specific pilot signature. The total system bandwidth B in Table 2.1 is calculated as

$$B = \sum_{n_F=1}^{N_F} B_{n_F}. \quad (3.83)$$

The pilot vector $\mathbf{p}^{(u)}$ of the u -th branch can be reused in the frequency domain at different sub-carriers. This reuse is reasonable in FMT systems [KWC04a], since the inter carrier interference (ICI) is negligible thanks to the proper design of the prototype filter [CEÖ02].

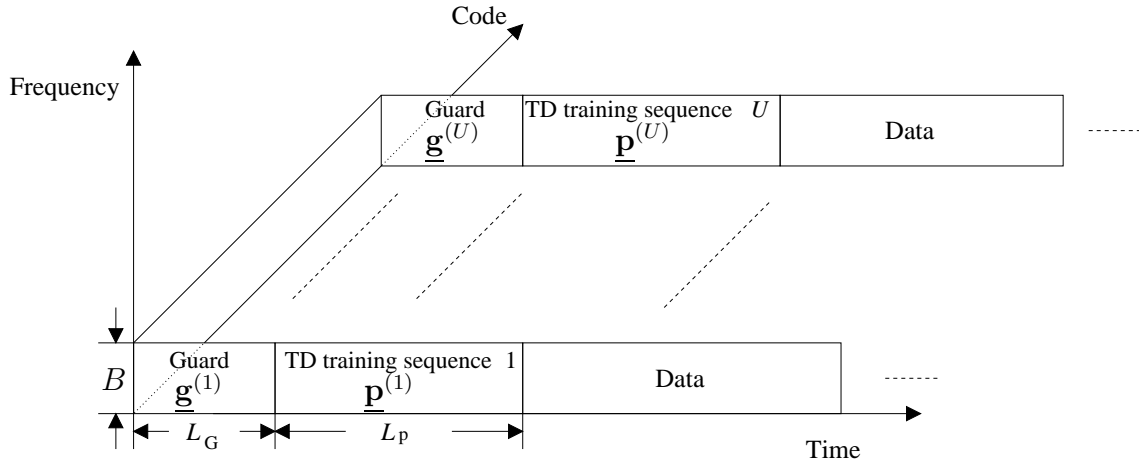


Fig. 3.5. Time multiplexing structure of the guard, the pilot and the data in the single carrier system.

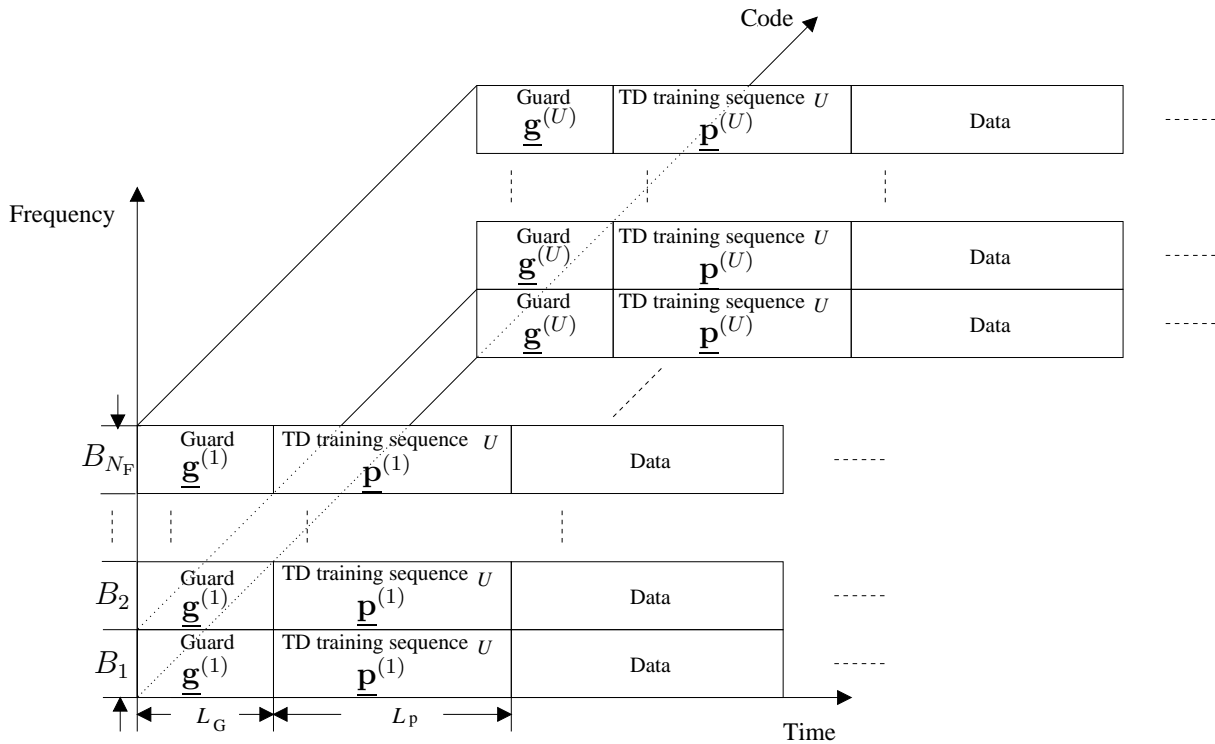


Fig. 3.6. Time multiplexing structure of the guard, the pilot and the data in the multi-carrier system.

3.4.4 TD-JCE

In this subsection, three TD-JCE algorithms will be derived from the FD-JCE algorithms described in Subsection 3.3.2 based on the shift property of DFT discussed in Subsection 3.4.2.

Substituting (3.71) into (3.32), by taking into account that

$$\tilde{\mathcal{F}}^H \tilde{\mathcal{F}} = \mathbf{I}, \quad (3.84)$$

the time domain MF JCE (TD-MF-JCE) is obtained as

$$\hat{\mathbf{h}}_{\text{MF}} = \mathbf{P}^H \mathbf{r} = \mathbf{P}^H \mathbf{P} \mathbf{h} + \mathbf{P}^H \mathbf{n}, \quad (3.85)$$

in which the time domain total pilot matrix \mathbf{P} is given in (3.70). From (3.85) the a-priori knowledge required by the TD-MF-JCE is the number of channel coefficients W and the transmitted pilot vectors $\mathbf{p}^{(u)}$, $u = 1 \cdots U$, of (3.1) of the U branches. The TD-MF-JCE of $\hat{\mathbf{h}}_{\text{MF}}$ is biased since (3.9) can not be fulfilled.

Similarly, substituting (3.71) into (3.34), the time domain LS JCE (TD-LS-JCE) is obtained as

$$\hat{\mathbf{h}}_{\text{LS}} = (\mathbf{P}^H \mathbf{P})^{-1} \mathbf{P}^H \mathbf{r} = \mathbf{h} + (\mathbf{P}^H \mathbf{P})^{-1} \mathbf{P}^H \mathbf{n}, \quad (3.86)$$

in which as in TD-MF-JCE, the number of channel coefficients W and the transmitted pilot vectors $\mathbf{p}^{(u)}$, $u = 1 \cdots U$, of (3.1) of the U branches should be a-priori known. From (3.86) it is obvious that the TD-LS-JCE is unbiased. The matrix $(\mathbf{P}^H \mathbf{P})^{-1} \mathbf{P}^H$ according to (3.86) is also called the pseudo-inverse of \mathbf{P} [Ste73].

If the noise covariance matrix \mathbf{R}_n of (3.7) is also a-priori known, and if (3.71) is substituted into (3.37), an unbiased time domain WLS JCE (TD-WLS-JCE) is obtained as

$$\hat{\mathbf{h}}_{\text{WLS}} = (\mathbf{P}^H \mathbf{R}_n^{-1} \mathbf{P})^{-1} \mathbf{P}^H \mathbf{R}_n^{-1} \mathbf{r} = \mathbf{h} + (\mathbf{P}^H \mathbf{R}_n^{-1} \mathbf{P})^{-1} \mathbf{P}^H \mathbf{R}_n^{-1} \mathbf{n}. \quad (3.87)$$

By comparing (3.87) with (3.86), if the noise \mathbf{n} of (3.79) at the receiver before the channel estimator is AWGN, i.e. its covariance matrix \mathbf{R}_n satisfies (3.8), the TD-WLS-JCE will reduce to the TD-LS-JCE.

From (3.81), the TD-JCE is only feasible if the number UW of unknown coefficients in the channel \mathbf{h} of (2.28) does not exceed the number L_p of components of the receive vector \mathbf{r} of (3.81).

3.4.5 SNR degradation

The MF-JCE maximizes the output SNR in the AWGN channel. From (3.85), neglecting the interference between the channel coefficients and MAI [Kle96], the SNR of the estimated j -th channel coefficient $\hat{h}_j, j = 1 \cdots UW$, at the output of the TD-MF-JCE of (3.85) is

$$\gamma_{\text{MF},j} = \frac{\mathbf{E}\{|\text{diag}(\mathbf{P}^{\text{H}}\mathbf{P})\mathbf{h}_j|^2\}}{\mathbf{E}\{|\mathbf{P}^{\text{H}}\mathbf{n}_j|^2\}} = |h_j|^2 \frac{\sum_{l_p=1}^{L_p} |p_{l_p,j}|^2}{2\sigma^2}. \quad (3.88)$$

From (3.86), with q_j denoting the j -th diagonal element of the matrix $(\mathbf{P}^{\text{H}}\mathbf{P})^{-1}$ and with the noise covariance matrix \mathbf{R}_n satisfying (3.8), the SNR of the estimated j -th channel coefficient $\hat{h}_j, j = 1 \cdots UW$, of the TD-LS-JCE is derived by

$$\gamma_{\text{LS},j} = \frac{\mathbf{E}\{|\mathbf{h}_j|^2\}}{\mathbf{E}\{|\mathbf{P}^{\text{H}}\mathbf{P})^{-1}\mathbf{P}^{\text{H}}\mathbf{n}_j|^2\}} = \frac{|h_j|^2}{2\sigma^2 q_j}. \quad (3.89)$$

From (3.87), if the noise is not white, i.e. (3.8) is not satisfied, but the noise covariance matrix \mathbf{R}_n is a-priori known, with t_j denoting the j -th diagonal element of the matrix $(\mathbf{P}^{\text{H}}\mathbf{R}_n^{-1}\mathbf{P})^{-1}$, the SNR of the estimated j -th channel coefficient $\hat{h}_j, j = 1 \cdots UW$, of the TD-WLS-JCE is given by

$$\gamma_{\text{WLS},j} = \frac{\mathbf{E}\{|\mathbf{h}_j|^2\}}{\mathbf{E}\{|\mathbf{P}^{\text{H}}\mathbf{R}_n^{-1}\mathbf{P})^{-1}\mathbf{P}^{\text{H}}\mathbf{R}_n^{-1}\mathbf{n}_j|^2\}} = \frac{|h_j|^2}{t_j}. \quad (3.90)$$

The SNR degradation $\gamma_{\text{LS},j}$ of (3.89) at the output of the TD-LS-JCE and the SNR $\gamma_{\text{WLS},j}$ of (3.90) at the output of the TD-WLS-JCE with respect to the SNR $\gamma_{\text{MF},j}$ of (3.88) at the output of the TD-MF-JCE gives the SNR degradation

$$\delta_{\text{MF-LS},j} = \frac{\gamma_{\text{MF},j}}{\gamma_{\text{LS},j}} = q_j \sum_{l_p=1}^{L_p} |p_{l_p,j}|^2 \quad (3.91)$$

of the j -th component of the estimated total CIR vectors $\hat{\mathbf{h}}_{\text{LS}}$ of (3.86) and the SNR degradation

$$\delta_{\text{MF-WLS},j} = \frac{\gamma_{\text{MF},j}}{\gamma_{\text{WLS},j}} = \frac{t_j \sum_{l_p=1}^{L_p} |p_{l_p,j}|^2}{2\sigma^2} \quad (3.92)$$

of the j -th component of the estimated total CIR vectors $\hat{\mathbf{h}}_{\text{WLS}}$ of (3.87), respectively.

If the noise at the input of the estimator is AWGN, i.e. (3.8) is fulfilled, the output SNRs $\gamma_{\text{LS},j}, j = 1 \cdots UW$, of (3.89) and $\gamma_{\text{WLS},j}, j = 1 \cdots UW$, of (3.90) of the two

estimators TD-LS-JCE and TD-WLS-JCE will be the same. If the noise at the input of the estimator is colored, i.e. (3.8) is not fulfilled, the output SNRs $\gamma_{\text{LS},j}$, $j = 1 \cdots UW$, of (3.89) and $\gamma_{\text{WLS},j}$, $j = 1 \cdots UW$, of (3.90) of the TD-LS-JCE and the TD-WLS-JCE will be different. In this case, if $L_p > UW$, it is expected that the TD-WLS-JCE will outperform TD-LS-JCE in terms of the estimation performance, since the noise covariance matrix $\underline{\mathbf{R}}_n$ of (3.7) is taken into account in TD-WLS-JCE [KWC04a].

3.4.6 MSE

In this subsection, the MSE of the TD-LS-JCE $\hat{\underline{\mathbf{h}}}_{\text{LS}}$ of (3.86) will be evaluated. With the definition of MSE of (3.47), by substituting the TD-LS-JCE $\hat{\underline{\mathbf{h}}}_{\text{LS}}$ of (3.86) into (3.47), and by using the exchangeability of the trace and the expectation operations, the MSE of the TD-LS-JCE

$$\epsilon_{\text{LS}} = 2\sigma^2 \text{tr}\{(\underline{\mathbf{P}}^H \underline{\mathbf{P}})^{-1}\} \quad (3.93)$$

is obtained, in which the noise is assumed to be AWGN. The MSE ϵ_{LS} of (3.93) depends only on the transmitted pilot vectors $\underline{\mathbf{p}}^{(u)}$, $u = 1 \cdots U$, of (3.1) on the U branches. It is reasonable to expect that some patterns of pilot vectors will bring the minimum MSE.

Considering the Fourier matrix $\tilde{\underline{\mathcal{F}}}$ of (3.12) and considering (3.84), (3.93) can be expressed as

$$\epsilon_{\text{LS}} = 2\sigma^2 \text{tr}\{(\underline{\mathbf{P}}^H \tilde{\underline{\mathcal{F}}}^H \tilde{\underline{\mathcal{F}}} \underline{\mathbf{P}})^{-1}\}. \quad (3.94)$$

By substituting (3.71) into (3.94), it is seen that (3.94) is the same as (3.50). Therefore, the minimum MSE $\epsilon_{\text{LS},\min}$ of the total CIR vector $\underline{\mathbf{h}}$ of (2.28) based on the time domain representation of the multi-branch system should be the same with the minimum MSE $\epsilon_{\text{LS},\min}$ of (3.58) of the total CIR vector $\underline{\mathbf{h}}$ of (2.28) based on the frequency domain representation of the multi-branch system, i.e.

$$\epsilon_{\text{LS},\min} = \frac{2UW\sigma^2}{E_p}, \quad (3.95)$$

in which

$$E_p = \frac{1}{2} \underline{\mathbf{p}}^{(u)} \underline{\mathbf{p}}^{(u)H}, u = 1 \cdots U, \quad (3.96)$$

which is equal to (3.11) by considering (3.13). The normalized minimum MSE

$$\epsilon'_{\text{LS},\min} = \frac{2W\sigma^2}{E_p} \quad (3.97)$$

is derived by multiplying the minimum MSE $\epsilon_{\text{LS},\min}$ of (3.95) with the factor $1/U$.

3.5 List of estimators

The frequency and time domain estimators considered in this chapter are listed in Table 3.1.

Table 3.1. Frequency and time domain estimators.

Domain	Estimation target	Name	Equation	Equation number
Frequency domain	CIR	FD-MF-JCE	$\hat{\mathbf{h}}_{\text{MF}} = \tilde{\mathbf{G}}^H \tilde{\mathbf{G}} \mathbf{h} + \tilde{\mathbf{G}}^H \tilde{\mathbf{n}}$	(3.32)
		FD-LS-JCE	$\hat{\mathbf{h}}_{\text{LS}} = \mathbf{h} + (\tilde{\mathbf{G}}^H \tilde{\mathbf{G}})^{-1} \tilde{\mathbf{G}}^H \tilde{\mathbf{n}}$	(3.34)
		FD-WLS-JCE	$\hat{\mathbf{h}}_{\text{WLS}} = \mathbf{h} + (\tilde{\mathbf{G}}^H \tilde{\mathbf{R}}_n^{-1} \tilde{\mathbf{G}})^{-1} \tilde{\mathbf{G}}^H \tilde{\mathbf{R}}_n^{-1} \tilde{\mathbf{n}}$	(3.37)
	CTF	FD-MF-JCE	$\hat{\mathbf{h}}_{\text{MF}} = \tilde{\mathcal{F}}_{\text{W,tot}} \tilde{\mathcal{F}}_{\text{W,tot}}^H \tilde{\mathbf{P}}^H \tilde{\mathbf{P}} \mathbf{h} + \mathbf{Z}_{\text{MF}} \tilde{\mathbf{n}}$	(3.39)
		FD-LS-JCE	$\hat{\mathbf{h}}_{\text{LS}} = \tilde{\mathbf{h}} + \mathbf{Z}_{\text{LS}} \tilde{\mathbf{n}}$	(3.40)
		FD-WLS-JCE	$\hat{\mathbf{h}}_{\text{WLS}} = \tilde{\mathbf{h}} + \mathbf{Z}_{\text{WLS}} \tilde{\mathbf{n}}$	(3.41)
Time domain	CIR	TD-MF-JCE	$\hat{\mathbf{h}}_{\text{MF}} = \mathbf{P}^H \mathbf{P} \mathbf{h} + \mathbf{P}^H \mathbf{n}$	(3.85)
		TD-LS-JCE	$\hat{\mathbf{h}}_{\text{LS}} = \mathbf{h} + (\mathbf{P}^H \mathbf{P})^{-1} \mathbf{P}^H \mathbf{n}$	(3.86)
		TD-WLS-JCE	$\hat{\mathbf{h}}_{\text{WLS}} = \mathbf{h} + (\mathbf{P}^H \mathbf{R}_n^{-1} \mathbf{P})^{-1} \mathbf{P}^H \mathbf{R}_n^{-1} \mathbf{n}$	(3.87)

4 Optimum and suboptimum pilots for JCE in noise limited systems

4.1 Introduction

In Section 3.3, considering the discrete frequency model, the SNR degradations $\tilde{\delta}_{\text{MF-LS},j}$, $j = 1 \cdots UN_{\text{F}}$, of (3.45) of the UN_{F} detected pilot symbols, the variation coefficient v_c of (3.68) and the MSE ϵ_{LS} of (3.50) are derived for the FD-LS-JCE. Furthermore, the SNR degradations $\tilde{\delta}_{\text{MF-WLS},j}$, $j = 1 \cdots UN_{\text{F}}$, of (3.46) of the UN_{F} detected pilot symbols is derived for the FD-WLS-JCE. Considering the discrete time model, the SNR degradation $\delta_{\text{MF-LS},j}$ of (3.91) and the MSE ϵ_{LS} of (3.93) are derived for the TD-LS-JCE, and the SNR degradation $\delta_{\text{MF-WLS},j}$ of (3.92) is derived for the TD-WLS-JCE. If we examine all above performance evaluations of JCE, we will see that they are all influenced by the the pilot vectors $\underline{\mathbf{p}}^{(u)}$, $u = 1 \cdots U$, of (3.1) or $\tilde{\underline{\mathbf{p}}}^{(u)}$, $u = 1 \cdots U$, of (3.10) that represent the pilots in the time domain and in the frequency domain, respectively, of a multi-branch system with U branches.

In this chapter, the issue of pilot design will be addressed for multi-branch systems represented in the time domain and in the frequency domain as illustrated in Fig. 1.4 and Fig. 1.5, respectively. In Subsection 1.3.1, the optimum pilots are defined as those by which there is no noise enhancement of a certain JCE algorithm compared with a reference matched filtering single branch JCE algorithm, therefore 0 dB SNR degradation is obtained. For the design of optimum pilots and suboptimum pilots discussed in this chapter, the SNR degradations $\tilde{\delta}_{\text{MF-LS},j}$ of (3.45) for the FD-LS-JCE and $\delta_{\text{MF-LS},j}$ of (3.91) for the TD-LS-JCE will be referred, i.e. with the frequency domain optimum pilots 0 dB SNR degradation $\tilde{\delta}_{\text{MF-LS},j}$ will be satisfied [MWS⁺02] and with the time domain optimum pilots 0 dB SNR degradation $\delta_{\text{MF-LS},j}$ will be satisfied [SJ94].

The design criteria for the frequency domain optimum pilots and for the time domain optimum pilots will be discussed in Section 4.2, in which the relationship between the time and the frequency domain optimum pilots will be also investigated. Based on the aforementioned design criteria, the optimum and suboptimum pilots will be constructed in Section 4.3 and Section 4.4, respectively. In Section 4.5, the numerical results of the SNR degradations of the constructed optimum and suboptimum pilots for TD-LS-JCE and FD-LS-JCE will be given to verify the theoretical method.

The issue of pilot design in interference environments will be discussed in Chapter 5.

4.2 Design criteria of optimum pilots

4.2.1 Frequency domain

The sufficient condition of 0 dB SNR degradation $\tilde{\delta}_{\text{MF-LS},j}$ of (3.45) can be obtained from the condition of minimum MSE $\epsilon_{\text{LS},\min}$ of (3.58) with the matrix $\tilde{\mathbf{G}}$ of (3.28) and from the discussion on the MSE of FD-LS-JCE in Subsection 3.3.4, the minimum MSE $\epsilon_{\text{LS},\min}$ is obtained if and only if all eigenvalues of the matrix $\tilde{\mathbf{G}}^{\text{H}} \tilde{\mathbf{G}}$ are equal, i.e. (3.57) is satisfied. Since the only positive definite matrix with constant eigenvalues is a diagonal matrix with constant diagonal elements, the minimum MSE $\epsilon_{\text{LS},\min}$ for the FD-LS-JCE will be achieved if and only if [KMW⁺04]

$$\tilde{\mathbf{G}}^{\text{H}} \tilde{\mathbf{G}} = E_p \mathbf{I}_{UW}, \quad (4.1)$$

in which \mathbf{I}_{UW} is an identity matrix of dimension $(UW) \times (UW)$. Substituting (4.1) into (3.45), we can derive

$$\tilde{\delta}_{\text{MF-LS},j} = 1, \quad j = 1 \cdots UN_F. \quad (4.2)$$

(4.2) demonstrates that the condition of (4.1) is sufficient for achieving 0 dB SNR degradation for each of the UN_F detected pilot symbols in the case of FD-LS-JCE. Therefore, for the multi-branch systems represented in the frequency domain the design of optimum pilots according to Fig. 1.5 should start from the sufficient condition of 0 dB SNR degradation of (4.1). However, the matrix $\tilde{\mathbf{G}}$ of (3.28) is obtained from the transmitted pilots $\tilde{\mathbf{p}}^{(u)}, u = 1 \cdots U$, of (3.10) and their Fourier transformations. It is hard to figure out from (4.1) directly the design criteria by which the frequency domain optimum pilots can be constructed. To solve this problem, the condition of (4.1) will be investigated in more detail in the following.

Let the $N_F \times (UW)$ matrix $\tilde{\mathbf{G}}$ of (3.28) be expressed as

$$\tilde{\mathbf{G}} = (\tilde{\mathbf{g}}^{(1)} \cdots \tilde{\mathbf{g}}^{(UW)}) \quad (4.3)$$

with the i -th column vector

$$\tilde{\mathbf{g}}^{(i)} = \left(\tilde{g}_1^{(i)} \cdots \tilde{g}_{N_F}^{(i)} \right)^{\text{T}}, \quad i = 1 \cdots UW. \quad (4.4)$$

The condition sufficient for 0 dB SNR degradation of (4.1) is therefore reformulated as

$$\tilde{\mathbf{G}}^{\text{H}} \tilde{\mathbf{G}} = \begin{pmatrix} |\tilde{\mathbf{g}}^{(1)}|^{\text{H}} \tilde{\mathbf{g}}^{(1)} & |\tilde{\mathbf{g}}^{(1)}|^{\text{H}} \tilde{\mathbf{g}}^{(2)} & \cdots & |\tilde{\mathbf{g}}^{(1)}|^{\text{H}} \tilde{\mathbf{g}}^{(UW)} \\ |\tilde{\mathbf{g}}^{(2)}|^{\text{H}} \tilde{\mathbf{g}}^{(1)} & |\tilde{\mathbf{g}}^{(2)}|^{\text{H}} \tilde{\mathbf{g}}^{(2)} & \cdots & |\tilde{\mathbf{g}}^{(2)}|^{\text{H}} \tilde{\mathbf{g}}^{(UW)} \\ \vdots & \vdots & \ddots & \vdots \\ |\tilde{\mathbf{g}}^{(UW)}|^{\text{H}} \tilde{\mathbf{g}}^{(1)} & |\tilde{\mathbf{g}}^{(UW)}|^{\text{H}} \tilde{\mathbf{g}}^{(2)} & \cdots & |\tilde{\mathbf{g}}^{(UW)}|^{\text{H}} \tilde{\mathbf{g}}^{(UW)} \end{pmatrix} = E_p \mathbf{I}_{UW}. \quad (4.5)$$

(4.5) implies that in order to design the optimum pilots for the frequency domain multi-branch systems, the two requirements

$$\underline{\tilde{\mathbf{g}}}^{(i)\text{H}} \underline{\tilde{\mathbf{g}}}^{(i)} = E_p, \quad i = 1 \cdots UW, \quad (4.6)$$

and

$$\underline{\tilde{\mathbf{g}}}^{(i_1)\text{H}} \underline{\tilde{\mathbf{g}}}^{(i_2)} = 0, \quad i_1 = 1 \cdots UW, i_2 = 1 \cdots UW, \quad i_1 \neq i_2 \quad (4.7)$$

must be fulfilled. (4.6) and (4.7) represent, respectively, the properties of the autocorrelation and the cross-correlation of the column vectors $\underline{\tilde{\mathbf{g}}}^{(i)}, i = 1 \cdots UW$, of (4.4) of the matrix $\tilde{\mathbf{G}}$ of (3.28) with which the frequency domain optimum pilots can be obtained.

The two requirements of (4.6) and (4.7) can be further analyzed in the following:

The matrix $\tilde{\mathbf{G}}$ of (3.28) can be expressed in detail as

$$\tilde{\mathbf{G}} = \tilde{\mathbf{P}} \tilde{\mathcal{F}}_{W,\text{tot}} = \begin{pmatrix} \underbrace{\tilde{p}_1^{(1)}}_{\underline{\tilde{\mathbf{g}}}^{(1)}} & \underbrace{\tilde{p}_1^{(1)}}_{\underline{\tilde{\mathbf{g}}}^{(2)}} & \cdots & \underbrace{\tilde{p}_1^{(1)}}_{\underline{\tilde{\mathbf{g}}}^{(W)}} & \cdots & \underbrace{\tilde{p}_1^{(U)}}_{\underline{\tilde{\mathbf{g}}}^{((U-1)W+1)}} & \cdots & \underbrace{\tilde{p}_1^{(U)}}_{\underline{\tilde{\mathbf{g}}}^{(UW)}} \\ \tilde{p}_2^{(1)} & \tilde{p}_2^{(1)} e^{-j \frac{2\pi}{N_F}} & \cdots & \tilde{p}_2^{(1)} e^{-j \frac{2\pi(W-1)}{N_F}} & \cdots & \tilde{p}_2^{(U)} & \cdots & \tilde{p}_2^{(U)} e^{-j \frac{2\pi(W-1)}{N_F}} \\ \vdots & \vdots & \ddots & \vdots & \ddots & \vdots & \ddots & \vdots \\ \tilde{p}_{N_F}^{(1)} & \tilde{p}_{N_F}^{(1)} e^{-j \frac{2\pi(N_F-1)}{N_F}} & \cdots & \tilde{p}_{N_F}^{(1)} e^{-j \frac{2\pi(N_F-1)(W-1)}{N_F}} & \cdots & \tilde{p}_{N_F}^{(U)} & \cdots & \tilde{p}_{N_F}^{(U)} e^{-j \frac{2\pi(N_F-1)(W-1)}{N_F}} \end{pmatrix}. \quad (4.8)$$

Considering the column vectors $\underline{\tilde{\mathbf{g}}}^{(i)}, i = 1 \cdots UW$, of the matrix $\tilde{\mathbf{G}}$ of (3.28), we obtain the autocorrelation of the column vectors

$$\underline{\tilde{\mathbf{g}}}^{(i)\text{H}} \underline{\tilde{\mathbf{g}}}^{(i)} = \sum_{n_F=1}^{N_F} \tilde{p}_{n_F}^{(u)*} \tilde{p}_{n_F}^{(u)} = \underline{\tilde{\mathbf{p}}}^{(u)\text{H}} \underline{\tilde{\mathbf{p}}}^{(u)}, \quad i = 1 \cdots UW, \quad U = 1 \cdots U, \quad U = \lfloor \frac{i}{W} \rfloor, \quad (4.9)$$

in which $\lfloor \cdot \rfloor$ means to round the element to the nearest integer towards minus infinity.

(4.6) can be satisfied from (4.9) since (3.11) has been assumed, i.e. the pilot vectors $\underline{\tilde{\mathbf{p}}}^{(u)}, u = 1 \cdots U$, of (3.10) on the U branches have the same energy E_p for transmission as described in (3.11).

For the cross-correlation of the column vectors $\underline{\tilde{\mathbf{g}}}^{(i)}$ of (4.4) of matrix $\tilde{\mathbf{G}}$, i.e. $\underline{\tilde{\mathbf{g}}}^{(i_1)\text{H}} \underline{\tilde{\mathbf{g}}}^{(i_2)}$, $i_1 = 1 \cdots UW, i_2 = 1 \cdots UW, i_1 \neq i_2$, from (4.8) we have

$$\underline{\tilde{\mathbf{g}}}^{(i_1)\text{H}} \underline{\tilde{\mathbf{g}}}^{(i_2)} = \sum_{n_F=1}^{N_F} \tilde{p}_{n_F}^{(u_1)*} \tilde{p}_{n_F}^{(u_2)} e^{-j \frac{2\pi(n_F-1)(w_2-w_1)}{N_F}}, \quad (4.10)$$

$$u_1 = 1 \cdots U, u_2 = 1 \cdots U, w_1 = 1 \cdots W, w_2 = 1 \cdots W, \quad i_1 \neq i_2,$$

$$u_1 = \lfloor \frac{i_1}{W} \rfloor, u_2 = \lfloor \frac{i_2}{W} \rfloor, w_1 = \text{mod}(i_1 - 1, W), w_2 = \text{mod}(i_2 - 1, W),$$

where $\text{mod}(x, y)$ stands for the modulo operation. (4.10) satisfying (4.7) requires that

$$\sum_{n_F=1}^{N_F} \tilde{\underline{p}}_{n_F}^{(u_1)*} \tilde{\underline{p}}_{n_F}^{(u_2)} e^{-j \frac{2\pi(n_F-1)(w_2-w_1)}{N_F}} = 0, \quad (4.11)$$

$$u_1 = 1 \cdots U, u_2 = 1 \cdots U, w_1 = 1 \cdots W, w_2 = 1 \cdots W.$$

(4.11) implicates that in order to satisfy the requirement of (4.7) for the cross-correlation of the column vectors $\tilde{\underline{\mathbf{g}}}^{(i)}$, $i = 1 \cdots UW$ of (4.4) of the matrix $\tilde{\underline{\mathbf{G}}}$, the pilot vectors $\tilde{\underline{\mathbf{p}}}^{(u)}$, $u = 1 \cdots U$, of (3.10) of any two branches u_1, u_2 with $u_1 = 1 \cdots U$ and $u_2 = 1 \cdots U$ should be phase shift orthogonal. The precondition $i_1 \neq i_2$ in (4.10) implies that $u_1 = u_2$ and $w_1 = w_2$ cannot be simultaneously satisfied in (4.11). Specifically, if $u_1 = u_2$ while $w_1 \neq w_2$, (4.11) indicates the phase shift orthogonality of the pilot $\tilde{\underline{\mathbf{p}}}^{(u)}$, $u = u_1 = u_2$, itself. In addition, if the phase shift relating parameter $w_1 = w_2$ while the branch indexes $u_1 \neq u_2$ and considering (4.11), we obtain

$$\sum_{n_F=1}^{N_F} \tilde{\underline{p}}_{n_F}^{(u_1)*} \tilde{\underline{p}}_{n_F}^{(u_2)} = 0, \quad u_1 = 1 \cdots U, u_2 = 1 \cdots U, \quad (4.12)$$

which means that the two pilots $\tilde{\underline{\mathbf{p}}}^{(u_1)}$ and $\tilde{\underline{\mathbf{p}}}^{(u_2)}$ should be orthogonal for any two branch u_1, u_2 with u_1 not equal to u_2 . (4.12) can be taken as a specific case of zero phase shift of (4.11). The requirement of (4.12) can be taken as the first step in the process of pilot design, i.e. only the pilots which are orthogonal to each other should be investigated further on the requirement of (4.11) for the optimum pilots.

Based on the above analysis from (4.8) through (4.12), the design criteria of optimum pilots for the frequency domain multi-branch systems can be summarized as

- the pilots of any two active branches u_1, u_2 with $u_1 = 1 \cdots U$ and $u_2 = 1 \cdots U$, in the considered SA should be phase shift orthogonal, i.e. (4.11) should be satisfied, and
- it is assumed that the pilots $\tilde{\underline{\mathbf{p}}}^{(u)}$ of (3.10) represented in the frequency domain on all branches have the same energy.

In Fig. 4.1 the property of optimum pilots for the frequency domain multi-branch systems with FD-LS-JCE is illustrated. As seen in Fig. 4.1, UW sequences are illustrated, with the U pilots $\tilde{\underline{\mathbf{p}}}^{(u)}$, $u = 1 \cdots U$, of (3.10) and the $W - 1$ phase shifts $\tilde{\underline{\mathbf{p}}}^{(u)} e^{-j \frac{2\pi(n_F-1)}{N_F}} \dots \tilde{\underline{\mathbf{p}}}^{(u)} e^{-j \frac{2\pi(n_F-1)(W-1)}{N_F}}$, $u = 1 \cdots U$, of each pilot. All the UW sequences represented by the UW rows illustrated in Fig. 4.1 should be mutually orthogonal.

$\tilde{\underline{p}}_1^{(1)}$	$\tilde{\underline{p}}_2^{(1)}$	$\tilde{\underline{p}}_{N_F}^{(1)}$
$\tilde{\underline{p}}_1^{(1)} e^{-j \frac{2\pi(n_F-1)}{N_F}}$	$\tilde{\underline{p}}_2^{(1)} e^{-j \frac{2\pi(n_F-1)}{N_F}}$	$\tilde{\underline{p}}_{N_F}^{(1)} e^{-j \frac{2\pi(n_F-1)}{N_F}}$
<div style="display: flex; justify-content: space-around; align-items: center;"> <div style="border: 1px solid black; padding: 5px;"> $\tilde{\underline{p}}_1^{(1)} e^{-j \frac{2\pi(n_F-1)(W-1)}{N_F}}$ </div> <div style="border: 1px solid black; padding: 5px;"> $\tilde{\underline{p}}_2^{(1)} e^{-j \frac{2\pi(n_F-1)(W-1)}{N_F}}$ </div> <div style="padding: 0 10px;">.....</div> <div style="border: 1px solid black; padding: 5px;"> $\tilde{\underline{p}}_{N_F}^{(1)} e^{-j \frac{2\pi(n_F-1)(W-1)}{N_F}}$ </div> </div>			
<div style="display: flex; justify-content: center; align-items: center;"> <div style="border: 1px solid black; padding: 5px; margin-right: 5px;"> \vdots </div> </div>			
$\tilde{\underline{p}}_1^{(U)}$	$\tilde{\underline{p}}_2^{(U)}$	$\tilde{\underline{p}}_{N_F}^{(U)}$
$\tilde{\underline{p}}_1^{(U)} e^{-j \frac{2\pi(n_F-1)}{N_F}}$	$\tilde{\underline{p}}_2^{(U)} e^{-j \frac{2\pi(n_F-1)}{N_F}}$	$\tilde{\underline{p}}_{N_F}^{(U)} e^{-j \frac{2\pi(n_F-1)}{N_F}}$
<div style="display: flex; justify-content: space-around; align-items: center;"> <div style="border: 1px solid black; padding: 5px;"> $\tilde{\underline{p}}_1^{(U)} e^{-j \frac{2\pi(n_F-1)(W-1)}{N_F}}$ </div> <div style="border: 1px solid black; padding: 5px;"> $\tilde{\underline{p}}_2^{(U)} e^{-j \frac{2\pi(n_F-1)(W-1)}{N_F}}$ </div> <div style="padding: 0 10px;">.....</div> <div style="border: 1px solid black; padding: 5px;"> $\tilde{\underline{p}}_{N_F}^{(U)} e^{-j \frac{2\pi(n_F-1)(W-1)}{N_F}}$ </div> </div>			

}

mutually orthogonal

Fig. 4.1. Orthogonal property of the frequency domain optimum pilots.

4.2.2 Time domain

By considering the equivalence between the time domain and the frequency domain representations of JCE in Section 3.4, we obtain from (3.71)

$$\tilde{\mathbf{G}}^H \tilde{\mathbf{G}} = \mathbf{P}^H \tilde{\mathcal{F}}^H \tilde{\mathcal{F}} \mathbf{P} = \mathbf{P}^H \mathbf{P}. \quad (4.13)$$

By substituting (4.13) into the condition of the frequency domain optimum pilots of (4.1), we derive

$$\mathbf{P}^H \mathbf{P} = E_p \mathbf{I}_{UW}. \quad (4.14)$$

Substituting (4.14) into (3.91), it follows for the SNR degradation

$$\delta_{\text{MF-LS},j} = 1, \quad j = 1 \cdots UW, \quad (4.15)$$

i.e. 0 dB SNR degradation for TD-LS-JCE can be obtained. That means, the condition of (4.14) is sufficient for the time domain optimum pilots by which 0 dB SNR degradation can be achieved. Therefore, the design of optimum pilots for the time domain multi-branch systems should start from (4.14).

From (3.70), (4.14) can be equivalently expressed as

$$\underline{\mathbf{P}}^{(u)H} \underline{\mathbf{P}}^{(u)} = E_p \mathbf{I}_W, \quad u = 1 \cdots U, \quad (4.16)$$

in which \mathbf{I}_W is an identity matrix of dimension $W \times W$, and

$$\underline{\mathbf{P}}^{(u_1)\text{H}} \underline{\mathbf{P}}^{(u_2)} = 0, \quad u_1 = 1 \cdots U, u_2 = 1 \cdots U, u_1 \neq u_2. \quad (4.17)$$

Furthermore, from the structure of $\underline{\mathbf{P}}^{(u)}$ of (3.69), (4.16) is represented as

$$\sum_{l_p=1}^{L_p} \underline{p}_{l_p}^{(u)*} \underline{p}_{l_p}^{(u)} = E_p, \quad u = 1 \cdots U, \quad (4.18)$$

and

$$\sum_{l_p=1}^{L_p} \underline{p}_{l_p}^{(u)*} \underline{p}_{l_p-w+1}^{(u)} = 0, \quad u = 1 \cdots U, w = 2 \cdots W. \quad (4.19)$$

Hence, (4.17) is represented as

$$\sum_{l_p=1}^{L_p} \underline{p}_{l_p}^{(u_1)*} \underline{p}_{l_p-w+1}^{(u_2)} = 0, \quad u_1 = 1 \cdots U, u_2 = 1 \cdots U, u_1 \neq u_2, w = 1 \cdots W. \quad (4.20)$$

Note that with the guard vector $\underline{\mathbf{g}}^{(u)}$ of (3.18) being composed of the cyclic shift of the pilot vector $\underline{\mathbf{p}}^{(u)}$ of (3.1) as illustrated in Fig. 3.4, we have

$$\underline{p}_{l_p-w+1}^{(u)} = \underline{p}_{L_p+l_p-w+1}^{(u)}, \text{ if } l_p \leq w-1, u = 1 \cdots U, w = 1 \cdots W. \quad (4.21)$$

(4.18) is satisfied if all the U branches use the same energy E_p for pilot transmission, i.e. (3.11) is satisfied, which is assumed in the thesis. (4.19) and (4.20) require, respectively, the shift orthogonal property of each pilot itself and between each pair of pilots. Therefore, the design criteria of the time domain optimum pilots can be summarized as

- the pilots of any two active branches u_1, u_2 with $u_1 = 1 \cdots U$ and $u_2 = 1 \cdots U$, in the considered SA should be shift orthogonal, i.e. (4.19) and (4.20) should be satisfied, and
- it is assumed that the pilots represented in the time domain on all branches have the same energy.

The design criteria of the time domain optimum pilots can be illustrated in Fig. 4.2. In order to make (4.19) and (4.20) satisfied, the UW sequences illustrated by the UW rows in Fig. 4.2 should be mutually orthogonal.

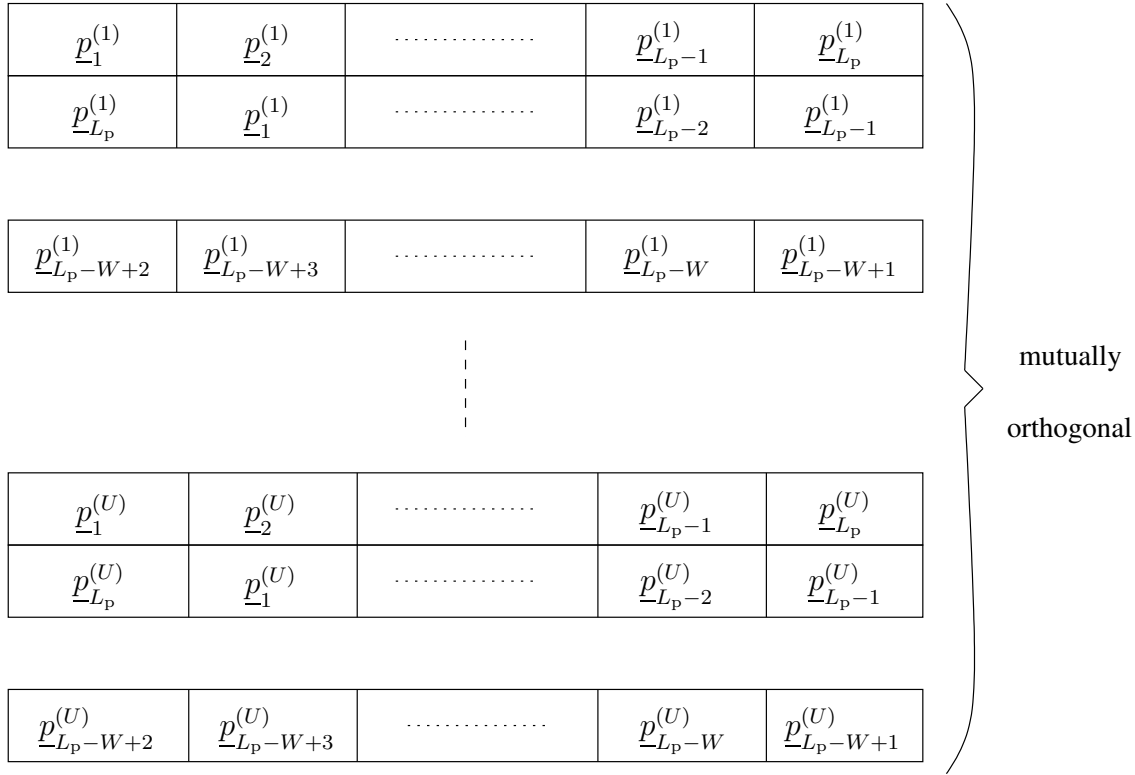


Fig. 4.2. Orthogonal property of the time domain optimum pilots.

4.2.3 Equivalence between the time and frequency domain design criteria of optimum pilots

In Section 3.4, the equivalence between the time and the frequency domain representations of the multi-branch systems has been explained. Since based on (4.13), the condition of the time domain optimum pilots of (4.14) can be obtained from the frequency domain optimum pilots of (4.1), and vice versa, the design criteria of the time domain optimum pilots of (4.19) and (4.20) is equivalent to the design criteria of the frequency domain optimum pilots of (4.11).

The equivalence between the design criteria of the time domain optimum pilots and the frequency domain optimum pilots implicates that we can design optimum pilots for the multi-branch systems either in the time domain according to the design criteria of (4.19) and (4.20) or in the frequency domain according to the design criteria of (4.11). By considering the relationship of the time and the frequency domain pilots of (3.13), we can conclude that the optimum pilots for the time domain multi-branch systems satisfying (4.19) and (4.20), after DFT, will also be the optimum pilots for the frequency domain multi-branch systems satisfying (4.11). Similarly, the optimum pilots for the frequency

domain multi-branch systems, after IDFT, will also be the optimum pilots for the time domain multi-branch systems. From literature [SJ94, MWS⁺02, KMW⁺04], separate pilot design either for the time domain or for the frequency domain is known, resulting in different classes of pilots for the time and the frequency domain JCEs. The equivalence between the time domain and the frequency domain design criteria of optimum pilots explained in this section increases the number of available optimum pilots for either time or frequency domain JCE in multi-branch systems.

4.3 Optimum pilots

4.3.1 Introduction

In this section, three kinds of optimum pilots, i.e. disjoint pilots, Walsh code based pilots, and CAZAC code based pilots, will be constructed. The former two kinds of pilots are shown to achieve 0 dB SNR degradation by simulation [MWS⁺02]. These two kinds of pilots will be proved to be optimum for the frequency domain multi-branch systems in this section since the design criteria of (4.11) can be satisfied. Besides that based on the criteria of (4.11) a new kind of optimum pilots, i.e. CAZAC code based pilots [KMW⁺04], will be constructed.

Although the optimum pilots can be designed either from the time domain or from the frequency domain due to the equivalence of their design criteria, the time and energy spending on finding a particular kind of pilots in the time domain design and in the frequency domain design might be different. This observation will be mentioned in the process of pilot construction in this section. Different kinds of pilots also challenge differently to the RF amplifier since they basically have different PAPR. This implementation related issue will be discussed in Chapter 6.

4.3.2 Disjoint pilots

The disjoint pilots can be designed from the design criteria of (4.11) for the frequency domain optimum pilots. To construct disjoint pilots, the N_F available subcarriers are subdivided among the U active branches inside a SA. Each branch uses its own specific subset of subcarriers exclusively to transmit pilots with the transmit energy E_p . The resulting pilots for the branch $u, u = 1 \cdots U$, is obtained as [MWS⁺02]

$$\tilde{\mathbf{p}}_D^{(u)} = \sqrt{\frac{2E_p}{W}} \underbrace{\left(\underbrace{0 \cdots 0}_{u-1} \underbrace{10 \cdots 0}_{U-u} 10 \cdots 10 \underbrace{0 \cdots 0}_{U-1} \underbrace{10 \cdots 0}_{U-u} \right)^T}_{\tilde{\mathbf{p}}_{D,b}^{(u)}}, \quad u = 1 \cdots U. \quad (4.22)$$

The term $\sqrt{\frac{2E_p}{W}}$ in (4.22) is to guarantee the transmit energy of the disjoint pilots to be E_p .

In a fully loaded system, the condition

$$N_F = UW \quad (4.23)$$

holds [SMW⁺01]. In an example case of $N_F = 16$ subcarriers, $U = 4$ branches and $W = 4$ channel coefficients, according to (4.22), the binary disjoint pilots $\tilde{\mathbf{p}}_{D,b}^{(u)}$ without considering the term $\sqrt{\frac{2E_p}{W}}$ for the U branches are constructed as

$$\begin{aligned} \tilde{\mathbf{p}}_{D,b}^{(1)} &= (1000100010001000)^T \\ \tilde{\mathbf{p}}_{D,b}^{(2)} &= (0100010001000100)^T \\ \tilde{\mathbf{p}}_{D,b}^{(3)} &= (0010001000100010)^T \\ \tilde{\mathbf{p}}_{D,b}^{(4)} &= (0001000100010001)^T \end{aligned} \quad (4.24)$$

Since the U pilots are orthogonal but not shift orthogonal, the disjoint pilots of (4.22) can only be designed from the two criteria (4.12) and (4.11) for the frequency domain multi-branch systems. That means, the disjoint pilots of (4.22) cannot be applied directly to the time domain multi-branch systems but have to resort to IDFT to obtain the time domain optimum pilots.

The disadvantage when choosing optimum pilots according to (4.22) is that the resulting set of pilots is the only possible set for the U branches in the considered SA. This means that adjacent SAs, if only disjoint pilots are applied, must apply the same set of pilots so that the interfering signals have similarities with the desired signals of the reference SA. This will adversely influence their performance in interference environments, which will be further discussed in Chapter 5.

4.3.3 Walsh code based pilots

The Walsh code based pilots can be designed from the frequency domain design criteria of (4.11). To construct Walsh code based pilots of dimension N_F , we consider a Hardamard matrix

$$\tilde{\mathbf{A}}_W = \begin{bmatrix} \mathbb{H}_1 & \mathbb{H}_1 \\ \mathbb{H}_1 & -\mathbb{H}_1 \end{bmatrix} \quad (4.25)$$

of dimension $N_F \times N_F$, in which \mathbb{H}_1 is a submatrix with dimension $\frac{N_F}{2} \times \frac{N_F}{2}$. The Hardamard matrix $\tilde{\mathbf{A}}_W$ can be also represented as

$$\tilde{\mathbf{A}}_W = [\tilde{\mathbf{w}}_1 \cdots \tilde{\mathbf{w}}_{n_F} \cdots \tilde{\mathbf{w}}_{N_F}], \quad n_F = 1 \cdots N_F, \quad (4.26)$$

with $\tilde{\mathbf{w}}_{n_F}$ being the n_F -th column vector of dimension N_F of matrix $\tilde{\mathbf{A}}_W$. The vectors $\tilde{\mathbf{w}}_{n_F}, n_F = 1 \cdots N_F$, represent the Walsh codes.

Walsh code based pilots are constructed from the specially selected column vectors of the Hardamard matrix [MWS⁺02]. Assuming the system to be fully loaded, for each fixed scenario characterized by the maximum number of channel coefficients W , the number of considered branches U and the number of subcarriers N_F , a total of W different sub-matrices of $\tilde{\mathbf{A}}_W$, say $\mathbb{P}_{W,1}, \mathbb{P}_{W,2}, \cdots, \mathbb{P}_{W,W}$, corresponding to W sets of Walsh code based pilots, each of which including U Walsh codes, can be constructed. N_F for the fast implementation of DFT is assumed to be powers of two. The W sets of Walsh code based pilots are constructed in the following way [MWS⁺02]:

$$\begin{aligned} \mathbb{P}_{W,1} &= [\tilde{\mathbf{w}}_1 \ \tilde{\mathbf{w}}_2 \ \tilde{\mathbf{w}}_3 \ \cdots \ \tilde{\mathbf{w}}_U], \\ \mathbb{P}_{W,2} &= [\tilde{\mathbf{w}}_{U+1} \ \tilde{\mathbf{w}}_{U+2} \ \tilde{\mathbf{w}}_{U+3} \ \cdots \ \tilde{\mathbf{w}}_{2U}], \\ &\vdots \\ \mathbb{P}_{W,W} &= [\tilde{\mathbf{w}}_{(W-1)U+1} \ \tilde{\mathbf{w}}_{(W-1)U+2} \ \tilde{\mathbf{w}}_{(W-1)U+3} \ \cdots \ \tilde{\mathbf{w}}_{N_F}], \end{aligned} \quad (4.27)$$

with each set forming the U Walsh code based pilots for the U branches in the frequency domain for the multi-branch system.

In the example case of $N_F = 16$, $U = 4$ and $W = 4$, according to (4.27), the Walsh code based pilots for the U branches can be obtained from the bold printed columns, i.e. from the first to the fourth column, of the following $N_F \times N_F$ matrix

$$\tilde{\mathbf{A}}_W = \begin{bmatrix} \mathbf{1} & \mathbf{1} & \mathbf{1} & \mathbf{1} & 1 & 1 & 1 & 1 & 1 & 1 & 1 & 1 & 1 & 1 & 1 & 1 \\ \mathbf{1} & -\mathbf{1} & \mathbf{1} & -\mathbf{1} & 1 & -1 & 1 & -1 & 1 & -1 & 1 & -1 & 1 & -1 & 1 & -1 \\ \mathbf{1} & \mathbf{1} & -\mathbf{1} & -\mathbf{1} & 1 & 1 & -1 & -1 & 1 & 1 & -1 & -1 & 1 & 1 & -1 & -1 \\ \mathbf{1} & -\mathbf{1} & -\mathbf{1} & \mathbf{1} & 1 & -1 & -1 & 1 & 1 & -1 & -1 & 1 & 1 & -1 & -1 & 1 \\ \mathbf{1} & \mathbf{1} & \mathbf{1} & \mathbf{1} & -1 & -1 & -1 & -1 & 1 & 1 & 1 & 1 & -1 & -1 & -1 & -1 \\ \mathbf{1} & -\mathbf{1} & \mathbf{1} & -\mathbf{1} & -1 & 1 & -1 & 1 & 1 & -1 & 1 & -1 & -1 & 1 & -1 & 1 \\ \mathbf{1} & \mathbf{1} & -\mathbf{1} & -\mathbf{1} & -1 & -1 & 1 & 1 & 1 & 1 & -1 & -1 & -1 & -1 & 1 & 1 \\ \mathbf{1} & -\mathbf{1} & -\mathbf{1} & \mathbf{1} & -1 & 1 & 1 & -1 & 1 & -1 & -1 & 1 & -1 & 1 & 1 & -1 \\ \mathbf{1} & \mathbf{1} & \mathbf{1} & \mathbf{1} & 1 & 1 & 1 & 1 & -1 & -1 & -1 & -1 & -1 & -1 & -1 & -1 \\ \mathbf{1} & -\mathbf{1} & \mathbf{1} & -\mathbf{1} & 1 & -1 & 1 & -1 & -1 & 1 & -1 & 1 & -1 & 1 & -1 & 1 \\ \mathbf{1} & \mathbf{1} & -\mathbf{1} & -\mathbf{1} & 1 & 1 & -1 & -1 & -1 & -1 & 1 & 1 & -1 & -1 & 1 & 1 \\ \mathbf{1} & -\mathbf{1} & -\mathbf{1} & \mathbf{1} & 1 & -1 & -1 & 1 & -1 & 1 & 1 & -1 & -1 & 1 & 1 & -1 \\ \mathbf{1} & \mathbf{1} & \mathbf{1} & \mathbf{1} & -1 & -1 & -1 & -1 & -1 & -1 & -1 & -1 & 1 & 1 & 1 & 1 \\ \mathbf{1} & -\mathbf{1} & \mathbf{1} & -\mathbf{1} & -1 & 1 & -1 & 1 & -1 & 1 & -1 & 1 & 1 & -1 & 1 & -1 \\ \mathbf{1} & \mathbf{1} & -\mathbf{1} & -\mathbf{1} & -1 & -1 & 1 & 1 & -1 & -1 & 1 & 1 & 1 & 1 & -1 & -1 \\ \mathbf{1} & -\mathbf{1} & -\mathbf{1} & \mathbf{1} & -1 & 1 & 1 & -1 & -1 & 1 & 1 & -1 & 1 & -1 & -1 & 1 \end{bmatrix} \quad (4.28)$$

It is seen from (4.27) that there are W sets, i.e. $\mathbb{P}_{W,1}, \mathbb{P}_{W,2}, \cdots, \mathbb{P}_{W,W}$, of codes available to be assigned to the U branches of the reference SA, i.e. adjacent SAs can apply different

sets of Walsh code based pilots, which allows perform JCE simultaneously using different sets of Walsh code based pilots in different SAs, even in the case of a large number of adjacent SAs.

The Walsh code based pilots are the frequency domain optimum pilots which satisfy the frequency domain design criteria of (4.11), as proved in Section 4.3.5 [KMW⁺04]. However, since the columns of the Hardamard matrix are not shift orthogonal, they cannot be constructed directly from the time domain design criterion of (4.14). However, from the equivalence of the time and the frequency domain design criteria of optimum pilots as described in Section 4.2.3, the Walsh code base pilots constructed as (4.27) will become the optimum pilots for the time domain JCE after IDFT.

Restricted by the construction of a Hardamard matrix, the dimension of the Walsh code based pilots N_F must be power of two.

4.3.4 CAZAC code based pilots

In this subsection, a new kind of optimum pilots, CAZAC code based pilots, is proposed and constructed. They are called CAZAC code based pilots because the pilots of the U branches are all CAZAC codes [Hei61, FZH62, Chu72, BC02]. The CAZAC codes are complex-valued pseudo-random noise (PN) sequences with constant amplitude assuming values on the unit circle and with cyclic correlation functions equal to zero apart from the only one peak at the starting point. For a CAZAC code

$$\tilde{\mathbf{c}} = \left(\tilde{c}_1 \quad \cdots \quad \tilde{c}_{N_F} \right)^T \quad (4.29)$$

of dimension N_F with the property

$$\tilde{c}_{k+N_F} = \tilde{c}_k, \quad k = 0 \cdots N_F - 1, \quad (4.30)$$

its cyclic correlation vector

$$\tilde{\mathbf{r}}_c = \left(\tilde{r}_{c,1} \quad \cdots \quad \tilde{r}_{c,N_F} \right)^T \quad (4.31)$$

is obtained by determining the elements [Hei61]

$$\tilde{r}_{c,i} = \sum_{k=0}^{N_F-1} \tilde{c}_{k+i} \tilde{c}_k^*, \quad i = 1 \cdots N_F. \quad (4.32)$$

The CAZAC codes are also called polyphase sequences [FZH62, Chu72]. The application of CAZAC codes alleviates the PAPR problem in OFDM systems [KMW⁺04], which will be discussed in Chapter 6.

The CAZAC code based pilots can be constructed from the frequency domain design criteria of (4.11). The CAZAC code $\underline{\tilde{\mathbf{c}}}$ can be constructed in several ways, such as in [Hei61] and [BC02]. According to [Hei61], the CAZAC code $\underline{\tilde{\mathbf{c}}}$ is defined as follows:

If P is an integer number greater than one, there are P different roots of unity, i.e. $\underline{\xi}_0, \underline{\xi}_1, \dots, \underline{\xi}_{P-1}$, with

$$\underline{\xi}_k = e^{-j(2\pi k/P)}, \quad 0 \leq k \leq P-1. \quad (4.33)$$

With the P roots of unity, a square matrix

$$\mathbf{C} = \begin{pmatrix} 1 & 1 & 1 & 1 & 1 \\ 1 & \underline{\xi}_1 & \underline{\xi}_1^2 & \dots & \underline{\xi}_1^{P-1} \\ 1 & \underline{\xi}_2 & \underline{\xi}_2^2 & \dots & \underline{\xi}_2^{P-1} \\ \vdots & \vdots & \vdots & \ddots & \vdots \\ 1 & \underline{\xi}_{P-1} & \underline{\xi}_{P-1}^2 & \dots & \underline{\xi}_{P-1}^{P-1} \end{pmatrix}. \quad (4.34)$$

of dimension $P \times P$ is formed. The CAZAC code vector $\underline{\tilde{\mathbf{c}}}$ of dimension $N_F = P^2$ is then generated by reading the matrix \mathbf{C} of (4.34) column by column, i.e.

$$\underline{\tilde{\mathbf{c}}} = (111 \dots 11 \underline{\xi}_1 \underline{\xi}_2 \underline{\xi}_3 \dots \underline{\xi}_{P-1} 1 \underline{\xi}_1^2 \underline{\xi}_2^2 \underline{\xi}_3^2 \dots \underline{\xi}_{P-1}^2 \dots 1 \underline{\xi}_1^{P-1} \underline{\xi}_2^{P-1} \underline{\xi}_3^{P-1} \dots \underline{\xi}_{P-1}^{P-1})^T. \quad (4.35)$$

In [Hei61], P is required to be a prime number. However, it was later pointed out in [FZH62] that P is not necessarily to be prime. With the generation of the CAZAC code $\underline{\tilde{\mathbf{c}}}$ according to (4.33) to (4.35), the dimension N_F of the CAZAC code $\underline{\tilde{\mathbf{c}}}$ is restricted to the square of an integer.

However, with the construction of the CAZAC code vector $\underline{\tilde{\mathbf{c}}}$ according to [BC02], the restriction on the dimension N_F of the CAZAC code vector $\underline{\tilde{\mathbf{c}}}$ is diminished, i.e. the dimension N_F of the CAZAC code vector $\underline{\tilde{\mathbf{c}}}$ could be any value. Let N_F and M be two integer numbers which are relatively prime. Hence, the elements $\tilde{c}_{l+1}, l = 0 \dots N_F - 1$, of the CAZAC code $\underline{\tilde{\mathbf{c}}}$ of dimension N_F according to [BC02] are derived as

$$\tilde{c}_{l+1} = \begin{cases} e^{j \frac{M\pi l^2}{N_F}}, & l = 0 \dots N_F - 1, \quad \text{if } N_F \text{ is even} \\ e^{j \frac{M\pi l(l+1)}{N_F}}, & l = 0 \dots N_F - 1, \quad \text{if } N_F \text{ is odd} \end{cases} \quad (4.36)$$

Generally, for a certain dimension N_F of the CAZAC code vector $\underline{\tilde{\mathbf{c}}}$ there is more than one number of M that is relatively prime to N_F . Therefore, there is more than one CAZAC code available based on the construction of the CAZAC code in [BC02]. Since the dimension N_F of Walsh code based pilots is limited to the power of two, CAZAC code based pilots might be more attractive regarding application than Walsh code based pilots in the case that the dimension of training sequences has to be flexible.

Taking the CAZAC code vector $\underline{\tilde{\mathbf{c}}}$ of (4.29) as a mother CAZAC code, a $N_F \times N_F$ matrix

$$\underline{\tilde{\mathbf{A}}}_C = [\underline{\tilde{\mathbf{c}}}_1 \dots \underline{\tilde{\mathbf{c}}}_{n_F} \dots \underline{\tilde{\mathbf{c}}}_{N_F}], \quad n_F = 1 \dots N_F \quad (4.37)$$

can be formed with the n_F -th column

$$\tilde{\mathbf{c}}_{n_F} = \begin{bmatrix} \mathbf{0} & \mathbf{I}_{n_F} \\ \mathbf{I}_{N_F-n_F} & \mathbf{0} \end{bmatrix} \tilde{\mathbf{c}}, \quad n_F = 1 \cdots N_F \quad (4.38)$$

being the CAZAC code vector cyclically shifted by $n_F - 1$ symbols from $\tilde{\mathbf{c}}$ of (4.29).

From the matrix $\tilde{\mathbf{A}}_C$ of (4.37), in the case of a fully loaded system, W submatrices

$$\begin{aligned} \mathbb{P}_{C,1} &= [\tilde{\mathbf{c}}_1 \tilde{\mathbf{c}}_{W+1} \tilde{\mathbf{c}}_{2W+1} \cdots \tilde{\mathbf{c}}_{(U-1)W+1}], \\ \mathbb{P}_{C,2} &= [\tilde{\mathbf{c}}_2 \tilde{\mathbf{c}}_{W+2} \tilde{\mathbf{c}}_{2W+2} \cdots \tilde{\mathbf{c}}_{(U-1)W+2}], \\ &\vdots \\ \mathbb{P}_{C,W} &= [\tilde{\mathbf{c}}_W \tilde{\mathbf{c}}_{2W} \tilde{\mathbf{c}}_{3W} \cdots \tilde{\mathbf{c}}_{N_F}] \end{aligned} \quad (4.39)$$

can be constructed, with each submatrix $\mathbb{P}_{C,w}$, $w = 1 \cdots W$, of dimension $N_F \times U$ containing U columns of the matrix $\tilde{\mathbf{A}}_C$.

In (4.39), each column in a submatrix $\mathbb{P}_{C,w}$, $w = 1 \cdots W$, corresponds to the pilot of one branch so that the U sequences in one submatrix correspond to the U pilots for the frequency domain multiple branches in one SA. The pilots in the other submatrices can be applied to the branches in the other SAs.

In an example case of $N_F = 16$, $U = 4$ and $W = 4$, according to (4.39), the CAZAC code based pilots for the U branches can be obtained as the bold printed columns, i.e. the first, the fifth, the ninth and the thirteenth column of the matrix

$$\tilde{\mathbf{A}}_C = \begin{bmatrix} \mathbf{1} & j & -1 & -j & \mathbf{1} & -1 & 1 & -1 & \mathbf{1} & -j & -1 & j & \mathbf{1} & 1 & 1 & 1 \\ \mathbf{1} & 1 & j & -1 & -\mathbf{j} & 1 & -1 & 1 & -\mathbf{1} & 1 & -j & -1 & \mathbf{j} & 1 & 1 & 1 \\ \mathbf{1} & 1 & 1 & j & -\mathbf{1} & -j & 1 & -1 & \mathbf{1} & -1 & 1 & -j & -\mathbf{1} & j & 1 & 1 \\ \mathbf{1} & 1 & 1 & 1 & \mathbf{j} & -1 & -j & 1 & -\mathbf{1} & 1 & -1 & 1 & -\mathbf{j} & -1 & j & 1 \\ \mathbf{1} & 1 & 1 & 1 & \mathbf{1} & j & -1 & -j & \mathbf{1} & -1 & 1 & -1 & \mathbf{1} & -j & -1 & j \\ \mathbf{j} & 1 & 1 & 1 & \mathbf{1} & 1 & j & -1 & -\mathbf{j} & 1 & -1 & 1 & -\mathbf{1} & 1 & -j & -1 \\ -\mathbf{1} & j & 1 & 1 & \mathbf{1} & 1 & 1 & j & -\mathbf{1} & -j & 1 & -1 & \mathbf{1} & -1 & 1 & -j \\ -\mathbf{j} & -1 & j & 1 & \mathbf{1} & 1 & 1 & 1 & \mathbf{j} & -1 & -j & 1 & -\mathbf{1} & 1 & -1 & 1 \\ \mathbf{1} & -j & -1 & j & \mathbf{1} & 1 & 1 & 1 & \mathbf{1} & j & -1 & -j & \mathbf{1} & -1 & 1 & -1 \\ -\mathbf{1} & 1 & -j & -1 & \mathbf{j} & 1 & 1 & 1 & \mathbf{1} & 1 & j & -1 & -\mathbf{j} & 1 & -1 & 1 \\ \mathbf{1} & -1 & 1 & -j & -\mathbf{1} & j & 1 & 1 & \mathbf{1} & 1 & 1 & j & -\mathbf{1} & -j & 1 & -1 \\ -\mathbf{1} & 1 & -1 & 1 & -\mathbf{j} & -1 & j & 1 & \mathbf{1} & 1 & 1 & 1 & \mathbf{j} & -1 & -j & 1 \\ \mathbf{1} & -1 & 1 & -1 & \mathbf{1} & -j & -1 & j & \mathbf{1} & 1 & 1 & 1 & \mathbf{1} & j & -1 & -j \\ -\mathbf{j} & 1 & -1 & 1 & -\mathbf{1} & 1 & -j & -1 & \mathbf{j} & 1 & 1 & 1 & \mathbf{1} & 1 & j & -1 \\ -\mathbf{1} & -j & 1 & -1 & \mathbf{1} & -1 & 1 & -j & -\mathbf{1} & j & 1 & 1 & \mathbf{1} & 1 & 1 & j \\ \mathbf{j} & -1 & -j & 1 & -\mathbf{1} & 1 & -1 & 1 & -\mathbf{j} & -1 & j & 1 & \mathbf{1} & 1 & 1 & 1 \end{bmatrix}. \quad (4.40)$$

In (4.40), the mother CAZAC code vector $\tilde{\mathbf{c}}$, i.e. the first column of matrix $\tilde{\mathbf{A}}_C$, the elements whose amplitude is 1, is obtained according to [Hei61]. The real and imagery

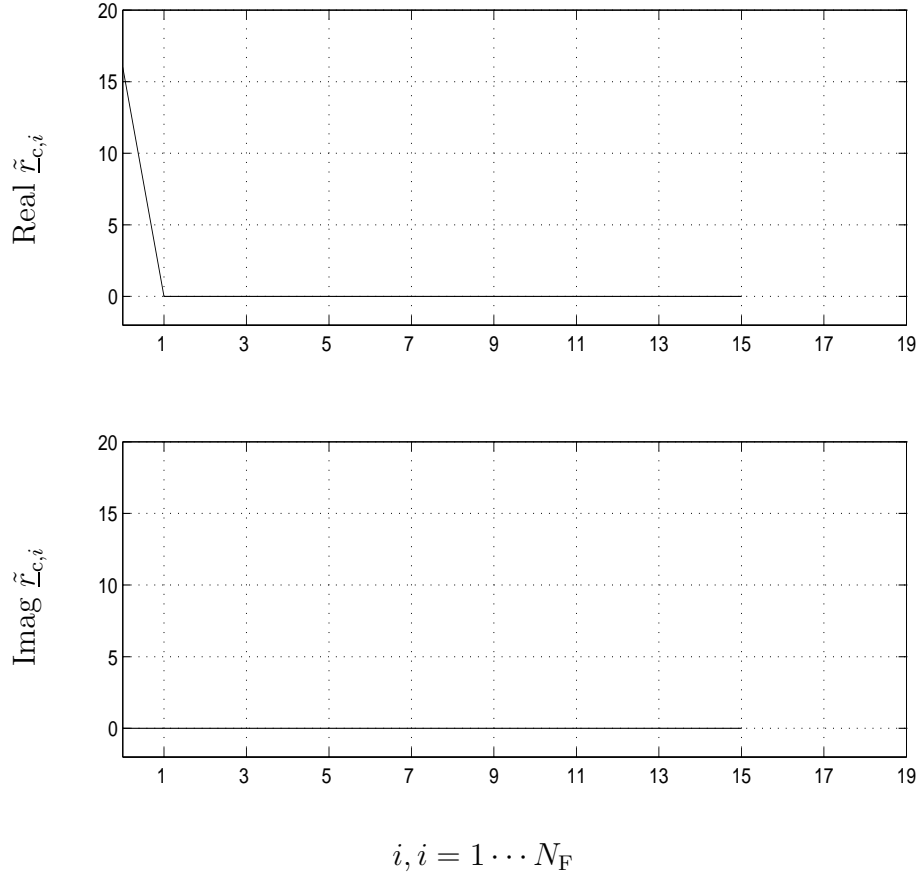


Fig. 4.3. Cyclic autocorrelation of the mother CAZAC code in (4.40).

parts $\text{Real } \tilde{\underline{r}}_{c,i}, i = 1 \dots N_F$, and $\text{Imag } \tilde{\underline{r}}_{c,i}, i = 1 \dots N_F$, of the elements of the cyclic correlation $\tilde{\underline{r}}_c$ of (4.31) of this mother CAZAC code is illustrated in Fig. 4.3.

It is seen from (4.39) that there is more than one set of codes available to be assigned to the U branches of the reference SA, i.e. adjacent SAs can apply different sets of CAZAC code based pilots. Besides, it should be noted that the generation of the pilots according to (4.39) is based on merely one mother CAZAC code $\tilde{\underline{c}}$. Hence, more CAZAC code based pilot resources can be assigned to the branches in all SAs than in the case of Walsh code based pilots, since for a certain dimension N_F there exists generally a certain amount of CAZAC codes, where each of which could act as the mother CAZAC code $\tilde{\underline{c}}$.

Furthermore, CAZAC code based pilots according to (4.39) are shift orthogonal since they have the cyclic correlation properties as shown in Fig. 4.3, they can also be directly constructed from the time domain design criteria of (4.14). This implies that the CAZAC code based pilots constructed according to (4.39) can be applied to the time domain multi-branch systems directly as the optimum pilots.

4.3.5 Proof of the optimum pilots

In this subsection, as an example, the Walsh code based pilots constructed according to (4.27) will be proved to be optimum pilots. The disjoint pilots constructed according to (4.22) and the CAZAC code based pilots constructed according to (4.39) can be verified to be optimum pilots in the similar way. Consequently, this will not be elaborately proved in this Subsection.

In the following, it is sufficient to prove that the design criterion of (4.11) can be fulfilled by their construction of (4.27) since the Walsh code based pilots are designed directly for the use in the frequency domain of multi-branch systems.

Since the column vectors of the Hardamard matrix of (4.26) are orthogonal, the pilots in each set of (4.27) will fulfill the correlation property given in (4.12) under the condition of $w_1 = w_2$. Therefore, in the following, it is to prove that Walsh code based pilots satisfy the design criterion (4.11) under the condition of $w_1 \neq w_2$.

In order to make (4.11) fulfilled, the equation

$$\sum_{n_F=1}^{N_F} e^{-j \frac{2\pi(n_F-1)(w_2-w_1)}{N_F}} = 0, \quad w_1 = 1 \cdots W, w_2 = 1 \cdots W, w_1 \neq w_2, \quad (4.41)$$

can be taken into account with the general assumption that N_F is power of two. The elements in the sum of (4.41) are distributed on the unit circle by exploiting the structure of the Hardamard matrix and by considering that the sum of any two elements which are symmetrical with respect to the center of the unit circle is equal to zero, we can prove that Walsh code based pilots satisfy (4.11) in the following way:

From the structure of the Hardamard matrix $\tilde{\mathbf{A}}_W$ of (4.25), it can be seen that in the case of $W > 1$, i.e. $W = 2, 4, 8, 16, \dots$, with the construction of pilots according to (4.27),

$$\begin{aligned} \tilde{p}_{n_{F1}}^{(u_1)*} \tilde{p}_{n_{F1}}^{(u_2)} &= \tilde{p}_{n_{F2}}^{(u_1)*} \tilde{p}_{n_{F2}}^{(u_2)}, \quad \forall n_{F1}, n_{F2} = 1 \cdots N_F, |n_{F2} - n_{F1}| = \frac{N_F}{2}, \\ u_1 &= 1 \cdots U, \quad u_2 = 1 \cdots U, \quad u_1 \neq u_2, \quad w_1 = 1 \cdots W, \quad w_2 = 1 \cdots W, \quad w_1 \neq w_2, \end{aligned} \quad (4.42)$$

is valid for any scenario with the given parameters N_F, U , and W in fully loaded systems. (4.42) implies that the two coefficients $\tilde{p}_{n_{F1}}^{(u_1)*} \tilde{p}_{n_{F1}}^{(u_2)}$ and $\tilde{p}_{n_{F2}}^{(u_1)*} \tilde{p}_{n_{F2}}^{(u_2)}$ in (4.11) in front of any two elements in (4.41) which are symmetrical to the center of the unit circle, i.e. $|n_{F2} - n_{F1}| = \frac{N_F}{2}$, are equal, which implies that

$$\begin{aligned} \tilde{p}_{n_F}^{(u_1)*} \tilde{p}_{n_F}^{(u_2)} e^{-j \frac{2\pi(n_F-1)(w_2-w_1)}{N_F}} + \tilde{p}_{n_F + \frac{N_F}{2}}^{(u_1)*} \tilde{p}_{n_F + \frac{N_F}{2}}^{(u_2)} e^{-j \frac{2\pi(n_F-1 + \frac{N_F}{2})(w_2-w_1)}{N_F}} &= 0 \\ \forall n_F = 1 \cdots \frac{N_F}{2}, u_1 = 1 \cdots U, u_2 = 1 \cdots U, u_1 \neq u_2, w_1 = 1 \cdots W, w_2 = 1 \cdots W, w_1 \neq w_2. \end{aligned} \quad (4.43)$$

(4.11) will be fulfilled by the summation over $\frac{N_F}{2}$ pairs, i.e. $n_F = 1 \dots \frac{N_F}{2}$, of (4.43). Therefore, the construction of Walsh code based pilots of (4.27) in the case $W > 1$ will fulfill (4.11). In the case of $W = 1$ we have $w_1 = w_2 = 1$. Then, the condition (4.11) is reduced to (4.12), which can be fulfilled by the orthogonality of Walsh codes.

4.4 Suboptimum pilots

The suboptimum pilots refer to those by which neither the time domain design criterion of (4.14) nor the frequency domain design criterion of (4.11) of optimum pilots can be fulfilled.

The easiest way to generate suboptimum pilots is to use random pilots [MWS⁺02]. Random pilots are randomly generated with elements from the set $-1, 1$. Random pilots are used in [MWS⁺02, KMW⁺04] and also in Chapter 7 of this thesis for the performance comparison with the optimum pilots, i.e. disjoint pilots, Walsh code based pilots and CAZAC code based pilots. In addition, a lot of other sequences can be used as the suboptimum pilots without the restriction of the optimum JCE performance in terms of 0 dB SNR degradation.

Basically, the time domain design criterion of (4.14) and the frequency domain design criterion of (4.11) call for sequences with ideal autocorrelation and cross-correlation characteristics, i.e. the sequences involved in Fig. 4.2 or Fig. 4.1 should be mutually orthogonal. The following families of codes, which do not have ideal autocorrelation and cross-correlation, are suboptimum pilots:

- maximum-length sequences (or m-sequences), which are generated using simple linear feedback shift register [BC02]. m-sequences have unideal but good autocorrelation characteristic [BC02].
- gold sequences, which are first proposed in [Gol67]. They are generated from m-sequences and can provide a large number of codes with the same correlation. Gold sequences have good autocorrelation and cross-correlation characteristics [BC02].
- Kasami sequences, which have good cross-correlation properties [Pro95].
- orthogonal Gold sequences, which result from simple modifications of Gold sequences and can provide zero cross-correlation at certain points [DJ98].

Furthermore, with the recent application of space-time block codes [Ala98] with two antennas to the WCDMA [WCDMA], some pilots are proposed for channel estimation.

For example, the two pilots

$$\begin{aligned} p^{(1)} &= (-1 - 111 - 1 - 1 - 11 - 1 - 1 - 1 - 1 - 1 - 111)^T, \\ p^{(2)} &= (-1 - 111111 - 1 - 1 - 1 - 1111 - 11)^T \end{aligned} \quad (4.44)$$

are proposed for the two antennas as the recommended pilots of dimension 16 [WCDMA]. These two pilots $p^{(1)}$ and $p^{(2)}$ are orthogonal. However, they are not shift orthogonal or phase shift orthogonal so that they are suboptimum pilots.

In addition, the pilots obtained by the exhaustive search in [SJ94] for the multiuser CDMA systems are also suboptimum.

4.5 Numerical results of SNR degradations

The numerical results of the SNR degradations $\tilde{\delta}_{\text{MF-LS},j}, j = 1 \cdots UN_{\text{F}}$, of (3.45) of the optimum pilots, i.e. disjoint pilots, Walsh code based pilots and CAZAC code based pilots, as well as of the suboptimum pilots such as random pilots will be shown in this section. The exemplary scenario with $N_{\text{F}} = 64$, $U = 16$, and $W = 4$ is adopted. Disjoint pilots, Walsh code based pilots and CAZAC code based pilots are constructed according to (4.22), (4.27) and (4.39), respectively. As for the CAZAC code based pilots, the mother CAZAC code $\tilde{\mathbf{c}}$ is constructed as in (4.33) through (4.35).

The aforementioned pilots are first applied to the multi-branch system represented in the frequency domain. In Fig. 4.4, the SNR degradations $\tilde{\delta}_{\text{MF-LS},j}$ of (3.45), $j = 1 \cdots UN_{\text{F}}$, of the four classes of pilots for the FD-LS-JCE are plotted versus the index $j, j = 1 \cdots UN_{\text{F}}$, whereas no interference from the neighboring SAs is assumed. It can be observed in Fig. 4.4 that the SNR degradations $\tilde{\delta}_{\text{MF-LS},j}$ have high values if random pilots are applied, while for disjoint pilots, Walsh code based pilots and CAZAC code based pilots, the SNR degradations are 0 dB, which confirms the theoretical analysis of the previous sections.

In the following evaluation, the aforementioned pilots are applied to the time domain multi-branch systems after the IDFT of these pilots. In Fig. 4.5, the SNR degradations $\delta_{\text{MF-LS},j}, j = 1 \cdots UW$, of (3.91) for the TD-LS-JCE of the resulted four kinds of pilots are shown. It is observed that the pilots obtained from the IDFT of the disjoint pilots, Walsh code based pilots and CAZAC code based pilots still result in 0 dB SNR degradations. This verifies the discussions of the equivalence between the time and frequency domain design criteria of optimum pilots in Subsection 4.2.3.

In addition, as discussed in Subsection 4.3.4, the CAZAC code based pilots designed in Subsection 4.3.4 can be directly applied to the time domain multi-branch systems because they fulfill also the time domain design criterion of (4.14). Fig. 4.6 shows the SNR

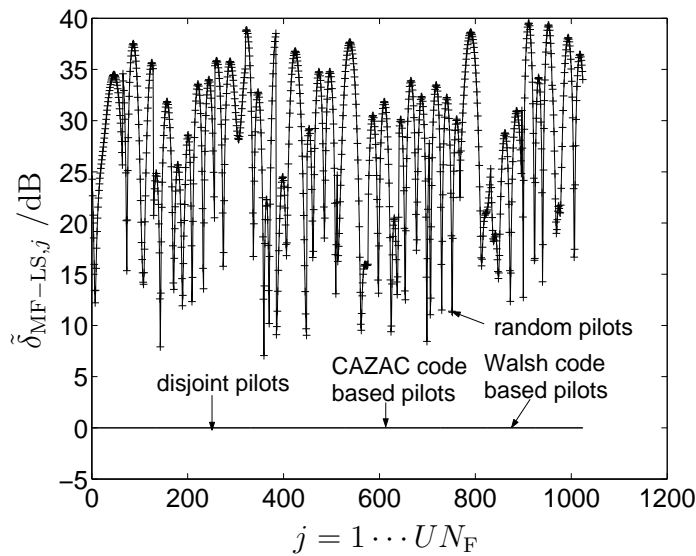


Fig. 4.4. SNR degradations $\tilde{\delta}_{\text{MF-LS},j}$, $j = 1 \dots UN_F$, in dB for the exemplary scenario of $N_F = 64$, $U = 16$ and $W = 4$. Random pilots, disjoint pilots, Walsh code based pilots and CAZAC code based pilots are directly applied to the frequency domain multi-branch system.

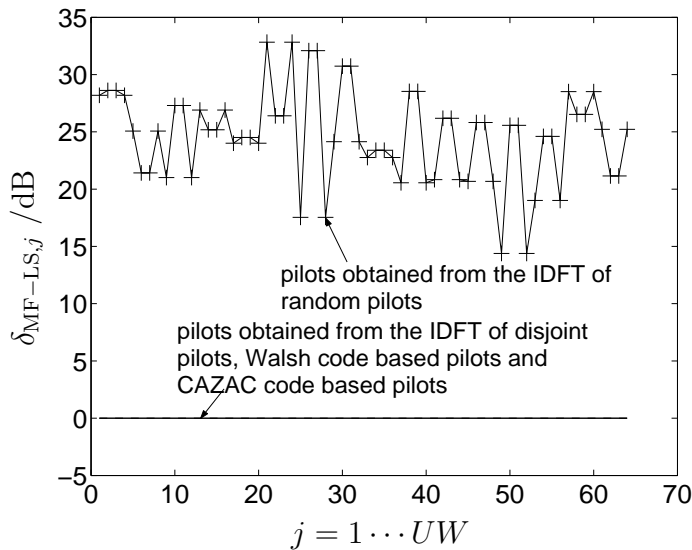


Fig. 4.5. SNR degradation $\delta_{\text{MF-LS},j}$, $j = 1 \dots UW$, in dB for the exemplary scenario of $N_F = 64$, $U = 16$ and $W = 4$. Random pilots, disjoint pilots, Walsh code based pilots and CAZAC code based pilots, after IDFT, are applied to the time domain multi-branch system.

degradations $\delta_{\text{MF-LS},j}$, $j = 1 \cdots UW$, of the time domain direct application of CAZAC code based pilots constructed as (4.33) through (4.35) and the random pilots. It is seen that the CAZAC code based pilots also result in 0 dB SNR degradation with their direct application to the time domain multi-branch systems.

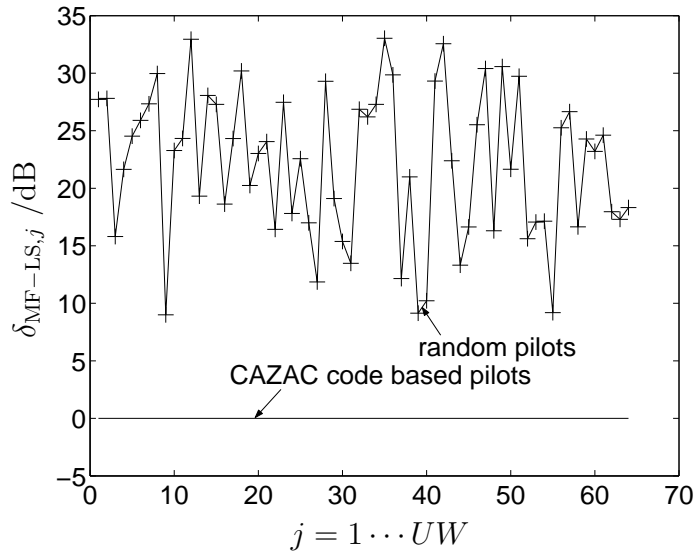


Fig. 4.6. SNR degradation $\delta_{\text{MF-LS},j}$, $j = 1 \cdots UW$, in dB for the exemplary scenario of $N_F = 64$, $U = 16$ and $W = 4$. Random pilots and CAZAC code based pilots are directly applied to the time domain multi-branch system.

5 Pilot assignment in multiple SA environments

5.1 Introduction

In Chapter 4, the pilots for the multiple branches are designed according to the SNR degradation evaluation in noisy environments by considering only one SA in the system. Optimum and suboptimum pilots have been constructed for the time and the frequency domain multi-branch systems. The sets of optimum pilots are disjoint pilots, Walsh code based pilots and CAZAC code based pilots.

In practical mobile radio systems, however, the interference from neighboring SAs is inevitable, which will adversely influence the capacity of the whole system. In the JOINT concept [WMS⁺02], JCE is applied to estimate the channels of the U MTs simultaneously in the considered SA and the MTs in other SAs appear to be interferers to the MTs in the considered SA. In Subsection 3.3.5, the performance of JCE in interference environments is evaluated by the variation coefficient, which, from its definition of (3.68), is influenced by the pilots used in the considered SA and its neighboring SAs. Therefore, it is a big challenge to the system designers to assign pilots to both the considered SA and the neighboring SAs so that the overall system performance can be improved.

The problem of pilot assignment in multiple SA environments is illustrated in Fig. 5.1. As an example, three SAs, SA1, SA2 and SA3, are shown, with three families of pilots, pilot family 1, pilot family 2 and pilot family 3 which are assigned to the MTs in each of the three SAs. Within each SA, the pilots for the multiple branches can be designed according to the investigations in Chapter 4, i.e. if 0 dB SNR degradation is required, the disjoint pilots, the Walsh code based pilots or the CAZAC code based pilots can be applied. However, we have to face with the question that if, for example, SA1 uses the Walsh code based pilots, should the same kind or the different kinds of pilots be selected for SA1, SA2 and SA3?

In this chapter the issue of pilot assignment for the multiple SA scenarios will be investigated. First, in Section 5.2 and Section 5.3, the scenario of two SAs, one reference SA and one neighboring SA, with one single discrete strong interfering signal originating from the adjacent SA, according to the interference model description in Section 2.5, will be considered. The variation coefficient discussed in Subsection 3.3.5 will be used to evaluate the performance in this scenario. If, instead, there are lots of interferers from the neighboring SAs and the signals from all the interferers are statistically independent and uniformly distributed, the pdf of the sum of the interfering signals will be Gaussian according to the central limit theorem [Pro95]. Thereby, the optimum pilots designed in Chapter 4 for one

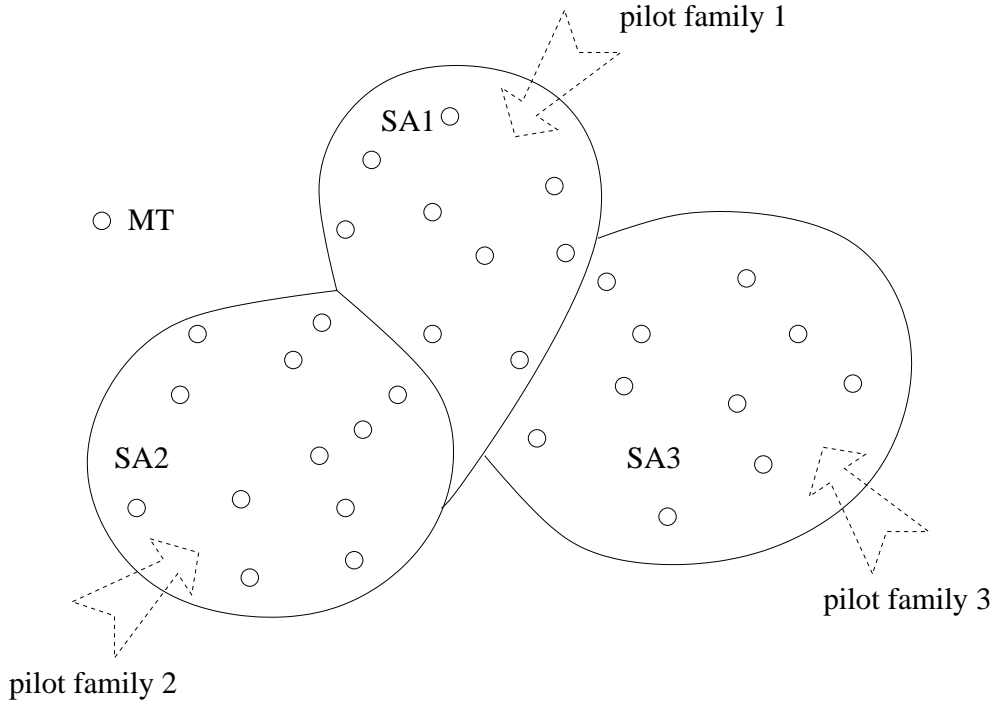


Fig. 5.1. Example of pilot assignment in multiple SAs/interference environments.

single SA in noisy environments will still be the optimum pilots no matter which kinds of optimum pilots are used in the adjacent SAs.

As an example, the frequency domain representation of JCE of Section 3.3 will be considered in each SA. By considering the equivalence between the time and the frequency domain representations of JCE which is discussed in Subsection 3.4.2, the conclusion obtained in this chapter applies also to the time domain multi-branch systems.

Finally, in Section 5.4, the pilot assignment schemes for multi-SA scenarios will be proposed based on the simulation results in Section 5.3.

5.2 Pilot assignment problem in interference environments

It is observed from (3.64) that the JCE error in interference environments depends on

- the correlation properties of the pilots applied to the reference SA characterized by $\tilde{\mathbf{P}}^H \tilde{\mathbf{P}}$ with the pilot matrix $\tilde{\mathbf{P}}$ according to (3.25),

- the correlation properties of the pilots applied to the reference SA and the neighboring SA characterized by $\tilde{\mathbf{P}}^H \tilde{\mathbf{P}}_I$ with the pilot matrix $\tilde{\mathbf{P}}$ of (3.25) and the interfering pilot matrix $\tilde{\mathbf{P}}_I$ of (3.60) of the neighboring SA, and
- the radio channel $\tilde{\mathbf{h}}_I$ of (3.61) between the interferer in the neighboring SA and the receiver in the considered AP.

In the case that the pilots in the reference SA are selected from the optimum pilots, such as disjoint pilots, Walsh code based pilots and CAZAC code based pilots, the sufficient condition of 0 dB SNR degradation of (4.5) will be fulfilled. Substituting (4.5) into the JCE error of (3.64) in multiple SA environment, the JCE error of (3.64) in this case will depend merely on the the correlation properties of the pilots applied to the reference SA and to the adjacent SA characterized by $\tilde{\mathbf{P}}^H \tilde{\mathbf{P}}_I$, and on the interfering radio channel $\tilde{\mathbf{h}}_I$. The design freedom for the good variation coefficient performance then lies in the pilots used in the reference SA embraced in $\tilde{\mathbf{P}}$ of (3.25) and the pilot used in the neighboring SA embraced in $\tilde{\mathbf{P}}_I$ of (3.60).

In particular, the pilots used in the considered SA are chosen among the optimum pilots of disjoint pilots, Walsh code based pilots and CAZAC code based pilots. While the pilot used in the neighboring SA is chosen from one of these three kinds of pilots. Basically, we have the following three options:

1. the interfering pilot is selected as one of the U pilots in the reference SA. Disjoint pilots, Walsh code based pilots and CAZAC code based pilots can be applied to this arrangement.
2. the interfering pilot is different from the U pilots in the reference SA. Nevertheless, it is described from the same kind of pilots as the U pilots in the reference SA. In this case, more pilot resource is required than the option 1. Walsh code based pilots and CAZAC code based pilots can be applied to this arrangement. For CAZAC code based pilots, the pilots in the reference SA and the pilot in the neighboring SA use the same mother CAZAC code.
3. the interfering pilot and the U pilots in the reference SA come from different kinds of pilots. For example, if disjoint pilots are used for the reference SA, then either one pilot from Walsh code based pilots or from CAZAC code based pilots can be used in the neighboring SA. The case that the pilots in the reference SA and its neighboring SA use different mother CAZAC codes is also within this option.

The variation coefficient performance for above three options of pilots will be illustrated in the next section. The variation coefficient v_c of (3.68) describes how uniformly the

interference power is distributed over the subcarriers of multiple branches in the reference SA. The more uniformly the interference spreading over all subcarriers of all branches, the smaller the variation coefficient. In the scenario of using all subcarriers for pilot transmission for both the MTs in the considered SA and the strong interferer from the neighboring SA, the ideal case of uniformly distributed interference power means that the interference signal from the neighboring SA looks like white Gaussian noise to the receiver in the reference SA. The random nature of the random pilots, when applied as the interfering pilot and the U pilots in the reference SA, makes the interfering pilot signal more like white Gaussian noise than the other pilots. Therefore, the random pilots discussed in Section 4.4 will be taken as the reference in the variation coefficient evaluation of various assignments of pilots.

5.3 Variation coefficient simulation

In this section, the variation coefficient performance with the three options for the pilot selection described in Section 5.2 will be demonstrated. Since random channels are considered in the simulation, the variation coefficient is a random variable. Therefore, the cumulative distribution function (cdf) of the variation coefficient v_c of (3.68) can be plotted. The exemplary scenario of $N_F = 64$, $U = 16$ and $W = 4$ is adopted in the simulations.

In the first case, the simulation results of the pdfs of the variation coefficient are shown in Fig. 5.2 according to option 1 in Section 5.2. Disjoint pilots, Walsh code based pilots and CAZAC code based pilots are considered and the random pilots are taken as the reference. For the disjoint pilots, as pointed out in Subsection 4.3.2, the U disjoint pilots constructed as (4.22) are the only possibility of disjoint pilots. The interfering pilot is obtained as the first one of the disjoint pilots derived by $u = 1$ according to (4.22). For the Walsh code based pilots, the pilots of the U branches in the reference SA are obtained from the first submatrix $\mathbb{P}_{W,1}$ of (4.27) and the interfering pilot is obtained from the first column vector $\tilde{\mathbf{w}}_1$ in this submatrix. As for the CAZAC code based pilots, the pilots of the U branches and the interfering pilot are obtained from the first submatrix $\mathbb{P}_{C,1}$ of (4.39) and the first column vector $\tilde{\mathbf{c}}_1$ in this submatrix, respectively. For the random pilots, both the U pilots in the reference SA and the interfering pilot are randomly selected. The random pilots have the same energy E_p as disjoint pilots, Walsh code based pilots and CAZAC code based pilots.

The x-axis V in Fig. 5.2 represents the threshold level of the variation coefficient, and the y-axis represents cdf of the variation coefficient, i.e. the probability of the logarithm of the variation coefficient v_c not exceeding the threshold V , i.e. $\text{Prob}\{10\lg_{10}v_c \leq V\}$. It is seen in Fig. 5.2 that with the arrangement of pilots according to option 1 in Section

5.2, the variation coefficient performances of disjoint pilot, Walsh code based pilots and CAZAC code based pilots are very close since the interfering pilot is the same with one of the U pilots in the reference SA in these cases. For a certain variation coefficient threshold V , the probability of the logarithm variation coefficient v_c not exceeding the threshold V for random pilots is much greater than the other three assignments of pilots. Therefore, the random pilots will produce better performance than the other three assignments of pilots in the system level.

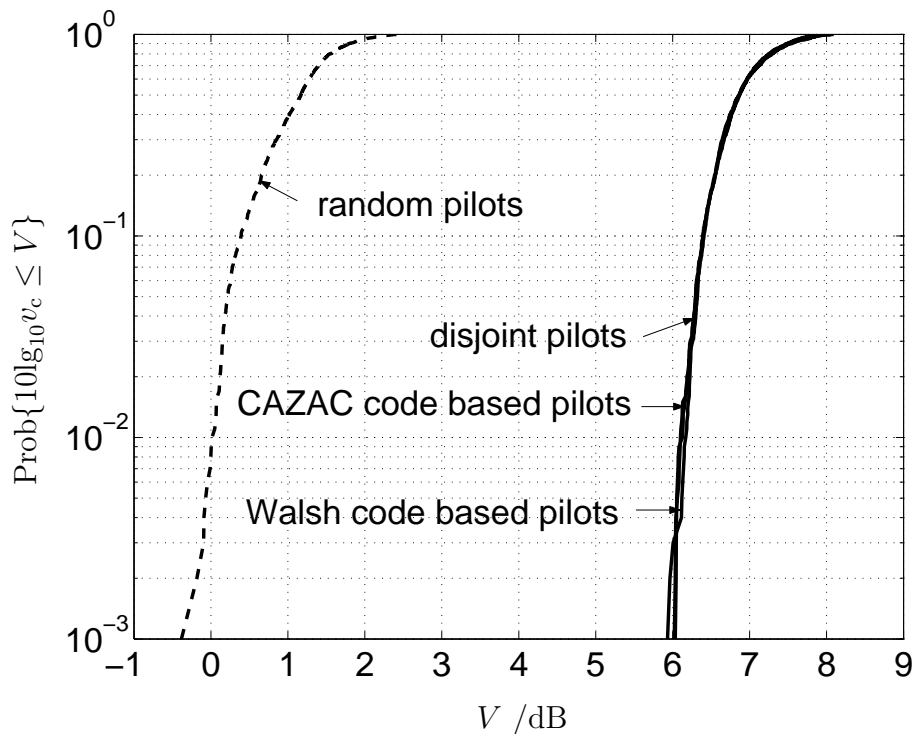


Fig. 5.2. Cdf of the variation coefficient v_c for the exemplary scenario of $N_F = 64$, $U = 16$ and $W = 4$ according to option 1.

In the second case, the simulation results of the cdfs of the variation coefficients based on the pilots arranged according to option 2 in Section 5.2 are demonstrated in Fig. 5.3. Walsh code based pilots and CAZAC code based pilots are applied and random pilots are used as the reference. For the Walsh code based pilots, the pilots of the U branches in the reference SA are obtained from the first submatrix $\mathbb{P}_{W,1}$ in (4.27) and the interfering pilot is selected as the first column vector $\tilde{\mathbf{w}}_{U+1}$ of the second submatrix $\mathbb{P}_{W,2}$ in (4.27). For the CAZAC code based pilots, the pilots of the U branches in the reference SA and the interfering pilot are obtained from the the first submatrix $\mathbb{P}_{C,1}$ and the first column vector $\tilde{\mathbf{c}}_2$ of the second submatrix $\mathbb{P}_{C,2}$ in (4.39), respectively.

It is observed that the performance of Walsh code based pilots and CAZAC code based pilots in the arrangement of pilots according to option 2 in Section 5.2 are close to each

other at lower value of variation coefficient threshold V since their interference pilots are basically constructed in the similar way. However, at higher threshold of V , CAZAC code based pilots underperform Walsh code based pilots. This is because the interfering pilot in the case of the CAZAC code based pilots comes from the same mother CAZAC code $\tilde{\mathbf{c}}$ as the U pilots in the reference SA as seen in (4.39). Therefore, the interfering pilot and the U pilots in the reference SA are more correlated or 'similar' in the case of CAZAC code based pilots than Walsh code based pilots. Both Walsh code based pilots and CAZAC code based pilots underperform random pilots with the arrangement of pilots according to option 2.

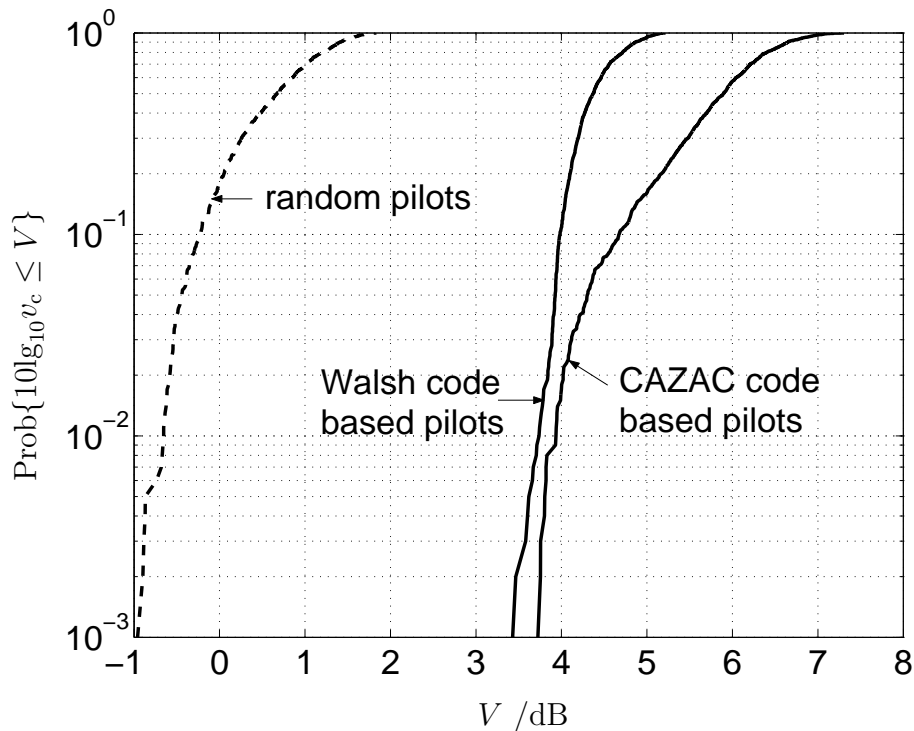


Fig. 5.3. Cdf of the variation coefficient v_c for the exemplary scenario of $N_F = 64$, $U = 16$ and $W = 4$ according to option 2.

In the third case, the cdfs of the variation coefficients based on the pilots arranged according to option 3 in Section 5.2 are investigated. The various combinations of pilots of the U pilots in the reference SA and the interfering pilot are listed in Table 5.1. There are in total six combinations C1 through C6 if disjoint pilots, Walsh code based pilots and CAZAC code based pilots are considered. For example, the combination C2 in Table 5.1 represents that the U pilots in the reference SA are obtained from the Walsh code based pilots, e.g. the submatrix $\mathbb{P}_{W,1}$ in (4.27), and the interfering pilot is obtained from one pilot $\tilde{\mathbf{p}}_D^{(1)}$ of (4.22) of the disjoint pilots.

The cdfs of variation coefficients of the six combination of pilots as Table 5.1 are demon-

Table 5.1. Various combination of pilots.

Combination index	The U pilots $\underline{\mathbf{P}}$ in the reference SA	The interfering pilot $\underline{\mathbf{P}}_I$
C1	disjoint pilots of (4.22)	a Walsh code $\underline{\tilde{\mathbf{w}}}_1$ in (4.27)
C2	Walsh code based pilots $\mathbb{P}_{W,1}$ in (4.27)	a disjoint pilot $\underline{\tilde{\mathbf{p}}}_D^{(1)}$ of (4.22)
C3	Walsh code based pilots $\mathbb{P}_{W,1}$ in (4.27)	a CAZAC code obtained from [Hei61]
C4	CAZAC code based pilots $\mathbb{P}_{C,1}$ in (4.39) whose mother CAZAC code comes from [Hei61]	a Walsh code $\underline{\tilde{\mathbf{w}}}_1$ in (4.27)
C5	disjoint pilots of (4.22)	a CAZAC code obtained from [Hei61]
C6	CAZAC code based pilots $\mathbb{P}_{C,1}$ in (4.39) whose mother CAZAC code comes from [Hei61]	a disjoint pilot $\underline{\tilde{\mathbf{p}}}_D^{(1)}$ of (4.22)

strated in Fig. 5.4. It is seen in Fig. 5.4 that the six combinations of pilots, C1 through C6, in Table 5.1 result in a variation coefficient performance which is comparable to the random pilots. In particular, the third combination C3 of the Walsh code based pilots $\mathbb{P}_{W,1}$ in (4.27) applied to the U branches in the reference SA and a pilot $\underline{\tilde{\mathbf{c}}}_1$ in (4.39) from the CAZAC code based pilots considered as the interfering pilot shows the best performance.

Furthermore, as stated in Subsection 4.3.4, for CAZAC code based pilots, the mother CAZAC code can be obtained from several methods, such as from [Hei61] whose generation is given by (4.33) through (4.35) and from [BC02] whose generation is given by (4.36). Even for one generation method of CAZAC codes, i.e. [BC02], for a certain dimension N_F of the pilots, more than one CAZAC code can be generated with the different choice M in (4.36), each of which can serve as a mother code in the construction of CAZAC code based pilots of (4.39). With different mother CAZAC codes, different CAZAC code based pilots of (4.39) can be obtained. The case of using different CAZAC code based pilots in different SAs is taken as the special case of option 3 in Section 5.2. In Table 5.2, the three combinations CA1 to CA3 of pilots based on different mother CAZAC code based pilots for the U pilots in the reference SA and the interfering pilot in the neighboring SA are listed. In the first combination CA1, the U pilots in the reference SA are obtained from the CAZAC code based pilots $\mathbb{P}_{C,1}$ in (4.39) whose mother CAZAC code is generated from [Hei61] as (4.33) through (4.35), while the interfering pilot is generated from [BC02]

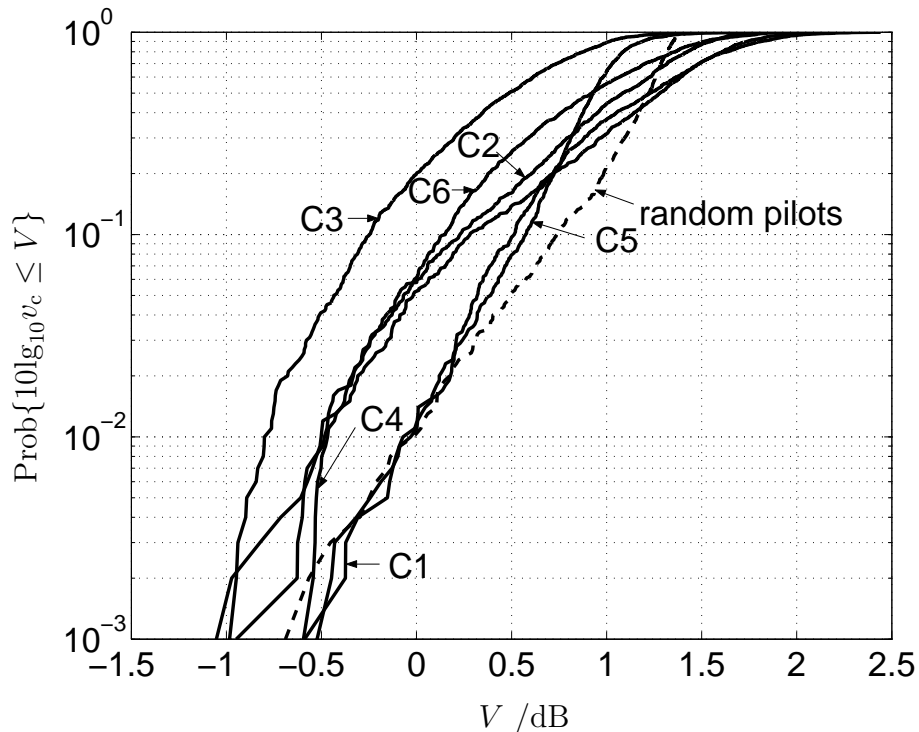


Fig. 5.4. Cdf of the variation coefficient v_c for the exemplary scenario of $N_F = 64$, $U = 16$ and $W = 4$ according to option 3 (see also Table 5.1).

with $M = 3$ in (4.36). In the second combination CA2, the U pilots in the reference SA are obtained from the CAZAC code based pilots $\mathbb{P}_{C,1}$ in (4.39) whose mother CAZAC code comes from [BC02] with $M = 3$ in (4.36), while the interfering pilot is obtained from [Hei61] as (4.33) through (4.35). In the third combination CA3, both the mother code of the U pilots for the reference SA and the interfering pilot are obtained from [BC02] as (4.36). However, they come from two different mother CAZAC codes with $M = 3$ and $M = 7$, respectively.

In Fig. 5.5 the cdfs of variation coefficient of the three combinations of pilots CA1, CA2 and CA3 of Table 5.2 are simulated. It is observed in Fig. 5.5 that all of the three combinations of CAZAC code based pilots produce the variation coefficient performance much better than the random pilots. For example, the combination of CA3 results the variation coefficient performance 4.4 dB better than the random pilots at the probability level of 10^{-2} . Comparing Fig 5.5 with Fig. 5.4, it is seen that the variation coefficient performance of the three combinations CA1 to CA3 of Table 5.2 is also better than the combinations C1 to C6 of Table 5.1. The simulation results of Fig. 5.5 encourages the use of CAZAC code based pilots with different mother codes to different SAs.

Table 5.2. Two combination of pilots based on CAZAC code based pilots.

Combination index	The U pilots $\underline{\mathbf{P}}$ for the reference SA	The interfering pilot $\underline{\mathbf{P}}_I$
CA1	CAZAC code based pilots $\mathbb{P}_{C,1}$ in (4.39), whose mother CAZAC code comes from [Hei61]	a CAZAC code obtained from [BC02] with $M = 3$
CA2	CAZAC code based pilots $\mathbb{P}_{C,1}$ in (4.39), whose mother CAZAC code comes from [BC02] with $M = 3$	a CAZAC code obtained from [Hei61]
CA3	CAZAC code based pilots $\mathbb{P}_{C,1}$ in (4.39), whose mother CAZAC code comes from [BC02] with $M = 3$	a CAZAC code obtained from [BC02] with $M = 7$

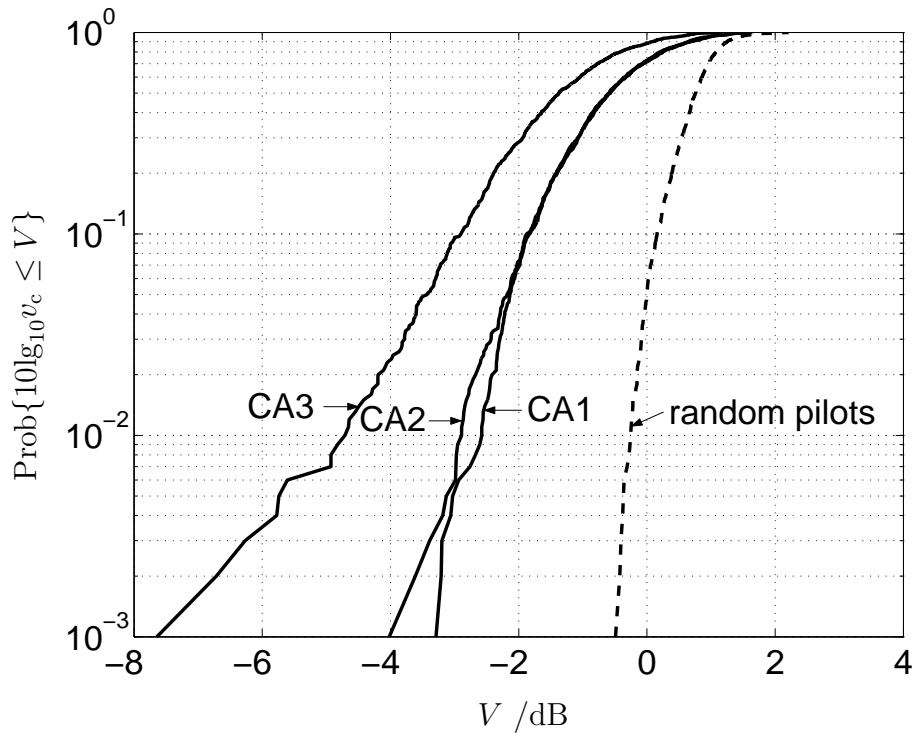


Fig. 5.5. Cdf of the variation coefficient v_c for the exemplary scenario of $N_F = 64$, $U = 16$ and $W = 4$ according to option 3 (see also Table 5.2).

5.4 Proposals of pilot assignment for multiple SAs

Comparing the curves in Fig. 5.4 and Fig. 5.5 with Fig. 5.2 and Fig. 5.3, it can be observed that the variation coefficient performance in the cases that different kinds of pilots, as in Table 5.1 or in Table 5.2, are applied to the reference SA and its neighboring SA will be much better than in the cases that the same kind of pilots, as the options 1 and 2 in Section 5.2, are applied to the different SAs.

The scenario of multiple SAs is the extension of the scenario of two SAs. Therefore, the observation in Section 5.3 based on the simulation results applies to the scenario of multiple SA also.

Based on the simulation results in Fig. 5.4, one scheme of pilot assignment is proposed in Fig. 5.6 providing one possible solution of a pilot assignment that could be beneficial from the interference point of view to the challenge of pilot assignment illustrated in Fig. 5.1. Basically, as shown in Fig. 5.6, different kinds of optimum pilots from the disjoint pilots, the Walsh code based pilots and the CAZAC code based pilots are assigned to different SAs. For example, if disjoint pilots are assigned to the U branches in the reference SA1, the CAZAC code based pilots and the Walsh code based pilots will be applied to the adjacent SA2 and SA3, respectively. Fig. 5.6 illustrates the basic cluster of pilot assignment, which can be extended physically by reusing the certain kind of pilots in the far SAs. With the pilot assignment as in Fig. 5.6, the U pilots for each SA are the optimum pilots with 0 dB SNR degradation, and the interference power with this arrangement of different kinds of pilots to different SAs fluctuates less than the other pilot arrangements of options 1 and 3 in Section 5.2, which makes the behavior of interference more similar to white noise. This will produce better channel estimation quality in multiple SA environment. Hence, less bit error rate (BER) can be expected. Or equivalently say, more users can be transmitted for a certain BER level. Therefore, the pilot assignment as proposed in Fig. 5.6 is expected to increase the system capacity than the other arrangements of options 1 and 3 in Section 5.2 when system level simulation is investigated.

However, as will be elaborately discussed in Chapter 6, the disjoint pilots and the Walsh code based pilots have worse PAPR performance than the CAZAC code based pilots [KMW⁺04]. So the former two kinds of pilots challenges the hardware implementation of the system. By considering this issue, another scheme of pilot assignment is proposed in Fig. 5.7, which is inspired by the simulation results in Fig. 5.5. Three different mother CAZAC codes are chosen in the three SAs, resulting CAZAC code based pilots 1, CAZAC based pilots 2 and CAZAC code based pilots 3 assigned to the multiple branches in SA1, SA2, and SA3, respectively. The advantages with the assignment of pilots as in Fig. 5.7 are

- the pilots in each SA are the optimum pilots by which 0 dB SNR degradation can be obtained,

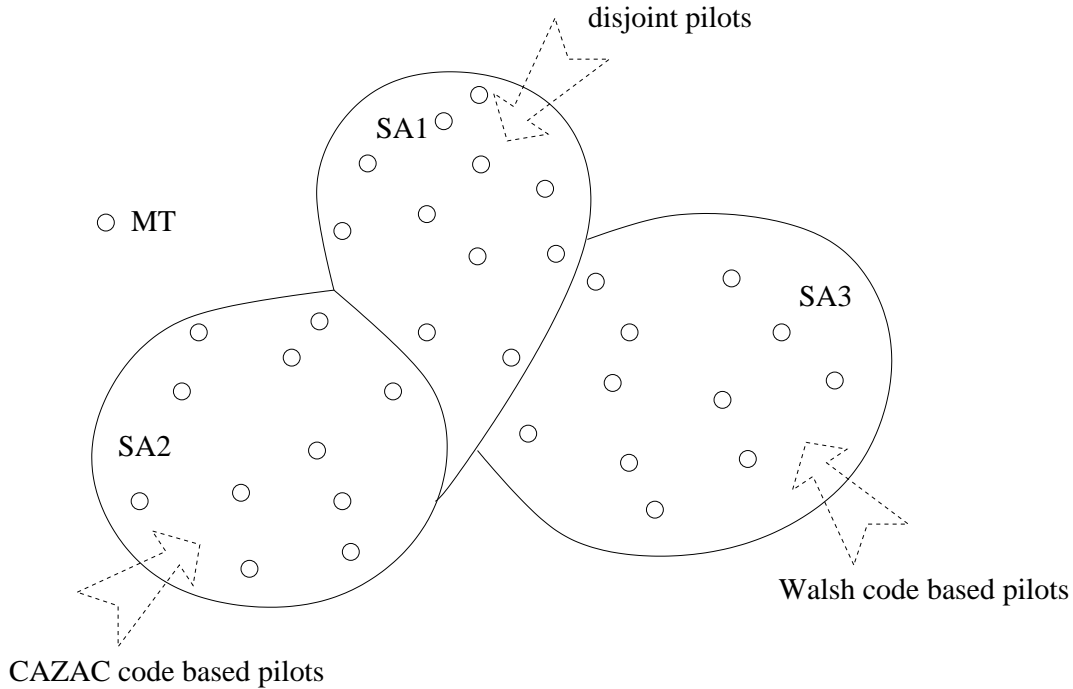


Fig. 5.6. The first proposal on the allocation of pilots to the multiple SAs.

- the interference power fluctuates slightly so that the good system performance can be expected,
- the PAPR problem is alleviated in each SA.

It is of particular interest with the arrangement of pilots as Fig. 5.7 in the scenario that more than three SAs are adjacent to the considered SA. In this scenario, since for a certain dimension N_F of pilots, there are normally amount of CAZAC code based pilots available with different mother CAZAC codes, the arrangement of pilots as indicated by Fig. 5.7 will be directly derivable. However, if the arrangement of pilots as indicated by Fig. 5.6 is taken, then some new kinds of optimum pilots apart from the disjoint pilots, Walsh code based pilots and CAZAC code based pilots have to be found and constructed in this scenario.

As discussed in Subsection 4.2.3, the equivalence between the time domain and the frequency domain design criteria of optimum pilots explained in this section increases the number of available optimum pilots for either time or frequency domain JCE in multi-branch systems. The increase of available optimum pilots raises the potential to assign different pilots to different SAs, therefore, to improve the overall system performance for both time and frequency domain multi-branch systems in multiple SA environments.

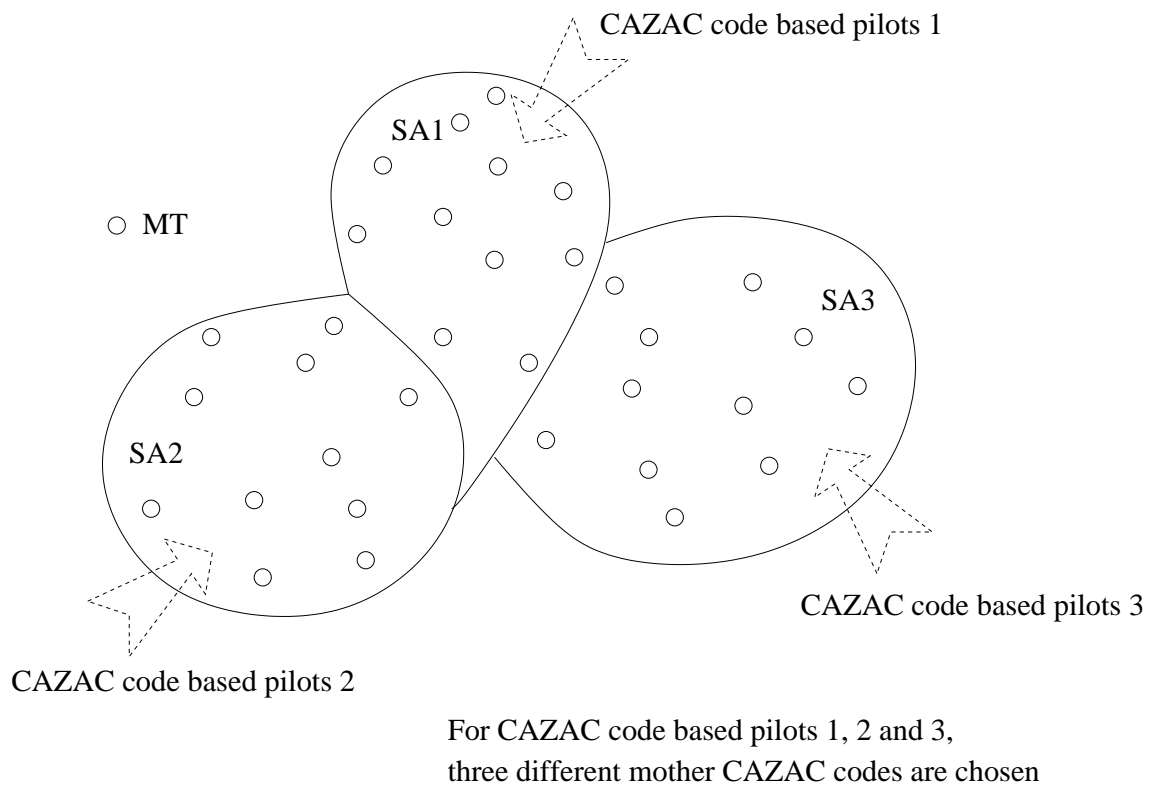


Fig. 5.7. The second proposal on the allocation of pilots to the multiple SAs.

6 Application of JCE in OFDM and FMT based multi-branch systems

6.1 Introduction

Despite the equivalence regarding time and frequency domain representations as discussed in Section 3.4, the JCE technique has practically developed into the time and frequency domain applications due to some implementation considerations concerning the implementation complexity and the PAPR. In this chapter, two application issues will be investigated concerning the JCE technique as well the pilots. The first investigation addresses the complexity evaluation of the TD-JCE and FD-JCE, based on which the choice of processing JCE in the time domain or the frequency domain according to the complexity will be made. The second investigation addresses the evaluation of PAPR of various pilots, which is critical, if the efficiency of the radio frequency (RF) power amplifier is taken into account.

In Section 6.2, the OFDM and FMT multi-carrier transmissions will be shortly introduced. In Section 6.3, the choice of either time or frequency domain JCE for OFDM and FMT systems will be discussed according to the evaluation of the processing complexity of the TD-LS-JCE and the FD-LS-JCE. The PAPR issue will be discussed in Section 6.4 especially for OFDM systems. A general discussion on the applications of various optimum pilots proposed in Section 4.3, i.e. disjoint pilots, Walsh code based pilots and CAZAC code based pilots, follows in Section 6.5 according to the performance of these pilots in a noisy environment, in an interference environment as well as to their PAPR properties.

6.2 Multi-carrier systems

6.2.1 Introduction

The application scenarios for JCE considered in this thesis are OFDM and FMT based multi-carrier multi-branch systems. Before discussing the suitability of either the time or the frequency domain JCE to OFDM and FMT based systems, which is carried out in the following Section 6.3, the well known OFDM and FMT multi-carrier modulation schemes will be briefly recapitulated in this section.

Both OFDM and FMT belong to the general family of filter bank multi-carrier (FB-MC) modulation systems, in which parallel data streams are filtered by interpolating filters with proper spectrum characteristics. If all the filters are frequency-shifted versions of

one prototype filter and the sub-carriers are equally spaced, then the FB-MC scheme can be efficiently implemented through a bank of prototype filters and FFT [BC02, Fil04].

The general FB-MC modulation will be described in Subsection 6.2.2, with a general model illustrated for the FB-MC modulation. Both the OFDM and the FMT modulated multi-carrier transmission can be depicted by this general model, which will be discussed in Subsections 6.2.3 and 6.2.4, respectively. Ideally the selected prototype filter in the general model should be well localized in both the time and frequency domains to guarantee the complete elimination of ISI and ICI [Bol99].

6.2.2 FB-MC modulation

Fig. 6.1 depicts the discrete time model of the general FB-MC modulation scheme. N_F represents the number of subcarriers, T denotes the multi-carrier symbol duration, i.e. the time separation between two consecutive data symbols transmitted on one subcarrier. F represents the subcarrier spacing. In this scheme the parallel data streams $\underline{a}_0(lT)$ through $\underline{a}_{N_F-1}(lT)$ are upsampled by a factor Q to produce the transmit signals with symbol rate Q/T . The resulting signals are then filtered by the same transmit prototype filter $\underline{c}_0(lT/Q)$ and are then allocated in the proper frequency region by the modulation $e^{j2\pi(0)FlT/Q}$ through $e^{j2\pi(N_F-1)FlT/Q}$ on each subcarrier.

With the subcarrier spacing

$$F = \frac{Q}{N_F T}, \quad (6.1)$$

and with reference to Fig. 6.1, the transmitted signal

$$\underline{x}\left(l\frac{T}{Q}\right) = \sum_{n_F=0}^{N_F-1} \sum_{n=0}^{+\infty} \underline{a}_{n_F}(nT) \underline{c}_0\left[(l-nQ)\frac{T}{Q}\right] e^{j2\pi\frac{n_F Q}{T N_F}\left(l\frac{T}{Q}\right)}, \quad l = 0 \cdots +\infty \quad (6.2)$$

is obtained. From (6.2) it may be observed that each data symbol $\underline{a}_{n_F}(nT)$ is associated with a signature

$$\underline{c}_{n_F}\left((l-nQ)\frac{T}{Q}\right) = \underline{c}_0\left[(l-nQ)\frac{T}{Q}\right] e^{j2\pi\frac{n_F Q}{T N_F}\left(l\frac{T}{Q}\right)}, \quad l = 0 \cdots +\infty, n = 0 \cdots +\infty. \quad (6.3)$$

The received signal $\underline{y}(lT/Q)$ is obtained as the convolution of the transmitted signal $\underline{x}(lT/Q)$ of (6.2) and the CIR $\underline{h}(\tau, lT/Q)$ corrupted by the AWGN noise $\underline{n}(lT/Q)$, i.e.

$$\underline{y}(lT/Q) = \sum_{\tau=0}^{+\infty} \underline{x}\left(l\frac{T}{Q} - \tau\right) \underline{h}\left(\tau, l\frac{T}{Q}\right) + \underline{n}\left(l\frac{T}{Q}\right), \quad l = 0 \cdots +\infty. \quad (6.4)$$

At the receiver, the receive signal $\underline{y}(lT/Q)$ is first demodulated by the multiplication with $e^{-j2\pi(n_F-1)FlT/Q}$, $n_F = 1 \cdots N_F$, on each subcarrier, and then passed through a bank of

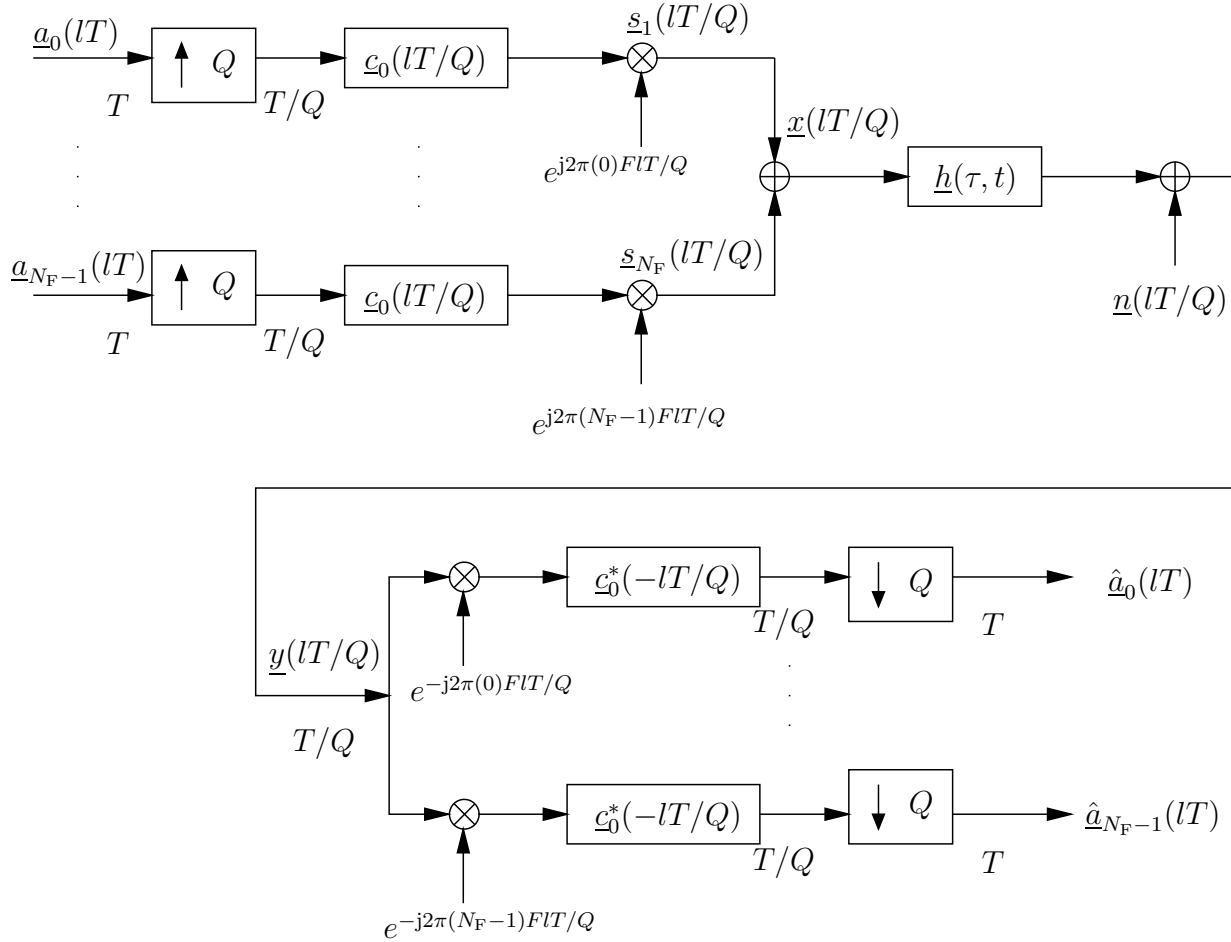


Fig. 6.1. The discrete time model of the general FB-MC modulation scheme.

receive prototype filter $\underline{c}_0^*(-lT/Q)$. The receive prototype filter $\underline{c}_0^*(-lT/Q)$ is matched to the transmit prototype filter $\underline{c}_0(lT/Q)$. The resulting signal is then down sampled by the factor Q to obtain the signal with the transmission rate $1/T$. The receive symbols $\hat{\underline{a}}_0(lT)$ through $\hat{\underline{a}}_{N_F-1}(lT)$ are expected to be further processed to improve the performance of the system.

6.2.3 OFDM modulation

With $Q = N_F$, the system is critically sampled [BC02]. This is the case for OFDM systems. In this case, by inverting the sums and letting

$$l \frac{T}{N_F} = mT + i \frac{T}{N_F}, \quad m = 0 \cdots +\infty, i = 0 \cdots N_F - 1, \quad (6.5)$$

(6.2) can be represented as [Fil04]

$$\underline{x}(mT + i\frac{T}{N_F}) = \sum_{n=0}^{+\infty} \sum_{n_F=0}^{N_F-1} \underline{a}_{n_F}(nT) e^{j2\pi i \frac{n_F}{N_F}} \underline{c}_0(mT + i\frac{T}{N_F} - nT), \quad m = 0 \cdots +\infty, i = 0 \cdots N_F - 1, \quad (6.6)$$

in which the second sum is the IDFT of the transmit symbols, i.e.

$$\underline{A}_i(nT) = \sum_{n_F=0}^{N_F-1} \underline{a}_{n_F}(nT) e^{j2\pi i \frac{n_F}{N_F}} = \text{IDFT}[\underline{a}_{n_F}(nT)]. \quad (6.7)$$

By substituting (6.7) into (6.6), it reads as

$$\underline{x}(mT + i\frac{T}{N_F}) = \sum_{n=0}^{+\infty} A_i(nT) \underline{c}_0(mT + i\frac{T}{N_F} - nT), \quad m = 0 \cdots +\infty, i = 0 \cdots N_F - 1. \quad (6.8)$$

With (6.8), the complexity of implementing the general FB-MC system illustrated in Fig. 6.1 is reduced significantly thanks to the use of the IDFT operation, which can be carried out via the FFT algorithm. The complexity can be further reduced by the polyphase decomposition which eliminates the multiplications by zero introduced by the upsampling operation [BC02].

In the OFDM system, the transmit prototype filter $\underline{c}_0(lT/Q)$ in Fig. 6.1 is chosen to have rectangular shape in the time domain, i.e.

$$\underline{c}_0(lT/Q) = \begin{cases} 1 & 0 \leq l \leq N_F - 1 \\ 0 & \text{elsewhere} \end{cases} \quad (6.9)$$

With (6.9) and with $0 \leq i \leq M - 1$, the elements of the sum in (6.8) are not zero only for $n = m$, so that (6.8) can be reduced to

$$\underline{x}(mT + i\frac{T}{N_F}) = A_i(mT), \quad m = 0 \cdots +\infty, i = 0 \cdots N_F - 1, \quad (6.10)$$

which is obtained by the IDFT of the input data stream.

Fig. 6.2 illustrates the frequency spectrum of an OFDM system with the exemplary case of $Q = 16$ and $N_F = 16$. The x-axis fT represents the normalized frequency band with respect to the subcarrier spacing F , which is the inverse of symbol duration T in the OFDM system. The y-axis $20\log_{10}(|C(f)|)$ /dB represents the amplitude of the spectrum in dB.

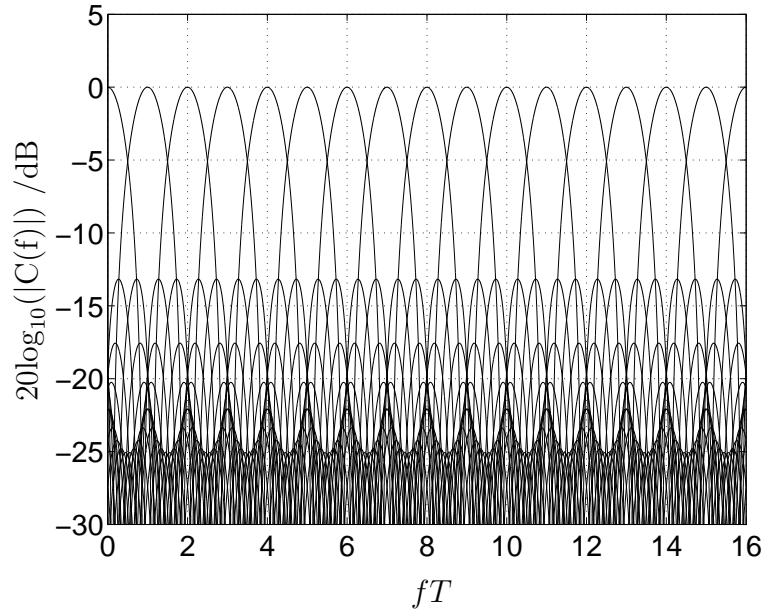


Fig. 6.2. Frequency spectrum in an OFDM system with the exemplary case of $Q = 16$ and $N_F = 16$.

6.2.4 FMT modulation

In the general FB-MC scheme illustrated in Fig. 6.1, with $Q > N_F$, the system is not critically sampled [BC02], which is the case in FMT systems. In this case, with every N_F input samples Q output samples are obtained. Therefore, a redundancy related to the factor Q/N_F is introduced. An excess bandwidth is introduced that allows the transition region of the prototype filter to be enlarged of a factor of $\alpha = Q/N_F$.

In Fig. 6.3 it is shown that a part of the bandwidth is used for the transition region of the prototype filter [Fil04]. With such an approach ICI is significantly reduced since ideally,

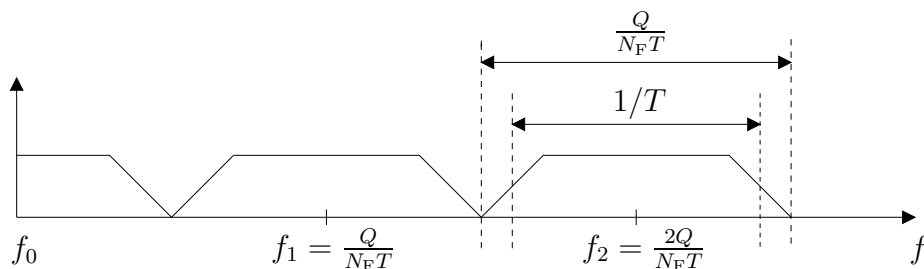


Fig. 6.3. Not critically sampling in FMT systems.

i.e. with infinitive length of the prototype filter, there is no crossover among adjacent carriers.

In the following, $m = 0 \cdots +\infty$ and $i = 0 \cdots N_F - 1$ are assumed. In the not critically sampled case with $Q > N_F$, by letting

$$l \frac{T}{N_F} = (mN_F + i) \frac{T}{N_F}, \quad (6.11)$$

(6.2) can be represented as [Fil04]

$$\underline{x}(mN_F \frac{T}{Q} + i \frac{T}{Q}) = \sum_{n=0}^{+\infty} \sum_{n_F=0}^{N_F-1} \underline{a}_{n_F}(nT) e^{j2\pi \frac{n_F Q}{T N_F} (mN_F \frac{T}{Q} + i \frac{T}{Q})} \underline{c}_0[(mN_F + i - nQ) \frac{T}{Q}]. \quad (6.12)$$

By considering (6.7), (6.12) can be rewritten as

$$\underline{x}(mN_F \frac{T}{Q} + i \frac{T}{Q}) = \sum_{n=0}^{+\infty} \underline{A}_i(nT) \underline{c}_0(mN_F \frac{T}{Q} + i \frac{T}{Q} - nTQ). \quad (6.13)$$

With (6.13), the complexity of implementing the not critically sampled FB-MC system is reduced by FFT algorithm. The complexity can be further reduced by polyphase decomposition [CEÖ02].

In the FMT system, the prototype filter $\underline{c}_0(lT/Q)$ is chosen to have a well localized shape in the frequency domain. Hence, by means of not critically sampling, it may be guaranteed that no overlapping (in the ideal case of the prototype filter with unlimited length) or almost no overlapping (in the practical case the prototype filter with limited length by windowing) occurs between adjacent sub-carriers. For example, the almost no overlapping condition may be fulfilled by windowing the prototype filter of a root raised cosine (rrcos) with roll-off factor $\rho \leq \alpha$, which is given by [Fil04]

$$\sqrt{\text{rcos}(x, \alpha)} = \begin{cases} 1 & \text{for } 0 \leq |x| \leq \frac{1-\alpha}{2}, \\ \cos\left(\frac{\pi}{2} \frac{|x| - \frac{1-\alpha}{2}}{\alpha}\right) & \text{for } \frac{1-\alpha}{2} < |x| \leq \frac{1+\alpha}{2}, \\ 0 & \text{for } |x| > \frac{1+\alpha}{2}. \end{cases} \quad (6.14)$$

Fig. 6.4 depicts the frequency spectrum in the case of rrcos with $\rho = 0.15$ for the not critically sampling with $Q = 18$ and $N_F = 16$. The x-axis fN_FT/Q represents the normalized frequency band with respect to the subcarrier spacing F , which is given by $Q/(N_FT)$ in the FMT system. The y-axis $20\log_{10}(|C(f)|)$ /dB represents the amplitude of the spectrum in dB. The high spectral containment of FMT systems as seen in Fig.6.4 makes them particularly robust to time and frequency synchronization offsets. This is achieved with the expense of bandwidth efficiency by introducing frequency redundancy.

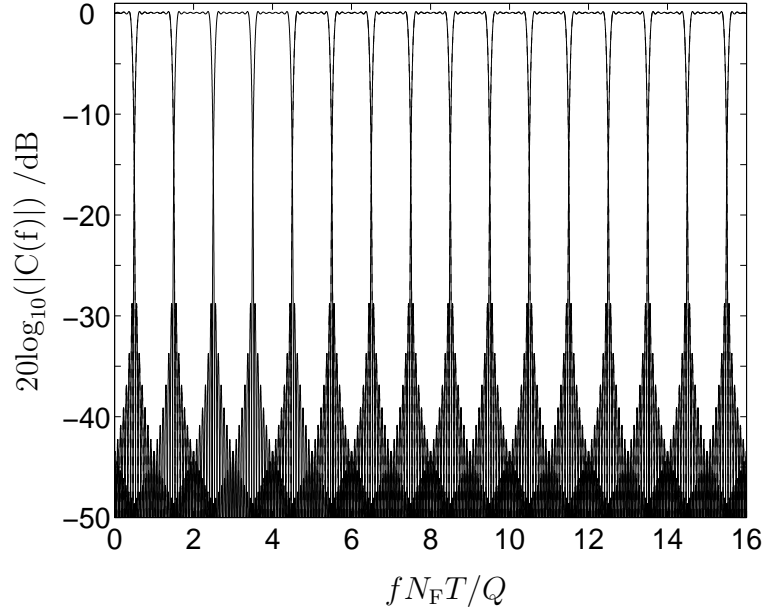


Fig. 6.4. Frequency spectrum of the square-root raised cosine prototype filter with the roll-off factor of 0.15 in the case of $Q = 18$, $N_F = 16$ in the FMT system.

6.3 Time versus frequency domain JCE for OFDM and FMT systems

In this section, the choice of either time or frequency domain JCE according to their processing complexity for OFDM and FMT systems is considered. For this reason, the processing complexity for implementing the TD-LS-JCE and the FD-LS-JCE is firstly evaluated and compared. $L_p = N_F$ is assumed in the evaluation.

With the time domain receive signal vector \mathbf{r} of dimension L_p , see (3.81), and with the time domain total pilot matrix \mathbf{P} of (3.70) of dimension $L_p \times (UW)$, the TD-LS-JCE estimate $\hat{\mathbf{h}}_{LS}$ of the total CIR \mathbf{h} of (2.28) is obtained according to (3.86). From (3.86), the process of the TD-LS-JCE can be decomposed into the two steps of matched filtering and sidelobe cancellation filter [FB92] as shown in Fig. 6.5. The matched filtering on the receive signal vector \mathbf{r} results the TD-MF-JCE $\hat{\mathbf{h}}_{MF}$ of (3.85). The sidelobe filtering of $\hat{\mathbf{h}}_{MF}$ yields the TD-LS-JCE $\hat{\mathbf{h}}_{LS}$ of (3.86).

With the frequency domain receive signal vector $\tilde{\mathbf{r}}$ of dimension N_F , see (3.28), and with the matrix $\tilde{\mathbf{G}}$ of (3.28) of dimension $N_F \times (UW)$, the FD-LS-JCE estimate $\hat{\mathbf{h}}_{LS}$ of the total CTF $\tilde{\mathbf{h}}$ of (3.20) is obtained according to (3.40). From (3.40), the process of the FD-LS-JCE can be decomposed into the three steps of matched filtering, sidelobe cancellation filter and the Fourier transformation as shown in Fig. 6.6. Matched filtering of the receive

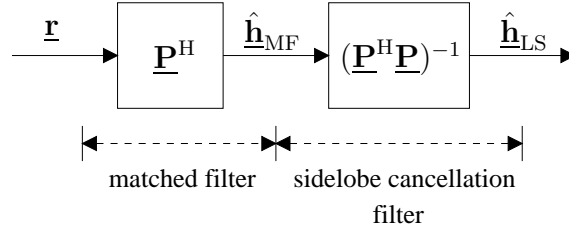


Fig. 6.5. Decomposition of the TD-LS-JCE.

signal vector $\tilde{\mathbf{r}}$ yields the FD-MF-JCE estimate $\hat{\mathbf{h}}_{\text{MF}}$ of (3.32) on the total CIR \mathbf{h} of (2.28). The sidelobe filtering of $\hat{\mathbf{h}}_{\text{MF}}$ results in the FD-LS-JCE estimate $\hat{\mathbf{h}}_{\text{LS}}$ of (3.34) of the total CIR \mathbf{h} of (2.28). The Fourier transformation of $\hat{\mathbf{h}}_{\text{LS}}$ results in the FD-LS-JCE estimate $\hat{\tilde{\mathbf{h}}}_{\text{LS}}$ of the total CTF $\tilde{\mathbf{h}}$ of (3.20).

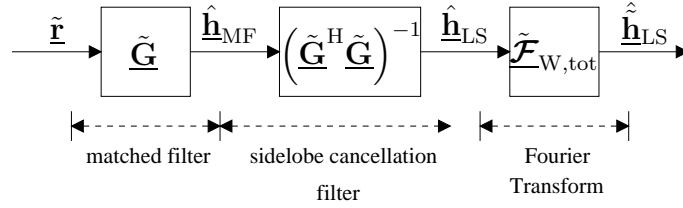


Fig. 6.6. Decomposition of the FD-LS-JCE.

As discussed in Subsections 4.2.1 and 4.2.2, with the optimum pilots used in the frequency and the time domain multi-branch transmissions, (4.14) and (4.1) can be fulfilled, respectively. Therefore, the inversion operation $(\mathbf{P}^H \mathbf{P})^{-1}$ in the structure shown in Fig. 6.5 and the inversion operation $(\tilde{\mathbf{G}}^H \tilde{\mathbf{G}})^{-1}$ in the structure shown in Fig. 6.6 will have the same complexity and both scale the estimate $\hat{\mathbf{h}}_{\text{MF}}$ by a factor $1/E_p$. Even if suboptimum pilots are considered by taking into account the expression of (4.13), these two inversion operations still have the same complexity. Therefore, for comparing the complexity of TD-LS-JCE and FD-LS-JCE, the two inversion operations $(\mathbf{P}^H \mathbf{P})^{-1}$ and $(\tilde{\mathbf{G}}^H \tilde{\mathbf{G}})^{-1}$ are omitted, i.e. only the complexity of the TD-MF-JCE of (3.85) of the total CIR \mathbf{h} and the complexity of FD-MF-JCE of (3.39) of the total CTF $\tilde{\mathbf{h}}$ will be considered. Particularly, in the following the number of complex multiplications and FFTs (IFFTs) in (3.85) and (3.39) will be calculated.

For the TD-MF-JCE of (3.85), the number

$$\eta_{\text{CM}_T} = UWL_p \quad (6.15)$$

of complex multiplications corresponding to the first step, i.e. the matched filtering, in the structure shown in Fig. 6.5 is required.

For the FD-MF-JCE of (3.39), by considering the definition of matrix $\tilde{\mathbf{G}}$ in (3.28), its complexity evaluation can be more clearly seen from Fig. 6.7.

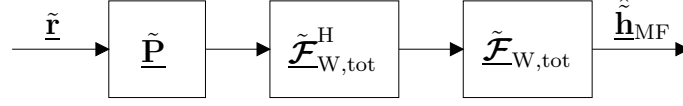


Fig. 6.7. Decomposition of the FD-MF-JCE.

From the discussion in Section 3.2, the three matrices in Fig. 6.7 $\tilde{\mathbf{P}}$, $\tilde{\mathcal{F}}_{W,\text{tot}}^H$ and $\tilde{\mathcal{F}}_{W,\text{tot}}$ should be a-priori known to the receiver. Therefore, the total matrix $\tilde{\mathcal{F}}_{W,\text{tot}} \tilde{\mathcal{F}}_{W,\text{tot}}^H \tilde{\mathbf{P}}$ of dimension $(UN_F) \times N_F$ is also a-priori known, which can be calculated off-line. A direct calculation of the complexity of the structure shown in Fig. 6.7 is based on the multiplication of the total matrix $\tilde{\mathcal{F}}_{W,\text{tot}} \tilde{\mathcal{F}}_{W,\text{tot}}^H \tilde{\mathbf{P}}$ with the receive signal vector $\tilde{\mathbf{r}}$. The number of complex multiplications

$$\eta_{\text{CM}_F} = UN_F^2 \quad (6.16)$$

is obtained in this direct calculation.

As discussed in Subsection 3.3.1, the number W of channel coefficients is typically smaller than the number N_F of subcarriers in OFDM systems [NP00]. Generally, N_F is at least 4 to 10 times larger than W [FAB02]. One reason for this is to minimize the fraction of overhead due to the insertion of the cyclic prefix at the beginning of each transmission block. When comparing (6.16) with (6.15), it is observed that the number of complex multiplications η_{CM_T} of (6.15) for the TD-MF-JCE is always smaller than the number of complex multiplications $\eta_{\text{CM}_{1F}}$ of (6.16) for the FD-MF-JCE under the assumption that $L_p = N_F$.

However, the complexity of FD-MF-JCE can be reduced by the fast implementation of the Fourier transformation. Generally, the N_F -point DFT can be fastly implemented by N_F -point FFT with $N_F \log_2(N_F)$ complex multiplications [BC02]. The first block in the structure shown in Fig. 6.7 brings UN_F complex multiplications, while the second and the third blocks in Fig. 6.7 in total require $2UN_F$ N_F -point FFTs, each of which has N_F inputs, while only W outputs are useful for the FD-MF-JCE. Hence, the total number of complex multiplications for the FD-MF-JCE in the structure shown in Fig. 6.7 is

$$\eta_{\text{CM}_F} = UN_F + 2UN_F \log_2(N_F). \quad (6.17)$$

From (6.15) and (6.17), with the same number of U branches in both the time and the frequency domain multi-branch transmissions, and under the assumption that $L_p =$

N_F , the complexity of TD-MF-JCE and FD-MF-JCE is related to the number N_F of subcarriers or the dimension L_p of the pilots as well as the number of channel coefficients W . It is derived from (6.15) and (6.17) that in the case

$$W > 1 + 2\log_2(N_F) \quad (6.18)$$

the complexity of TD-MF-JCE of (6.15) is greater than the complexity of FD-MF-JCE of (6.17). Therefore, the FD-LS-JCE should be chosen according to the complexity evaluation. In contrast to this, in the case

$$W < 1 + 2\log_2(N_F) \quad (6.19)$$

the complexity of the TD-MF-JCE of (6.15) is less than the complexity of FD-MF-JCE of (6.17). Therefore, the TD-LS-JCE should be chosen according to the complexity evaluation.

From (6.18) and (6.19), the choice of TD-LS-JCE or FD-LS-JCE according to their complexity evaluation is illustrated in Fig. 6.8. The horizontal axis represents the dimension N_F of the frequency domain pilot or the dimension L_p of the time domain pilot. The vertical axis represents the number W of channel coefficients. The curve in Fig. 6.8 illustrates the function $1 + 2\log_2(N_F)$ as in (6.18) and (6.19). Therefore, if the implementing complexity is the critical factor in choosing either the TD-LS-JCE or the FD-LS-JCE, the range above the curve in Fig. 6.8 corresponding to the case that (6.18) can be satisfied represents the scenario in which FD-LS-JCE should be selected. In contrast to this, the range below the curve in Fig. 6.8 corresponding to the case that (6.19) can be satisfied represents the scenario in which TD-LS-JCE should be selected. Since the number of branches U influences the complexity of both the TD-LS-JCE which is reduced to (6.15) in the case of optimum pilots and the FD-LS-JCE which is reduced to (6.17) in the case of optimum pilots linearly, Fig. 6.8 is valid for the systems with any number of branches.

Based on above discussions, the choice of the processing domain of JCE for OFDM and FMT based multi-branch multi-carrier systems can be discussed according to the complexity evaluation of JCE.

The dominant propagation impairment of multipath in broadband wireless access systems causes multiple echoes of the transmitted signal to be received with excess delays of up to tens of microseconds [EMG99]. For symbol rates in the range of tens of megabits per second, this translates to intersymbol interference that can span up to 100 or more data symbols [FAB02]. For the parameters of beyond 3G systems given in Table 2.1, the symbol rate of 20 MHz and the maximum excess delay of 5 μ s in the worse scenario of outdoor mean that $W = 100$ channel coefficients can be resolved if we sample with the symbol rate at the receiver. If, e.g. there are 512 subcarriers in the considered multi-branch OFDM system, the FD-LS-JCE should be used [SWB02, MWS⁺02] according to Fig. 6.8 with respect to obtain low complexity.

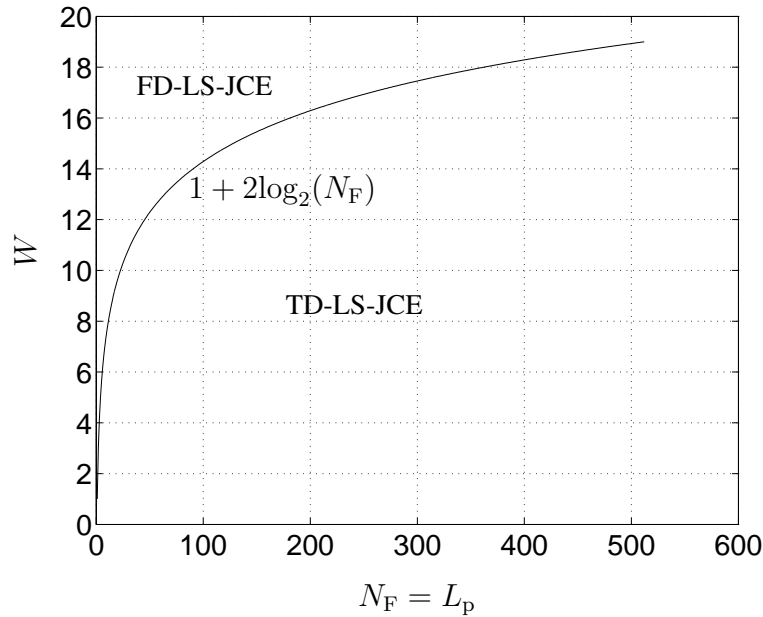


Fig. 6.8. The choice of TD-LS-JCE and FD-LS-JCE according to the complexity.

As for the FMT systems, with the appropriately designed prototype filter, the ICI between the subchannels in FMT systems is negligible [BC02], as demonstrated in Fig. 6.4 as an example. Therefore, the signal processing, e.g. the JCE, at the receiver is normally carried out subcarrier wise [BTT02, KWC04a]. With the total symbol rate of 20 MHz over the broadband channel, by considering, e.g. 16 subcarriers in the FMT system, the $5 \mu\text{s}$ excess delay in the worse case of outdoor given in Table 2.1 means that about $W = 6$ channel taps can be resolved, if we sample with the symbol rate on each subcarrier at the receiver. Therefore, according to Fig. 6.8, for the pilot dimension L_p e.g. around 30, it is more preferable to adopt TD-LS-JCE on each subcarrier with respect to obtain low complexity [KWC04a].

6.4 PAPR issue in OFDM systems

6.4.1 General

In wireless communication systems, the RF transmitter dominates power consumption and heat generation at the MT and at the BS or AP [SG01]. The PAPR of the transmitted waveform determines the bias point and efficiency of the transmit power amplifier. For a given required power output, the greater the PAPR, the greater the required power amplifier back-off, and, therefore, the lower the amplifier efficiency. Hence, the PAPR issue should be considered in the signal processing such as in the channel estimation.

It is found out that the PAPR in a single carrier system, in which the signals are processed and transmitted in the time domain, is 4.5 to 5 dB lower than that in an OFDM system, in which the signals are first allocated in the frequency domain and then transformed into the time domain by IFFT for transmission, with 256 or 512 subcarriers using QPSK modulation [SG01]. That means that the signals transmitted in OFDM systems are more crucial with respect to the PAPR problem. Therefore, the discussion on the PAPR issue will be restricted to the frequency domain channel estimation in this section. Particularly, the PAPR issue will be investigated for the three optimum pilots, namely disjoint pilots, Walsh code based pilots and CAZAC code based pilots proposed in Section 4.3.

6.4.2 PAPR comparison of various pilots

Based on the fact that the time domain pilot symbol $\underline{p}^{(u, l_p)}$, $u = 1 \cdots U$, $l_p = 1 \cdots l_p$, in (3.1) presents in the physical transmission models as shown in Fig. 1.4 and Fig. 1.5, from (3.1), by assuming $L_p = N_F$, the discrete time PAPR

$$\eta^{(u)} = \frac{\max_{n_F \in (1, N_F)} |\underline{p}^{(u, n_F)}|^2}{E\{|\underline{p}^{(u, n_F)}|^2\}}, \quad u = 1 \cdots U, \quad (6.20)$$

for the u -th branch is derived [MH97, WNW01]. The PAPR $\eta^{(u)}$ of (6.20) is the square of the crest factor [MH97].

The optimum pilots of disjoint pilots, Walsh code based pilots and CAZAC code based pilots in Section 4.3 are designed and expressed in the frequency domain. From (3.13), the time domain expression of the pilot on the u -th branch

$$\underline{\mathbf{p}}^{(u)} = \underline{\mathcal{F}}^{-1} \underline{\tilde{\mathbf{p}}}^{(u)}, \quad u = 1 \cdots U, \quad (6.21)$$

can be obtained, i.e. the time domain expression of the pilot on the u -th branch is the IDFT of the frequency domain expression of the pilot on the u -th branch.

The numerical results of the power of one snapshot of the time domain expression of the disjoint, Walsh and CAZAC pilots, i.e. $|\underline{p}^{(u, n_F)}|^2$, $n_F = 1 \cdots N_F$, of one branch u versus the time discrete point n_F is shown in Fig. 6.9. The exemplary scenario of $N_F = 64$, $U = 16$ and $W = 4$ is considered. The x-axis in Fig. 6.9 represents N_F time discrete points of the time domain expression of these pilots, and the y-axis represents the power of these pilots over these discrete points. It is observed that apart from the CAZAC pilot, the other two pilots exhibit time-variant power. Among disjoint pilot, Walsh pilot and CAZAC pilot, Walsh pilot has the highest peak power, while CAZAC pilot has the lowest power and uniform power distribution over the N_F discrete time points. This tendency of different pilots holds also for the other branches.

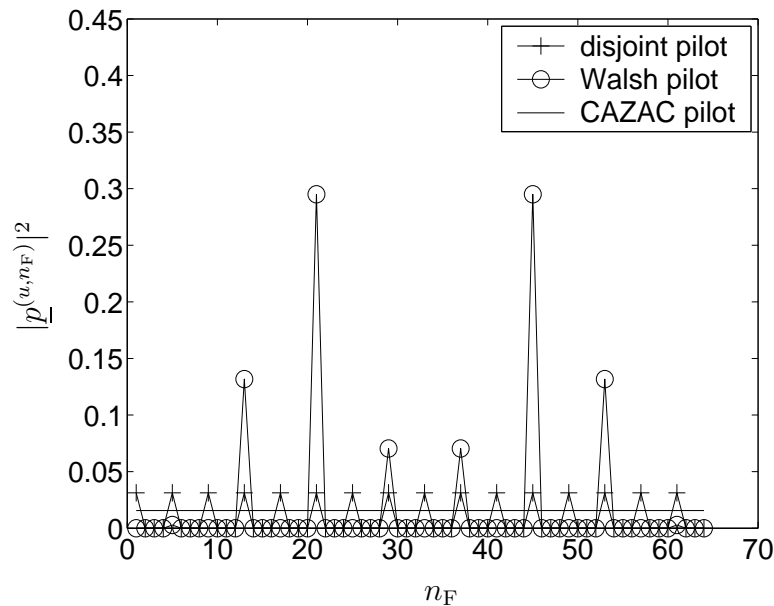


Fig. 6.9. The power of the time domain pilot sequence $|\underline{p}^{(u,n_F)}|^2$, $u = 1 \cdots U$, $n_F = 1 \cdots N_F$, for the exemplary scenario of $N_F = 64$, $U = 16$ and $W = 4$.

To evaluate the PAPR, the U branch specific PAPRs of (6.20) are averaged. The averaged PAPR

$$\eta = \frac{1}{U} \sum_{u=1}^U \eta^{(u)} \quad (6.22)$$

in dB is shown in Table 6.1. Also the exemplary scenario of $N_F = 64$, $U = 16$ and $W = 4$ is considered. It is observed in Table 6.1 that among the disjoint pilots, the Walsh code based pilots and the CAZAC code based pilots, the Walsh code based pilots have the highest average PAPR, which is 14.7882 dB. The average PAPR of the disjoint pilots is in between while the PAPR of the CAZAC code based pilots is 0 dB. That means, comparing with disjoint pilots and Walsh code based pilots, CAZAC code based pilots alleviate the problem of PAPR in OFDM based systems greatly. It would be challenging to the hardware, such as A/D, D/A converters and RF power amplifier, if, e.g. Walsh code based pilots are applied directly to multi-user OFDM systems for JCE.

Table 6.1. Averaged PAPR of different pilots.

Pilots	Averaged PAPR /dB
Disjoint pilots	6.0206
Walsh code based pilots	14.7882
CAZAC code based pilots	0

6.5 Applications of various optimum pilots

In this section, some general discussions on the three kinds of optimum pilots in Section 4.3, i.e. disjoint pilots, Walsh code based pilots and CAZAC code based pilots will be made for their applications in multi-branch multi-carrier systems.

Up to now, the presented three kinds of optimum pilots have been investigated in three aspects, i.e. their performance in terms of SNR degradation in noisy environments as in Section 4.5, their performance in interference environments in terms of variation coefficient as in Section 5.3, as well as their implementation issue concerning PAPR in Subsection 6.4.2. As seen in Section 4.5, in noisy environments, disjoint pilots, Walsh code based pilots and CAZAC code based pilots have the same performance in terms of SNR degradation. In interference environments, as seen in Fig. 5.4, the choice of using different kinds of pilots, i.e. disjoint pilots, Walsh code based pilots and CAZAC code based pilots, to different SAs appears to have good variation coefficient performance. However, by considering the PAPR performance of various pilots, it would be challenging to the RF front end if Walsh code based pilots are used in one of the SAs. The choice of using CAZAC code based pilots, but with different mother CAZAC code to different SAs, will produce not only the best variation coefficient performance, as seen in Fig. 5.5, but also the ideal PAPR performance in each SA. Therefore, with this arrangement of pilots, the best solution of pilots in terms of the best performance in noise and interference environments, as well as of the best PAPR performance, can be obtained.

The performance advantage of CAZAC code based pilots is obtained at the price of higher hardware requirement. Since CAZAC code based pilots are normally composed of non-binary elements, they require more memory than Walsh code based pilots, which consist of binary elements. However, this disadvantage of CAZAC code based pilots could be balanced by alleviating the implementation complexity of the A/D and D/A converter as well as the RF power amplifier, due to their ideal PAPR performance.

7 Simulations of JCE in OFDM and FMT based multi-branch systems

7.1 General

In this chapter, the performance of JCE in terms of MSE and BER by applying Walsh code based pilots, disjoint pilots, CAZAC code based pilots and random pilots in OFDM and FMT based multi-branch systems is demonstrated by simulations .

While considering the operations of the two systems in indoor and outdoor environments, throughout this chapter, the WSSUS channel model introduced in Chapter 2 is adopted in the simulations. In Section 7.2, the parameters used for the simulations in OFDM and FMT based multi-carrier multi-branch systems are given for the indoor and outdoor scenarios. In Section 7.3, the MSE performance of JCE and the BER performance in the multi-branch OFDM system are simulated using the well known Monte Carlo simulation method. In Section 7.4, the MSE performance of JCE and the BER performance in the multi-branch FMT system are simulated. Besides, the subchannels of the WSSUS beyond 3G broadband channel obtained by OFDM and FMT modulations are also simulated to justify the presented JCE algorithms in Section 7.3 and 7.4, respectively.

It should be mentioned that although the BER performance of the OFDM and FMT based multi-branch systems is presented in this chapter, the aim is not to compare these two systems. Actually, the OFDM and FMT based multi-branch systems are chosen for the applications of FD-LS-JCE and TD-LS-JCE, respectively, using various pilots to verify the the previous theoretical investigations on channel estimation especially in Chapter 3, Chapter 4 and Chapter 6. The multiple access scheme, the detection scheme as well as some simulation parameters such as the pilot and data multiplexing factor, which are irrelative to the verification on channel estimation, are chosen randomly in this chapter.

7.2 Simulation scenarios

7.2.1 OFDM simulation parameters

With reference to the channel parameters in Table 2.1 for the beyond 3G indoor and outdoor channels, the simulation parameters for the multi-branch OFDM system are given in Table 7.1.

An available infrastructure of multi-branch OFDM system is JOINT, which is introduced in Subsection 1.1.2. Within the infrastructure of JOINT, the number of APs K_A should

be no less than the number of MTs K , with the K MTs occupying the same time and frequency resources, as illustrated in Fig. 3.3. This arrangement indicates a space division multiple access (SDMA) scheme. In the simulations, the number of MTs K is chosen as 1, 2, 4 and 8. The number of APs K_A is the same with the number of MTs K . Only one antenna is equipped in each MT and AP. The number of transmit branches U is calculated as (1.1). In addition, according to Table 7.1, based on the discussion in Section 6.3 concerning the implementation complexity of JCE algorithm, the FD-LS-JCE of (3.34) is applied in the multi-branch OFDM system which has 512 subcarriers. The subcarrier spacing F in Table 7.1 is calculated from the system bandwidth B and the number of subcarriers N_F , which is given by

$$F = \frac{B}{N_F}. \quad (7.1)$$

F is equal to 39.1 KHz according to the parameters in Table 7.1. A subcarrier-wise zero-forcing JD scheme [SWB⁺01] is used in the simulation link for the simulation of BER performance. Channel coding and decoding are not used in the simulation link.

Fig. 3.3 is referred for the multiplexing structure of the pilot and the data for the multi-branch OFDM system. For the indoor simulations, in front of every 10 data blocks (D) of dimension 512 occupying the whole 512 subcarriers, one pilot block (P) of dimension 512 occupying the whole 512 subcarriers is inserted for channel estimation, corresponding to a multiplexing factor P:D of 1:10. For the outdoor simulations, in front of every 5 data blocks (D) of dimension 512 one pilot block (P) of dimension 512 is inserted for channel estimation, corresponding to the multiplexing factor P:D of 1:5. The choice of the lower multiplexing factor in the indoor environment than in the outdoor environment is justified by the subchannel simulation of the OFDM system, which will be given in Subsection 7.3.1 and which will illustrate the more severe time variance of the CTF in the outdoor environment than the indoor environment. The more severe the time variance of the channel, the more frequent the insertion of pilot [LSA01]. The radio channel obtained by JCE during the transmission of the pilot block is used as the a-priori knowledge in the data detection during the transmission of the the following data blocks.

The guard interval is assumed to be longer than the channel maximum delay τ_{\max} according to the design of OFDM systems [NP00]. In addition, there is no leakage of energy of a certain channel tap to the neighboring taps, and the number of channel coefficients W used in the blockdiagonal matrix $\tilde{\mathcal{F}}_{W,\text{tot}}$ of (3.21) is assumed to be the same with the number of channel taps, which is fixed to 64 in the WSSUS channel model in the simulations. If above assumptions are fulfilled, the channel is called 'sufficiently' estimated in the following, or equivalently say, the channel estimation is 'sufficient'. With sufficient channel estimation, there is no error floor in the MSE and BER performance resulting from channel estimation. The error floor free performance is obtained at the expense of the increased dimension of the $UN_F \times UW$ blockdiagonal matrix $\tilde{\mathcal{F}}_{W,\text{tot}}$ of (3.21) therefore the estimation complexity and delay. In the case of sufficient channel estimation,

the vectors $\hat{\mathbf{h}}$ and \mathbf{h} in (3.47) have the same dimension, and the MSE of FD-LS-JCE is perfectly expressed as (3.50).

Table 7.1. Simulation parameters for the multi-branch OFDM system.

OFDM System Parameters	Indoor	Outdoor
System bandwidth B	20 MHz	20 MHz
Carrier frequency f_c	5.5 GHz	5.5 GHz
Number of subcarriers N_F	512	512
Subcarrier spacing F	39.1 kHz	39.1 kHz
Vehicle speed v	3 km/h	50 km/h or 200 km/h
Multi-path excess delay τ	0.8 μ s	5 μ s
Doppler frequency f_D	15.28 Hz	257 kHz or 1 kHz
Number of MTs K	1,2,4,8	1,2,4,8
Number of antennas $K_{M,k}$ of each MT	1	1
Number of transmit branches U	1,2,4,8	1,2,4,8
Number of APs K_A	1,2,4,8	1,2,4,8
Number of antennas k_a of each AP	1	1
Multiple access scheme	SDMA	SDMA
Symbol number in one pilot transmission	512	512
Symbol number in one data transmission	10*512	5*512
Multiplexing factor P:D	1:10	1:5
Modulation	QPSK	QPSK
Channel estimation	FD-LS-JCE	FD-LS-JCE
Detection	zero-forcing JD	zero-forcing JD

7.2.2 FMT simulation parameters

With reference to the channel parameters in Table 2.1 for the beyond 3G indoor and outdoor channels, the simulation parameters for the multi-branch FMT system are given in Table 7.2.

The rros prototype filter with roll-off factor $\rho = 0.15$ is used in the FMT modulation. With 16 subcarriers and with the oversampling factor $Q = 18$, it is shown in Fig. 6.4 that due to the filter characteristics the adjacent subcarrier suppression is at least -20dB. Therefore, the ICI between subcarriers is negligible in the considered FMT system, which implies that the signals on each subcarrier can be processed independently while allowing a negligible loss in JCE and data detection performance.

The system structure of multiple transmit branches with only one receive branch is taken in the simulation link of the multi-branch FMT system. As seen in Table 7.2, the number

of MTs K is considered as 1, 2 and 3 in the simulations with only one antenna for each MT. The number of transmit branches U is calculated as (1.1). There is only one AP equipped with one antenna for the receive of signals. The multiple MTs are identified by orthogonal Walsh spreading code of dimension 4, corresponding to a CDMA scheme on each subcarrier. Based on the discussion in Subsection 6.3 concerning the implementation complexity of JCE algorithm, the subcarrier-wise TD-LS-JCE of (3.86) is applied in multi-branch FMT system with 16 subcarriers. The subcarrier spacing F is equal to 1.25 MHz, which is calculated according to (7.1) with the given parameters in Table 7.2. For the simulation of the BER performance, a zero-forcing JD scheme for the typical CDMA system [Kle96] is used on each subcarrier. Channel coding and decoding are not used in the simulation link.

Fig. 3.5 can be referred as the multiplexing structure on each subcarrier of the pilot and the data for the considered multi-branch FMT system. For the indoor simulations, in front of every 10 data blocks (D) of dimension 64 occupying 64 continuous symbols, one pilot block (P) of dimension 24 occupying 24 continuous symbols is inserted for channel estimation, corresponding to a multiplexing factor P:D of 3:80. For the outdoor simulations, in front of every 2 data blocks (D) of dimension 64, one pilot block (P) of dimension 24 is inserted for channel estimation, corresponding to a multiplexing factor P:D of 3:16. The choice of the lower multiplexing factor in an indoor environment than in an outdoor environment is justified by the subchannel simulation of the FMT system, which will be given in Subsection 7.4.1 and which will illustrate the more severe time variance of the CTF in an outdoor environment than an indoor environment. The radio channel estimated during the transmission of this pilot block is used as the a-priori knowledge in the data detection during the transmission of the the following data blocks.

The WSSUS channel used for the simulations in the multi-branch FMT system is slightly different from that used for the simulations in the multi-branch OFDM system. In the former case, the number of taps in the WSSUS channel is randomly changed. However, the number of channel coefficients W used in the pilot matrix $\underline{\mathbf{P}}^{(u)}$ of (3.69) on each subcarrier is fixed to 8 during the simulation. Due to the mismatch between the number of channel taps, which is a random number, and the number of channel coefficients W in the pilot matrix $\underline{\mathbf{P}}^{(u)}$ of (3.69), an insufficient channel estimation is resulted and the error floor is expected in the MSE and BER simulation results of the multi-branch FMT system.

Table 7.2. Simulation Parameters for the multi-branch FMT system.

FMT Simulation Parameters	Indoor	Outdoor
System bandwidth B	20 MHz	20 MHz
Carrier frequency f_c	5.5 GHz	5.5 GHz
Number of subcarriers N_F	16	16
Subcarrier bandwidth F	1.25 MHz	1.25 MHz
Oversampling factor K	18	18
Vehicle speed v	3 km/h	50 km/h
Multi-path excess delay τ	0.8 μ s	5 μ s
Doppler frequency f_D	15.28 Hz	257 kHz
Number of MTs K	1,2,3	1,2,3
Number of antennas $K_{M,k}$ of each MT k	1	1
Number of transmit branches U	1,2,3	1,2,3
Number of APs K_A	1	1
Number of antennas k_a of each AP	1	1
Multiple access scheme	CDMA	CDMA
Spreading factor	4	4
Symbol number in one pilot transmission	24	24
Symbol number in one data transmission	10*64	2*64
Multiplexing factor P:D	3:80	3:16
Modulation	BPSK	BPSK
Channel estimation	TD-LS-JCE	TD-LS-JCE
Detection	zero-forcing JD	zero-forcing JD

7.2.3 Definition of SNR

Let us assume the average signal power to be P_s and the average noise power to be P_n . The average signal power P_s is related to the average symbol energy E_s and the symbol duration T_s , which is given as [BC02, Pro95]

$$P_s = \frac{E_s}{T_s} = E_s R_s, \quad (7.2)$$

in which

$$R_s = 1/T_s \quad (7.3)$$

is the symbol rate. The average noise power P_n is related to the one sided noise power spectral density N_0 and the noise bandwidth, which is normally limited by the total system bandwidth B , which is given as [Pro95]

$$P_n \approx N_0 B. \quad (7.4)$$

With (7.2) and (7.4), the average SNR γ at the input of the matched filter at the receiver is defined as [BC02, Pro95]

$$\gamma = \frac{P_s}{P_n} = \frac{E_s R_s}{N_0 B}. \quad (7.5)$$

Let us suppose M is the modulation order. For example, $M = 2$ in BPSK modulation and $M = 4$ in QPSK modulation [Pro95]. By considering the relationship between the symbol rate R_s and the bit rate R_b , i.e.

$$R_s = R_b / \log_2 M, \quad (7.6)$$

and the relationship between the average bit energy E_b and the average symbol energy E_s [BC02, Pro95], i.e.

$$E_b = E_s / \log_2 M, \quad (7.7)$$

(7.5) can be represented as

$$\gamma = \frac{E_b R_b}{N_0 B}. \quad (7.8)$$

With (7.3) and (7.6), the bit rate R_b is given by

$$R_b = \frac{\log_2 M}{T_s}. \quad (7.9)$$

Substituting (7.9) into (7.8), we obtain

$$\gamma = \frac{E_b \log_2 M}{N_0 B T_s}. \quad (7.10)$$

In conventional SC systems in which the Nyquist assumptions are verified, the rate $BT_s = 1$. With BPSK modulation, $\gamma = E_b/N_0$ satisfies.

7.3 Performance of JCE in the multi-branch OFDM system

7.3.1 Subchannel simulation

For the observation of the subchannel of the WSSUS channel obtained by the OFDM modulation, only one transmit branch is considered.

As shown in Table 7.1, the subcarrier spacing in the considered OFDM system is 39.1 kHz. As an example, the simulation results of the amplitude of the CTF for the first subchannel, i.e. $|\tilde{h}_1(f, t)|$, which is obtained directly from the samples of the broadband

CTF $\tilde{\underline{h}}(f, t)$ of (2.5), are presented in Fig. 7.1a for indoor and in Fig. 7.1b for outdoor environments. The f -axis represents the bandwidth in MHz and the t -axis represents the propagation time in ms. To illustrate the influence of the velocity on the time variance of the CTF in outdoor environments, a vehicle speed of 200 km/h is considered in the simulation. It is observed that the OFDM subchannel is flat in the frequency domain in an indoor environments as shown in Fig. 7.1a and almost flat in the frequency domain in outdoor environments as shown in Fig. 7.1b. These observations justify the process of one-tap equalization per subchannel as normally done in OFDM systems [NP00]. The fluctuation of $|\tilde{\underline{h}}_1(f, t)|$ on the t -axis in the OFDM indoor and outdoor subchannels as in Figs. 7.1a and 7.1b, respectively, although is alleviated compared with that for the broadband CTF $\tilde{\underline{h}}(f, t)$ as in Figs. 2.1 and 2.2, is obvious. The higher time variance in outdoor environments than in indoor environments is the reason for the more frequent insert of pilots in the outdoor transmission than in indoor transmission.

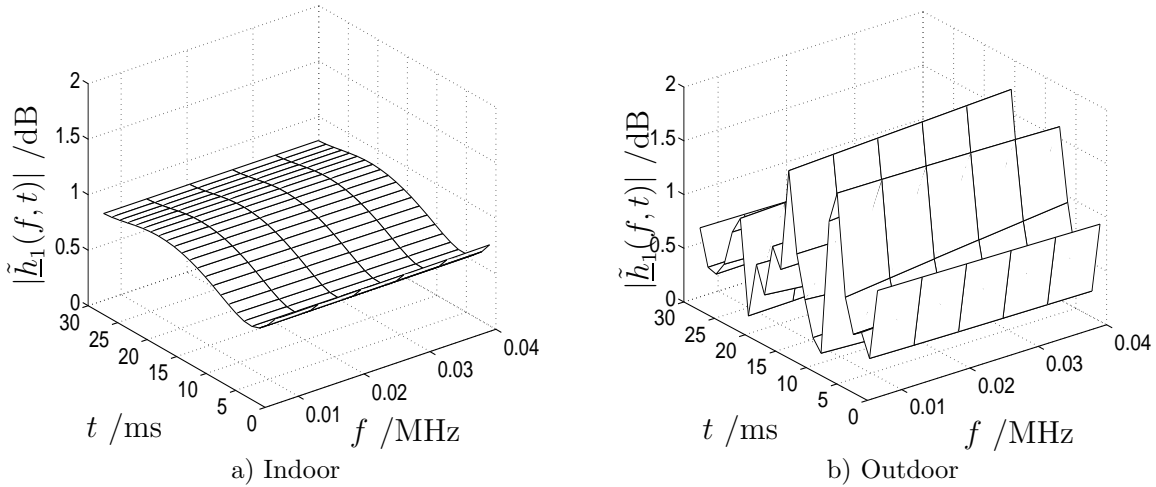


Fig. 7.1. The amplitude of the transfer function, i.e. $|\tilde{\underline{h}}_1(f, t)|$, for the 1st OFDM subchannel; a) indoor environment; b) outdoor environment.

When two or more adjacent subcarriers are simulated, there exists some frequency correlation between subchannels, which can be observed in Figs. 7.2a and 7.2b for indoor and outdoor environments, respectively, in which 6 adjacent subchannels are simulated for the considered OFDM system. This frequency correlation can be taken advantage of in the JCE of multi-branch OFDM systems to reduce the number of unknowns [SMW⁺01, MWS⁺02], which has been used in the derivation from (3.27) to (3.28) in Subsection 3.3.1.

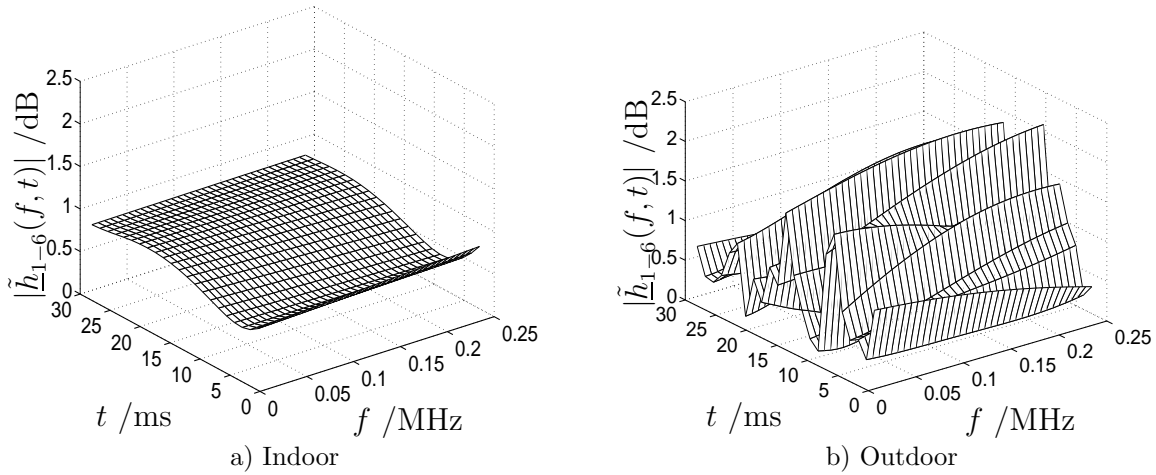


Fig. 7.2. The amplitude of the transfer function, i.e. $|\tilde{h}_{1-6}(f, t)|$, for the 1st to the 6th OFDM subchannels; a) indoor environment; b) outdoor environment.

7.3.2 MSE simulation

The MSE in this subsection evaluates the performance of the FD-LS-JCE $\hat{\mathbf{h}}_{LS}$ of (3.34) during the transmission of the pilot block with respect to the real channel during this transmission period. Therefore, the real estimation performance is reflected and the time variance of the channels from the transmission of the regarding pilot block to the transmission of the following data blocks is not considered. The normalized MSE

$$\epsilon'_{LS} = \epsilon_{LS}/U, \quad (7.11)$$

which is obtained by dividing the MSE ϵ_{LS} of (3.50) by the number of branches U , is presented in the simulation results. The optimum disjoint pilots, Walsh code based pilots and CAZAC pilots constructed in Subsection 4.3.2, Subsection 4.3.3 and Subsection 4.3.4, respectively, and the suboptimum random pilots discussed in Section 4.4 are used as the pilots transmitted on the multiple branches in the simulations. A vehicle speed of 50 km/h is assumed and the channel is sufficiently estimated by FD-LS-JCE $\hat{\mathbf{h}}_{LS}$ of (3.34) as explained in Subsection 7.2.1.

First, the indoor environments are considered. In Fig. 7.3 and Fig. 7.4, the normalized MSEs ϵ'_{LS} of (7.11) for the FD-LS-JCE $\hat{\mathbf{h}}_{LS}$ of (3.34) with Walsh code based pilots, disjoint pilots, CAZAC code based pilots and random pilots are simulated under consideration of 1 MT and 1 AP, 2 MTs and 2 APs, 4 MTs and 4 APs as well as 8 MTs and 8 APs as in Figs. 7.3a, 7.3b, 7.4a and 7.4b, respectively. The corresponding normalized minimum MSE $\epsilon'_{LS, \min}$ of (3.59) is also shown in Figs. 7.3 and 7.4. It is seen that the normalized MSE ϵ'_{LS} of (7.11) of the FD-LS-JCE $\hat{\mathbf{h}}_{LS}$ of (3.34) with the optimum pilots like disjoint pilots, Walsh code based pilots and CAZAC code based pilots always coincides with the

normalized minimum MSE $\epsilon'_{LS,\min}$ of (3.59). For the FD-LS-JCE $\hat{\mathbf{h}}_{LS}$ of (3.34) using random pilots, its MSE performance coincides with the normalized minimum MSE $\epsilon'_{LS,\min}$ of (3.59) in the scenario of 1 MT and 1 AP of Fig. 7.3a. This is because in the case of sufficient channel estimation, the MSE ϵ_{LS} obtained by applying FD-LS-JCE with any pilots is calculated by 3.50. With one transmit branch, the random pilots statistically produce the same value $\text{tr}\{((\tilde{\mathbf{G}}^H \tilde{\mathbf{G}})^{-1})\}$ as the other pilots. However, in the multi-branch cases of Figs. 7.3b, 7.4a and 7.4b, the higher the number of branches U , the worse the MSE performance of FD-LS-JCE with random pilots compared to the normalized minimum MSE $\epsilon'_{LS,\min}$ of (3.59). This is because the inter-branch interference is always present for the FD-LS-JCE with random pilots. With large number of branches such as with 8 MTs and 8 APs as in Fig. 7.4b, the MSE performance of FD-LS-JCE with random pilots is extremely bad in comparison with the optimum pilots due to the inter-branch interference. The simulation results in Figs. 7.3 and 7.4 demonstrate the necessity of the investigation in this thesis on the design of optimum pilots for the multi-branch systems especially with large number of branches.

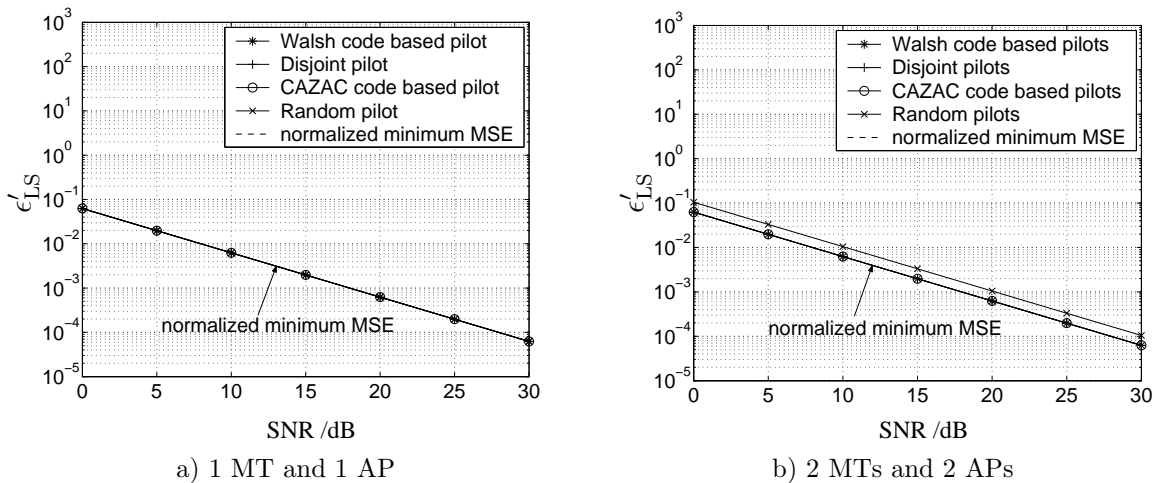


Fig. 7.3. The normalized MSE ϵ'_{LS} of (7.11) and the normalized minimum MSE $\epsilon'_{LS,\min}$ of (3.59) for FD-LS-JCE with Walsh code based pilots, disjoint pilots, CAZAC code based pilots and random pilots in the multi-user OFDM system in an indoor environment; a) 1 MT and 1 AP; b) 2 MTs and 2 APs.

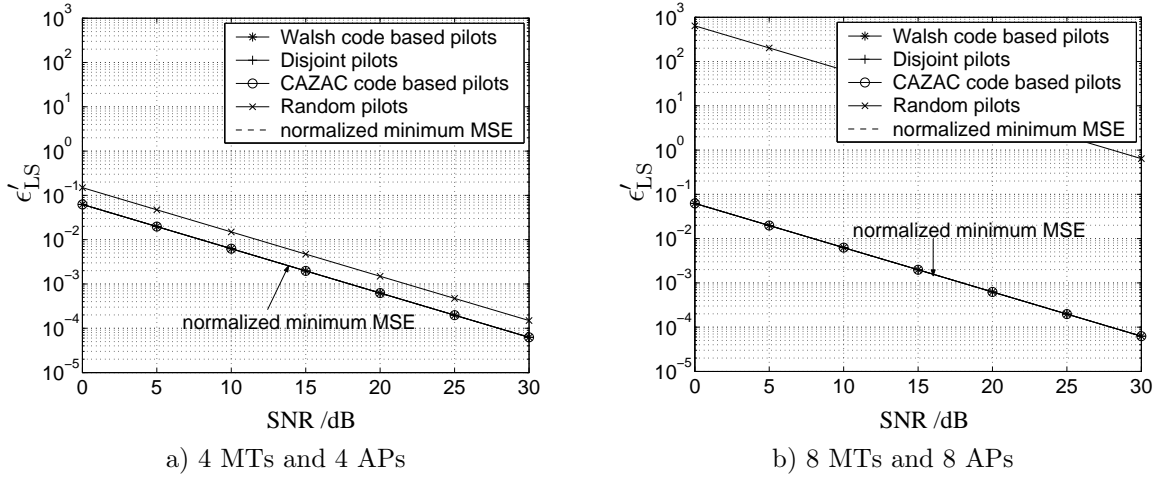


Fig. 7.4. The normalized MSE ϵ'_{LS} of (7.11) and the normalized minimum MSE $\epsilon'_{LS,\min}$ of (3.59) for FD-LS-JCE with Walsh code based pilots, disjoint pilots, CAZAC code based pilots and random pilots in the multi-user OFDM system in an indoor environment; a) 4 MTs and 4 APs; b) 8 MTs and 8 APs.

Figs. 7.5a and Fig. 7.5b are obtained from some curves in Figs. 7.3 and 7.4 with emphasis on the influence of the number of branches to the normalized MSEs ϵ'_{LS} of (7.11) for FD-LS-JCE $\hat{\mathbf{h}}_{LS}$ of (3.34) with optimum pilots, e.g. CAZAC code based pilots, and suboptimum pilots, e.g. random pilots, in indoor environments. As seen in Fig. 7.5a, the number of branches has no influence to the normalized MSEs ϵ'_{LS} of (7.11) of FD-LS-JCE using CAZAC code based pilots, which coincides always with the normalized minimum MSE $\epsilon'_{LS,\min}$ of (3.59). This demonstrates that, with optimum pilots such as CAZAC code based pilots, the MSE performance of FD-LS-JCE in multi-branch scenarios, e.g. 2 MTs and 2 APs, 4 MTs and 4 APs as well as 8 MTs and 8 APs, is the same with that in single-branch scenario, e.g. 1 MT and 1 AP. This validates the theoretical expectation in Chapter 4, i.e. the optimum pilots like CAZAC code based pilots should achieve the normalized minimum MSE $\epsilon'_{LS,\min}$ of (3.59), which is independent of the number of branches U . However, as in Fig. 7.5b, with random pilots, the inter-branch interference makes the MSE performance of FD-LS-JCE worse in the multi-branch scenarios than in the single branch scenario. The more the number of branches U , the worse the MSE performance for FD-LS-JCE using random pilots.

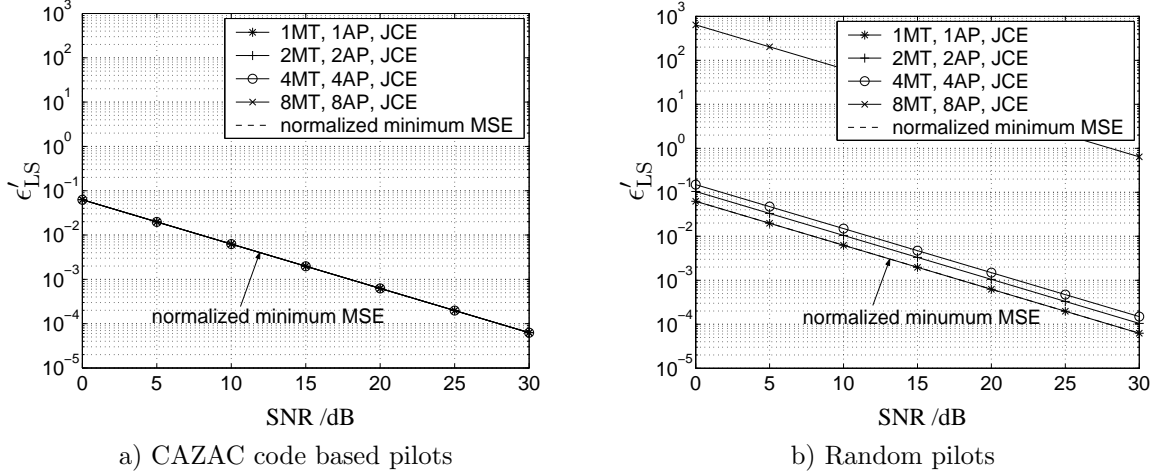


Fig. 7.5. The normalized MSE ϵ'_{LS} of (7.11) and the normalized minimum MSE $\epsilon'_{LS,\min}$ of (3.59) in the scenarios of 1MT-1AP, 2MT-2AP, 4MT-4AP and 8MT-8AP in multi-user OFDM system in an indoor environment; a) CAZAC code based pilots; b) random pilots.

In the following, the outdoor environments are considered. In Fig. 7.6 and Fig. 7.7, the normalized MSEs ϵ'_{LS} of (3.50) for the FD-LS-JCE $\hat{\mathbf{h}}_{LS}$ of (3.34) applying Walsh code based pilots, disjoint pilots, CAZAC code based pilots and random pilots is simulated under the scenarios of 1 MT and 1 AP, 2 MTs and 2 APs, 4 MTs and 4 APs as well as 8 MTs and 8 APs in Figs. 7.6a, 7.6b, 7.7a and 7.7b, respectively. The same tendency can be seen as in indoor environments, i.e. the normalized MSEs ϵ'_{LS} of (7.11) of FD-LS-JCE with optimum pilots coincides with the normalized minimum MSE $\epsilon'_{LS,\min}$ of (3.59), while the MSE performance of the FD-LS-JCE with random pilots gets worse when the number of branches U increases.

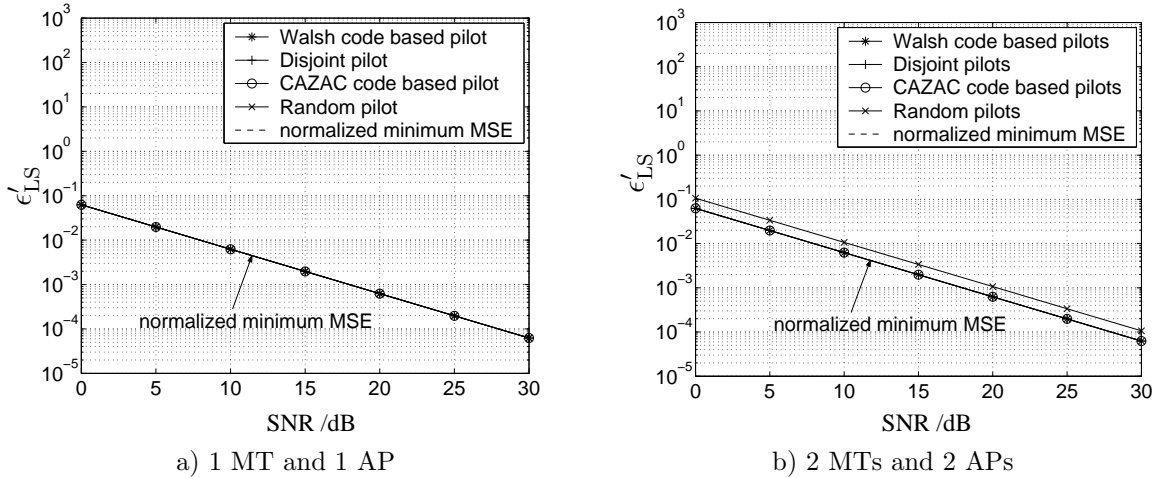


Fig. 7.6. The normalized MSE ϵ'_{LS} of (7.11) and the normalized minimum MSE $\epsilon'_{LS,\min}$ of (3.59) for FD-LS-JCE with Walsh code based pilots, disjoint pilots, CAZAC code based pilots and random pilots in the multi-user OFDM system in an outdoor environment; a) 1 MT and 1 AP; b) 2 MTs and 2 APs.

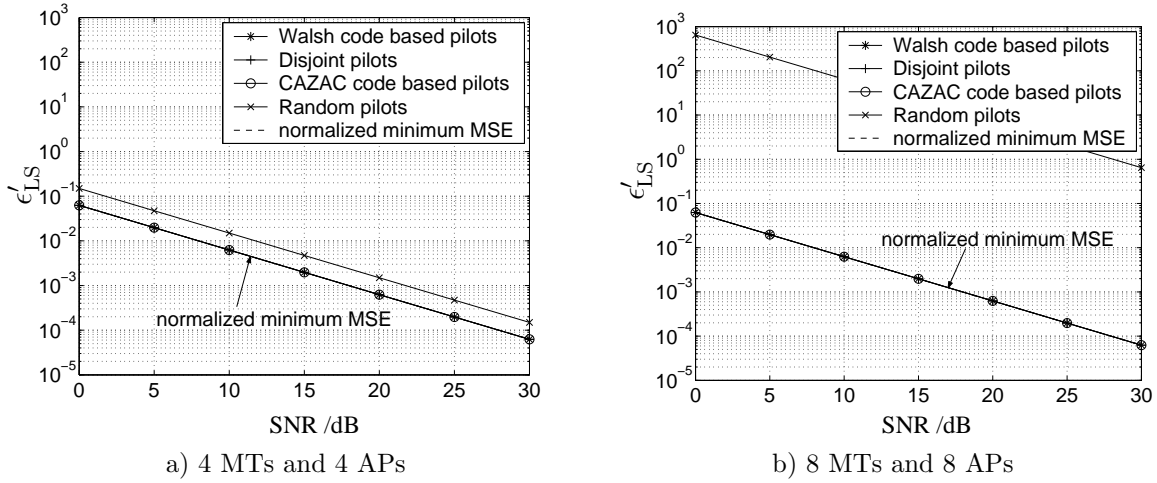


Fig. 7.7. The normalized MSE ϵ'_{LS} of (7.11) and the normalized minimum MSE $\epsilon'_{LS,\min}$ of (3.59) for FD-LS-JCE with Walsh code based pilots, disjoint pilots, CAZAC code based pilots and random pilots in the multi-user OFDM system in an outdoor environment; a) 4 MTs and 4 APs; b) 8 MTs and 8 APs.

In Fig. 7.8, the normalized MSEs ϵ'_{LS} of (7.11) for FD-LS-JCE $\hat{\mathbf{h}}_{LS}$ of (3.34) using CAZAC code based pilots and random pilots are illustrated with respect to the number of branches U for outdoor environments. Similar to the simulation results in Fig. 7.5 for indoor environments, in outdoor environments, the normalized MSEs ϵ'_{LS} of (7.11) of FD-LS-JCE with CAZAC code based pilots is independent on the number of considered branches U , while using random pilots it is sensitive to the number of branches U , as seen in Figs. 7.8a and 7.8b, respectively.

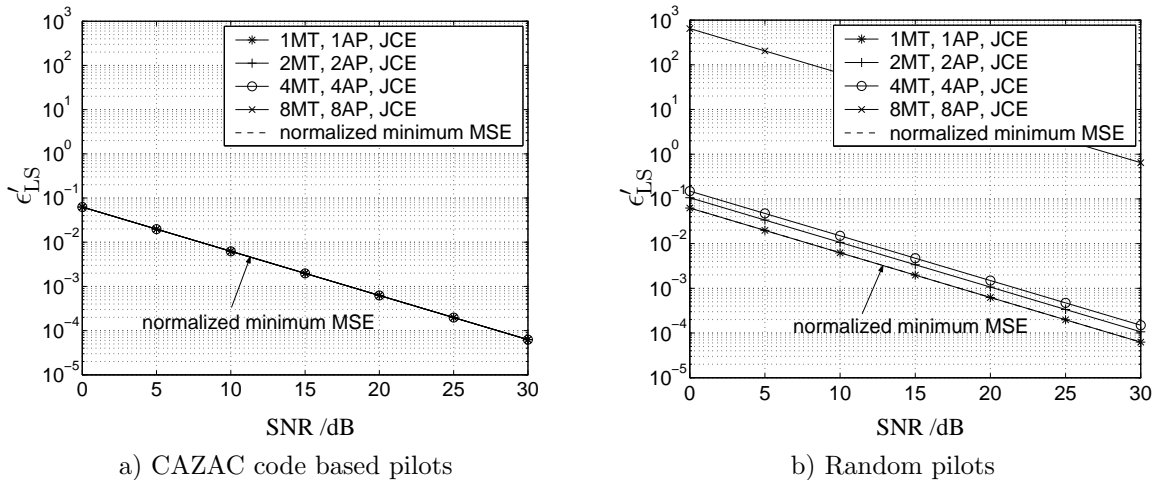


Fig. 7.8. The normalized MSE ϵ'_{LS} of (7.11) and the normalized minimum MSE $\epsilon'_{LS,\min}$ of (3.59) in the scenarios of 1MT-1AP, 2MT-2AP, 4MT-4AP and 8MT-8AP in the multi-user OFDM system in an outdoor environment; a) CAZAC code based pilots; b) random pilots.

To summarize this subsection, in the sufficient channel estimation case, as explained in Subsection 7.2.1, the normalized MSE ϵ'_{LS} of (7.11) for FD-LS-JCE $\hat{\mathbf{h}}_{LS}$ of (3.34) using optimum pilots always coincides with the normalized minimum MSE $\epsilon'_{LS,\min}$ of (3.59). The number of branches U has only influence to the normalized MSE ϵ'_{LS} of (7.11) for FD-LS-JCE $\hat{\mathbf{h}}_{LS}$ of (3.34) using suboptimum pilots like random pilots.

Although the MSE simulation results of only FD-LS-JCE are presented, it can be expected that for the optimum pilots, e.g. disjoint pilots, Walsh code based pilots and CAZAC code based pilots, there is no MSE performance difference between FD-MF-JCE and FD-LS-JCE. This is because for optimum pilots, the matrix $\tilde{\mathbf{G}}^H \tilde{\mathbf{G}}$ in (3.34) is identity matrix when the FD-LS-JCE $\hat{\mathbf{h}}_{LS}$ of (3.34) is compared with FD-MF-JCE $\hat{\mathbf{h}}_{MF}$ of (3.32). Besides, for the multi-branch OFDM system, there is no MSE performance difference between FD-LS-JCE and FD-WLS-JCE schemes. This is because for the OFDM modulation, the noise before the channel estimator at the receiver is Gaussian [Fil04], i.e. the noise covariance matrix is identity, when the FD-WLS-JCE $\hat{\mathbf{h}}_{WLS}$ of (3.37) is compared with FD-LS-JCE $\hat{\mathbf{h}}_{LS}$ of (3.34).

7.3.3 BER simulation

The BER performance is obtained by comparing the detected data with the real transmitted data during the transmission of data blocks. Since the channel information, which is needed for equalization and/or reliable detection, is obtained by JCE before the transmission of data blocks, the time variance of the subchannel, which is slow in indoor environments according to the simulation result in Fig. 7.1a and fast in outdoor environments according to the simulation result in Fig. 7.1b, will influence adversely the BER performance with FD-LS-JCE $\hat{\mathbf{h}}_{LS}$ of (3.34), even with the application of the optimum pilots like Walsh code based pilots, disjoint pilots, and CAZAC code based pilots. In the following JCE is called ideal JCE if the a-priori channel knowledge for data detection is obtained as the real channel knowledge during the transmission of the data blocks. The corresponding BER performance is illustrated in this subsection by the dotted curves. Therefore, the BER curves with ideal JCE represent the best case without channel estimation error due to the time variance of the channel during the data transmission period. The vehicle speed of 50 km/h is taken in the simulations, and the channel is sufficiently estimated by FD-LS-JCE as explained in Subsection 7.2.1 during the pilot transmission period.

First, the indoor environments are considered. Figs. 7.9 and 7.10 illustrate the BER performance when using Walsh code based pilots, disjoint pilots, CAZAC code based pilots and random pilots for JCE in the cases of 1 MT and 1 AP, 2 MTs and 2 APs, 4 MTs and 4 APs as well as 8 MTs and 8 APs. It is seen in Fig. 7.9a that in the case of 1 MT and 1 AP, the BER performance when using the four kinds of pilots coincides with

each other, which is slightly worse than the ideal JCE case due to the slow time variance of the channel in indoor environments. In the case of 2 MTs and 2 APs, as seen in Fig. 7.9b, the system with random pilots slightly underperforms that with the optimum pilots of Walsh code based pilots, disjoint pilots and CAZAC code based pilots. By comparing the curves in Fig. 7.9b with the curves in Figs. 7.10a and 7.10b, it is seen that the higher the number of branches U , the worse the BER performance using random pilots than the other optimum pilots. In general, the tendency of BER performance coincides with the tendency of MSE performance as seen in Fig. 7.3 and Fig. 7.4. The higher the number of branches U , the worse the BER performance of any optimum and suboptimum pilots than the ideal JCE case due to the superposition of the signals on the multiple branches at the receiver with the time variance of the channel on each branch.

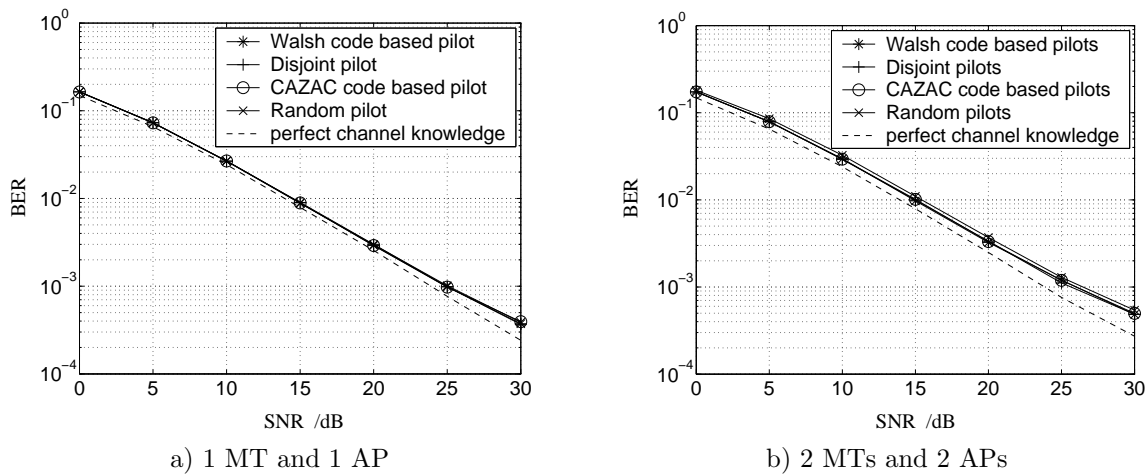


Fig. 7.9. The BER for Walsh code based pilots, disjoint pilots, CAZAC code based pilots and random pilots in an indoor environment; a) 1 MT and 1 AP; b) 2 MTs and 2 APs.

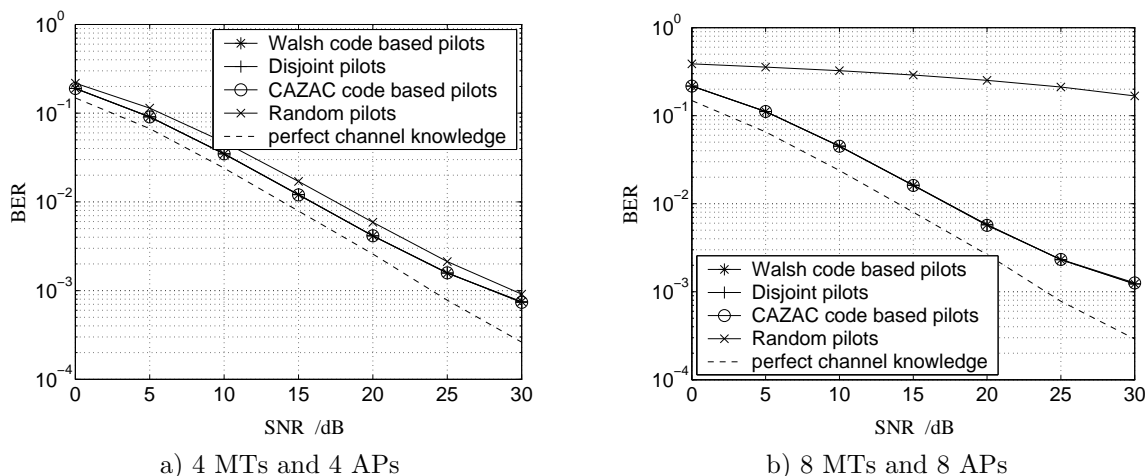


Fig. 7.10. The BER for Walsh code based pilots, disjoint pilots, CAZAC code based pilots and random pilots in an indoor environment; a) 4 MTs and 4 APs; b) 8 MTs and 8 APs.

In Fig. 7.11, the BER performance under consideration of 1 MT and 1 AP, 2 MTs and 2 APs, 4 MTs and 4 APs, as well as 8 MTs and 8 APs in an indoor environment is compared for CAZAC code based pilots, as illustrated in Fig. 7.11a, and for random pilots, as illustrated in Fig. 7.11b. It is seen that in indoor environments, the BER performance for the multi-branch OFDM system with CAZAC code based pilot transmission is slightly sensitive to the number of branches U , while the BER performance with random pilot transmission is very sensitive to the number of branches U . This is because with CAZAC code based pilot transmission, the time variance of the indoor channel makes the estimated channel of each branch by FD-LS-JCE $\hat{\mathbf{h}}_{LS}$ of (3.34) during the pilot transmission slightly different from the real channel of each branch during the following data transmission. While with random pilot transmission, not only the time variance of the indoor channel during the pilot and data transmission influences adversely the BER performance, but also the inter-branch interference in FD-LS-JCE $\hat{\mathbf{h}}_{LS}$ of (3.34) coming from the suboptimum pilot transmission significantly deteriorates the BER performance. In the case of 8 MTs and 8 APs, the BER performance with random pilot transmission is extremely bad. These simulation results verify the necessity of the design of optimum pilots for FD-LS-JCE especially in systems with large number of branches U .

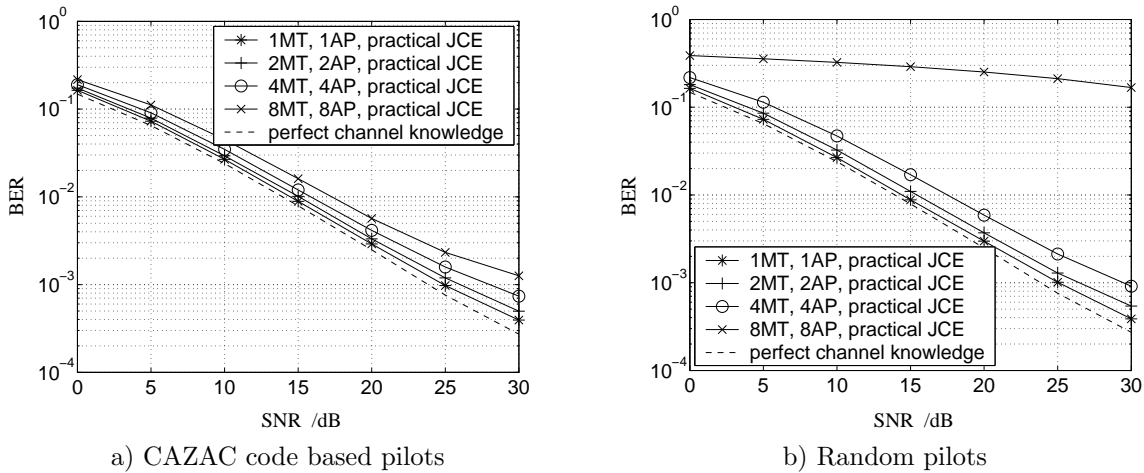


Fig. 7.11. The BER considering 1MT-1AP, 2MT-2AP, 4MT-4AP and 8MT-8AP in an indoor environment; a) CAZAC code based pilots; b) Random pilots.

Next, the BER performance in outdoor environments is presented. Figs. 7.12 and 7.13 show the BER curves when using Walsh code based pilots, disjoint pilots, CAZAC code based pilots and random pilots and assuming 1 MT and 1 AP, 2 MTs and 2 APs, 4 MTs and 4 APs as well as 8 MTs and 8 APs. It is seen in Figs. 7.12a, 7.12b and 7.12a that when considering a small number of branches U , there is little BER performance difference between choosing optimum or suboptimum pilots for the pilot transmission. That is because in both cases, the fast time variance of the outdoor channel during the transmission of the pilot block and the following data blocks is more critical to the BER

performance than the inter-branch interference in FD-LS-JCE $\hat{\mathbf{h}}_{LS}$ of (3.34) with optimum and suboptimum pilots. The time variance of the outdoor channel causes also an error floor in the BER performance. However, in the case of large number of branches U , as shown in Fig. 7.13b, the performance difference of BER between the suboptimum pilots like random pilots and the optimum pilots like Walsh code based pilots, disjoint pilots and CAZAC code based pilots is obvious since the inter-branch interference is getting critical. Some similar BER performance tendency as in the indoor environments can be observed, i.e. the higher the number U of branches, the worse the BER performance using random pilots than the other optimum pilots. This is due to the inter-branch interference during the FD-LS-JCE process with random pilots. In general, the higher the number of branches, the worse the BER performance of any optimum and suboptimum pilots in comparison with the ideal JCE case due to the time variance of the channel on each subchannel. The performance gap between the practical and the ideal JCEs in outdoor environments can be reduced by some adaptive filtering techniques [LSA01, LAS⁺02] by which the time variance is taken into account for channel estimation and tracking.

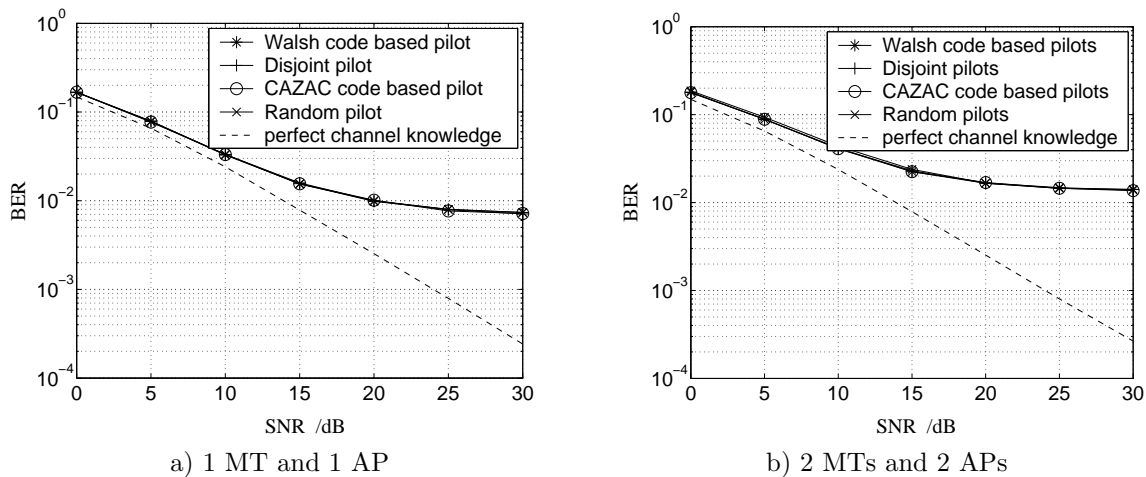


Fig. 7.12. The BER for Walsh code based pilots, disjoint pilots, CAZAC code based pilots and random pilots in an outdoor environment; a) 1 MT and 1 AP; b) 2 MTs and 2 APs.

In Fig. 7.14, the BER performance when considering 1 MT and 1 AP, 2 MTs and 2 APs, 4 MTs and 4 APs, as well as 8 MTs and 8 APs in the outdoor environment is compared for the applications of CAZAC code based pilots and random pilots. It is seen that in the outdoor environment, the BER performance with both CAZAC code based pilot transmission, as seen in Fig. 7.14a, and random pilot transmission, as seen in Fig. 7.14b, is sensitive to the number of branches U due to the time variance of channel on each branch. In the case of high number of branches U such as 8 MTs and 8 APs, the BER performance with random pilot transmission is extremely bad comparing with that in the ideal JCE case. The sensibility of the BER performance using various pilots to the number of branches U in outdoor environments is expected to be reduced also by some adaptive filtering techniques [LSA01, LAS⁺02].

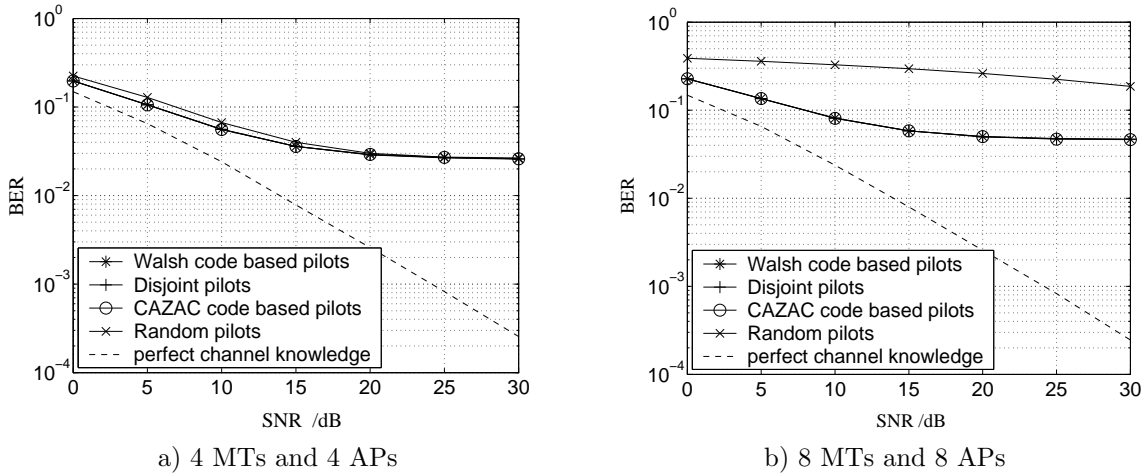


Fig. 7.13. The BER for Walsh code based pilots, disjoint pilots, CAZAC code based pilots and random pilots in an outdoor environment; a) 4 MTs and 4 APs; b) 8 MTs and 8 APs.

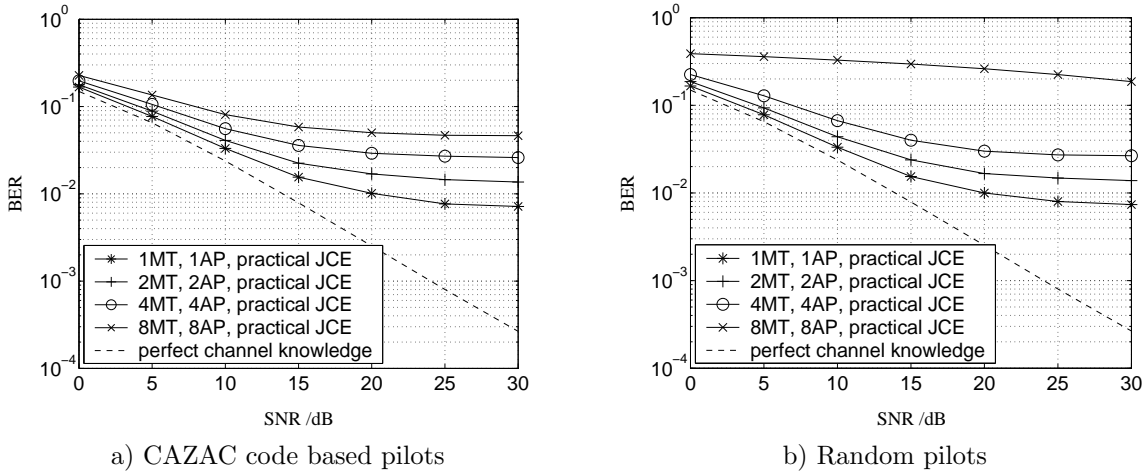


Fig. 7.14. The BER in the scenarios of 1MT-1AP, 2MT-2AP, 4MT-4AP and 8MT-8AP in an outdoor environment; a) CAZAC code based pilots; b) Random pilots.

To summarize this subsection, in the sufficient channel estimation case as explained in Subsection 7.2.1 in the considered multi-branch OFDM system, the BER performance with FD-LS-JCE $\hat{\mathbf{h}}_{LS}$ of (3.34) deviates from that with ideal JCE in indoor and outdoor environments for the applications of both optimum and suboptimum pilots. This results from the time variance of the channel on each branch during the pilot transmission and the following data detection. For the same reason, the BER performance in indoor and outdoor environments for both optimum and suboptimum pilots gets worse when the number of branches U increases.

Although the BER simulation results of only FD-LS-JCE are presented, it can be expected that for the optimum pilots, e.g. disjoint pilots, Walsh code based pilots and CAZAC code based pilots, there is no BER performance difference for the system with FD-MF-

JCE and for the system with FD-LS-JCE. This is because for optimum pilots, there is no performance difference between FD-LS-JCE $\hat{\mathbf{h}}_{\text{LS}}$ of (3.34) and FD-MF-JCE $\hat{\mathbf{h}}_{\text{MF}}$ of (3.32) as explained in Subsection 7.3.2. Besides, for the multi-branch OFDM system, there is no BER performance difference between the systems with FD-LS-JCE and with FD-WLS-JCE schemes since for OFDM modulation, the noise before the channel estimator at the receiver is Gaussian [Fil04] with identity covariance matrix.

7.4 Performance of JCE in multi-branch FMT systems

7.4.1 Subchannel simulation

As seen in Table 7.2, the subchannel bandwidth is 1.25 MHz in the considered FMT system. The amplitude of the CTF of the subchannel with bandwidth 1.25 MHz of the WSSUS broadband channel obtained by the FMT modulation is simulated in Fig. 7.15a for indoor and in Fig. 7.15b for outdoor environments. The CTF of the i -th subchannel $\tilde{h}_i(f, t)$, $i = 1 \cdots N_{\text{F}}$, is obtained by filtering the broadband channel $\tilde{h}(f, t)$ of (2.5) with the FMT demodulation [CEÖ02]. As an example, the amplitude of the CTF of the first subchannel $|\tilde{h}_1(f, t)|$ is presented in Figs. 7.15a and 7.15b. The f -axis represents the bandwidth in MHz and the t -axis represents the propagation time in ms.

It is shown in Fig. 7.15a that in the indoor environment the subchannel in the FMT system keeps time invariant for a long period. By comparing the subchannel in Fig. 7.15a with the broadband channel in Fig. 2.1, it appears that the time variance, i.e. the influence of the Doppler shift, is much alleviated on each subchannel by the FMT demodulation. However, the subchannel in the FMT system is still frequency selective, although its frequency selectivity is not as strong as the broadband indoor channel shown in Fig. 2.1. This frequency selectivity on each subchannel means that it is not suitable to use one-tap equalization per subcarrier as done in OFDM systems [NP00]. It also means that the interference between the channel coefficients in the channel estimation process and the ISI in the data detection process have to be considered on each subchannel of the FMT system.

From Fig. 7.15b, it is seen that the amplitude of the subchannel transfer function of the considered FMT system in outdoor environments fluctuates in both time and frequency. However, the fluctuations are less intensive compared to the broadband outdoor channel as shown in Fig. 2.2. Similar to the discussion on the indoor subchannel of the considered FMT system of Fig. 7.15a, the influence of the Doppler shift is much alleviated on each outdoor subchannel by the FMT demodulation and the interference between the channel coefficients in the channel estimation process and the ISI in the data detection process have to be dealt with on each outdoor subchannel of the considered FMT system.

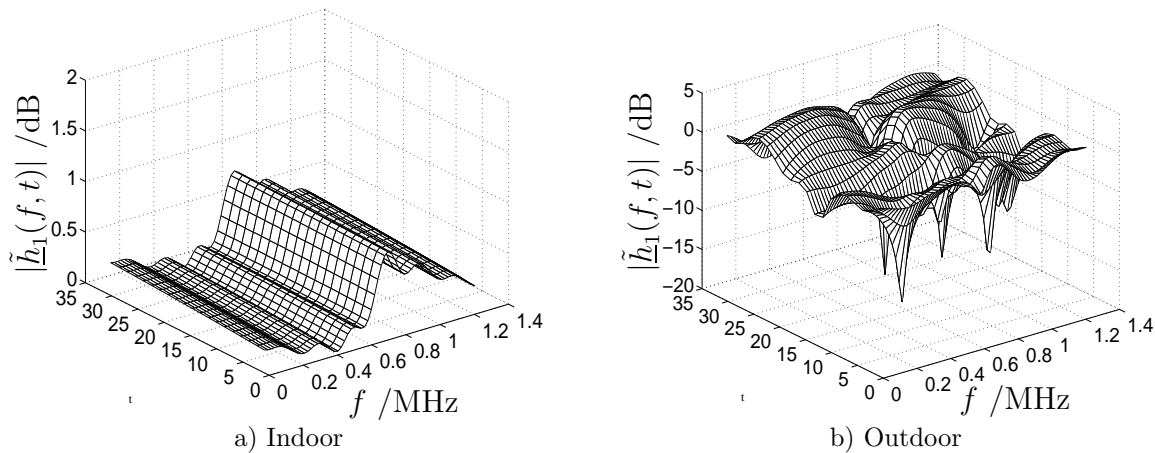


Fig. 7.15. The amplitude of the transfer function, i.e. $|\tilde{h}_1(f, t)|$ for the 1st FMT subchannel; a) Indoor; b) Outdoor.

7.4.2 MSE simulation

In this subsection, the simulation results of the normalized MSE ϵ'_{LS} of (7.11) for TD-LS-JCE $\hat{\mathbf{h}}_{LS}$ of (3.86) over WSSUS channel in the multi-branch FMT systems are presented. The optimum CAZAC code based pilots and the suboptimum random pilots are used as the pilots transmitted on the multiple branches in the simulations.

In Fig. 7.16, the normalized MSE ϵ'_{LS} of (7.11) for the multi-branch FMT system with CAZAC code based pilots and random pilots in an indoor environment is simulated. Figs. 7.16a, 7.16b and 7.16c illustrate the cases with 1 MT and 1 AP, 2 MTs and 1 AP as well as 3 MTs and 1 AP, respectively. It is seen that in the lower SNR range in the case of 1 MT and 1 AP, the MSE performance of TD-LS-JCE $\hat{\mathbf{h}}_{LS}$ of (3.86) with CAZAC code based pilot is close to that with random pilot. Increasing the SNR, the MSE curve comes to an error floor for TD-LS-JCE with random pilot transmission. While the error floor has not appeared until the SNR of 25 dB for the MSE curve with CAZAC code based pilot transmission. In the insufficient channel estimation, as explained in Subsection 7.2.2, this error floor obtained by applying random pilot demonstrates that the TD-LS-JCE $\hat{\mathbf{h}}_{LS}$ of (3.86) with random pilot is more sensitive than the CAZAC code based pilot to the residue energy leakage by the mismatch between the number of channel coefficients W and the number of channel taps, which is a random value. In the case of 2 MTs and 1 AP, the TD-LS-JCE $\hat{\mathbf{h}}_{LS}$ of (3.86) with CAZAC code based pilots outperforms significantly than that with random pilots in terms of the normalized MSE for the multi-branch FMT system especially in the higher SNR range. This is because the inter-branch interference in TD-LS-JCE using random pilots makes the error floor appear at low SNR value, while there is no inter-branch interference in TD-LS-JCE using CAZAC code based pilots. In the case of 3 MTs and 1 AP, the error floor can be observed for both CAZAC code based pilot and random pilot transmissions. This is because the residue energy leakage of

the channel taps on each transmit branch is getting influential to both pilots. However, the performance advantage of TD-LS-JCE $\hat{\mathbf{h}}_{LS}$ of (3.86) using CAZAC code based pilots compared to random pilots is not as significant as in the case of 2 MTs and 1 AP. From the simulation results in Fig. 7.16, we can conclude that the TD-LS-JCE $\hat{\mathbf{h}}_{LS}$ of (3.86) with optimum pilots outperforms that with suboptimum pilots in terms of MSE. In the case of insufficient channel estimation, using the optimum pilots, the error floor of the MSE appears at higher SNR value than using the suboptimum pilots.

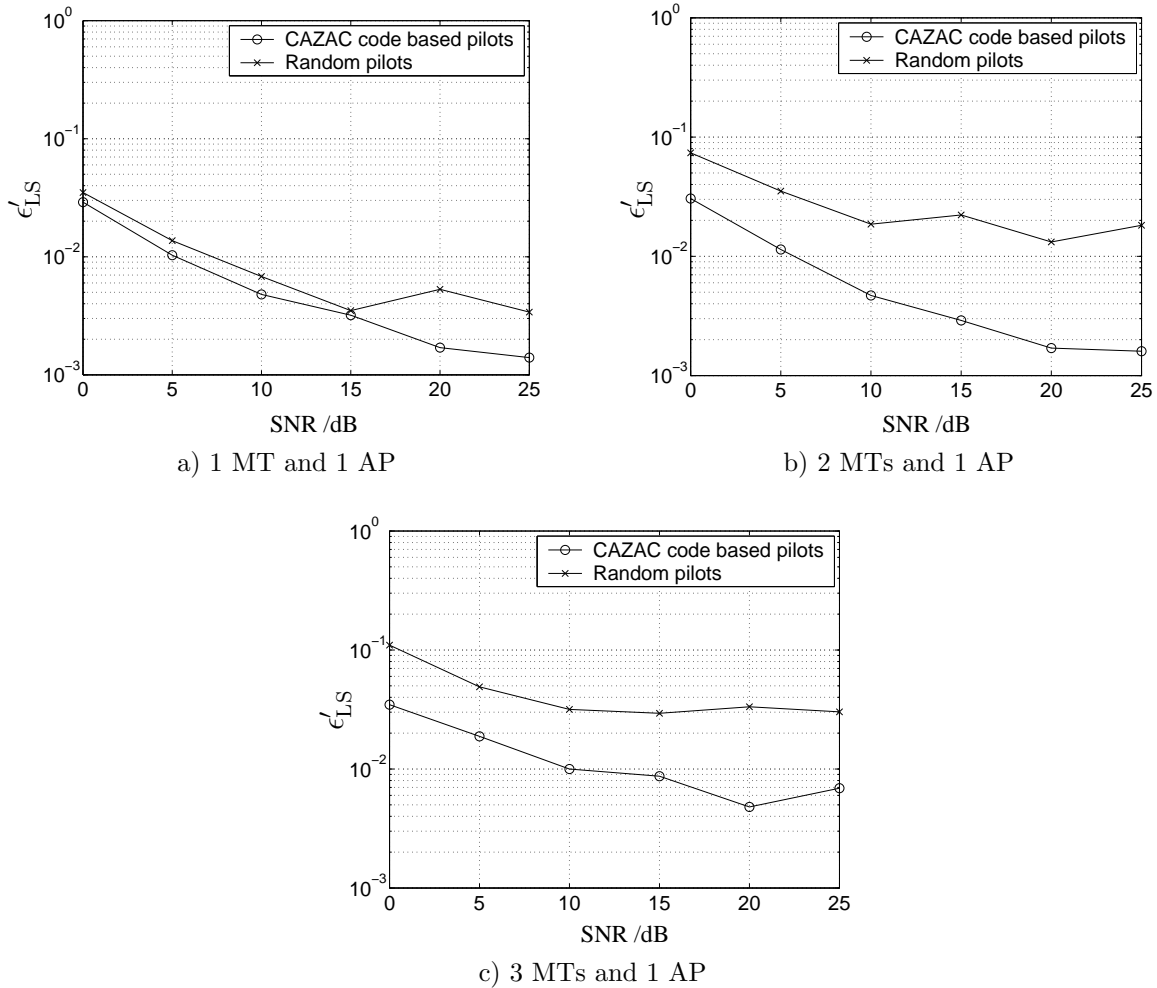


Fig. 7.16. The normalized MSE ϵ'_{LS} of (7.11) for the multi-branch FMT system with CAZAC code based pilots and random pilots in an indoor environment; a) 1 MT and 1 AP; b) 2 MTs and 1 AP; c) 3 MTs and 1 AP.

In Fig. 7.17, the normalized MSE ϵ'_{LS} of (7.11) for the multi-branch FMT system when considering 1MT and 1 AP, 2 MTs and 1 AP, and 3 MTs and 1 AP in an indoor environment is simulated. For the case of CAZAC code based pilots, as seen in Fig. 7.17a, the normalized MSE ϵ'_{LS} of (7.11) in the case of 1 MT and 1 AP is very close to the case of 2 MTs and 1 AP. This is because the inter-branch interference is avoided by the design of optimum pilots for the TD-LS-JCE. However, in the case of 3 MTs and 1 AP, the error

floor due to the insufficient channel estimation becomes significant so that the benefit of TD-LS-JCE with CAZAC code based pilots in terms of the inter-branch interference free estimation is not clearly seen. Nevertheless, when comparing Fig. 7.17a with Fig. 7.17b, in which the random pilots are applied in the TD-LS-JCE for the multi-branch FMT system, it is seen that with random pilots, the MSE performance of TD-LS-JCE suffers not only from the error floor due to the insufficient channel estimation but also from the inter-branch interference even in the case of low number of branches such as two transmit branches.

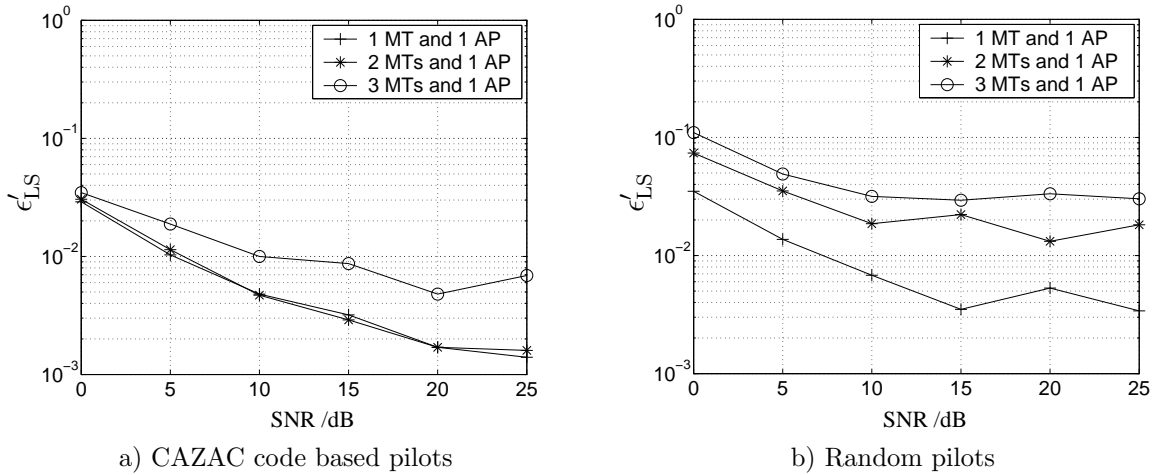


Fig. 7.17. The normalized MSE ϵ'_{LS} of (7.11) for the multi-branch FMT system considering 1 MT and 1 AP, 2 MTs and 1 AP, as well as 3 MTs and 1 AP in an indoor environment; a) CAZAC code based pilots; b) Random pilots.

In Fig. 7.18, the normalized MSE ϵ'_{LS} of (7.11) for the multi-branch FMT system with CAZAC code based pilots and random pilots in an outdoor environment is illustrated for the cases of 1 MT and 1 AP, as shown in Fig. 7.18a, 2 MTs and 1 AP, as shown in Fig. 7.18b as well as 3 MTs and 1 AP, as shown in Fig. 7.18c. It is seen in Fig. 7.18a that with only one transmit branch, the TD-LS-JCE $\hat{\mathbf{h}}_{LS}$ of (3.86) with CAZAC code based pilot performs similar to that with random pilot transmission in terms of the normalized MSE in the FMT system in lower SNR case. In higher SNR case, the TD-LS-JCE with random pilot underperforms that with CAZAC code based pilot. The TD-LS-JCE with both pilots suffers from more severe error floor in the MSE performance than in the indoor environment as in Fig. 7.16. This is because in the outdoor environment, the maximum channel delay is $5 \mu\text{s}$, which is longer than $0.8 \mu\text{s}$, which is assumed the maximum delay in the indoor environment. In both environments, as mentioned in Subsection 7.2.2, the number of channel coefficient W is set to 8, resulting in a more severe sensibility of TD-LS-JCE for any pilots in the outdoor environment due to residue energy leakage of channel taps. With two transmit branches, as seen in Fig. 7.18b, the TD-LS-JCE with CAZAC code based pilots outperforms significantly than that with random pilots in terms of MSE in the multi-branch FMT system. This is because the TD-LS-JCE with CAZAC code based pilots has no inter-branch interference, while with random pilots has significant

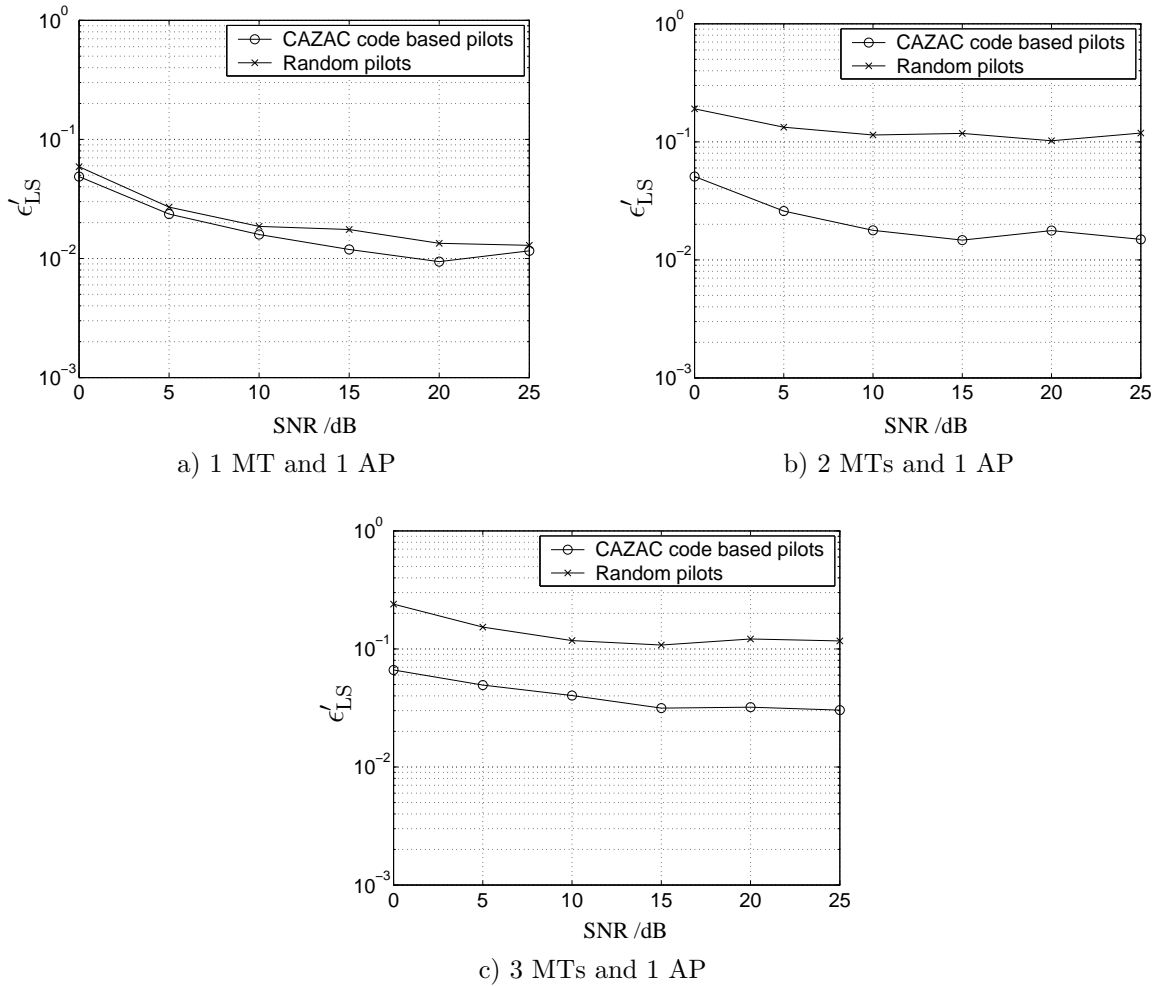


Fig. 7.18. The normalized MSE ϵ'_{LS} of (7.11) for the multi-branch FMT system with CAZAC code based pilots and random pilots in an outdoor environment; a) 1 MT and 1 AP; b) 2 MTs and 1 AP; c) 3 MTs and 1 AP.

inter-branch interference. With three transmit branches, as seen in Fig. 7.18c, the TD-LS-JCE with CAZAC code based pilots performs also much better than that with random pilots in terms of the normalized MSE in the multi-branch FMT system. However, the advantage of CAZAC code based pilots over random pilots in the three branch case is not as significantly as that in the two branch case due to the error floor in both cases which comes from the insufficient channel estimation on each branch.

In Fig. 7.19, the normalized MSE ϵ'_{LS} of (7.11) for the multi-branch FMT system considering 1 MT and 1 AP, 2 MTs and 1 AP, as well as 3 MTs and 1 AP in an outdoor environment is illustrated. It is seen in Fig. 7.19a that with CAZAC code based pilots, for the lower SNR range, the normalized MSE ϵ'_{LS} of (7.11) in the 2 MTs and 1 AP case is similar to that with 1 MT and 1 AP case. This verifies the theoretical analysis in Chapter 4 that the normalized MSE performance for TD-LS-JCE with optimum pilots like CAZAC code based pilots is not influenced by the number of branches U . However,

in the higher SNR range and assuming a higher number U of branches such as three branches, the MSE performance of CAZAC code based pilots is sensitive to the number of branches due to the error floor that results from the insufficient channel estimation on each branch. In comparison with the CAZAC code based pilots, with random pilots, as shown in Fig. 7.19b, the MSE performance is very sensitive to the number of branches with lower number of branches such as two branches. In the case of higher number of branches such as three branches, the error floor of the MSE performance using random pilot transmission appears at low SNR value due to the insufficient channel estimation on each branch and the inter-branch interference. Therefore, it looks like the MSE performance with random pilot transmission is not sensitive to the number of branches U when U takes higher value.

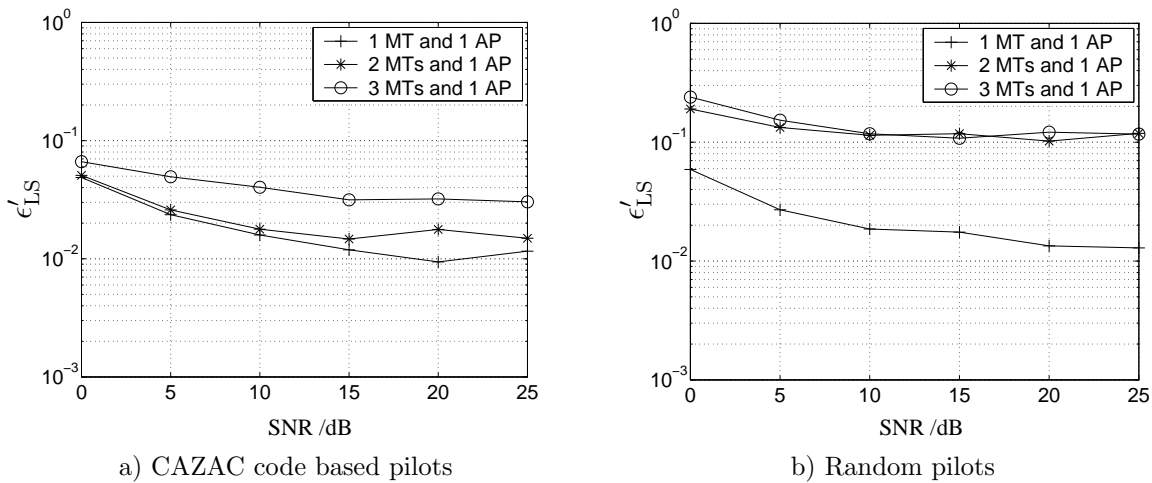


Fig. 7.19. The normalized MSE ϵ'_{LS} of (7.11) of the multi-branch FMT system considering 1 MT and 1 AP, 2 MTs and 1 AP, as well as 3 MTs and 1 AP in an outdoor environment; a) CAZAC code based pilots; b) Random pilots.

From above simulation results of MSE of the normalized MSE ϵ'_{LS} of (7.11) of the estimated channel in a multi-branch FMT system with various number of branches and with various pilots, it is seen that in the scenario of insufficient channel estimation, the TD-LS-JCE $\hat{\mathbf{h}}_{LS}$ of (3.86) with CAZAC code based pilot transmission outperforms that with random pilot transmission in both indoor and outdoor environments. In addition, for the TD-LS-JCE with CAZAC code based pilot transmission, the error floor appears at higher value than that with random pilot transmission in both indoor and outdoor environments. This is because although the MSE performance of TD-LS-JCE with both kinds of pilots suffers from insufficient channel estimation, the TD-LS-JCE with random pilots deteriorates the MSE performance further due to the inter-branch interference in channel estimation.

Although the MSE simulation results of only TD-LS-JCE are presented, it can be expected that for the optimum pilots, e.g. CAZAC code based pilots, there is no MSE performance difference for the system with TD-MF-JCE and for the system with TD-LS-JCE. This

is because for optimum pilots, the matrix $\mathbf{P}^H\mathbf{P}$ in (3.86) is identity matrix when the TD-LS-JCE $\hat{\mathbf{h}}_{LS}$ of (3.86) is compared with TD-MF-JCE $\hat{\mathbf{h}}_{MF}$ of (3.85). However, for the multi-branch FMT system, there is MSE performance difference between TD-LS-JCE and TD-WLS-JCE schemes [KWC04a]. This is because for the FMT modulation, the noise before the channel estimator at the receiver is not Gaussian [KWC04a] after the FMT demodulation at the receiver, i.e. the noise covariance matrix is not identity, when the TD-WLS-JCE $\hat{\mathbf{h}}_{WLS}$ of (3.87) is compared with TD-LS-JCE $\hat{\mathbf{h}}_{LS}$ of (3.86).

7.4.3 BER simulation

In this subsection, the simulation results of the BER performance of the multi-branch FMT system with TD-LS-JCE $\hat{\mathbf{h}}_{LS}$ of (3.86) are presented.

Fig. 7.20 shows the simulated BER curves for the multi-branch FMT system with CAZAC code based pilots and random pilots in an indoor environment. In the case of 1 MT and 1 AP, as seen in Fig. 7.20a, the BER performance with CAZAC code based pilot transmission is close to that with random pilot transmission. In the case of 2 MTs and 1 AP, as seen in Fig. 7.20b, and in the case of 3 MTs and 1 AP, as seen in Fig. 7.20c, the BER performance with CAZAC code based pilots applied to TD-LS-JCE outperforms TD-LS-JCE with random pilots. Generally the inter-branch interference exists in both the channel estimation and data detection stages. In Fig. 7.16, a significant MSE performance advantage by using CAZAC code based pilots is seen than using random pilots for the cases with two and three branches. This is because the inter-branch interference in channel estimation is cancelled by TD-LS-JCE with CAZAC code based pilots. However, in the corresponding BER performance in Fig. 7.20, such significant advantage by using CAZAC code based pilots over random pilots is not observed for the cases with two and three branches. This is because the inter-branch interference in data detection adversely significantly influences the BER performance using both CAZAC code based pilot transmission and random pilot transmission. By introducing some advanced interference suppressing and cancellation technologies in CDMA systems [Kle96], the inter-branch interference in data detection will be mitigated, and the BER performance advantage by using CAZAC code based pilot transmission over random pilot transmission is expected to be significant.

In Fig. 7.21, the BER performance for the multi-branch FMT system considering 1 MT and 1 AP, 2 MTs and 1 AP, and 3 MTs and 1 AP in an indoor environment is illustrated for the application of CAZAC code based pilots, as shown in Fig. 7.21a, and for random pilots, as shown in Fig. 7.21b. It is seen that with CAZAC code based pilots, the BER performance for the multi-branch FMT system is not much sensitive to the number of branches U . However, with random pilots, the BER performance is obviously worse in the

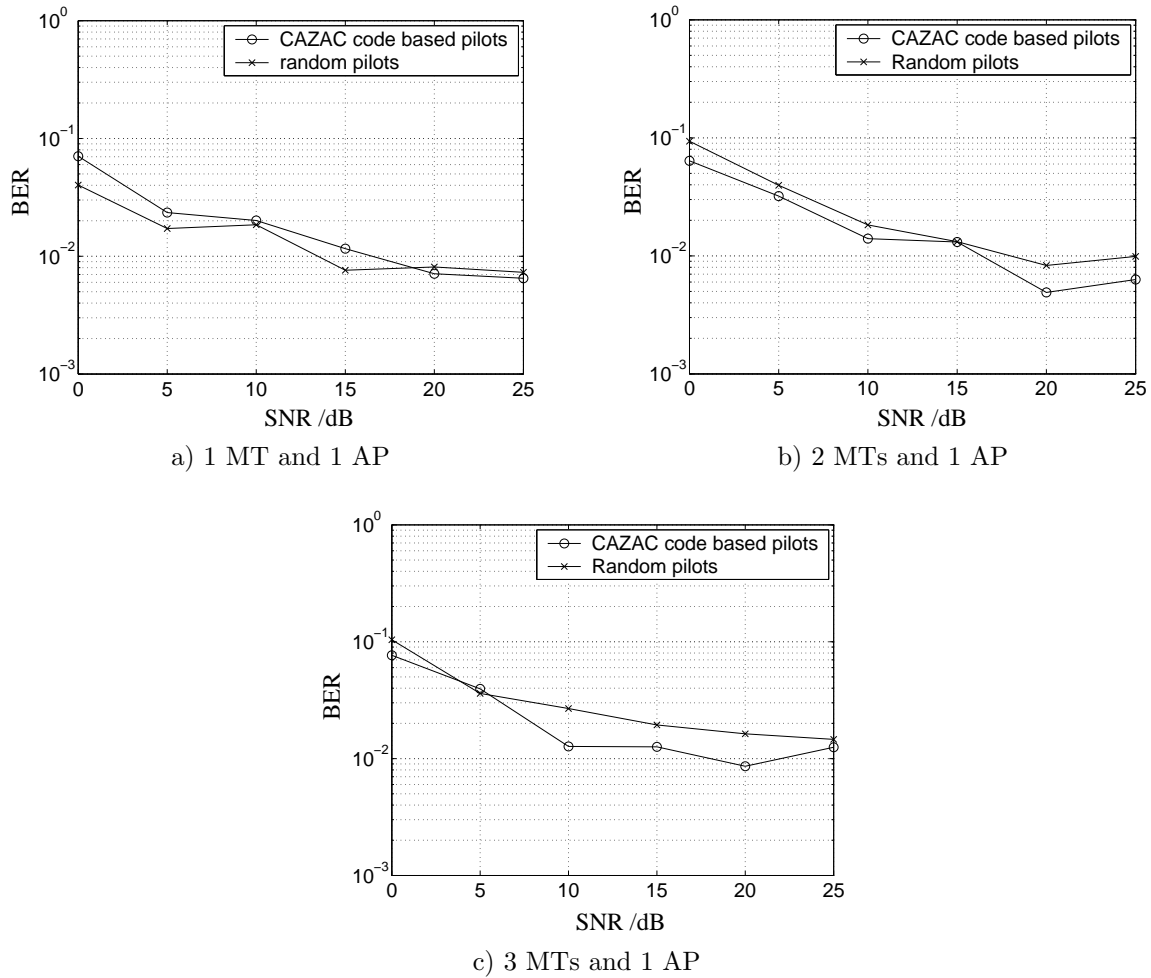


Fig. 7.20. BER of the multi-branch FMT system with CAZAC code based pilots and random pilots in an indoor environment; a) 1 MT and 1 AP; b) 2 MTs and 1 AP; c) 3 MTs and 1 AP.

case of more branches than in the case of less branches due to the inter-branch interference in both the channel estimation and data detection processes.

Fig. 7.22 illustrates the BER performance for the multi-branch FMT system with CAZAC code based pilots and random pilots in an outdoor environment. When comparing the three figures of BER performance in Fig. 7.22, i.e. Fig. 7.22a for the case of 1 MT and 1 AP, Fig. 7.22b for the case of 2 MTs and 1 AP as well as Fig. 7.22c for the case of 3 MTs and 1 AP, with the three figures of MSE performance in Fig. 7.18, i.e. Figs. 7.18a, 7.18b and 7.18c, it is seen that the BER performance of the multi-branch system in Fig. 7.22 has a similar tendency as the MSE performance of the TD-LS-JCE in Fig. 7.18. That is, the system with CAZAC code based pilot transmission outperforms that with random pilot transmission in terms of both BER and MSE, especially in the case of 2 Tx and 1 Rx. This similarity between the BER performance and the MSE performance demonstrates that the channel estimation and the pilots applied are critical to the overall

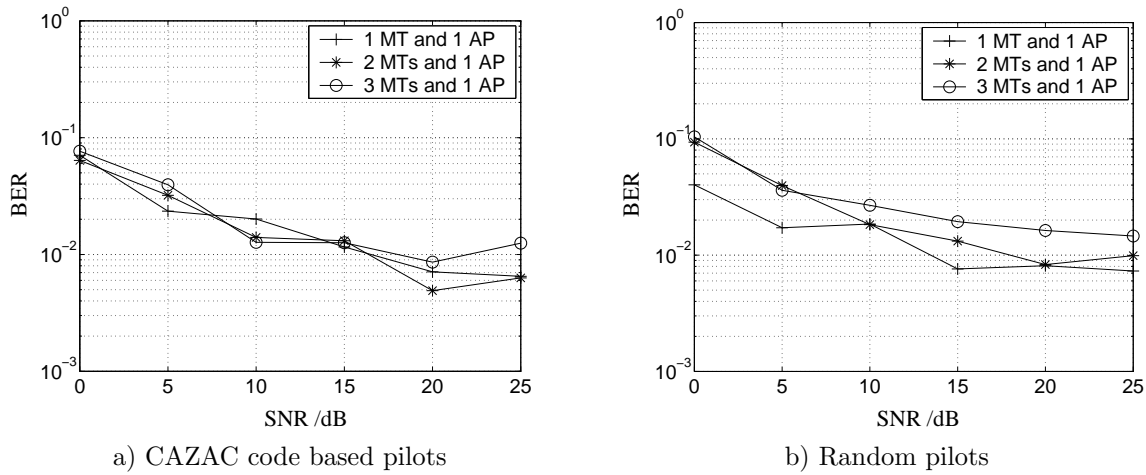


Fig. 7.21. BER of the multi-branch FMT system in the scenarios of 1 MT and 1 AP, 2 MTs and 1 AP, as well as 3 MTs and 1 AP in an indoor environment; a) CAZAC code based pilots; b) Random pilots.

system performance in the multi-branch FMT system.

In Fig. 7.23, the BER of the multi-branch FMT system considering 1 MT and 1 AP, 2 MTs and 1 AP, as well as 3 MTs and 1 AP in an outdoor environment is shown. When the two subfigures in Fig. 7.23, i.e. Fig. 7.23a for CAZAC code based pilots and Fig. 7.23b for random pilots, are compared with the two figures in Fig. 7.19, i.e. Fig. 7.19a and Fig. 7.19b, it is seen that the BER performance tendency for CAZAC code based pilots and random pilots in the scenarios of various branches is the same as the MSE performance tendency in the corresponding scenarios. This similarity also demonstrates that the channel estimation and the pilots applied are influential to the overall system performance in the multi-branch FMT system.

From above simulation results for the multi-branch FMT system of BER with various number of branches and with various pilots, it is seen that in the scenario of insufficient channel estimation, the BER performance has the similar tendency as the MSE performance in both indoor and outdoor environments. Therefore, the investigations on the channel estimation, especially on the pilot design in multi-branch systems, as carried out in this thesis, is significant to the improvement of the overall system performance.

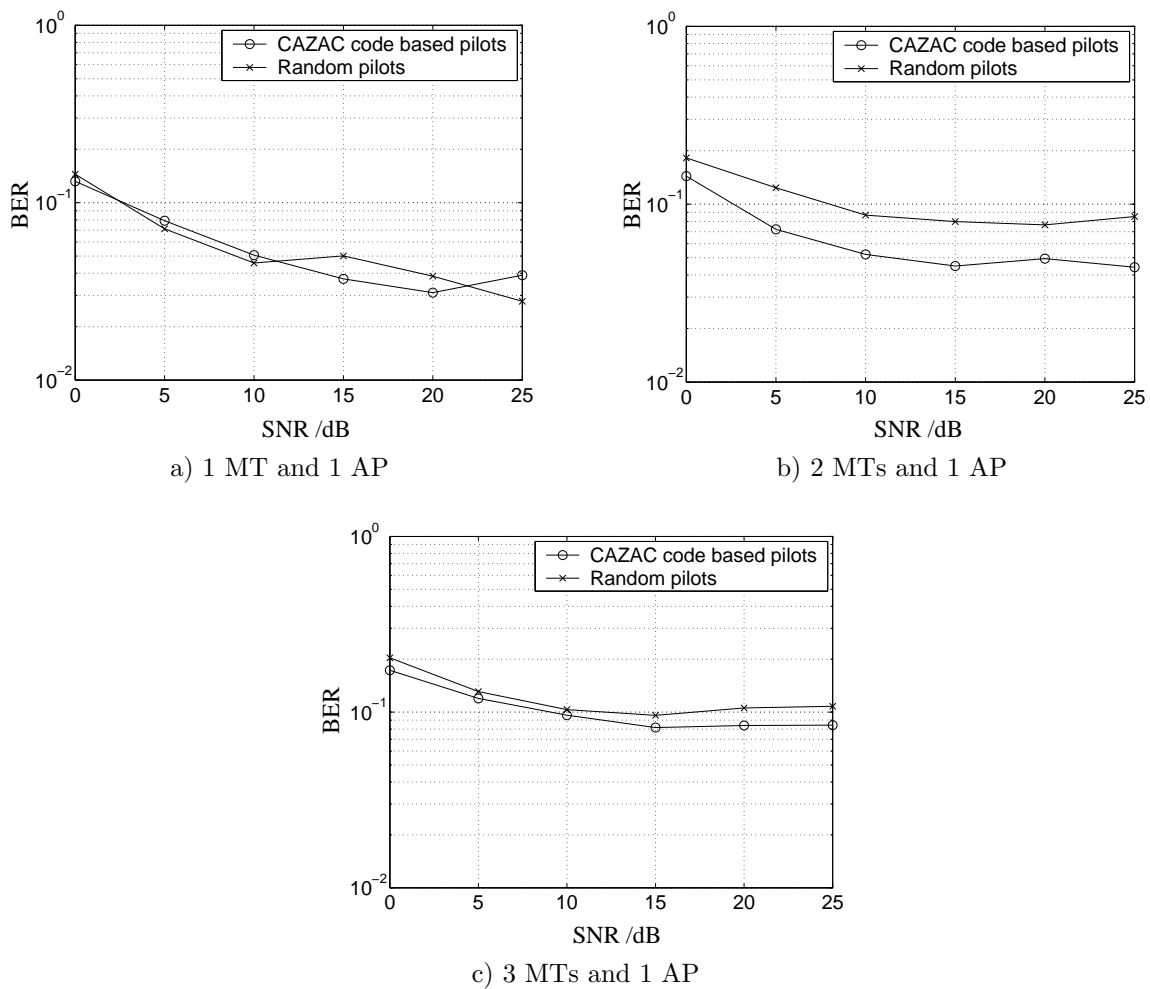


Fig. 7.22. BER of the multi-branch FMT system with CAZAC code based pilots and random pilots in an outdoor environment; a) 1 MT and 1 AP; b) 2 MTs and 1 AP; c) 3 MTs and 1 AP.

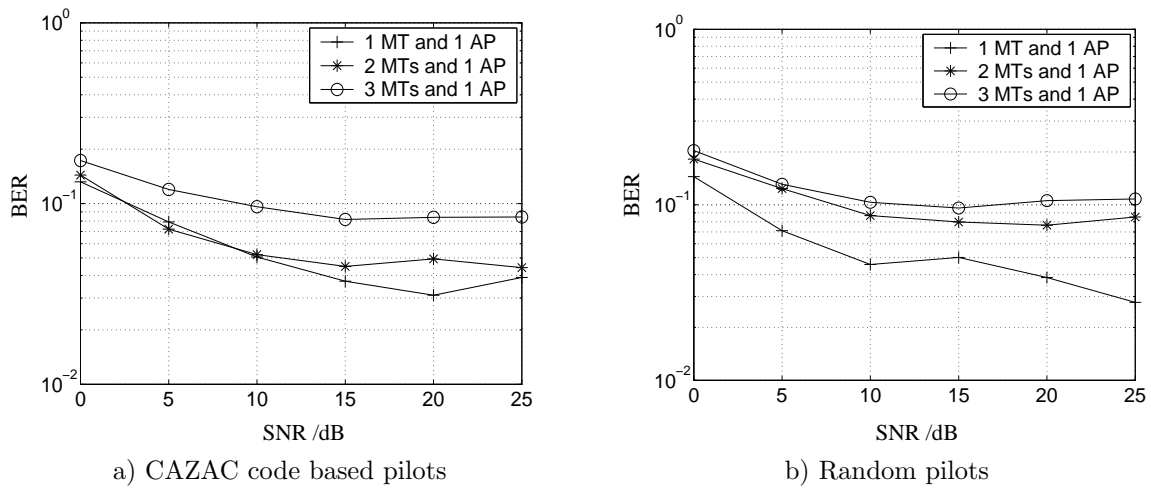


Fig. 7.23. BER of the multi-branch FMT system considering 1 MT and 1 AP, 2 MTs and 1 AP, as well as 3 MTs and 1 AP in an outdoor environment; a) CAZAC code based pilots; b) Random pilots.

8 Summary

8.1 English

Channel estimation is of great importance in many wireless communication systems, since it influences the overall performance of a system significantly. Especially in multi-user and/or multi-antenna systems, i.e. generally in multi-branch systems, the requirements on channel estimation are very high, since the training signals or so called pilots that are used for channel estimation suffer from multiple access interference. Recently, in the context with such systems more and more attention is paid to concepts for joint channel estimation (JCE) which have the capability to eliminate the multiple access interference and also the interference between the channel coefficients. The performance of JCE can be evaluated in noise limited systems by the SNR degradation and in interference limited systems by the variation coefficient. Theoretical analysis carried out in this thesis verifies that both performance criteria are closely related to the patterns of the pilots used for JCE, no matter the signals are represented in the time domain or in the frequency domain. Optimum pilots like disjoint pilots, Walsh code based pilots or CAZAC code based pilots, whose constructions are described in this thesis, do not show any SNR degradation when being applied to multi-branch systems. It is shown that optimum pilots constructed in the time domain become optimum pilots in the frequency domain after a discrete Fourier transformation. Correspondingly, optimum pilots in the frequency domain become optimum pilots in the time domain after an inverse discrete Fourier transformation. However, even for optimum pilots different variation coefficients are obtained in interference limited systems. Furthermore, especially for OFDM-based transmission schemes the peak-to-average power ratio (PAPR) of the transmit signal is an important decision criteria for choosing the most suitable pilots. CAZAC code based pilots are the only pilots among the regarded pilot constructions that result in a PAPR of 0 dB for the transmit signal that originates in the transmitted pilots. When summarizing the analysis regarding the SNR degradation, the variation coefficient and the PAPR with respect to one single service area and considering the impact due to interference from other adjacent service areas that occur due to a certain choice of the pilots, one can conclude that CAZAC codes are the most suitable pilots for the application in JCE of multi-carrier multi-branch systems, especially in the case if CAZAC codes that originate in different mother codes are assigned to different adjacent service areas. The theoretical results of the thesis are verified by simulation results. The choice of the parameters for the frequency domain or time domain JCE is oriented towards the evaluated implementation complexity. According to the chosen parameterization of the regarded OFDM-based and FMT-based systems it is shown that a frequency domain JCE is the best choice for OFDM and a time domain JCE is the best choice for FMT applying CAZAC codes as pilots. The results of this thesis can be used as a basis for further theoretical research and also for future JCE implementation in wireless systems.

8.2 German

In zahlreichen drahtlosen Kommunikationssystemen kommt der Kanalschätzung eine große Bedeutung zu, da sie die Gesamtperformanz eines Systems in erheblichem Maße beeinflusst. Insbesondere in Mehrteilnehmersystemen und/oder Mehrantennensystemen, d.h. allgemein in Systemen mit mehreren Übertragungszweigen, werden hohe Anforderungen an die Kanalschätzung gestellt, da die zur Kanalschätzung verwendeten Trainingssignale, die sogenannten Piloten, Vielfachzugriffsinterferenzen unterliegen. Für solche Systeme werden zunehmend Verfahren zur gemeinsamen Kanalschätzung (engl. Joint Channel Estimation, JCE) betrachtet, die sowohl die Vielfachzugriffsinterferenzen als auch die Interferenz zwischen den Kanal-Koeffizienten eliminieren. Die Performanz der JCE kann in rauschbegrenzten Szenarien anhand der SNR-Degradation und in interferenzbegrenzten Szenarien durch den Variationskoeffizienten evaluiert werden. Theoretische Analysen, die in der vorliegenden Arbeit enthalten sind, zeigen, dass beide Performanzkriterien eng mit der Struktur der zur Kanalschätzung verwendeten Piloten zusammenhängen, unabhängig davon, ob die Piloten im Zeitbereich oder Frequenzbereich repräsentiert werden. Optimale Piloten, wie beispielsweise nicht-gemeinsame Piloten, Walsh-Code-basierende Piloten oder CAZAC-Code-basierende Piloten, deren Konstruktion in der vorliegenden Arbeit beschrieben wird, weisen keine SNR-Degradation bei der Anwendung in Systemen mit mehreren Übertragungszweigen auf. Es wird gezeigt, dass optimale Piloten, die im Zeitbereich konstruiert werden, nach einer diskreten Fouriertransformation zu optimalen Piloten im Frequenzbereich werden. Entsprechend werden optimale Piloten im Frequenzbereich durch eine inverse diskrete Fouriertransformation zu optimalen Piloten im Zeitbereich. In interferenzbegrenzten Systemen zeigen sich jedoch selbst für optimale Piloten unterschiedliche Performanzen hinsichtlich des jeweiligen Variationskoeffizienten. Insbesondere bei OFDM-basierten Übertragungsverfahren ist ein weiteres Kriterium zur Wahl geeigneter Piloten das durch das Senden der Pilotsignale entstehende Verhältnis zwischen maximalem Sendesignalpegel und mittlerem Sendesignalpegel (engl. Peak-to-average power ratio, PAPR). CAZAC-Code-basierte Piloten ermöglichen als einzige der hier betrachteten Piloten eine PAPR von 0 dB für die für die Kanalschätzung erforderlichen Signalanteile. Fasst man die Analysen hinsichtlich SNR-Degradation, Variationskoeffizienten und PAPR bezogen auf einen Versorgungsbereich zusammen und betrachtet man die Auswirkungen auf die Interferenz, die zwischen unterschiedlichen Versorgungsbereichen durch das Verwenden bestimmter Piloten erzeugt wird, so lässt sich erkennen, dass CAZAC-Codes, die von unterschiedlichen Mutter-Codes stammend unterschiedlichen Versorgungsbereichen zugeordnet werden, die am besten geeigneten Piloten für eine gemeinsame Kanalschätzung in einem Mehrträger-Übertragungsverfahren mit mehreren Übertragungszweigen sind. Die theoretischen Ergebnisse dieser Arbeit sind durch Simulationen verifiziert. Die Wahl der Zeitbereichs-Kanalschätzung oder Frequenzbereichs-Kanalschätzung richtet sich nach der Implementierungskomplexität. Bei der gewählten Parametrisierung der betrachteten OFDM-basierten und FMT-basierten Systeme zeigt sich, dass für OFDM eine Kanalschätzung im Frequenzbe-

reich und für FMT eine Kanalschätzung im Zeitbereich unter Verwendung von CAZAC-Codes als Piloten die beste Wahl ist. Die vorliegende Arbeit kann sowohl als Basis für weiterführende theoretische Analysen der gemeinsamen Kanalschätzung als auch als Basis für zukünftige Systemimplementierungen dienen.

Appendix

A.1 Abbreviations

1G	<u>1</u> st <u>G</u> eneration
2G	<u>2</u> nd <u>G</u> eneration
3G	<u>3</u> rd <u>G</u> eneration
4G	<u>4</u> th <u>G</u> eneration
AP	<u>A</u> ccess <u>P</u> oint
AWGN	<u>A</u> dditive <u>W</u> hite <u>G</u> aussian <u>N</u> oise
BER	<u>B</u> it <u>E</u> rror <u>R</u> ate
BS	<u>B</u> ase <u>S</u> tation
CAZAC	<u>C</u> onstant <u>A</u> mplitude <u>Z</u> ero <u>A</u> uto <u>c</u> orrelation
cdf	<u>c</u> umulative <u>d</u> istribution <u>f</u> unction
CDMA	<u>C</u> ode <u>D</u> ivision <u>M</u> ultiple <u>A</u> ccess
CIR	<u>C</u> hannel <u>I</u> mpulse <u>R</u> esponse
CP	<u>C</u> yclic <u>P</u> refix
CTF	<u>C</u> hannel <u>T</u> ransfer <u>F</u> unction
CU	<u>C</u> entral <u>U</u> nit
DFT	<u>D</u> iscrete <u>F</u> ourier <u>T</u> ransformation
FB-MC	<u>F</u> ilter <u>B</u> ank <u>M</u> ulti- <u>C</u> arrier
FD-JCE	<u>F</u> requency <u>D</u> omain <u>J</u> oint <u>C</u> hannel <u>E</u> stimation
FD-MF-JCE	<u>F</u> requency <u>D</u> omain <u>M</u> F <u>J</u> CE
FD-LS-JCE	<u>F</u> requency <u>D</u> omain <u>L</u> S <u>J</u> CE
FD-WLS-JCE	<u>F</u> requency <u>D</u> omain <u>W</u> eighted <u>L</u> S <u>J</u> CE
FDMA	<u>F</u> requency <u>D</u> ivision <u>M</u> ultiple <u>A</u> ccess
FFT	<u>F</u> ast <u>F</u> ourier <u>T</u> ransformation
FMT	<u>F</u> iltered <u>M</u> ultit <u>o</u> ne
IC	<u>I</u> nterference <u>C</u> ancellation
ICI	<u>I</u> nter <u>C</u> arrier <u>I</u> nterference
GSM	<u>G</u> lobal <u>S</u> ystem for <u>M</u> obile <u>C</u> ommunications
IDFT	<u>I</u> nverse <u>D</u> iscrete <u>F</u> ourier <u>T</u> ransformation
IFFT	<u>I</u> nverse <u>F</u> ast <u>F</u> ourier <u>T</u> ransformation
ISI	<u>I</u> ntersymbol <u>I</u> nterference
JCE	<u>J</u> oint <u>C</u> hannel <u>E</u> stimation
JD	<u>J</u> oint <u>D</u> etection
JOINT	<u>J</u> oint <u>T</u> ransmission and <u>D</u> etection <u>I</u> ntegrated <u>N</u> etwork
JT	<u>J</u> oint <u>T</u> ransmission
LOS	<u>L</u> ine- <u>o</u> f- <u>S</u> ight
LS	<u>L</u> east <u>S</u> quare

MAI	<u>M</u> ultiple <u>A</u> ccess <u>I</u> nterference
MF	<u>M</u> atched <u>F</u> iltering
MF-JCE	<u>M</u> atched <u>F</u> iltering <u>J</u> oint <u>C</u> hannel <u>E</u> stimation
MISO	<u>M</u> ultiple <u>I</u> nput <u>S</u> ingle <u>O</u> utput
ML	<u>M</u> aximum <u>L</u> ikelihood
MSE	<u>M</u> ean <u>S</u> quare Estimation <u>E</u> rror
MMSE	<u>M</u> inimum <u>M</u> ean <u>S</u> quare <u>E</u> rror
MT	<u>M</u> obile <u>T</u> erminal
NLOS	<u>N</u> o <u>L</u> ine-of- <u>S</u> ight
OFDM	<u>O</u> rthogonal <u>F</u> requency <u>D</u> ivision <u>M</u> ultiplexing
PAPR	<u>P</u> eak to <u>A</u> verage <u>P</u> ower <u>R</u> atio
pdf	probability <u>d</u> ensity <u>f</u> unction
PN	<u>P</u> seudo <u>N</u> oise
QoS	<u>Q</u> uality of <u>S</u> ervice
RF	<u>R</u> adio <u>F</u> requency
rrcos	<u>r</u> oot <u>r</u> aised <u>c</u> osine
SA	<u>S</u> ervice <u>A</u> rea
SISO	<u>S</u> ingle <u>I</u> nput <u>S</u> ingle <u>O</u> utput
SS	<u>S</u> pread <u>S</u> pectrum
SNR	<u>S</u> ignal-to- <u>N</u> oise <u>R</u> atio
TD-CDMA	<u>T</u> ime <u>D</u> ivision <u>C</u> DMA
TDD	<u>T</u> ime <u>D</u> ivision <u>D</u> uplex
TD-JCE	<u>T</u> ime <u>D</u> omain <u>J</u> CE
TDMA	<u>T</u> ime <u>D</u> ivision <u>M</u> ultiple <u>A</u> ccess
TD-MF-JCE	<u>T</u> ime <u>D</u> omain <u>M</u> F <u>J</u> CE
TD-LS-JCE	<u>T</u> ime <u>D</u> omain <u>L</u> S <u>J</u> CE
TD-WLS-JCE	<u>T</u> ime <u>D</u> omain <u>W</u> eighted <u>L</u> S <u>J</u> CE
TF	<u>T</u> ransfer <u>F</u> unction
TD-SCDMA	<u>T</u> ime <u>D</u> ivision <u>S</u> ynchronous <u>C</u> DMA
WCDMA	<u>W</u> ideband <u>C</u> DMA
WLS	<u>W</u> eighted <u>L</u> east <u>S</u> quare
WSSUS	<u>W</u> ide- <u>S</u> ense <u>S</u> tationary <u>U</u> ncorrelated <u>S</u> cattering
WSS	<u>W</u> ide- <u>S</u> ense <u>S</u> tationary

A.2 Symbols

$\tilde{\mathbf{A}}_C$	the matrix generated from the cyclic shifts of a CAZAC code
$\tilde{\mathbf{A}}_W$	Hardamard matrix
B	system bandwidth
B_C	channel coherence bandwidth
c	speed of light

$\tilde{\mathbf{c}}$	CAZAC code
$\tilde{\mathbf{c}}_{n_F}$	the CAZAC code vector cyclically shifted by $n_F - 1$ symbols from $\tilde{\mathbf{c}}$
\mathbb{C}	a square matrix forming a CAZAC code
$()^*$	complex conjugate
$()^{*T}$	complex conjugate and transpose or complex Hermitian
$\delta(\cdot)$	Kronecker delta function
δ_{f_D}	Doppler spread
$\delta_{\text{MF-LS},j}$	SNR degradation of the TD-LS-JCE $\gamma_{\text{LS},j}$ in comparison to that of the TD-MF-JCE $\gamma_{\text{MF},j}$
$\tilde{\delta}_{\text{MF-LS},j}$	SNR degradation of the j -th CTF component \tilde{h}_j of FD-LS-JCE in comparison with the reference FD-MF-JCE method
$\delta_{\text{MF-WLS},j}$	SNR degradation of the TD-WLS-JCE $\gamma_{\text{WLS},j}$ in comparison to that of the TD-MF-JCE $\gamma_{\text{MF},j}$
$\tilde{\delta}_{\text{MF-WLS},j}$	SNR degradation of the j -th CTF component \tilde{h}_j of FD-WLS-JCE in comparison with the reference FD-MF-JCE method
$\text{diag}(\cdot)$	diagonal matrix containing the diagonal elements of the matrix in the argument
$\text{E}(\cdot)$	expectation operation
E_b	average bit energy
E_p	energy of the pilot at each branch
ϵ	mean square estimation error for the estimated CIR
$\tilde{\epsilon}$	mean square estimation error for the estimated CTF
ϵ_{LS}	mean square estimation error for the TD-LS-JCE
ϵ'_{LS}	normalized mean square estimation error
$\epsilon_{\text{LS},\min}$	minimum mean square estimation error for the TD-LS-JCE
$\epsilon'_{\text{LS},\min}$	normalized minimum mean square estimation error
$\tilde{\epsilon}_{\text{LS}}$	mean square estimation error for the FD-LS-JCE
$\tilde{\epsilon}_{\text{LS},\min}$	minimum mean square estimation error for the FD-LS-JCE
ϵ_{WLS}	mean square estimation error for the TD-WLS-JCE
E_s	average symbol energy
η	the averaged peak to average power ratio
$\eta^{(u)}$	peak to average power ratio for the u -th branch
η_{CM_F}	the number of complex multiplications
f	frequency
F	subcarrier spacing
$\tilde{\mathcal{F}}$	Fourier matrix
\mathfrak{f}	degree of freedom
f_c	carrier frequency
f_D	Doppler shift
f_{D,w_τ}	Doppler shift on the w_τ -th path, $w_\tau = 1 \cdots W_\tau$
$\tilde{\mathcal{F}}_W$	block matrix containing the first W columns of the Fourier matrix $\tilde{\mathcal{F}}$
$\tilde{\mathcal{F}}_{W,\text{tot}}$	blockdiagonal matrix whose diagonal block is composed of first W columns of the Fourier matrix

γ	SNR
$\tilde{\mathbf{G}}$	the matrix obtained from the multiplication of matrix $\tilde{\mathbf{P}}$ and $\tilde{\mathcal{F}}_{W,\text{tot}}$
$\mathbf{g}^{(u)}$	guard vector for the u -th branch
$\gamma_{\text{LS},j}$	SNR of the TD-LS-JCE of the j -th channel tap \underline{h}_j
$\tilde{\gamma}_{\text{LS},j}$	SNR of the FD-LS-JCE at the j -th CTF component \tilde{h}_j
$\gamma_{\text{MF},j}$	SNR of the TD-MF-JCE of the j -th channel tap \underline{h}_j
$\tilde{\gamma}_{\text{MF},j}$	SNR at the output of the FDMF JCE at the j -th CTF component \tilde{h}_j
$\gamma_{\text{WLS},j}$	SNR of the TD-WLS-JCE of the j -th channel tap \underline{h}_j
$\tilde{\gamma}_{\text{WLS},j}$	SNR of the FD-WLS-JCE at the j -th CTF component \tilde{h}_j
$\tilde{\gamma}_{\text{ref},j}$	SNR of the j -th CTF component $\hat{\tilde{h}}_j$ in the reference single branch scenario
$(\)^{\text{H}}$	complex Hermitian
\mathbb{H}_1	submatrix of the Hardamard matrix
$\underline{h}(\tau)$	time invariant CIR as a function of delay τ
$\underline{h}(\tau, t)$	time variant CIR as a function of delay τ and time t
$\underline{\mathbf{h}}$	the total CIR vector of U branches
$\hat{\underline{\mathbf{h}}}$	estimation to the total CIR $\underline{\mathbf{h}}$
$\tilde{\underline{\mathbf{h}}}_{\text{I}}$	the CTF of the interferer
$\hat{\underline{\mathbf{h}}}_{\text{LS}}$	least square estimation to the total CIR $\underline{\mathbf{h}}$
$\hat{\underline{\mathbf{h}}}_{\text{LS}}$	least square estimation to the total CTF $\tilde{\underline{\mathbf{h}}}$
$\hat{\underline{\mathbf{h}}}_{\text{LS,A}}$	the FD-LS-JCE of the total CTF in the interference scenario
$\hat{\underline{\mathbf{h}}}_{\text{MF}}$	matched filtering estimation to the total CIR $\underline{\mathbf{h}}$
$\hat{\underline{\mathbf{h}}}_{\text{MF}}$	matched filtering estimation to the total CTF $\tilde{\underline{\mathbf{h}}}$
$\hat{\underline{\mathbf{h}}}_{\text{WLS}}$	weighted least square estimation to the total CIR $\underline{\mathbf{h}}$
$\hat{\underline{\mathbf{h}}}_{\text{WLS}}$	weighted least square estimation to the total CTF $\tilde{\underline{\mathbf{h}}}$
$\tilde{\underline{\mathbf{h}}}$	the total CTF vector of U branches
$\underline{\mathbf{h}}^{(u)}$	CIR vector between each transmit branch u and the receiver, $u = 1 \cdots U$
$\tilde{\underline{\mathbf{h}}}$	CTF vector between each transmit branch u and the receiver, $u = 1 \cdots U$
$\hat{\underline{\mathbf{h}}}$	estimation to the CIR $\underline{\mathbf{h}}^{(u)}$ of the u -th branch, $u = 1 \cdots U$
$\underline{h}^{(u,w)}$	the w -th element of the vector $\underline{\mathbf{h}}^{(u)}$, $u = 1 \cdots U$, $w = 1 \cdots W$
$\tilde{h}(f)$	time invariant CTF as a function of frequency f
$\tilde{h}(f, t)$	time variant CTF as a function of frequency f and time t
$\tilde{h}_{i-j}(f, t)$	the transfer function of subchannels i through j , $i = 1 \cdots N_{\text{F}}$, $j = 1 \cdots N_{\text{F}}$, $i < j$
$\tilde{h}_i(f, t)$	transfer function of the i -th subchannel, $i = 1 \cdots N_{\text{F}}$, as a function of frequency f and time t
\mathbf{I}	identity matrix
\tilde{I}	mean value of the interference power of $\tilde{I}^{(j)}$
$\tilde{I}^{(j)}$	interference power on the j -th channel estimation sample $\hat{\underline{h}}_{\text{LS,A}}^{(j)}$
$\mathbf{I}_{L_{\text{p}}}$	$L_{\text{p}} \times L_{\text{p}}$ identity matrix
$\mathbf{I}_{N_{\text{F}}}$	$N_{\text{F}} \times N_{\text{F}}$ identity matrix

\mathbf{I}_{UW}	identity matrix of dimension $(UW) \times (UW)$
\mathbf{I}_W	identity matrix of dimension $W \times W$
J	Lagrange cost function
K	number of MTs simultaneously active in a cell or SA
k_a	number of antennas at each AP
K_A	number of APs
$K_{M,k}$	number of antennas at each MT k , $k = 1 \cdots K$
$\tilde{\lambda}_j$	j -th eigenvalue of the matrix $\tilde{\mathbf{G}}^H \tilde{\mathbf{G}}$
L_G	guard interval length
L_p	length of the pilot at each branch
M	modulation order
$\tilde{\mathbf{M}}$	frequency domain estimation matrix
\mathbf{n}	time domain noise vector
$\tilde{\mathbf{n}}$	frequency domain noise vector
N_0	one sided noise power spectral density
N_F	number of subcarriers
\mathbf{P}	a total time domain pilot matrix of U branches
$\tilde{\mathbf{P}}$	a total frequency domain pilot matrix of U branches
$\mathbb{P}_{C,w}$	a $N_F \times U$ submatrix containing U columns of the matrix $\tilde{\mathbf{A}}_C$
$p(f_D)$	pdf of the Doppler shift
$p(f_D, \tau)$	joint pdf of the Doppler shift f_D and the time delay τ
$p(\tilde{h})$	pdf of the CTF $\tilde{h}(f, t)$
$p \tilde{h} $	pdf of the absolute value of the CTF $\tilde{h}(f, t)$
$\phi_h(\tau, f_D)$	the scattering function of the channel, which is obtained from the Fourier transformation of $\phi_h(\tau, \Delta t)$
$\phi_h(\tau_1, \tau_2, t_1, t_2)$	autocorrelation function of the time-variant CIR $h(\tau, t)$ as a function of τ_1, τ_2, t_1, t_2
$\phi_h(\tau, \Delta t)$	autocorrelation function of the time-variant CIR $h(\tau, t)$ as a function of $\tau, \Delta t$
$\tilde{\phi}_h(\Delta t, \Delta f)$	the time-frequency correlation function of the channel, which is obtained from the Fourier transformation of the autocorrelation function $\phi_h(\Delta t, \tau)$
$\phi_h(\tau)$	power delay profile of the channel
$\tilde{\mathbf{P}}$	frequency domain total pilot matrix
$\tilde{\mathbf{P}}_D^{(u)}$	disjoint pilot for the u -th branch
$\tilde{\mathbf{P}}_I$	pilot matrix of the interferer
ψ_{w_τ}	direction of the terminal movement relative to the w_τ -th path direction
$p(f_D)$	pdf of the Doppler shift f_D
P_n	average noise power
P_s	average signal power
$p(\tau)$	pdf of the channel delay τ
$p(\tau, f_D)$	joint pdf of the Doppler shift f_D and time delay τ

$\underline{\mathbf{p}}^{(u)}$	vector representing the time domain pilot transmit at each branch $u, u = 1 \dots U$
$\underline{\mathbf{p}}_{\text{E}}^{(u)}$	extended pilot vector from the guard vector $\underline{\mathbf{g}}^{(u)}$ and the pilot vector $\underline{\mathbf{p}}^{(u)}$ at the u -th branch
$\tilde{\underline{\mathbf{p}}}^{(u)}$	vector representing the frequency domain pilot transmit at each branch $u, u = 1 \dots U$
$\underline{\mathbf{P}}^{(u)}$	a branch specific pilot matrix in time domain
$\tilde{\underline{\mathbf{P}}}^{(u)}$	a diagonal branch specific pilot matrix in frequency domain
$\underline{p}^{(u, l_p)}$	the time domain pilot symbol value of the l_p -th symbol at the u -th branch, $l_p = 1 \dots L_p, u = 1 \dots U$
$p(\varphi)$	pdf of the path phase
$\mathbb{P}_{\text{W}, w}$	the w -th Walsh code based pilots
Q	upsampling factor in filter bank multi-carrier systems
$\underline{\mathbf{r}}$	the time domain receive signal vector
$\tilde{\underline{\mathbf{r}}}$	the frequency domain receive signal vector
$\underline{\mathbf{R}}$	correlation matrix of the total vector of CIR $\underline{\mathbf{h}}$
$\tilde{\underline{\mathbf{r}}}_{\text{A}}$	the interfered receive signal in the considered SA in the interference scenario
R_{b}	bit rate
$\tilde{\underline{\mathbf{r}}}_{\text{c}}$	cyclic correlation vector of the CAZAC code
$\underline{R}(i, j)$	the element in the correlation matrix $\underline{\mathbf{R}}$
$\underline{\mathbf{R}}_{\text{h}}$	correlation matrix of the total CIR vector $\underline{\mathbf{h}}$
$\underline{\mathbf{R}}_{\text{n}}$	covariance matrix of the time domain noise vector $\underline{\mathbf{n}}$
$\tilde{\underline{\mathbf{R}}}_{\text{n}}$	covariance matrix of the frequency domain noise vector $\tilde{\underline{\mathbf{n}}}$
R_{s}	symbol rate
σ^2	power of the complex Gaussian noise vector
σ_{h}^2	variation of the CTF $\tilde{\underline{h}}(t, f)$
σ_{τ}	channel delay spread
$\tilde{\sigma}_{\text{I}}^2$	mean square deviation of the interference power $\tilde{I}^{(j)}$
s_{max}	maximum vehicle speed
t	time
τ	path delay in the radio channel
τ_{max}	maximum multi-path propagation delay
$\tau_{w_{\tau}}$	propagation delay of the w_{τ} -th path, $w_{\tau} = 1 \dots W_{\tau}$
T	multi-carrier symbol duration
T_{C}	channel coherence time
T_{G}	guard interval duration
T_{OFDM}	total OFDM symbol duration
$\text{tr}(\cdot)$	trace operation
$(\cdot)^{\text{T}}$	transpose of matrix
T_{s}	symbol duration of the baseband signal
U	number of branches

v	vehicle speed
V	threshold level of the variation coefficients
v_{\max}	maximum vehicle speed
$\tilde{\mathbf{V}}$	unitary matrix
v_c	variation coefficient
φ	random variable of the initial phase
φ_{w_τ}	phase rotation of the w_τ -th path, $w_\tau = 1 \cdots W_\tau$
W	number of channel coefficients
$\tilde{\mathbf{w}}_{n_F}$	the n_F -th Walsh code obtained from the Hadamard matrix $\tilde{\mathbf{A}}_W$
W_τ	number of channel taps
$\underline{\mathbf{Z}}_{\text{LS}}$	the estimation matrix in FD-LS-JCE
$\underline{\mathbf{Z}}_{\text{MF}}$	the estimation matrix in FD-MF-JCE
$\underline{\mathbf{Z}}_{\text{WLS}}$	the estimation matrix in FD-WLS-JCE
$[\cdot]_{x,y}$	the element in the x -th row and the y -th column of a matrix in the bracket
$[\cdot]_{x_1,y_1}^{x_2,y_2}$	the submatrix bounded by the rows and and the columns and of a matrix in the bracket

References

- [Ala98] S.M. Alamouti, "A Simple Transmit Diversity Technique for Wireless Communications", *IEEE Journal on Selective Areas in Communications*, vol. 16, 1998, pp. 1451–1458.
- [Arf85] G. Arfken, *Mathematical Methods for Physicists*, Academic Press, 1985.
- [BaM02] P.W. Baier, M. Meurer, "Air interface enhancements for 3G and beyond-3G mobile radio communications", *Proc. 9th International Conference on Telecommunications (ICT '02)*, 2002, pp. 284–291.
- [BBT02] R. Berezdivin, R. Breinig, R. Topp, "Next-generation wireless communications concepts and technologies", *IEEE Communications Magazine*, vol. 40, 2002, pp. 108–116.
- [BC02] N. Benvenuto, G. Cherubini, *Algorithms for Communications Systems and Their Applications*, John Wiley & Sons, 2002.
- [Bel63] P.A. Bello, "Characterization of randomly time-variant linear channels", *IEEE Trans. Communication Systems*, vol. CS-11, Dec. 1963, pp. 363–393.
- [BES⁺95] J.v.d. Beek, O. Edfors, M. Sandell, S.K. Wilson, P.O. Börjesson, "On channel estimation in OFDM systems", *Proc. IEEE 45th Vehicular Technology Conference, (VTC '95)*, vol. 2, 1995, pp. 815–819.
- [BJW01] P.W. Baier, C.A. Jötten, T. Weber, "Review of TD-CDMA", *Proc. 3rd International Workshop on Commercial Radio Sencors and Communications Techniques, (CRSCT '01)*, 2001, pp. 11–20.
- [BKN⁺94a] J.J. Blanz, A. Klein, M.M. Naßhan and A. Steil, "Capacity of a cellular CDMA mobile radio system applying joint detection", *COST 231 Temporary Document TD (94) 2*, Lisbon, 1994.
- [BLM02] I. Barhumi, G. Leus, M. Moonen, "Optimal trainging sequences for channel estimation in MIMO OFDM systems in mobile wireless channels", *International Zurich Seminar on Broadband Communications, Access, Transmission, Networking*, 2002, pp. 44-1–44-6.
- [Bol99] H. Bolcskei, 'Efficient design of pulse shaping filters for OFDM systems', *Proc. SPIE*, vol. 3813, July 1999, pp. 625–636.
- [BP95] K. Berberidis and J. Palicot, "A frequency domain decision feedback equalizer for multipath echo cancellation," *Proc. IEEE Global Telecommunications Conference, (GLOBECOM '95)*, vol. 1, 1995, pp. 98–102.
- [BMW⁺00] P.W. Baier, M. Meurer, T. Weber, H. Tröger, "Joint Transmission (JT), an alternative rationale for the downlink of time division CDMA using multi-element transmit antennas", *Proc. IEEE 6th International Symposium on Spread Spectrum Techniques & Applications, (ISSSTA '00)*, vol. 1, 2000, pp. 1–5.

- [BT02] N. Benvenuto, S. Tomasin, "On the comparison between OFDM and single carrier modulation with a DFE using a frequency-domain feedforward filter", *IEEE Transactions on Communications*, vol. 50, 2002, pp. 947–955.
- [BTT02] N. Benvenuto, S. Tomasin, L. Tomba, "Equalization methods in OFDM and FMT systems for broadband wireless communications", *IEEE Transactions on Communications*, vol. 50, 2002, pp. 1413–1418.
- [BTT02a] N. Benvenuto, S. Tomasin, L. Tomba, "Receiver architectures for FMT broadband wireless communications", *Proc. IEEE 53th Vehicular Technology Conference, (VTC '01)*, vol. 1, 2001, pp. 643–647.
- [CD02] Z. Cheng, D. Dahlhaus, "Time versus frequency domain channel estimation for OFDM systems with antenna arrays", *Proc. IEEE 6th International Conference on Signal Processing*, vol. 2, 2002, pp. 1340–1343.
- [CEÖ02] G. Cherubini, E. Eleftheriou, S. Öker, "Filtered multitone modulation for very high-speed digital subscriber lines", *IEEE Journal on Selected Areas in Communications*, vol. 20, 2002, pp. 1016–1028.
- [CEÖ+00] G. Cherubini, E. Eleftheriou, S. Öker, J.M. Cioffi, "Filter bank modulation techniques for very high speed digital subscriber lines", *IEEE Communications Magazine*, vol. 38, 2000, pp. 98–104.
- [CFW03] E. Costa, A. Filippi, M. Weckerle, E. Schulz, "Comparison of FMT-FDMA and OFDMA in asynchronous uplink applications", *Proc. 8th International OFDM Workshop (InOWo '03)*, 2003.
- [ChM00] W. Chen, U. Mitra, "Frequency domain versus time domain based training sequence optimization", *Proc. IEEE International Conference on Communications, (ICC '00)*, vol. 2, 2000, pp. 646–650.
- [Chu72] D.C. Chu, "Polyphase codes with good periodic correlation properties", *IEEE Transactions on Information Theory*, vol. 18, July 1972, pp. 531–532.
- [ChM00a] W. Chen, U. Mitra, "Training sequence optimization: comparisons and an alternative criterion", *IEEE Transactions on Communications*, vol. 48, Dec. 2000, pp. 1987–1991.
- [CM98] G. Caire, U. Mitra, "Training sequence design for adaptive equalization of multi-user systems", *Proc. 32nd Asilomar Conference on Signals, Systems & Computers*, vol. 2, 1998, pp. 1479–1483.
- [COS89] COST 207, "Digital land mobile radio communications", Final Report COST Action 207, Office for Official Publications of the European Communities, Luxembourg, 1989.
- [COS01] COST 259, "Wireless flexible personalized communications", Final Report COST Action 259, edited by L.M. Correia, John Wiley & Sons Inc., 2001.
- [CS00] J. Chuang, N. Sollenberger, "Beyond 3G: wideband wireless data access based on OFDM and dynamic packet assignment", *IEEE Communications Magazine*, vol. 38, 2000, pp. 78–87.

- [CWG⁺01] M.V. Clark, T.M. Willis III, L.J. Greenstein, A.J. Rustako Jr., V. Erceg, R.S. Roman, "Distributed versus centralized antenna arrays in broadband wireless networks", Proc. IEEE 53th Vehicular Technology Conference, (VTC '01), vol. 1, 2001, pp. 33–37.
- [DGE01] L. Deneire, B. Gyselinckx, M. Engels, "Training sequences versus cyclic prefix – a new look on single carrier communication", IEEE Communications Letters, vol. 5, July 2001, pp. 292–294.
- [DJ98] E.H. Dinan, B. Jabbari, "Spreading codes for direct sequence CDMA and wideband CDMA cellular networks", IEEE Communications Magazine, vol. 36, Sept. 1998, pp. 48–54.
- [ECS⁺98] R.B. Ertel, P. Cardieri, K.W. Sowerbi, T.S. Rappaport and J.R. Reed, "Overview of spatial channel models for antenna array communication systems", IEEE Personal Communications Magazine, vol. 5, Feb. 1998, pp. 10–22.
- [EGL93] M. Ewerbring, B. Gudmundson, G. Larsson, and P. Teder, "CDMA with interference cancellation: A technique for high capacity wireless systems", Proc. International Conference on Communications, May 1993, pp. 1901–1906.
- [EMG99] V. Erceg, D.G. Michelson, S.S. Ghassemzadeh, L.J. Greenstein, et al., "A model for the multipath delay profile of fixed wireless channels", IEEE Journal on Selected Areas in Communications, vol. 17, March 1999, pp. 399–410.
- [FAB02] D. Falconer, S.L. Ariyavisitakul, A. Benyamin-Seeyar, B. Eidson, "Frequency domain equalization for single-carrier broadband wireless systems", IEEE Communications Magazine, vol. 40, April 2002, pp. 58–66.
- [FAT03] C. Fragouli, N. Al-Dhahir, W. Turin, "Training-based channel estimation for multiple-antenna broadband transmissions", IEEE Transactions on Wireless Communications, vol. 2, March 2003, pp. 384–391.
- [FB92] T. Felhauer, P.W. Baier, "Optimum radio channel estimation with periodic spread spectrum signal adjusted to amplifier nonlinearities", Proc. IEEE Second International Symposium on Spread Spectrum Techniques and Applications (ISSSTA '92), 1992, pp. 309–312.
- [Fel93] T. Felhauer, "Digital signal processing for optimum wideband channel estimation in the presence of noise", Proc. IEEE F Radar and Signal Processing, vol. 140, June 1993, pp. 179–186.
- [Fel94] T. Felhauer, Optimale erwartungstreue Algorithmen zur Hochauflösenden Kanalschätzung mit Bandspreizsignalformen, Fortschrittberichte VDI, series 10, no. 278, VDI-Verlag, Düsseldorf, 1994.
- [FG98] G.J. Foschini, M.J. Gans, "On limits of wireless communications in a fading environment when using multiple antennas", Wireless Personal Communications, vol. 6, 1998, pp.311–335.

- [Fil04] A. Filippi, Non-conventional Multi-carrier Air Interface for the 4th Generation Mobile Radio Systems, PhD thesis, 2004.
- [Fis76] M. Fisz, Wahrscheinlichkeitsrechnung und Mathematische Statistik, Deutscher Verlag der Wissenschaften, Berlin, 1976.
- [Fos96] G.J. Foschini, "Layered space-time architecture for wireless communication in a fading environment when using multi-element antennas", Bell Labs Technical Journal, Autumn 1996.
- [FRB97] J. Fuhl, J.P. Rossi and E. Bonek, "High resolution 3-D direction-of-arrival determination for urban mobile radio", IEEE Transactions on Antennas and Propagation, vol. 45, 1997, pp. 672-681.
- [FZH62] R.L. Frank, S.A. Zadoff, R. Heimiller, "Phase shift pulse codes with good periodic correlation properties", IRE Transactions on Information Theory, vol. 8, Oct. 1962, pp. 381-382.
- [Gal01] D. Galda, "The stochastic WSSUS broadband channel model and its implications on the OFDM system design", Technique Report of Joint Research beyond 3G (JRB3G) by Siemens, Aug. 2001.
- [Gol67] R. Gold, "Optimal binary sequences for spread spectrum multiplexing", IEEE Transactions on Information Theory, vol. 13, Oct. 1967, pp. 619-621.
- [GSM88] ETSI/TC GSM Recommendations, series 01-12, 1988.
- [Gar99] V.K. Garg, IS-95 CDMA & CDMA2000: Cellular/PCS Systems Implementation, Prentice-Hall, 1999.
- [Hei61] R.C. Heimiller, "Phase shift pulse codes with good periodic correlation properties", IRE Transactions on Information Theory, vol. 7, Oct. 1961, pp. 254-257.
- [Hoe92] P. Hoehner, "A statistical discrete-time model for the WSSUS multipath channel", IEEE Transactions on Vehicular Technology, vol. 41, Nov. 1992, pp. 461-468.
- [HT02] H. Holma, A. Toskala, WCDMA for UMTS: Radio Access for Third Generation Mobile Communications, John Wiley & Sons, 2002.
- [Kal95] C.K. Kahl, "Channel equalization for block transmission systems", IEEE Journal on Selected Areas in Communications, vol. 13, Jan. 1995, pp. 110-121.
- [Kat97] R. Kattenbach, Charakterisierung zeitvarianter Indoor-Funkkanäle anhand ihrer System- und Korrelationsfunktionen, Shaker Verlag, Aachen, 1997.
- [Kay93] S.M. KAY, Fundamentals of Statistical Signal Processing: Estimation theory, Prentice-Hall, New Jersey, 1993.

- [KCW⁺03] G. Kang, E. Costa, M. Weckerle, E. Schulz, "Optimum channel estimation over frequency-selective fading channel in multiple antenna systems", Proc. IEEE International Conference on Communication Technology, (ICCT '03), vol. 2, 2003, pp. 1799–1803.
- [KIH87] R. Kohno, H. Imai, M. Hatori, and S. Pasupathy, "Adaptive cancellation of interference in direct-sequence spread-spectrum multiple access systems", Proc. Global Telecommunications Conference, Nov. 1987, pp. 630–634.
- [KJC⁺03] Y. Kim, B.J. Jeong, J. Chung, C. Hwang, J.S. Ryu, K. Kim, Y.K. Kim, "Beyond 3G: vision, requirements, and enabling technologies", IEEE Communications Magazine, vol. 41, 2003, pp. 120–124.
- [KKB96] A. Klein, K. Kaleh, P.W. Baier, "Zero forcing and minimum-mean-square-error equalization for multiuser detection in code-division multiple-access channels", IEEE Transactions on Vehicular Technology, vol. 45, May 1996, pp. 276–287.
- [Kle96] A. Klein, Multi-user Detection of CDMA Signals – Algorithms and Their Applications to Cellular Mobile Radio, VDI-Verlag GmbH, Düsseldorf, 1996.
- [KMT96] A. Klein, W. Mohr, R. Thomas, P. Weber and B. Wirth, "Direction-of-arrival of partial waves in wideband mobile radio channels for intelligent antenna concepts", Proc. IEEE 46th Vehicular Technology Conference (VTC '96), Atlanta, 1996, pp. 849–853.
- [KMW⁺04] G. Kang, I. Maniatis, M. Weckerle, E. Costa, T. Weber, "Optimum pilots for joint channel estimation in multi-user OFDM systems", IEEE Transactions on Wireless Communications, 2004, submitted.
- [KWC04] G. Kang, M. Weckerle, E. Costa, "Time and frequency domain joint channel estimation in multi-branch systems", ICC '04, submitted.
- [KWC04a] G. Kang, M. Weckerle, E. Costa, "Space-time joint channel estimation in filtered multi-tone based multi-carrier multi-branch systems", Proc. IEEE Wireless Communications and Networking Conference WCNC '04, Atlanta, March 2004, pp. 1844–1849.
- [Li00] Y. Li, "Optimum training sequences for OFDM systems with multiple transmit antennas", Proc. IEEE Global Telecommunications Conference, (GLOBECOM '00), vol. 3, 2000, pp. 1478–1482.
- [LL99] S. Li, J. Li, "TD-SCDMA: standardization and prototype development", 5th Asia-Pacific Conference on Communications and 4th Optoelectronics and Communications Conference, (APCC/OECC '99), vol. 2, 1999, pp. 1715.
- [LSA99] Y. Li, N. Seshadri, S. Ariyavisitakul, "Channel estimation for OFDM systems with transmitter diversity in mobile wireless channels", IEEE Journal on Selected Areas in Communications, vol. 17, 1999, pp. 461–471.
- [LSA01] L. Lindbom, M. Sternad, A. Ahlén, "Tracking of time-varying mobile radio channels—part I: the Wiener LMS algorithm", IEEE Transactions on Communications, vol. 49, Dec. 2001, pp. 2207–2217.

- [LAS⁺02] L. Lindbom, A. Ahlén, M. Sternad, M. Falkenström, "Tracking of time-varying mobile radio channels—part II: a case study", *IEEE Transactions on Communications*, vol. 50, Jan. 2002, pp. 156–167.
- [MH97] S.H. Müller, J.B. Huber, "OFDM with reduced peak-to-average power ratio by optimum combination of partial transmit sequences", *Electronics Letters*, vol. 33, Feb. 1997, pp. 368–369.
- [MWS⁺02] I. Maniatis, T. Weber, A. Sklavos, Y. Liu, E. Costa, H. Haas, E. Schulz, "Pilots for joint channel estimation in multiuser OFDM mobile radio systems", *Proc. IEEE 7th International Symposium on Spread Spectrum Techniques & Applications, (ISSSTA '02)*, vol. 1, 2002, pp. 44–48.
- [NP00] R.V. Nee, R. Prasad, *OFDM for Wireless Multimedia Communications*, Artech House, 2000.
- [Pap00] A. Papathanassiou, *Adaptive antennas for mobile radio systems using Time Division CDMA and joint detection*, *Forschungsberichte Mobilkommunikation*, vol. 6, University of Kaiserslautern, 2000, ISBN 3–925178–48–1.
- [Par92] J.D. Parsons, *The mobile radio propagation channel*, Pentech Press, London, 1992.
- [Pau94] A. Paulraj, et al., "Increasing capacity in wireless broadcast system using distributed transmission/directional reception", U.S. Patent no. 5345599, 1994.
- [PL95] K. Pahlavan and A.H. Levesque, *Wireless Information Networks*, New York: Wiley, 1995.
- [Pro95] J.G. Proakis, *Digital communications*, McGraw–Hill, New York, 3rd edition, 1995.
- [Rap96] T.S. Rappaport, *Wireless Communications principles and practice*, Prentice-Hall, 1996.
- [RGG01] H. Rohling, R. Grünheid, D. Galda, "OFDM air interface for the 4-th generation if mobile communication systems", *Proc. 6th International OFDM-workshop (InOWo '01)*, Hamburg, Germany, Sept. 2001.
- [Sch89] H. Schulze, "Stochastische modelle und digitale simulation von mobilfunkkanälen", in *Kleinheubacher Berichte*, no. 32, 1989.
- [SG01] P. Struhsaker, K. Griffin, "Analysis of PHY waveform peak to mean ratio and impact on RF amplification", *IEEE 802.16a cont. IEEE 802.16.3c-01/46*, Mar. 6, 2001.
- [SJ94] B. Steiner, P. Jung, "Optimum and suboptimum channel estimation for the uplink of CDMA mobile radio systems with joint detection", *European Transactions on Communications*, vol. 5, 1994, pp. 39–49.
- [Sk197] B. Sklar, "Rayleigh fading channels in mobile digital communication systems Part I: characterization", *IEEE Communications Magazine*, Sept. 1997, pp. 136–146.

- [SMH02] D. Schafhuber, G. Matz, F. Hlawatsch, "Pulse-shaping OFDM/BFDM systems for time-varying channels: ISI/ICI analysis, optimal pulse design, and efficient implementation", Proc. IEEE 13th International Symposium on Personal, Indoor and Mobile Radio Communications, (PIMRC '02), vol. 3, 2002, pp. 1012–1016.
- [SMW⁺01] A. Sklavos, I. Maniatis, T. Weber, P.W. Baier, E. Costa, H. Haas, E. Schulz, "Joint channel estimation in multi-user OFDM systems", Proc. 6th International OFDM-workshop (InOWo '01), 2001, pp. 3-1–3-4.
- [SWB⁺01] A. Sklavos, T. Weber, P.W. Baier, E. Costa, "Beyond 3G radio interface JOINT: optimum uplink data detection when applying OFDM", Proc. 7th International OFDM-workshop (InOWo '02), 2002, pp. 11–15.
- [Ste73] G.W. Stewart, Introduction to Matrix Computations, Academic Press, New York, 1973.
- [SWB02] A. Sklavos, T. Weber, P.W. Baier, E. Costa, "Beyond 3G radio interface JOINT: Optimum uplink data detection when applying OFDM", Proc. 7th International OFDM Workshop (InOWo '02), 2002, pp. 11–15.
- [Tel95] E. Telatar, "Capacity of multi-antenna Gaussian channels", AT&T Bell Labs Internal Techn. Memo., June 1995.
- [TM97] F. Tufvesson, T. Maseng, "Pilot assisted channel estimation for OFDM in mobile cellular systems", Proc. IEEE 47th Vehicular Technology Conference, (VTC '97), vol. 3, 1997, pp. 1639–1643.
- [TSC98] V. Tarokh, N. Seshadri, A.R. Calderbank "Space-time codes for high data rate wireless communication: performance criterion and code construction", IEEE Trans. on Information Theory, vol. 44, 1998, pp. 744–765.
- [Ver98] S. Verdú, Multiuser detection, Cambridge University Press, Cambridge, 1998.
- [VT01] F.W. Vook, T.A. Thomas, "MMSE multi-user channel estimation for broadband wireless communications", Proc. Global Telecommunications Conference (GLOBECOM '01), 2001, pp. 470–474.
- [Wec02] M. Weckerle, Utilization of Correlation Matrices in Adaptive Array Processors for Time-slotted CDMA Uplinks, Kaiserslautern University, Dissertation, 2002.
- [WeM02] T. Weber, M. Meurer, "Iterative multiuser detection for TD-CDMA exploiting data estimate refinement techniques", Proc. IEEE 56th Vehicular Technology Conference, (VTC '02 Fall), vol. 3, Sept. 2002, pp. 1642–1646.
- [Wha71] A.D. Whalen, Detection of Signals in Noise, Academic Press, New York, 1971.
- [WCDMA] WCDMA specifications, "Physical channels and mapping of transport channels onto physical channels (FDD)", 3GPP TS 25.211, v4.2.0, Sept. 2001.

-
- [WMS⁺02] T. Weber, I. Maniatis, A. Sklavos, Y. Liu, E. Costa, H. Haas, E. Schulz, "Joint transmission and detection integrated network (JOINT), a generic proposal for beyond 3G systems", Proc. 9th International Conference on Telecommunications, (ICT '02), vol. 3, 2002, pp. 479–483.
- [WNW01] D.A. Wiegandt, C.R. Nassar, Z. Wu, "Overcoming peak-to-average power ratio issues in OFDM via carrier interferometry codes", Proc. Vehicular Technology Conference, (VTC '01), vol. 2, 2001, pp. 660–663.
- [YMC02] K. Yang, A. Madhukumar, F. Chin, "Optimum pilot design for multipath channel estimation of a single carrier cyclic prefix-assisted CDMA system", Proc. International Conference on Communication Systems, (ICCS '02), vol. 1, 2002, pp. 279–283.
- [Zol93] E. Zollinger, Eigenschaften von Funkübertragungsstrecken in Gebäuden, Doctoral Dissertation, Eidgenössische Technische Hochschule Zürich, 1993.

Tabellarischer Lebenslauf

Name: Guixia Kang

Birthday: 26. December 1972

Birth place: Tangshan, Heibei, China

Family status: Married

Nationality: Chinese

Education: Sept 1979 – July 1984
Elementary School of Tianranqi Company, Daqing, Heilongjiang, China

Sept 1984 – July 1985
Elementary School of the Second Extraction Factory, Daqing, China

Sept 1985 – July 1988
The 30th Middle School of Daqing, Daqing, China

Sept 1988 – July 1991
The Tieren High School of Daqing, Daqing, Heilongjiang, China

Study: Sept 1991 – July 1995
Study of Industrial automation
in Tianjin University

Graduation: Banchelor

Sept 1997 – Sept 2001
Study of Wireless Communications
in Beijing University of Posts and Telecommunications

Graduation: PhD

Work experience: August 1995 – August 1997
Beijing Factory of Radio Instruments

Sept 1999 – July 2002
Research scientist in Beijing University of Posts and Telecommunications

Since July 2002
Free coworker of Siemens AG in Munich